Characteristics of Stay Cable Dry Galloping and Effectiveness of Spiral Protuberance Countermeasures

Vo Duy Hung

2016

Characteristics of Stay Cable Dry Galloping and Effectiveness of Spiral Protuberance Countermeasures

斜ケーブルドライギャロッピングの特性とスパイラル突起による対策の有効性

A Dissertation Submitted in Partial Fulfillment of the
Requirements for the Degree of
Doctor of Philosophy

By

Vo Duy Hung

Department of Civil Engineering

YOKOHAMA NATIONAL UNIVERSITY

September 2016

Table of Contents

List of Figures

List of Tables

List of Equations

Abstract

In the past, during construction or once the bridge was completed and in service stage, stay cable had known to vibrate due to rain-wind combination, which named rain-wind induced vibration (RWIV). Recently, it was also proved that stayed-cables could be excited even though in no rain condition that called dry galloping (DG). For RWIV, rain plays an important role in forming the lower and upper rivulets on cable surface that change the cable aerodynamic characteristics, and then excite galloping. This phenomenon can be mitigated by shape modification or increasing the Scruton number of cable. Together with that, dry galloping is classified as one of the wind-induced large amplitude vibration phenomena in dry weather (without rain), usually occurs at relatively high-reduced wind speed, it also showed some characteristics of limited amplitude vibration, however. Some studies showed the existence of dry galloping, in both wind tunnel test and the site observation. Nevertheless, its characteristics and mechanism are not fully understood as well as control methods for this phenomenon are under developing. Recently, some authors pointed out that current aerodynamic mitigation methods can adapted for RWIVs but not for the DG. The present research is therefore an effort to investigate insight of DG characteristics and its mechanism as well as develop an effective countermeasure for DG and RWIV. Experimental and analytical results proved that DG depends on wind attack angles and it is less sensitive to the cable damping change rather than frequency and it can occur in subcritical Re region. Moreover, there is a strong recovery of surface pressure in leeward side and in presence of single spiral protuberances, cable surface pressure redistributed. The mechanism of DG relate to the interruption of Karman vortex shedding and the excitation from low frequency flow/vortices at high wind speed. Further, its interaction with axial flow, wind attack angle are significant in forming dry galloping conditions.

In addition, to assess the efficiency of current control methods for suppression the DG and RWIV, parallel protuberances and pattern-indented surface cables are investigated in low Scruton number range to reconfirm the efficiency. The results reaffirmed that DG

only occurred in specific condition of wind-cable angle, wind speeds. Further, the cable with indented surface and parallel protuberances still exhibited large amplitude vibration in low Scruton number. Due to the fact like that, this study will continue developing an aerodynamically cable for suppressing wind and rain-wind induced vibration, named spiral protuberances. The recommendation for fabrication of spiral protuberance cable will be issued in considering the selective fillet sizes and fillet pitches and number of protuberances. Finally, the suppression mechanism of spiral protuberance cable and its stability characteristic will be discussed in detail.

To my beloved family and respectable teachers

Acknowledgements

After five years in Japan, the author has encountered a lot of difficulty in life and study. Without kindly helps from his supervisors and his friends, the author could not finish my course as well as enjoy the life here. Now is the time for author to express his gratitude to all of them.

The author would like to express the heartfelt and sincere gratitude to Professor Hiroshi Katsuchi for his encouragement and guidance throughout the development of the works described in this dissertation. His contagious enthusiasm has often inspired author to keep pressing on through the inevitable discouragements, which author has encountered, and his openhearted teaching has made our time working together truly a pleasure.

The author would like to express the deepest gratitude Professor Hitoshi Yamada for his kind advices and supervision. Owning to his contribution, this research work has been improved better and better. The author also obtained much of fruitful knowledge from his lectures. Importantly, author is really appreciated for his contributions in training young Vietnamese scientists in general and especially for The University of Da Nang - Vietnam.

The author would like to send many thanks to Associate Professor Mayuko Nishio for her advices and correction. With her contribution and her lectures, author gained a lot of valuable knowledge.

The author would like to thank Professor Tatsuya Tsubaki and Associate Professor Dionysius M. Siringoringo. Their comments helped to ameliorate the thesis.

The author is highly obliged and grateful to Japanese Government (文部科学省: MEXT) for their incessant financial assistance and Japanese people for their friendly attitude during his study period in Japan.

The author would like to apologize to his mother for not being close to her when she need and through this paper would like to thank her for the sacrifice, which she made.

Thank you.

Vo Duy Hung

Chapter 1: Introduction

1.1 Background

Cable-stayed bridge has widely been applied for medium and long span bridges. Thanks to advanced construction technology and structural materials, its span length is being broken time by time. At the completion, Tatara Bridge in Japan with a main span of 890 meters used to be known as the longest stay cable bridge in the world. Nevertheless, it was rapidly passed over by Sutong Bridge (2008), Stonecutters Bridge (2009), E'dong Yangtze River Bridge (2010) and Russky Island Bridge (2012). The detail of top five longest stayed cable and its cable length are illustrated in Table 1.1.

Table 1.1 List of longest cable-stayed bridge spans and their cables length

Rank	Name	Longest span (m)	Cable length (m)	References
1	Russky Bridge	1104	579.83	[1]
2	Sutong Bridge	1088	577	[2]
3	Stonecutters Bridge	1018	540	[3]
4	E'dong Bridge	926	> 500	[4]
5	Tatara Bridge	890	460	[5]

With 1104 meters of the main span, Russky Island Bridge is the longest stay cable bridge in all over the world. Due to the increase of main span, cable length becomes longer and itself stiffness getting lower (as Figure 1-1). Like instance, the cable length excessed 540m in case of Stonecutter Bridge or around 580m for Russky Stay Cable Bridge. Additionally, its inherent damping ratio is as low as under 0.1% of critical and their mass is

quite low at around 50-150kg/m. This leads to the Scruton number of cables become very low. Therefore, stayed-cable is not able to dissipate much of the excitation energy, rendering them susceptible to large amplitude vibration. Further, stay cables are laterally flexible structural members with very low natural frequency. Due to the range of different lengths and frequencies, the number of stay cables on a cable-stayed bridge has a practical continuum of fundamental and higher mode frequencies. Thus, any excitation mechanism with any arbitrary frequency is likely to find one or more cables with either a fundamental or higher mode frequency sympathetic to the excitation. For these reasons, stay cables become more and more vulnerable to external excitation, especially wind or rain-wind combination.

Figure 1-1 Russky bridge with 580m length of longest cable stay

Common vibration types are rain-wind induced vibration, dry galloping, vortex-induced vibration (VIV) and wake galloping. RWIV phenomenon was observed first time in Meiko-Nishi Bridge [6], and then later it was reported occurring frequently on site of cable-stayed bridges [7-9]. In detail, there have been numerous field observations of stay cable vibrations over the past 20-30 years. The experience of large amplitude vibration has been figured out [7] for the Farø bridge in Denmark, the Ben-Ahin and Wandre bridges in Belgium, and more recently, for the Second Severn bridge in UK and the Erasmus bridge in the Netherlands. In Japan, besides the Meiko-Nishi Bridge (West Meiko), the Aratsu, the Higashi Kobe, the Tempozan and the Central Meiko bridges have also experienced rain-wind vibration. In the USA, rain vibration occurred at the Weirton-Steubenville Bridge, in

West Virginia, and at the Fred Hartman and East Huntington bridges, located in Texas and West Virginia, respectively. Moreover, in Australia, rain vibration amplitudes of several meters have been observed at the Glebe Island Bridge. Although majority of the observed stay cable vibration belongs to the rain–wind induced vibration, it has been found both in field [9-11] and wind tunnel tests [12-17] that dry inclined cables can also suffer large amplitude vibration without precipitation. The galloping of stay cables not only cause severe structural damages for the cables themselves and the bridge deck, but also it can cause fatigue and damages in cable attachments as Figure 1-2, 1-3 and 1-4. Further, excessive vibrations caused by wind could be unsettling to bridge operators and users. To tackle these problems and find better control methods, it is imperative to investigate the mechanisms underlying different conditions.

Many researches have been carried out during the past few decades to give a better understand the excitation mechanisms of large amplitude oscillation of bridge stay cables. RWIV phenomenon is nearly full understanding whereas the mechanisms of the DG are somehow ambiguous and need to be investigated more and more. Although a significant amount of effort has been made through the field observations, wind tunnel tests, and with the aid of Computational Fluid Dynamics, extensive research is still required to unveil the complex mechanisms of wind-induced cable vibration phenomena and to provide a better countermeasure for real bridges.

Figure 1-2 Cable damages due to cable vibration [18]

Figure 1-3 Dry galloping evidence without rain [18]

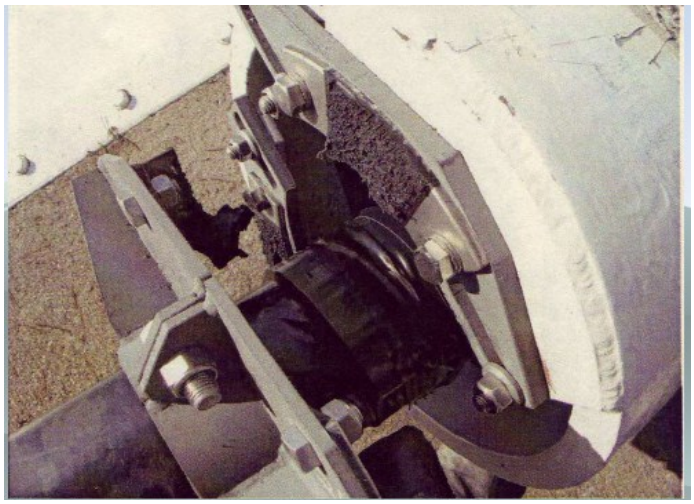

Figure 1-4 Damper-damages due to cable vibration [18]

1.2 Motivations

When rain-wind induced vibration was reported at the first time, cable manufacturers proposed some types of surface modification on cable sheathing in order to prevent forming water rivulet along the cable. The proposed control methods are based on researches carried out mainly in Japan and Europe, for instance: a high-density polyethylene tube with twelve parallel protuberances [19], a high-density polyethylene tube with indented surfaces [12] and a HDPE with single spiral wire [20] (as Figure 1-5). It has been found to promote the stabilization of these kinds of surface modification cable under rain-wind interaction.

(a) Parallel protuberances [21]

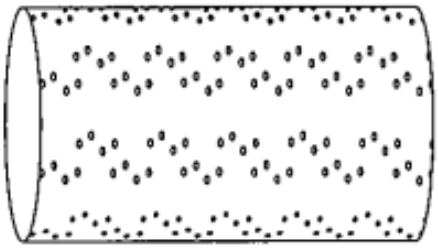

(b) Indented surface [22]

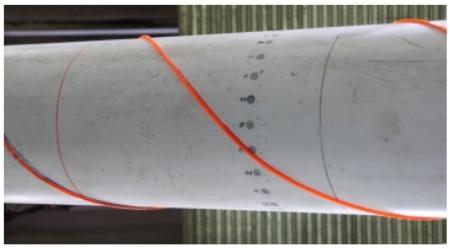

(c) Single spiral wire [23]

Figure 1-5 Surface of cable models

On the other hand, it was also pointed out that circular stay cables could be excited under no precipitation condition, which called DG [10, 13-17]. Generally, DG is classified as one of the wind-induced large amplitude vibration phenomena under no precipitation conditions, usually occurs at relatively high-reduced wind speed, it also showed some characteristics of limited amplitude vibration, however. An earlier wind tunnel study of Saito et al. suggested that the onset condition of DG could be easily satisfied by most of existing stayed-cables, which caused great concerns bridge engineers [13]. The current state of research on dry inclined stay cable galloping has confirmed the possible occurrence of such phenomenon on site of cable-stayed bridges through wind tunnel studies as well as the field observations[9-11, 13-17]. Additionally, Katsuchi and Yamada reported that dry galloping occurred in case of an indented cable under smooth flow and 30° of yawed angle at low Scruton number[16].

Therefore, suppression efficiency of indented surface as well as parallel protuberance for DG is still suspected. To give a better understanding about mitigation efficiency of current control methods, further investigation should be carried out. In addition, to propose a proper countermeasure, it is important to put more effort on investigating dry galloping characteristic as well as it mechanism.

It was also found that the presence of the spiral protuberance significantly reduced the shedding correlation length. Wind-tunnel tests was conducted with a single spiral protuberance for controlling RWIV[24]. Consequently, experiment results showed that a strong reduction of RWIV through the disruption of upper rivulet formation under rain condition. Nevertheless, it should be paid attention to that recent full-scale monitoring at Øresund Bridge [25] revealed that single helical wires were not effective as initially expected. Recently, a cable with twelve spiral protuberances wound with 27^0 was proposed as an optimized winding angle for reducing the drag force of cable [26]. However, a full wind tunnel test to observe cable response in dry and rain condition has not been done yet. Hence, it is imperative to develop a proper countermeasure, which must be adaptive for both RWIV and DG.

1.3 Objectives

So far, the characteristics of DG are still debating to a certain extent and its control methods have not developed yet. Besides that, the countermeasure for dry galloping must satisfy controlling RWIV as well. Therefore, this study aims at further extending the available insight of the aerodynamics characteristics of dry galloping and then proposes a proper countermeasure for not only DG but also RWIV. The goals and objectives of the current study are proposed to be:

- **Goal 01:** Shed a light on dry galloping characteristics and its generation mechanism

- To investigate the DG characteristics under considering various aspects: Scruton number effect, frequency dependence and aerodynamic damping characteristic.
- To give a better understanding of DG mechanism by investigating the flow field around cable, include axial flow, wake flow. Finally, the insight of generation mechanism will be discussed on.

- To examine galloping characteristic of parallel protuberance cable and indented surface cable in low Scruton number range.
    - ❖ **Goal 02:** Propose design recommendation for spiral protuberance cable in mitigating cable DG and taking in account suppressing RWIV.
- To propose a better countermeasure for dry galloping, “spiral protuberance cable” will be optimized in this study. The design recommendations for fabricating this method will be issued by number of protuberances, size of protuberances, pitches effect and winding direction. Furthermore, the suppression of RWIV will be also taken in to account.
- To elucidate the suppression mechanism of spiral protuberance.
- To compare the vibration mitigation level between spiral protuberances, indented surface and parallel protuberances to give a better understanding about the efficiency level of spiral protuberances countermeasures.

For these purposes, intensive wind tunnel tests with more than 300 cases were conducted to capture cable vibration amplitude with various relative cable-wind angle and to compare each other. Further, the insight of these flow field characteristics will be investigated and shed light on.

1.4 Organization of the dissertation

The main body of this dissertation has six chapters. The organizations are as follows:

- **Chapter 1:** Give general information regarding the stay cable vibration. In addition, the imperative need of proposing a more proper countermeasure for both DG and RWIV. Then, the necessary of this research will be addressed. On the other hand, this chapter clearly defines the research aim, objectives, methodology and motivation.
- **Chapter 2:** A general background of the current state of research on the wind-induced vibrations of bridge stay cables will be presented. The most commonly observed wind-induced vibration phenomena of stay cables with and without the presence of rain will be reviewed. As the primary focus of this study, dry galloping, which is a type of wind-induced vibration of stay cables under no precipitation condition, will be discussed in details. Then, previous studies related to wind or rain-wind induced cable vibration, galloping are also considered. Finally, the needs to further investigation on this field will be addressed.

- **Chapter 3:** Give introduction about the methodology of this study about wind tunnel facilities and various wind parameters. In addition, the flow condition, wind attack angle as well as rain condition of experiment will be described in this chapter. Furthermore, the rain wind induced cable vibration will be carried for validating the experiment system and for reference.
- **Chapter 4:** Examination of the cable dry galloping characteristics by wind tunnel will be presented. Firstly, dry galloping will be reproduced to confirm the existence of this phenomenon. Then, the effect of Scruton number, natural frequency dependence, aerodynamic damping ratio and surface pressure will be also figured out. Moreover, to give the suitable explanation for dry galloping, insight characteristics of wake flow fields will be shed a light on. Then, the DG generation mechanism will be also shed a light on. Furthermore, the unstable vibration of parallel protuberances and indented surface cables in low Scruton number range are also discussed. Due to the instability of current control method under dry galloping, it is imperative to develop more effective control method.
- **Chapter 5:** Propose a better control method for DG and take into account suppressing RWIV. In this chapter, cable with various spiral protuberance cable will be fabricated and conducted the experiments for optimizing. Consequently, number of protuberances, size of protuberances, pitches and winding direction will be recommended for the fabrication design of this cable type. Finally yet importantly, the suppression characteristic and mechanism of spiral protuberance will be elucidated fully. The mechanism of aerodynamic damping, axial flow and wake flow near the wake of cable will be addressed.
- **Chapter 6:** Major conclusions obtained from the previous chapters are summarized.

Bibliography

1. *https://en.wikipedia.org/wiki/Russky_Bridge*.
2. *http://www.worldrecordacademy.com/biggest/longest_cable-stayed_bridge-the_Sutong_Bridge_sets_world_record_80280.htm*.
3. *http://www.roadtraffic-technology.com/projects/stonecutters/*.
4. *https://en.wikipedia.org/wiki/Edong_Yangtze_River_Bridge*.
5. Wilson, A. *A critical analasis of Tatara bridge, Japan*. in *Bridge Engineering 2 Conference*. 2009. University of Bath, Bath, UK.
6. Hikami, Y. and N. Shiraishi, *Rain–wind induced vibrations of cables in cable-stayed bridges.* Journal of Wind Engineering and Industrial Aerodynamics, 1988. **29**: p. 409-418.
7. Caetano, E.d.S., *Cable Vibrations in Cable-Stayed Bridges (Book)*, ed. I.A.f.B.a.S. Engineering. 2007: IABSE-AIPC-IVBH ETH Honggerberg CH-8093 Zurich, Switzerland
8. Ni, Y.Q., X.Y. Wang, and Z.Q. Chen, Ko, J.M., *Field observations of rain-wind-induced cable vibration in cable-stayed Dongting Lake Bridge.* J. Wind Eng. Ind. Aerodyn., 2007. **95**: p. 303-328.
9. Zuo, D., N.P. Jones, and J.A. Main, *Field observation of vortex and rain-wind-induced stay-cable vibrations in a three-dimensional environment.* J. Wind Eng. Ind. Aerodyn, 2008. **96**: p. 1124–1133.
10. Matsumoto, M., et al., *Dry-galloping characteristics and its mechanism of inclined/yawed cables.* Journal of Wind Engineering and Industrial Aerodynamics, 2010. **98**: p. 317-327.
11. Matsumoto, M., et al. *Field observation system of cable aerodynamics in natural wind*. in *Proceedings of the 4th International Symposium on Cable Dynamics*. 2001. Montreal, Canada.
12. Miyata, T., H. Yamada, and T. Hojo. *Aerodynamic response of PE stay cables with pattern-indented surface*. in *International Conference on Cable-Stayed and Suspension Bridges (AFPC)*. 1994. Deauville, France.
13. Saito, T., M. Matsumoto, and M. Kitazawa. *Rain-wind Excitation of Cables on Cable-stayed Higashi-Kobe Bridge and Cable Vibration Control*. in *Proc. of Cable-stayed and Suspension Bridges*. 1994.
14. Honda, A., et al. *Wind tunnel test on rain-induced vibration of the stay cable*. in *Proceedings of International Symposium on Cable Dynamics*. 1995. Lie`ge, Belgium.

15. Cheng, S., et al., *Experimental study on the wind-induced vibration of a dry inclined cable -Part I: Phenomena.* Journal of Wind Engineering and Industrial Aerodynamics, 2008. **96**: p. 2231-2253.

16. Katsuchi, H. and H. Yamada. *Wind-tunnel Study on Dry-galloping of Indented-surface Stay Cable*. in *11th Americas conference on wind engineering*. 2009. Puerto Rico.

17. J.B. Jakobsen, et al., *Wind-induced response and excitation, characteristic of an inclined cable model in the critical Reynolds number range.* Journal of Wind Engineering and Industrial Aerodynamics, 2012. **110**: p. 100-112.

18. Matsumoto, M. *Review of Bridge Cable Vibrations in Japan*. in *Wind Induced Vibration of Cable Stay Bridges Workshop*. 2006. Kyoto, Japan.

19. Matsumoto, M., M. Kitazawa, and H. Kanaji, *Wind tunnel test for stay cables of Higashi Kobe Ohashi Bridge -part 2 (in Japanese).* Proc. Of 44th Annual Conference of JSCE, 1989 p. 802-803.

20. Flamand, O. *Rain/wind-induced vibration of cables*. in *Proc. of the International Conference on Cable-Stayed and Suspension Bridges (AFPC)*. 1994. Deauville, France.

21. *http://www.netis.mlit.go.jp/NetisRev/Search/NtDetailPreview.asp?REG_NO=KT-140029&pFlg=1*.

22. Hojo, T., S. Yamazaki, and H. Okada, *Development of low drag aerodynamically stable cable with indented processing*. 2000.

23. Larose , G., et al. *Wind-tunnel investigations of an inclined stay cable with a helical fillet*. in *6th European and African Wind Engineering Conference*. 2013.

24. Larose, G. and W. Smitt. *Rain/wind induced vibrations of parallel stay cables*. in *Proc. of the IABSE Conference, Cable-Stayed Bridges-Past, Present and Future*. 1999. Malmo, Sweden.

25. Acampora, A. and C.T. Georgakis. *Recent monitoring of the Oresund Bridge: rain–wind induced cable vibrations*. in *The 13th International Wind Engineering Conference*. 2011. Amsterdam.

26. Yagi, T.O., et al. *Modification of surface configurations of stay cables for drag force reduction and aerodynamic stabilization*. in *The 13th International Conference on Wind Engineering*. 2011. Amsterdam.

Chapter 2: General Background

Wind effect estimation plays an important role in the design of cable-stayed bridges, particularly of stay cables. These stay cables suffer not only direct excitation along the surface but also indirect action on the bridge deck and supports. The study of wind effects is normally conducted by separating the static component, associated with a mean flow velocity of air, and the dynamic component, related with vortex shedding and atmospheric turbulence [1]. The current chapter presents a brief description of wind loads applied to stay cables, concentrating RWIV and DG of bridge stay cables. Since the target of the current study is on the DG and its control method, it is crucial to understand the general mechanism of this phenomenon and state of control methods. Therefore, field observations of RWIV and DG will be reviewed. Subsequently, the literature of DG and its countermeasure will be addressed. The last but not least, the needs for better countermeasure to mitigate both DG and rain wind-induced vibration will be presented and the scope of this thesis will be defined.

2.1 Wind-induced stay cables vibration

Generally, wind-induced cable vibrations can be classified into several types. Apart from the dynamic properties of the cable, excitation of stay cables may be characterized by the amplitude of vibration, the critical wind speed range, the cable orientation, the relative angle between wind direction and cable axis and the rain condition. Several observed phenomena then might be categorized in general manner as: Buffeting due to wind gust, vortex-induced vibration, classical galloping with iced cables, wake galloping, parametric excitation, Reynolds number related drag instability, rain–wind induced vibration, high-

speed vortex excitation and dry galloping [2]. Among these vibration types, vortex induced vibration and buffeting due to wind gust are generally small amplitude while the last three types are mainly related to stay cables with larger amplitude vibration and the rain–wind induced vibration is the one most frequently observed on site of bridge. Furthermore, mechanism of rain–wind vibration has been fully elucidated in recent years, and some effective control methods have been successfully applied in practice. In particular, dry galloping is still less understood and it would require more intensive research. According to the above mention, buffeting due to wind gust, vortex-induced vibration, classical galloping with iced cables, wake galloping, parametric excitation and Reynolds number related drag instability, which have exhibited lower amplitudes of vibration, and thus have a lower degree of importance. Therefore, only RWIV, DG and its control methods will be discussed within the context of current study.

2.1.1 Rain-wind induced vibration

The RWIV of power lines had been reported in literature around 1970s. For stay cable bridges, it was recorded the first time on Koehbrand Bridge in 1974. Then, this kind of vibration was identified again during the construction of Meiko Nishi Bridge [3, 4]. Later, same vibration phenomena were also frequently reported in many cable stay bridges as Table 2-1. It is presently considered that RWIV caused about 95% of the reported vibration problems in cable-stayed bridges [5]. Despite the intense research developed both through wind tunnel tests and through observation of prototypes, the mechanisms of RWIVs are yet to be fully elucidated.

The field observation that prompted the study in RWIV were the strong vibrations exhibited by many cables of the Meiko-Nishi bridge during construction stage, under the interacted of rain and wind at a relatively low wind velocity of 14 m/s (Figure 2-1) [3]. In order to find causes of the vibration and to seek the effective method of prevention, the measurement was carried out for five months. Consequently, Hikami and Shiraishi (1988) found that the occurrences of the cable vibration were accompanied by rain in all the cases. Further, the 10 hours record showed that, although the wind speed and direction were almost the same, the vibrations occurred only during the rainfall (Figure 2-2). Therefore, these distinct behaviors in connection with rain indicate that the vibrations are caused by the combined influences of rain and wind. Finally, the occurrence of cable vibration was limited to the cables that geometrically declined in the direction of the wind.

Table 2.1 Field observations of RWIV

Bridge	Country	Year	Peak to peak Amplitude	Reference
Koehlbrand	Germany	1974	approx. 1m	[6]
Brottonne	France	1977	approx. 0.6m	[7]
Meiko-Nishi	Japan	1984	approx. .55m	[3, 4]
Farø	Denmark	1985	approx. 2m	[8]
Aratsu	Japan	1988	approx. 0.6m	[9, 10]
Ben Ahin	Belgium	1988	approx. 1m	[11]
Erasmus	Netherlands	1996	approx. 1.4m	[12]
Cochrane	Alabama	2002	approx. 1.5m	[13, 14]

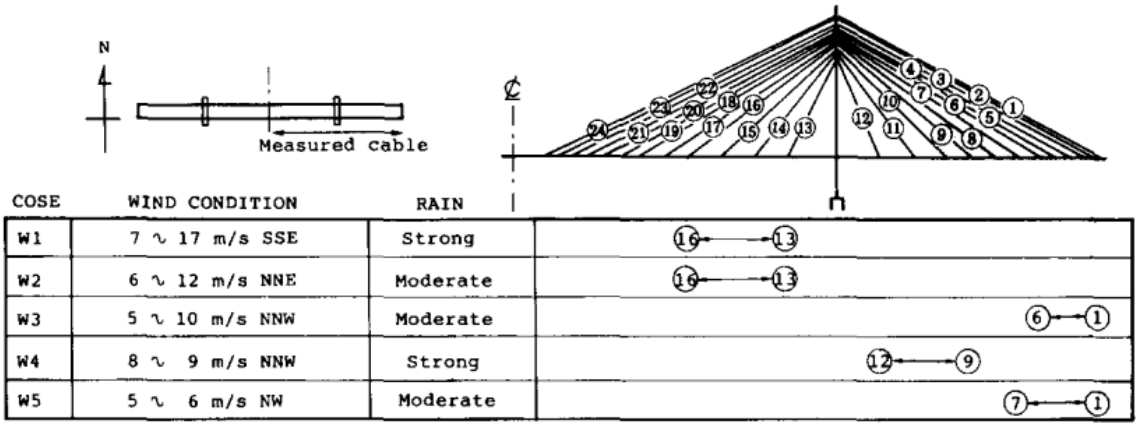

Figure 2-1 Observation at the Meiko-Nishi bridge

Continuously, Hikami and Shiraishi[4] conducted series of wind tunnel test to simulate the generating mechanism of rain-wind induced vibration. In particular, the formation and role of the water rivulet along the cable in excitation mechanism was investigated. Results showed that a second rivulet was formed along the upper windward surface of the cable at an angle θ equal to 45°. The formation of this upper rivulet was associated with wind speed. As the wind speed increased to a certain value, the raindrops would overcome the gravity and friction forces to form the upper rivulet. The relationship between the angle of formation and wind speed is shown in Figure 2-3. The lower rivulet was found to have a stabilizing effect, whereas the upper rivulet would generate aerodynamic force to excite RWIV. Therefore, the RWIV used to be assigned with the effect of upper rivulet.

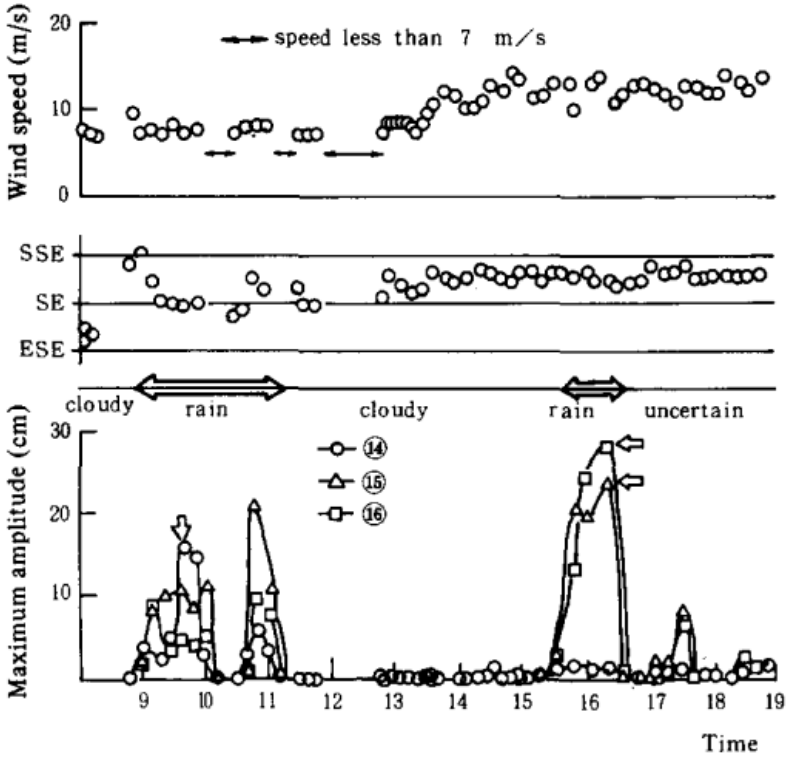

Figure 2-2 Ten hour record of vibration amplitudes and weather conditions

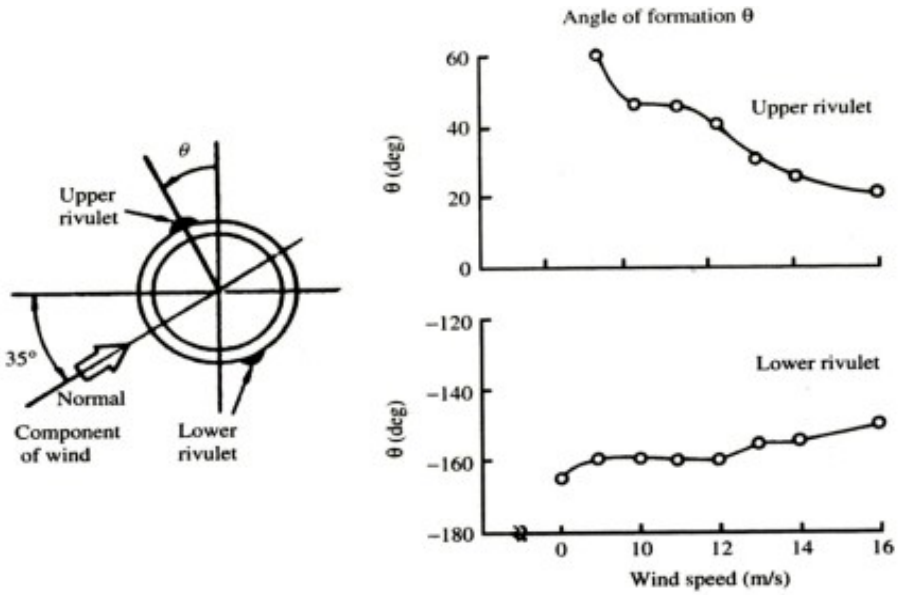

Figure 2-3 Variation of the angle of formation of the water rivulet with wind speed

Despite of the observations from Hikami and Shiraishi were essential to clarify the role of the circumferential oscillation of the rivulets at the cable frequencies, further studies have led to the identification of a little bit different mechanisms of vibration. Venviebe [15] additionally found that almost vertical cables could suffer from RWIVs. He identified three different mechanisms of rain-wind excitation. The first one occurs when the wind is in the direction of the cable. In the other expression, the flow angle is equal to 90°. The second is that wind speed must be great enough to separate the windward rivulet into two symmetric

rivulets in the lateral areas of the cable (As Figure 2-4). Lastly, the rivulet oscillation of with the vibration of the cable promotes a change in cable aerodynamic forces, thereby accelerating the vibration, which are maximum when inclined angle is 30° and wind speed of 25m/s.

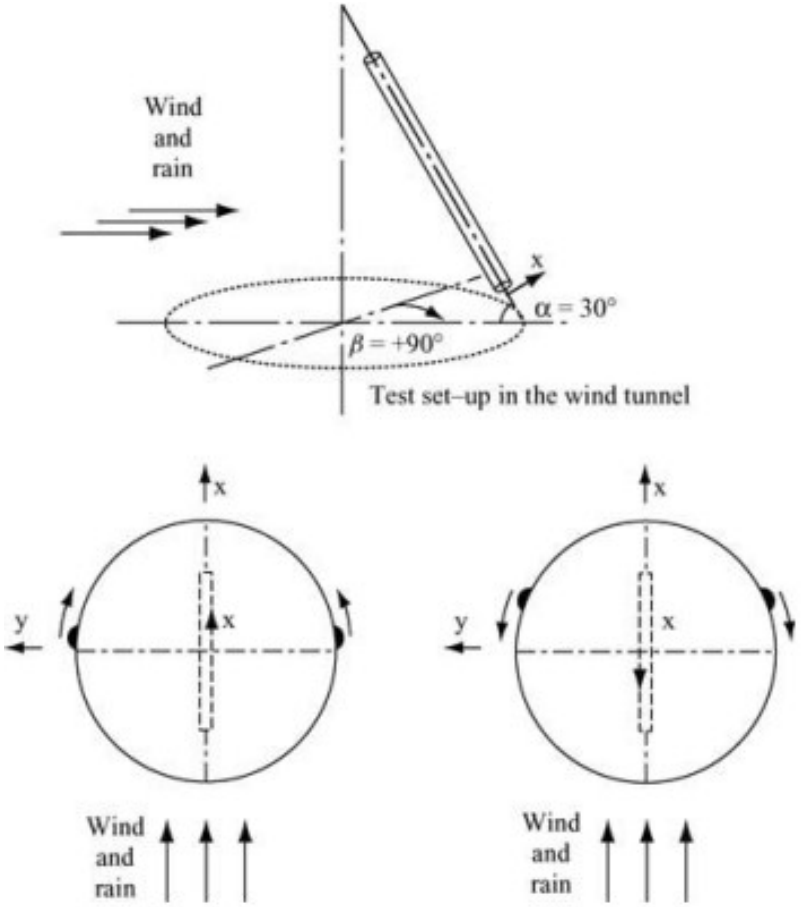

Figure 2-4 Rain-wind exciting mechanism for along-wind vibrations

Several possible mechanisms of RWIV were reported during years of research. Yamaguchi (1990) and Bosdogianni and Olivari (1996) investigated and explained RWIV using galloping theory[16, 17]. Later, Matsumoto et al. (2001) considered rain-wind induced cable vibration as a special vortex-induced vibration caused by the interactions between Karman vortex and axial vortex [18]. Tanaka (2003) outlined some aspects of RWIV as follow [19]: First of all, it is under the interaction of rain and wind at specific attack angles and rainfall intensity, that rivulets form at the upper and lower surfaces of the cable. The formation of rain rivulets as the result of the balance of gravity, aerodynamic force and surface friction forces, leads to a change of symmetry of the cable cross-section, and leading to a difference on aerodynamic forces on the cable. Eventually, a decrease in the drag force coefficient and a negative slope of the lift force coefficient associated with a small variation

of the angle of attack may lead to a negative aerodynamic damping, resulting in a instability of the Den Hartog type galloping. Once the cable starts oscillating, the rivulets tend to oscillate circumferentially with the same frequency. A coupling of this oscillation with the flexural oscillation of the cable may lead to aerodynamic instability, which is likely to intensify the vibrations. Further studies [20, 21] suggested that RWIV was a vortex-induced vibration at high-reduced wind speed caused by the vortex shedding that is different from the classical Karman vortex. Nevertheless, the precise mechanism of RWIV remains unknown owing to the lack of quantitative measurements to quantify the upper rivulet oscillation.

Combining the results of field measure, wind tunnel experiment and theoretical analyze in the past 30 years [12, 15, 22-35], characters of rain-wind induced cable vibration can be described as following:

a) RWIV mostly occurs on bridge located in level terrain or constructed above sea due to the low atmosphere turbulence identity in those places. It rarely happen when inflow turbulence identify is relatively high.

b) RWIV mainly emerge on cables with smooth surface, 80~200mm diameter (or 140~225mm diameter presented by some researchers), and 6×10^4-2×10^5 of Reynolds number. Larger and smaller diameter cables scarcely confront the process.

c) RWIV usually appear at 1st -3rd modes, but the fourth order mode vibration was also reported. When fundamental frequency of cable stay is higher than 3Hz, RWIV is hard to happen or amplitude is relatively small.

d) As inclination angle of stay cables (α) is among 20°-50°, possibility of rain- wind induced vibration is increased considerably.

e) As cable stay plane and inflow included flow angle (β) is among 20°-60°, possibility of RWIV is great.

f) Cables in tower leeward side (cables down-dip along average wind direction or project of up waterway along average wind direction is positive) are easy to vibrate. The phenomenon that one cable plane vibrate while the other do not do appear usually.

g) RWIV starting wind velocity is arranged between 6.0 and 18.0m/s, and reduced wind speed is 20-90 respectively. Cables scarcely confront the process under large and less wind velocity.

h) Precipitation affects RWIV to some extent. Vibration of cables with different space shapes, diameters, surface types also have various rain precipitation conditions.

i) Upper rivulet oscillates circumferentially along cable stay surface during RWIV cable vibration. It can be concluded that form of upper rivulet is the necessary condition of RWIV to some degree. Nevertheless, there are reports about RWIV without upper rivulet or rain precipitation.

j) Rain-wind vibration is hard to appear when cable stay damping ratio bigger than 0.5%.

k) RWIV is a kind of vibration in plane principally. Nevertheless, it is also accompanied with vibration out of plane, which made the oscillation trace as ellipse shape.

l) Although mechanism about RWIV is not recognized unitized at present, certain measures have been taken to depress the vibration, main aspects of which are adapting damper or changing cable surface status.

In summary, RWIV is a violent vibration of cables in certain space shape induced by integrated function of wind and rain under certain wind velocity range. It is one of the most violent oscillation forms of cable stay known now.

2.1.2 Dry galloping (DG)

DG of stay cables is a relatively new term and its concept has become clearer only recently. It was pointed out that stay cables could be excited even though in the condition without rain, which is called DG. In general definition, DG is classified as one of the wind-induced large amplitude vibration phenomena in dry weather (no rain condition), usually occurs at relatively high-reduced wind speed, it also showed some characteristics of limited amplitude vibration, however. Though there are reported field observations of large amplitude violent cable motions [32, 36], no site measurements were conducted for further clarification of possible cause. Recently, some studies showed the existence of this phenomenon by wind tunnel test and the field observation. Nevertheless, its characteristics do not fully understand, as well as control methods for DG are unknown. DG of inclined cable was observed in wind tunnel tests by Saito et al [23], Honda et al. [24] and Matsumoto et al.[36] in the subcritical Reynolds number regime, and Miyata et al.[37], Cheng et al. and Jackobsen et al. [38-40] in the transition and critical Reynolds number regime. Therefore, the possibility of its occurrence on real bridges should be regarded.

Generally, DG can be classified two types of cable vibration. The first one is limited amplitude vibration (restricted response), which considered as restricted amplitude. The other is divergent type galloping which is violent oscillation of cable. The divergent type

galloping is associated with the occurrence of negative aerodynamic damping, which, when large enough to overcome the positive structural damping, will result in negative effective damping of the cable. The response amplitude of the oscillating cable will thus increase strongly, leading to a divergent type motion. Hence, assessing aerodynamic damping of a stay cable could be an effective way of studying the mechanisms of DG. The conventional way is to apply the classical Den Hartog criterion to derive aerodynamic damping of a vibration cable under wind attack [41]. Macdonald and Larose (2006) extended the classical Den Hartog approach and rendered it applicable to a cylindrical body with an arbitrary cross-sectional shape vibrating along any arbitrary direction normal to its axis [42]. Later, a two-degree-of freedom model was then proposed by Macdonald and Larose (2008a & 2008b) to better simulate this phenomenon [43, 44].

In parallel, Nakamura et al. [45] indicated that the galloping generation mechanism is interruption of communication between upper and lower separation flows. Because communication of two separated flows can tend to make pressure on upper and lower surfaces of cable become no difference. Matsumoto et al. [36] shed light on the role of axial flow for galloping instability by conducting wind tunnel test with and without artificial axial flow along the wake of cable (Figure 2-5). The test results indicated clearly that the axial flow in near wake could excite galloping. Before of that, Matsumoto at el also had pointed out that the axial flow also was visualized in the real bridge by using the light strings for the proto-type stayed cable with wind angle around 40º-50º[46]. However, the axial flow mechanisms still less understood.

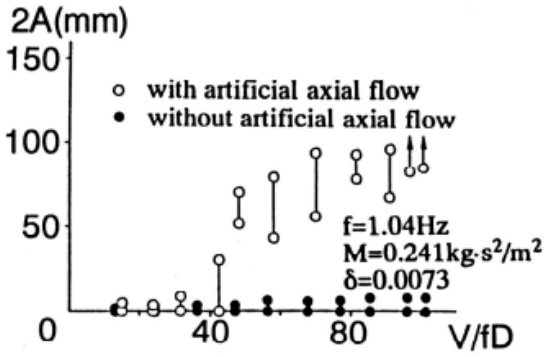

Figure 2-5 Galloping appearance with/without artificial axial flow

Furthermore, Matsumoto (2010) explained the differences between the Saito criterion and FHWA criterion in Scruton number dependence by classifying galloping into divergent galloping and unsteady galloping with limited amplitude. In Scruton number and reduced wind speed diagram, it is found that FHWA criterion and Saito criterion correspond steady

galloping and unsteady galloping, respectively, which can be seen in Figure 2-6. Nevertheless, further confirmation should be carried out. In the experiments of Cheng et al.[38], both divergent type of motion and limited-amplitude vibration at high-reduced wind speed were also recorded. However, the characteristics and excitation conditions of these two phenomena are separately different. The former has similar response as galloping while the latter occurs only in limited range of reduced wind speed and they have different restricted amplitude. Apart from that, Katsuchi and Yamada [47] conducted wind tunnel test for comparing the characteristics of dry-galloping between normal and indented cable surface. They figured out that DG occurred in both cases of the indented and normal cable models with the wind angle of 30 degrees. According to Figure 2-7, the indented cable surface could not mitigate the DG effectively. Their test results showed that root mean square value of fluctuating surface pressure became large at the leeward surface and upstream position of the cable model. Finally yet importantly, the onset reduced wind speed of DG was in between 90 and 110 respectively.

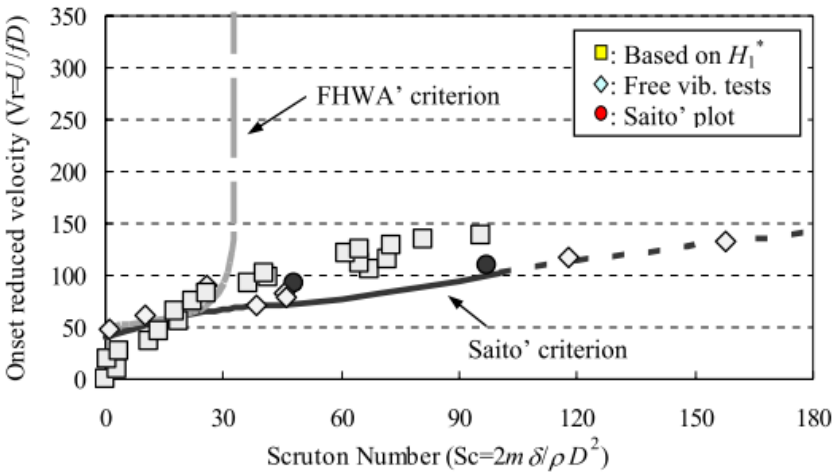

Figure 2-6 Field observation data at prototype

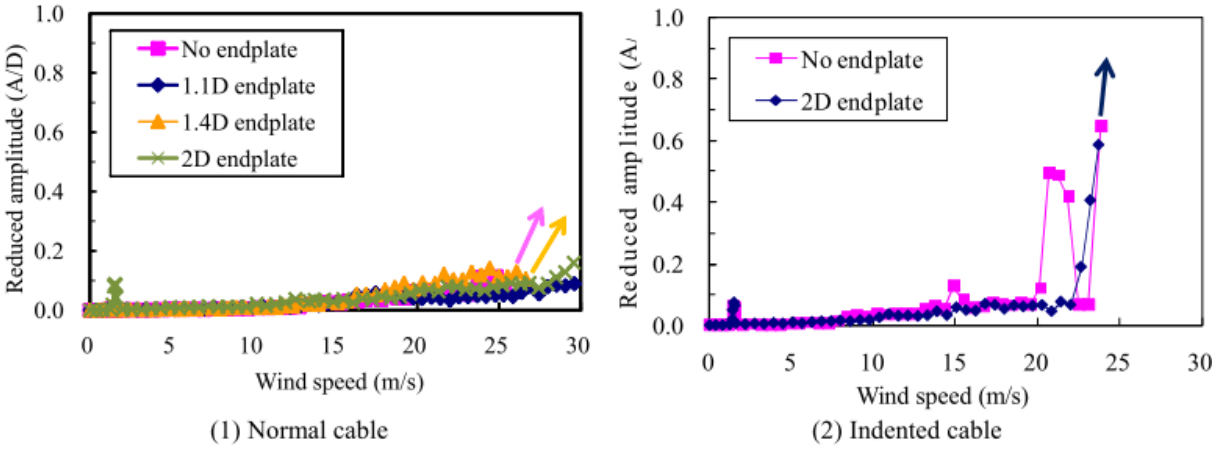

Figure 2-7 Wind-induced vibration amplitude with different endplate conditions

Jakobsen et al. (2012) concluded that the most violent dry galloping were observed at 60^0 of inclination with damping ratios below 0.2% and significant "lock-in'' between the lift force and the large sway cable response was identified[39]. However, Nikitas and Macdonald (2015) concluded that the effect of transitional behavior is central for dry galloping. The inherent flow pattern unsteadiness in the critical Re range and its interaction with wind turbulence and inclined angle are significant in forming the DG conditions. Something similar was also found for wake-induced vibrations, where quasi-steady features have to combine with unsteadiness to yield excessive unconventional dynamic response. Abrupt transitions, varying time delays between load and motion, and a stiffness-like wind force component are other characteristics in common between that cases and the current one [40].

Many researchers have attempted wind tunnel investigation on DG since then and extensive outcomes have been made available. Some general characteristics of DG can be described as below:

a. Cable DG does exist as a highly possible instability, which can damage cable stay itself as well as cable attachments.
b. When DG occurs, cable can oscillate with divergent vibration or restricted amplitude vibration.
c. It is a unique aerodynamic phenomenon for a cable, which is yawed/ inclined against wind.
d. Instability takes place in the subcritical and critical Reynolds number range. Further, mechanism of DG seems to be relates to existence of axial flow and wake flow field.
e. There are a few specific orientations where the cable could become instability.

In the existing studies, characteristics of cable DG have been elucidated to some extent and many approaches have been applied to study on this problem. However, there are still a little bit conflict between those conclusions about the mechanism of dry galloping. In addition, the flow field around cable for dry galloping still suspected and unclear. Therefore, to fulfill the literature for dry galloping, further investigation should be carried out.

2.2 Cable vibration control methods

To control stay cable vibration induced by various factors, especially rain-win induced vibration, many control methods have been developed with different levels of efficiency. Those methods can simply be categorized in two groups. The first is aerodynamic control methods, which related to modification the aerodynamic characteristic of stay cable. On other hand, the second group is mechanical control methods, which typically install the external dampers or use crosstie system. Consequently, the damping of cable will be enhanced or natural frequency be decreased and thus mitigate the vibration of cable. In this section, these countermeasures will be addressed and revised.

2.2.1 Mechanical control methods

The mechanical control of vibration is achieved by installing damping devices at specific positions along cables. Mechanical control is the most popularly used mitigation method on bridge site to control cable vibration. Crossties and external dampers are commonly used for this purpose.

2.2.1.1 Crossties system

To increase the in-plane stiffness and its natural frequency, stay cables can be connected together with a set of additional auxiliary wire, named as crossties-system. From a dynamic perspective, the properties of the single cables are modified by the presence of the lateral constraints that influence their oscillation characteristics. Figure 2-8 shows an example of cable crosstie systems applied to a bridge.

Figure 2-8 Auxiliary wire system of the Yobuko Bridge [2]

This countermeasure has been applied for many cable-stayed Bridges such as Normandy Bridge in France, the Second Severn Bridge in the United Kingdom, the Helgeland Bridge in Norway, and the Meiko Nishi Bridge and Yobuko Bridge in Japan [48]. By the addition of crosstie system, two or more stay cables are interconnected. Therefore, the in-plane stiffness (natural frequencies) can be enhanced. This could effectively suppress stay cables vibration in low frequencies. Nevertheless, the drawback of crossties system is that it is still defective in controlling out-of-plane vibration. This further suggests the significant of using external dampers in coordination with these systems. To apply the crosstie system, it should not consider only on structural performance considerations but also on cost estimation due to design work, installation and periodic maintenance. In this manner, the preferred countermeasure should be suggested perhaps through a more extended optimization technique.

2.2.1.2 External dampers

The other way to prevent cable vibration is by adding external dampers, which can be active damper, semi-active damper and passive damper. Active damper control requires the input of external power, so it is not frequently used in mitigating cable vibration. On the other hand, semi-active dampers are becoming more popular in recent years. Magneto rheological damper (MR damper) is the most common type of semi-active control device in the site of bridges. MR damper is short for magneto-rheological damper. It filled with magneto-rheological fluid, which could change its damper size by varying magnetic field. However, MR damper is always requires an external power source. MR damper installs on a cable-stayed bridge as Figure 2-9. The main drawback of MR damper is that this method requires high sophisticated technique in fabricating and designing.

Figure 2-9 MR damper installed on cable-stayed bridges [49]

At present, majority of the external dampers are applying on bridge site belong to passive damper. It has variety of types such as high-damping rubber (HDR), friction damper and oil damper. The first is high-damping rubber damper, which consists of several rubber pads, which have high damping. Recently much attention has been paid to high-damping rubber material because of its potential in the vibration control of a structural response. The cable vibration energy is absorbed by shear deformation of the rubber pads. HDR damper is normally installed inside the cable casing between the cable and the steel tube near the bridge deck anchorage. It retains aesthetic appearance of the bridge since the size this rubber damper is small. Figure 2-10 shows a rubber damper installed on the Tatara Bridge in Japan [2]. However, this kind of countermeasure could not control totally the large amplitude vibration such as rain wind induced vibration, dry galloping or parametric vibration. Therefore, it frequently applies for stay cable bridges that have short to medium span.

The second is friction damper, which consists of two parts (Figure 2-11). There are steel wings in a plane normal to the cable and attached on the cable by a collar. Pressed on them are the spring blades, which are rigidly fixed on the bridge deck. As a result, when the steel wings move with the cable, they will dissipate energy by frictional contact with the spring blade [2]. Friction damper was invented to increase the damping of cable-damper system in a simple and cost-effective way [50]. However, it is hard to obtain the high efficiency in mitigating different vibration types that have different vibration amplitude.

The last one is oil damper, which have simple mechanism. Oil damper consists of a cylindrical container filled with viscous oil, and a piston, which can move through the oil. Oil provides viscous resistance while piston moves in the damper cylinder. The resistance force is the damping force. Oil dampers have many advantages such as wide range of damping capacity, technology maturity, low cost and so on. Its application on cable-stayed bridges is common. Since oil damper can only provide axial damping force along its cylindrical direction, in order to control both in-plane and out-of-plane cable vibration, two oil dampers are required to be installed on one cable at certain inclination angle. The main disadvantage of this control method is that the liquid viscosity depends on temperature and natural frequency of cable and lead to change the damping coefficient. Figure 2-12 shows such an oil damper installation scheme on the second Aratsu Bridge in Japan.

Figure 2-10 HDR damper installed on Tatara bridge and Shonan Ginza Bridge

Figure 2-11 Friction damper installed on Uddevalla Bridge

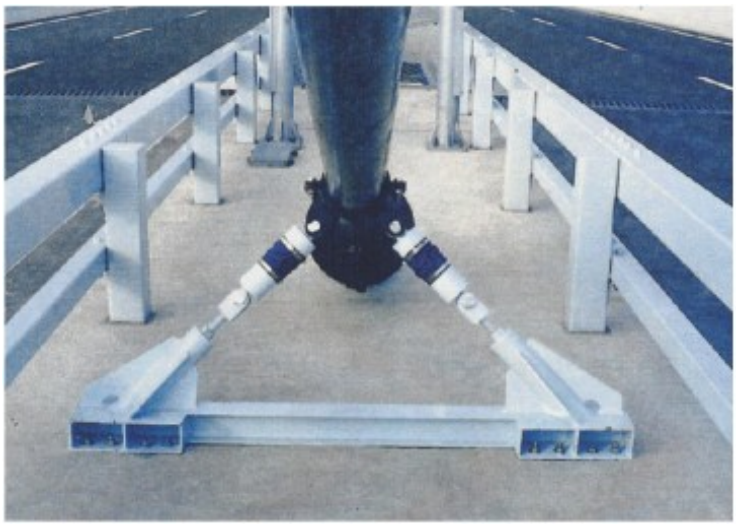

Figure 2-12 Oil dampers on the Aratsu Bridge [2]

2.2.2 Aerodynamic control

Aerodynamic control is a passive control method that modifies aerodynamic feature of the cable cross-section. It is most effective in controlling rain-wind-induced cable vibration by preventing accumulation of rain to form water stream on the surface of cable. In the past, some types of cable surface modification had been proposed to suppress RWIV. There popular type was applied are spiral protuberance, indented surface and parallel protuberance cable.

2.2.2.1 Spiral fillet (spiral protuberances)

Spiral fillet works on the principle of disrupting the coherence of vortex formation, helps avoiding the rain induced vibrations by destruction the generation of upper rain rivulets and they also introduce a three-dimensional disturbance in the flow, which can help suppressing vortex induced vibrations [51]. Flamand [22] used helical fillets of 1.5 mm on the cable surface of Normandy Bridge and this countermeasure was proven effectively for mitigation rain wind vibration. However, the drag force was still high as Figure 2-13. Additionally, Ming Gu and Xiaoqin Du [30] clarified the effect of spiral wire to suppress the vibration of cable in some extend (Figure 2-14). They concluded that only proper spacing of the helical fillet could destroy suppress rain–wind-induced vibration of cables. Further, the spiral wire twined on the surface of the cable is effective in mitigating the rain–wind-induced vibration through carefully selecting the diameter, pitch and twine direction of the spiral wire. However, they did not conclude the general guidelines as well as the optimum parameters for application.

Apart from that, Phelan et al.(2006) showed some test cases about this kind of countermeasure to suppress rain-wind-induced vibration[31]. Recently, K. Kleissl et al. [52] presented the smoke visualizations of the near-wake flow structures of the cable for 45^{o} relative wind angle. In this experiment, a channel of axial flow was observed clearly along the leeward side of plain cable case (normal surface). Nevertheless, this type of flow was found to be nearly suppressed in the wind tunnel test with the helical fillets at low wind speed (Figure 2-15). These test findings affirmed that helical fillet could eliminate the axial that is one of mechanism of DG. Nevertheless, it should pay attention that these wind tunnel tests were conducted under static condition and very low wind speed. Until now, the control methods for eliminating DG are under developing.

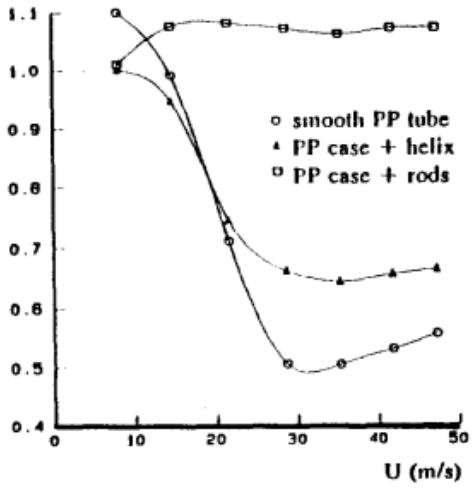

Figure 2-13 Drag coefficient of different surface modification

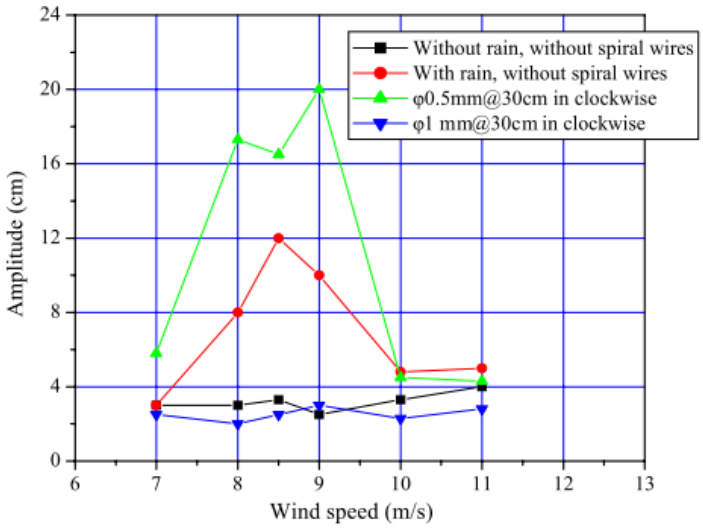

Figure 2-14 Effect of pitch of spiral wires on mitigation efficiency

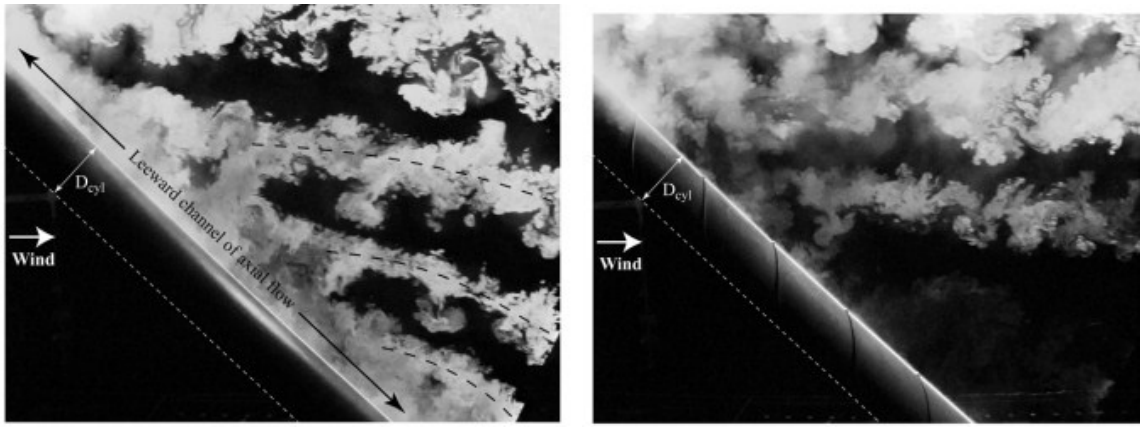

Figure 2-15 Axial flow near wake of plain cable and helically filleted

2.2.2.2 Parallel protuberances

The use of parallel protuberance was developed in Japan for Higashi-Kobe Bridge. The idea was to have these deep parallel protuberances along the cable, which would drive the water down without allowing any transverse movements[53]. The cable cross section can be seen as Figure 2-16. In a preliminary investigation, cable with parallel, spiral, wave, and other forms were examined. Consequently, parallel protuberance cable were found as the most effective solution in restraining RWIV [54]. However, it was reported on site that this kind of cable still exhibited large vibration to some extent as Figure 2-17[55]. In addition, the drag force for this type of cable was still high around 1.2 of drag force coefficient.

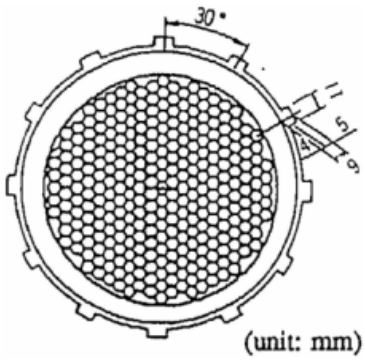

Figure 2-16 Cross section of the cable used for the Higashi-Kobe Bridge

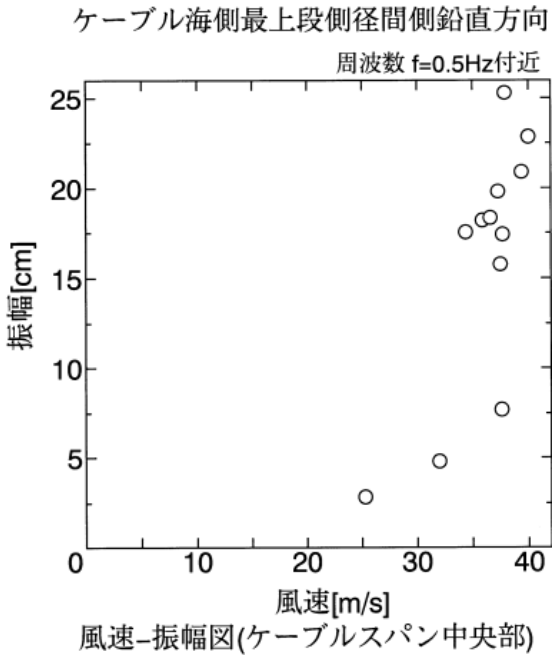

Figure 2-17 Vertical vibration of top cable of East Kobe cable-stayed Bridge

2.2.2.3 Indented surface cable

For controlling RWIV, indented surface (dimple) was firstly developed by Miyata et al. in 1994 [37]. This type of cable was applied firstly in Tatara Stayed Cable Bridge in Japan, which is the longest stay cable at completion time. The indents was formed after the cable was coated with the extruded polyethylene as the Figure 2-18. This control method was effective in suppressing rain wind with low drag force coefficient as smooth surface. The detail responses of indented cable under rain condition and different frequencies can be seen as Figure 2-19. Generally, rain wind induced vibration was suppressed by this countermeasure. Moreover, its effectiveness in real scale confirmed as no rain wind induced vibration occurred after opening about one year [56].Nevertheless, this control method still exhibited the large amplitude vibration in the original stage. Indented cable with Scruton number around 21, started vibrating with large amplitude from 10m/s of wind speed and became divergent around 30m/s of wind speed (Figure 2-20) [56]. In addition, it was reported by Katsuchi and Yamada recently that DG could occur for an indented cable in low Scruton number. [47]. According to Figure 2-21 and Figure 2-22, indented stay cable galloped divergently at around 23m/s and it was not so sensitive to the Scruton number change. Furthermore, the health monitoring of Tatara stay cable bridge recently revealed that indented surface exhibited limited vibration[57]. However, the amplitude is still in allowable range.

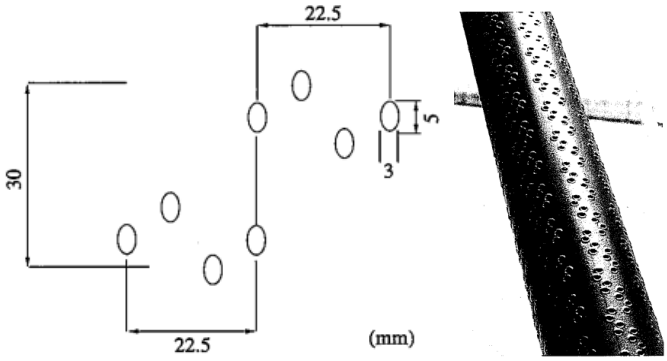

Figure 2-18 Indent pattern and indented cable of Tatara Bridge [56]

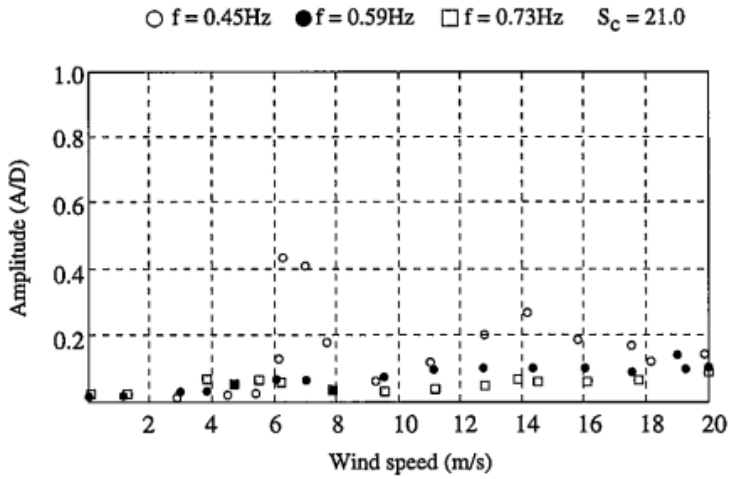

Figure 2-19 Responses of indented cable under rain condition

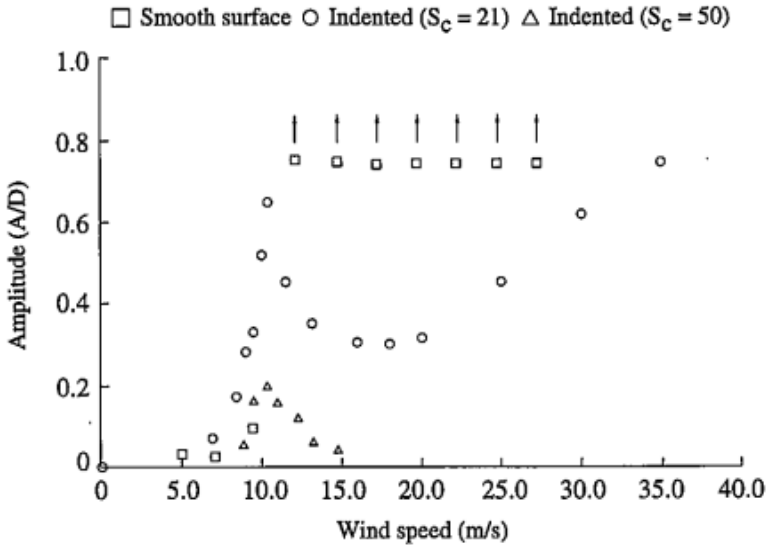

Figure 2-20 Vibration of indented surface under no precipitation

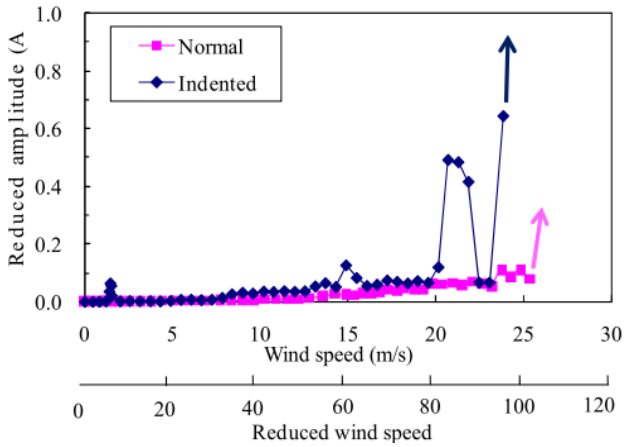

Figure 2-21 Wind-induced vibration amplitude of normal and indented cable model (No endplate, wind angle of 30 degrees, Sc = 17.9 for normal and 19.7 for indented)

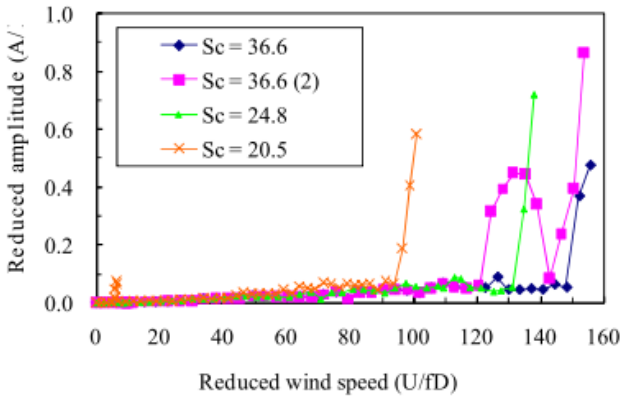

(2) Reduced amplitude and reduced wind speed

Figure 2-22 Wind-induced vibration amplitude versus Scruton number (Indented cable, no endplate and wind angle of 30 degrees)

2.3 Summary of chapter 2

Rain wind induced vibration has been investigated fully and many control methods has been applied widely. Nevertheless, each method is still defective in controlling DG and need to be improved. On the other scenario, the occurrence of dry galloping of stay cable has confirmed by several field observations and many wind tunnel tests. However, its characteristics are still debating and its mitigation countermeasure has not proposed yet. In addition, the generation mechanism of DG is lack of understanding. To conservative the safety of stay cables and their attachment under attack of wind or rain wind interaction, it is imperative to propose a new cable surface treatment, which can suppress both dry galloping and rain-wind induced vibration.

Bibliography

1. Caetano, E.d.S., *Cable Vibrations in Cable-Stayed Bridges (Book)*, ed. I.A.f.B.a.S. Engineering. 2007: IABSE-AIPC-IVBH ETH Honggerberg CH-8093 Zurich, Switzerland

2. Fujino Y., Kimura K., and Tanaka H., *Wind Resistant Design of Bridges in Japan: Developments and Practices (Book)*. 2012: Springer.

3. Hikami, Y., *Rain Vibrations of Cables of a Cable-Stayed Bridge.* Journal of Wind Engineering (Japan) 1986 **27 (In Japanese)** p. 17-28.

4. Hikami, Y. and N. Shiraishi, *Rain–wind induced vibrations of cables in cable-stayed bridges.* Journal of Wind Engineering and Industrial Aerodynamics, 1988. **29**: p. 409-418.

5. Wagner, P. and J.-P. Fuzier. *Health Monitoring of Structures with Cables-Which Solutions. Dissemination of the Results of the IMAC European Project"* in *Fifth International Symposium on Cable Dynamics, "Tutorial on Health Monitoring of Structures with Cables"*. 2003. Santa Margherita Ligure, Italy.

6. Ruscheweyh H. and Hirsch G., *Vibration measurements at the cable stayed Koehlbrand Bridge in Hamburg (in German)*, in *Technical Report*. 1974, Institute for Lightweight Structures, University of Aachen (RWTH).

7. Wianecki, J. *Cables wind excited vibrations of cable-stayed bridges*. in *Proceedings of the 5th ICWE*. 1979. Fort Collins, Colorado.

8. Langsø, H. and O. Larsen. *Generating mechanisms for cable-stay oscillations at the Farø Bridge*. in *The international conference on cable-stayed bridges*. 1987. Bangkok, Thailand.

9. Yoshimura, T., et al. *A study on the aerodynamic stability of the Aratsu Bridge*. in *The Japan-Canada workshop on bridge aerodynamics*. 1989. Ottawa, Canada.

10. Yoshimura, T., M. Savage, and H. Tanaka. *Wind induced vibrations of bridge stay-cables*. in *The 1st ISCD*. 1995. Lie`ge.

11. Lilien, J. and A. Pinto, *Vibration amplitudes caused by parametric excitation of cable stayer structures.* Journal Sound and Vibration 1994. **174**(1): p. 69-90.

12. Geurts, C., et al., *Numerical modelling of rain–wind-induced vibration: Erasmus bridge, Rotterdam.* Struct Eng Int, 1998. **8**(2): p. 129-135.

13. Irwin, P. *Field monitoring of cable supported bridges*. in *The 6th ISCD*. 2005. Charleston, South Carolina.

14. Irwin, P., Nedim A., and T. N. *Wind induced stay cable vibrations – A case study*. in *The 3rd ISCD*. 1999. Trondheim.

15. Venviebe, C. *Rain-Wind-Induced Vibrations of Cables and Bars* in *Larsen, A. and Esdahl, S. (eds), "Bridge Aerodynamics"*. 1998. Balkema.

16. Yamaguchi, H., *Analytical study on growth mechanism of rain vibration of cables.* J. Wind Eng. Ind. Aerodyn., 1990. **33**(1-2): p. 73-80.

17. Bosdogianni, A. and D. Olivari, *Wind- and rain-induced oscillations of cables of stayed bridges.* J. Wind Eng. Ind. Aerodyn., 1996. **64**(2 - 3): p. 171 - 185.

18. Matsumoto, M., et al., *Vortex-induced cable vibration of cable-stayed bridges at high reduced wind velocity.* J. Wind Eng. Ind. Aerodyn., 2001. **89**(7-8): p. 633-647.

19. Tanaka, H. *Aerodynamics of Cables*. in *Fifth International Symposium on Cable Dynamics*. 2003. Santa Margherita Ligure, Italy.

20. Matsumoto, M., et al., *Rain-wind-induced vibration of inclined cables at limited high reduced wind velocity region.* J. Wind Eng. Ind. Aerodyn., 2003b. **91**(1-2): p. 1-12.

21. Zuo, D. and J.P. Jones, *Interpretation of fi eld observations of wind- and rain-wind-induced stay cable vibrations.* . J. Wind Eng. Ind. Aerodyn. , 2010. **98**(2): p. 73-87.

22. Flamand, O. *Rain/wind-induced vibration of cables*. in *Proc. of the International Conference on Cable-Stayed and Suspension Bridges (AFPC)*. 1994. Deauville, France.

23. Saito, T., M. Matsumoto, and M. Kitazawa. *Rain-wind Excitation of Cables on Cable-stayed Higashi-Kobe Bridge and Cable Vibration Control*. in *Proc. of Cable-stayed and Suspension Bridges*. 1994.

24. Honda, A., et al. *Wind tunnel test on rain-induced vibration of the stay cable*. in *Proceedings of International Symposium on Cable Dynamics*. 1995. Lie`ge, Belgium.

25. Matsumoto, M. *Observed behaviour of prototype cable vibration and its generation mechanism*. in *Bridge Aerodynamics*. 1998. Balkema, Rotterdam.

26. Larose, G. and W. Smitt. *Rain/wind induced vibrations of parallel stay cables*. in *Proc. of the IABSE Conference, Cable-Stayed Bridges-Past, Present and Future*. 1999. Malmo, Sweden.

27. Main, J. and N. Jones. *Full-scale measurements of stay cable vibration*. in *The 10th International Conference on Wind Engineering*. 1999. Copenhagen, Denmark.

28. Main, J., N. Jones, and H. Yamaguchi. *Characterization of rain-wind induced stay-cable vibrations from full-scale measurements,* . in *4th International Symposium on Cable Aerodynamics*. 2001. Montreal, Canada.

29. Matsumoto, M., et al. *Field observation system of cable aerodynamics in natural wind*. in *Proceedings of the 4th International Symposium on Cable Dynamics*. 2001. Montreal, Canada.

30. Gu, M. and X. Du, *Experimental investigation of rain-wind- induced vibration of cables in cable-stayed bridges and its mitigation.* Journal of Wind Engineering and Industrial Aerodynamics, 2005. **93**: p. 79-95.

31. Phelan, R., P. Sarkar, and K. Mehta, *Full-Scale Measurements to Investigate Rain-Wind Induced Cable-Stay Vibration and Its Mitigation.* Journal of Bridge Engineering, 2006. **11**(3): p. 293- 304.

32. Ni, Y.Q., X.Y. Wang, and Z.Q. Chen, Ko, J.M., *Field observations of rain-wind-induced cable vibration in cable-stayed Dongting Lake Bridge.* J. Wind Eng. Ind. Aerodyn., 2007. **95**: p. 303-328.

33. Cheng, S., et al., *Experimental study on the wind-induced vibration of a dry inclined cable -Part I: Phenomena.* Journal of Wind Engineering and Industrial Aerodynamics, 2008. **96**: p. 2231-2253.

34. Zuo, D., N.P. Jones, and J.A. Main, *Field observation of vortex and rain-wind-induced stay-cable vibrations in a three-dimensional environment.* J. Wind Eng. Ind. Aerodyn, 2008. **96**: p. 1124–1133.

35. Wen-Li, C., et al., *In fluence of Dynamic Properties and Position of Rivulet on Rain – Wind-Induced Vibration of Stay Cables.* Journal of Bridge Engineering, 2013. **18**(10): p. 1021-1031.

36. Matsumoto, M., et al., *Dry-galloping characteristics and its mechanism of inclined/yawed cables.* Journal of Wind Engineering and Industrial Aerodynamics, 2010. **98**: p. 317-327.

37. Miyata, T., H. Yamada, and T. Hojo. *Aerodynamic response of PE stay cables with pattern-indented surface*. in *International Conference on Cable-Stayed and Suspension Bridges (AFPC)*. 1994. Deauville, France.

38. Cheng, S., et al. *Aerodynamic instability of inclined cables*. in *The 5th ISCD*. 2003. Santa Margherita.

39. J.B. Jakobsen, et al., *Wind-induced response and excitation, characteristic of an inclined cable model in the critical Reynolds number range.* Journal of Wind Engineering and Industrial Aerodynamics, 2012. **110**: p. 100-112.

40. Nikitas, N. and J.H.G. Macdonald, *Aerodynamic forcing characteristics of dry cable galloping at critical Reynolds numbers.* European Journal of Mechanics B/Fluids, 2015. **49**: p. 243-249.

41. Den Hartog, J.P., *Mechanical Vibrations, 4th ed.* 1956: McGraw-Hill, New York.

42. Macdonald, J. and G. Larose, *A unified approach to aerodynamic damping and drag/lift instabilities, and its application to dry inclined cable galloping.* J. Fluids Struct., 2006. **22**: p. 229-252.

43. Macdonald, J. and G. Larose, *Two-degree-of-freedom inclined cable galloping-Part 1: General formulation and solution for perfectly tuned system.* J. Wind Eng. Ind. Aerodyn., 2008a. **96**: p. 291-307.

44. Macdonald, J. and G. Larose, *Two-degree-of-freedom inclined cable galloping-Part 2: Analysis and prevention for arbitrary frequency ratio.* J. Wind Eng. Ind. Aerodyn., 2008b. . **96**: p. 308-326.

45. Nakamura, Y., K. Hirata, and T. Urabe, *Galloping of rectangular cylinders in the presence of a splitter plate.* Journal of Fluids and Structures, 1991. **5**: p. 521-549.

46. Matsumoto, M., et al. *Aerodynamic Behavior of Inclined Circular Cylinders Cable Aerodynamics*. in *International Colloquium on Bluff Bodies Aerodynamics and Applications*. 1990.

47. Katsuchi, H. and H. Yamada. *Wind-tunnel Study on Dry-galloping of Indented-surface Stay Cable*. in *11th Americas conference on wind engineering*. 2009. Puerto Rico.

48. Kumarasena, S., et al., *Wind Induced Vibration of Stay Cables*, in *Report No. FHWA-HRT-05-083*. 2007, Federal Highway Administration: McLean, Virginia.

49. Söhne, M., *MAURER Stay Cable Dampers*. Maurer Söhne Frankfurter Ring 193, D-80807 München.

50. Lopez, I., J.M. Busturia, and H. Nijmeijer, *Energy dissipation of a friction damper.* Journal of Sound and Vibration, 2004: p. 539-561

51. Wong. H. Y. *An aerodynamic means of suppressing vortex excited oscillation. Part 2* in *Proc. Inst. Ar. Eng.* 1977.

52. K. Kleissl and C.T. Georgakis, *Comparison of the aerodynamics of bridge cables with helical fillets and a pattern-indented surface.* Journal of Wind Engineering and Industrial Aerodynamics, 2012. **104-106**: p. 166-175.

53. Matsumoto, M., M. Kitazawa, and H. Kanaji, *Wind tunnel test for stay cables of Higashi Kobe Ohashi Bridge -part 2 (in Japanese).* Proc. Of 44th Annual Conference of JSCE, 1989 p. 802-803.

54. Saito, T., M. Matsumoto, and M. Kitazawa. *Rain-wind excitation of cables on cable-stayed Higashi-Kobe bridge and cable vibration control*. in *The International Conference on Cable-Stayed and Suspension Bridges*. 1994. Deauville.

55. Matsumoto, M. *Review of Bridge Cable Vibrations in Japan*. in *Wind Induced Vibration of Cable Stay Bridges Workshop*. 2006. Kyoto, Japan.

56. Hojo, T., S. Yamazaki, and H. Okada, *Development of low drag aerodynamically stable cable with indented processing*. 2000.

57. Kusuhara, S., *Vibration and countermeasures for cable structure of Honshu-Shikoku bridges.* ISFA 2016, 2016. **1**: p. CD Room.

Chapter 3: Wind Tunnel Test for Cable

Wind tunnel test (WTT) will be used as a main tool to investigate the wind-induced cable galloping characteristics and to develop its countermeasures. In this chapter, the detail of wind tunnel facilities as well as the wind tunnel test parameters will be illustrated. In addition, the fabrication works for different cable surface modifications as well as the validation of section model will be addressed. Besides that, various wind parameters and experimental procedure will be introduced. In last section of this chapter, rain-wind induced cable vibration will be confirmed and discussed.

3.1 Wind tunnel

3.1.1 Introduction

The wind tunnel is an opened circuit wind tunnel at Yokohama National University, Japan. The wind tunnel is mainly used to perform experiments in uniform flow at high flow velocity of up to 20 m/s. The size of the working section is 1.3m wide and 1.3m high. In this study, a cable model was supported by single degree of freedom (1-DOF) spring system in vertical plane and small wire system was used in horizontal plane in order to keep cable model unmoved laterally. Referring to previous study that the responses of 1DOF and 2DOF system was not so different [1], Cable's position can be changed by flow angle and inclined angle as shown in Figure 3-1.

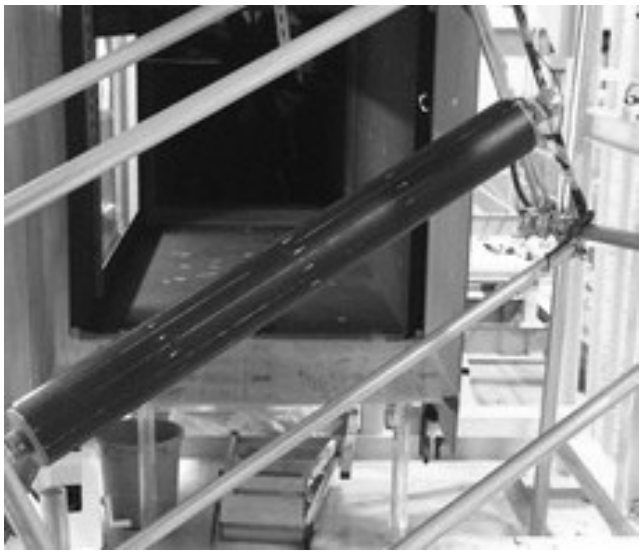

Figure 3-1 Cable model suspension frame

3.1.2 Flow profile

To confirm the uniformity of the flow field, turbulence intensity of flow inside wind tunnel was examined. The flow conditions were measured at cable model position by hot wire anemometer. The measurement data showed that turbulence intensities around 0.479–0.62% were recorded for several wind speeds as Table 3-1. To confirm the difference of wind speed at entrance of wind tunnel where the cable model located and inside wind tunnel where is the location of Pitot tube, the wind speed was recorded by handy hot wire as Figure 3-2 at each place. Generally, the wind speeds of two locations are similar by different wind speed as the Table 3-2. The calibration factor for wind speed at cable location is around 1.03 which taken from wind speed range 3m/s - 20m/s.

Table 3.1 Turbulence intensity

No.	Mean U (m/s)	I_u	I_w
1	6.71	0.59%	0.60%
2	9.20	0.59%	0.62%
3	11.68	0.56%	0.59%
4	14.15	0.60%	0.61%
5	19.06	0.48%	0.62%

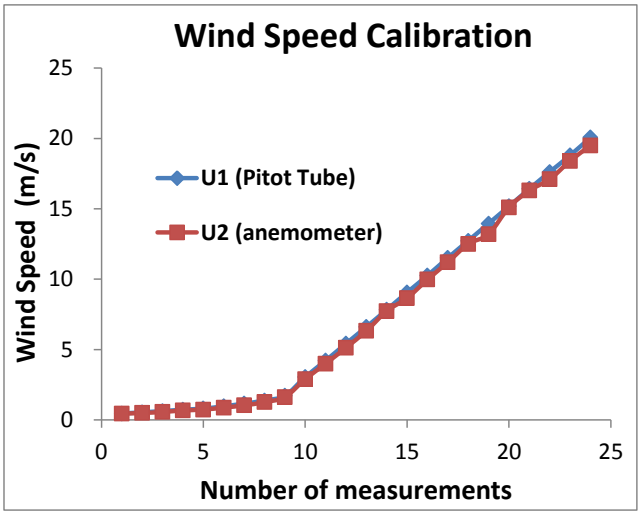

Figure 3-2 Wind speed calibration

Table 3.2 Wind speed comparison

No.	U_1 (m/s)	U_2 (m/s)	U_1/U_2
	Pitot tube	Anemometer	
1	0.45	0.44	1.024
2	0.54	0.49	1.095
3	0.62	0.56	1.114
4	0.72	0.67	1.081
5	0.80	0.73	1.099
6	0.96	0.87	1.109
7	1.16	1.03	1.123
8	1.38	1.26	1.093
9	1.72	1.62	1.059
10	3.04	2.89	1.051
11	4.21	3.99	1.055
12	5.41	5.13	1.055
13	6.60	6.32	1.045
14	7.82	7.73	1.012
15	9.06	8.66	1.046
16	10.25	9.97	1.028
17	11.51	11.20	1.028
18	12.73	12.50	1.018
19	13.95	13.20	1.057
20	15.18	15.10	1.005
21	16.42	16.30	1.007
22	17.62	17.10	1.030
23	18.79	18.40	1.021
24	20.07	19.50	1.029

3.1.3 Section model and Scaling

The section model and full model have been widely applied so far in the wind tunnel to investigate the aerodynamic characteristic of structures. In this study, the section model will be used for investigate the characteristics of cable vibration and its mechanism. The validity of a section model to represent response of long prototype cable was figured out by Delong Zou et al [2]. By comparing the section model and full-scale measurement, Delong Zou et al found that sectional model could reproduce the full-scale response. Therefore, sectional model enable to capture the main characteristic of cable vibration. In addition, section model commonly used to determine the aerodynamic response characteristics of a prototype body with a particular cross sectional shape. Examples of prototypes that may be studied with section models include airplane wings, bridge decks or other bodies whose length is large enough to make full-scale model testing difficult in the wind tunnel, like stay-cables. A section model is an appropriately scaled and detailed geometrical model of a typical two-dimensional section of a body. The model is typically suspended from an elastic support system that allows freedom of motion similar to the expected motion of the prototype. In this way, the static and dynamic forces expected on the prototype can be investigated. Section modeling often provides fundamental aerodynamic data that is used as a basis for comprehensive analytical studies.

To obtain higher possible Reynolds number, it is necessary to use cylinders a little large regarding the degree of blockage, which typically has a maximum acceptable value around 10-15% of the test section width [3]. Moreover, different types of similarity laws available such as Froude's law or Reynolds' law, but as it is not physical possible to fully fulfill the Principle of Similitude, it should be flexible. It is therefore essential to identify the important parameters for the WTT and to interpret the information obtained from the tests. The complete list of scaling relationships for Froude's and Reynolds' laws are referred at Table 3-3.

With the length scale α given as:

$$\alpha = \frac{D_P}{D_M} \tag{3.1}$$

Where

$\mathbf{D_P}$ is the diameter of the prototype

$\mathbf{D_M}$ the diameter of the model.

In this study, the test model was fabricated with the same 1:1 scale with prototype body. Therefore, length scale α equal to 1.

Table 3.3 Scaling relationship of Froude's law and Reynolds' law

	Froude's law	**Reynolds' law**
Length [m]	α	α
Area [m^2]	α^2	α^2
Volume [m	α^3	α^3
Mass [kg]	α^3	α^3
Time [s]	$\alpha^{1/2}$	α^2
Frequency [s^{-1})	$\alpha^{-1/2}$	α^{-2}
Velocity [m/s]	$\alpha^{1/2}$	α^{-1}
Acceleration [m/s^2]	1	α^{-3}
Force [N]	α^3	1
Pressure [N/m^2]	α	α^{-2}
Energy [J]	α^4	α
Effect [J/s]	$\alpha^{7/2}$	α^{-1}

3.1.4 Model fabrication and its verification

The section model consists two main parts. The first is the steel core, which is fabricated from steel tube with relevant length and approximate 50mm of diameter. The second part is the high polyethylene tube cover with different diameter. The fabricated cable model are shown in Figure 3-3. In this figure, there are mainly four types of cable including circular cylinder with smooth surface, indented surface, parallel protuberance and spiral protuberances. The diameter of cable section model are 110mm, and 158mm taking into account the typical prototype cable diameters. Currently, the indented surface cable and parallel cable are being applied for Tatara Bridge and Higashi Kobe Bridge respectively. In addition, a typical circular cylinder is used to investigate the dry galloping and rain-wind induced vibration. Besides that, the spiral protuberance cable will be also fabricated and tested. The parallel protuberance and spiral protuberance will be fabricated by adding the rubber fillets on the cable surfaces. On the other hand, the indented surface will used same indent scale of Tatara bridge cable.

Figure 3-3 Experimental cable models

3.1.5 Supporting system

To simulate the same various kinds of cable orientations, the frame system was made from circular steel tube and was connected together. Suspension systems commonly use springs support system as a means of restraining the translational motion of the model in a given direction. In this study, a cable model was supported by a 1-DOF spring system in vertical plane and small wire system was used in horizontal plane in order to keep cable model unmoved laterally. Cable's position can be changed by flow angle and inclined angle as shown in Figure 3-4. According to previous studies, the responses of 1-DOF and 2DOF systems was almost similar [4, 5], so current 1DOF system can capture the galloping characteristic of stay cable.

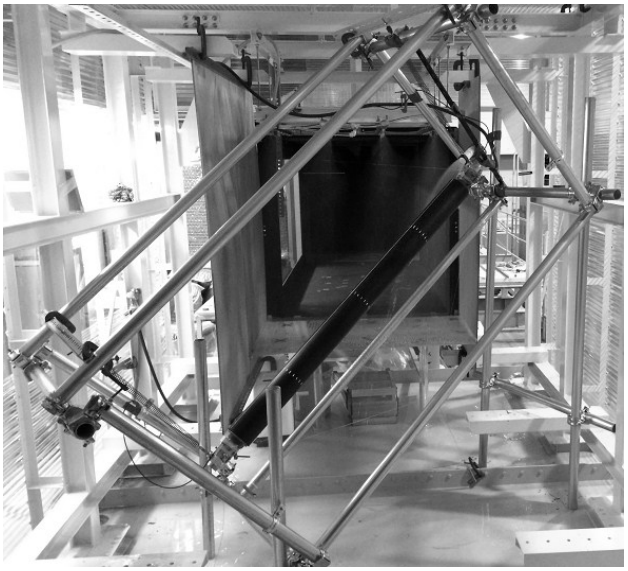

Figure 3-4 Supporting system

3.1.6 Rain simulator system

In this experiment, rain condition can be simulated by an overhead nozzle system as shown in Figure 3-5. Rain volume at the cable model position is controlled around 40-60mm/h in the wind-speed range (around 8-15m/s), which was adjusted to create the critical rain wind induced amplitude. The volume adjustment system located outside of wind tunnel, so it is easy to change volume to critical value. Moreover, nozzles can be changed by different types to get the suitable one. The detail of rain fall by different wind speed can be referred in table 3.4.

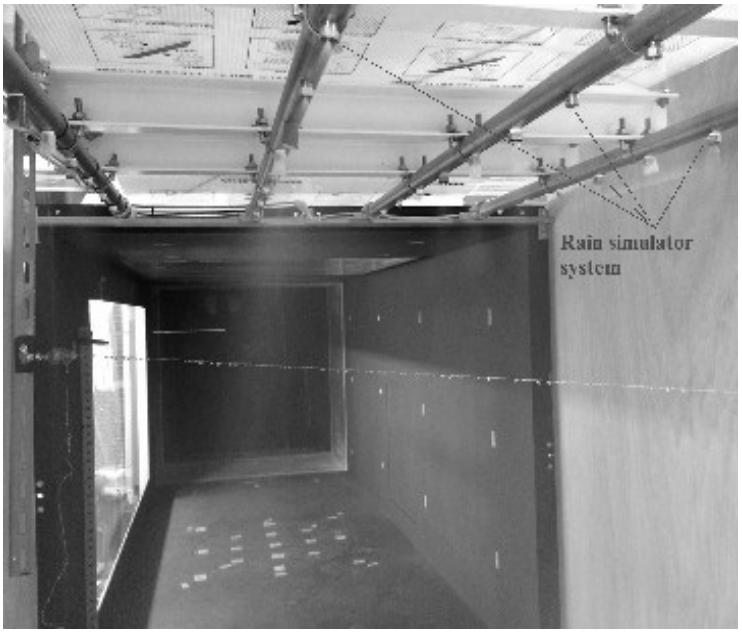

Figure 3-5 Rain simulator system

Table 3.4 Rain volume at different wind speed

U	**Rain volume**
(m/s)	(mm/ hour)
8.75	61.5
11.3	51
13.75	42

3.2 Data acquisition equipment

The arrangement of measurement systems can be seen in Figure 3-6. In this system, dynamic pressure was measured by Pitot Tube and it connect to the Manometer. Besides that, accelerators and dynamic strain amplifier were used for capturing cable vibration. All of equipment will be connect to PC to recording data through Keygen Analog (NR-HA08). In addition, the atmospheric pressure was displayed by Barometer.

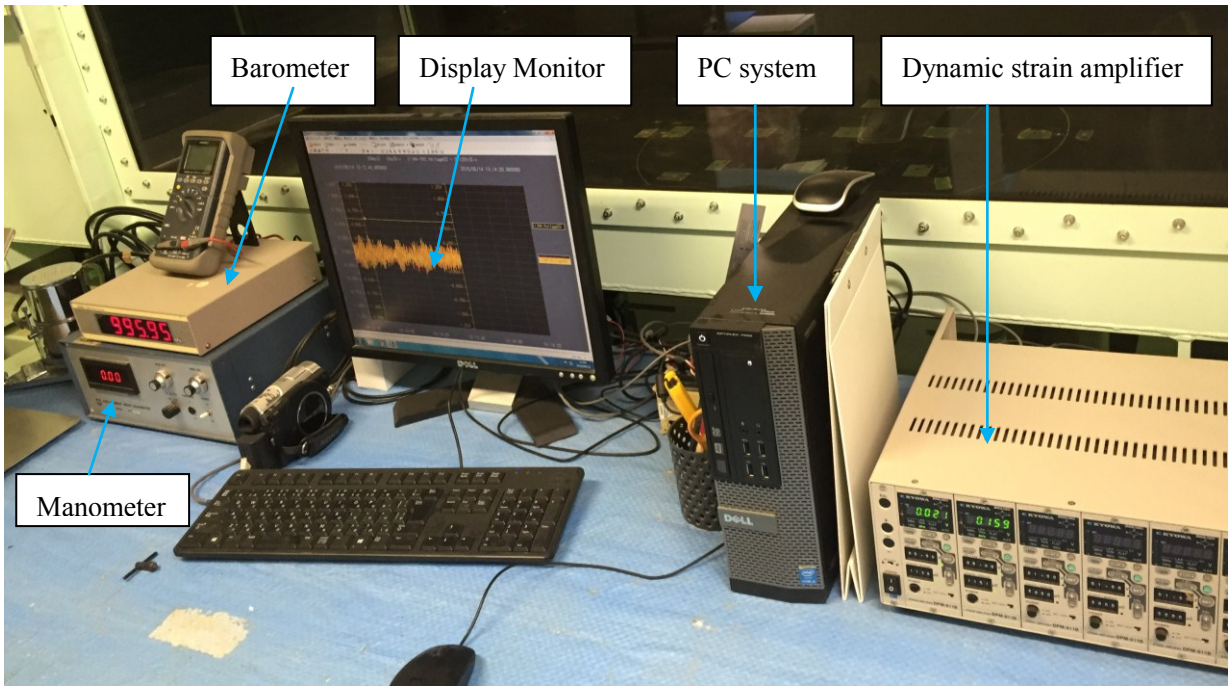

Figure 3-6 Arrangement of measurement system

3.2.1 Accelerometers

Accelerometers were manufactured by Kyowa Electronic Instruments Co., LTD. The model name is ASW-5A with rate capacity 49.03m/s^2. A couple of accelerometers were used to capture acceleration of the cable motion. Two accelerometers were mounted exactly at the top of each cable end as Figure 3-7. Then, the average value will be taken by these accelerometers. In wind tunnel, the sampling frequency was set at 50Hz and the recording duration was 60 seconds, which enable capturing all vibrations of cable model.

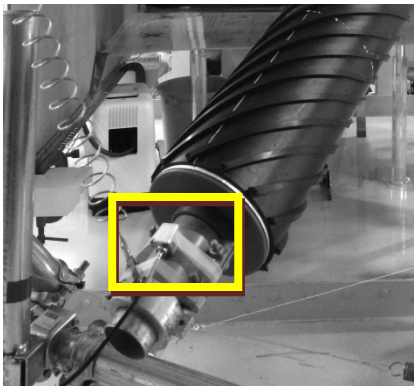

Figure 3-7 Accelerometers are mounted on the surface of cable

3.2.2 Dynamic strain amplifier

The dynamic strain amplifier system is illustrated in Figure 3-8. It was manufactured by Kyowa Electronic Instruments Co., LTD. The model name is DPM-911B. The two accelerometers were connected to this data logger to record experimental data.

Figure 3-8 Data acquisition system

3.2.3 Precision differential manometer

The wind speed was easily calculated from dynamic pressure. In this study, the fluctuation of dynamic pressure was measured by Pitot tube system as Figure 3-9. Firstly, dynamic pressure were recorded by Pitot tube, then it will transfer and display in a precision differential manometer with Model ISP-3200 which were manufactured by SIBATA company. In addition, the accompanied data acquisition displaying and extracting software provided a real time monitoring of the data.

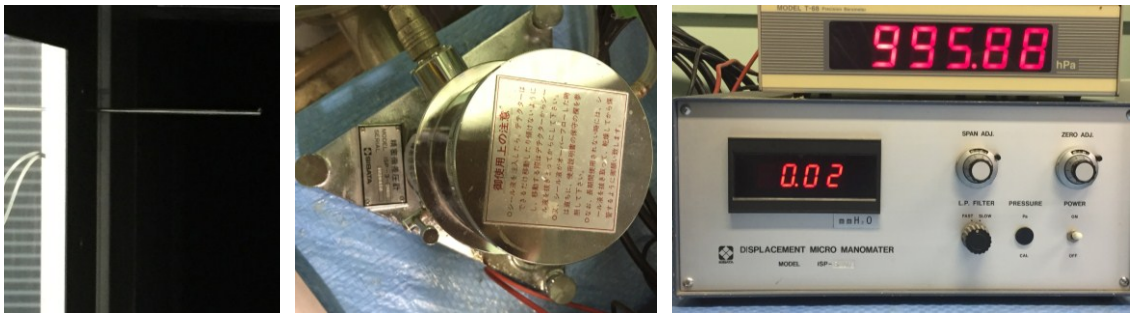

Figure 3-9 Precision differential manometer IPS-3200

3.2.4 Convert acceleration data to vibration amplitude

From accelerator data, vibration amplitude can be easily calculated. The equilibrium motion equation that governs a mass-spring system can be written as:

$$m.\ddot{y} + \xi.\ddot{y} + k.y = 0 \tag{3.2}$$

$y(t)$ = vibration amplitude
m = mass $(m > 0)$
ξ = damping constant $(\xi \geq 0)$
k = spring (Hooke's) constant $(k > 0)$

By considering the motion system as an undamped free vibration (no damping system), the motion equation can rewrite as follow:

$$m.\ddot{y} + k.y = 0 \tag{3.3}$$

Then the vibration amplitude can be obtained from:

$$y = \frac{m.\ddot{y}}{k} = \frac{\ddot{y}}{\omega^2} = \frac{\ddot{y}}{4\pi f^2} \tag{3.4}$$

f : Natural frequency of motion structure

$\ddot{y}$: Acceleration which is recorded from accelerators

3.3 Scope of wind tunnel test

3.3.1 Wind tunnel test campaign

Wind tunnel test campaign is divided into three stages. First stage carries out experiments with a circular cylinder for the baseline. In this stage, the DG and rain wind induced vibration will be reproduced. Then, several characteristics of DG will continue being investigated. The second part deal with examining the effectiveness of indented surface and parallel protuberances for DG. Then, third stage tries to propose optimized parameters for spiral protuberance countermeasures in size, pitch and number of fillets.

3.3.2 Angle of attack

Various wind attack angles can be simulated by changing the supporting frame system through inclined angle α and flow angle β. Then, wind relative angle β*, which defines the angle between wind direction and cable axis as shown in Figure 3-10, can be calculated by following formula:

$$\beta^* = \sin^{-1}\left(\cos\alpha \times \sin\beta\right) \tag{3.5}$$

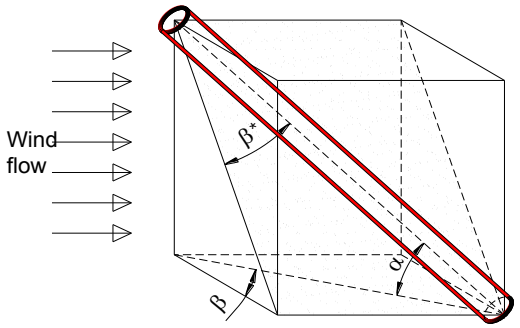

Figure 3-10 Definition of inclined angle and flow angle

In this experiment, the inclined angle was fixed at 40°, 25° and 9° combined with the flow angle of 0°, 15°, 30°, 45° and 60°. Inclined angles of 40° and 25° were selected to take

into account an inclined angle of stay cables in middle and top section of a normal cable-stayed bridge, respectively. On the other hand, the inclination of 9° was also take into account to consider the longest cable of a long-span cable-stayed bridge with lower tower height due to the aviation restriction.

3.3.3 Test procedure

The test procedure can be seen as the Figure 3-11 below. Current experiments will deal with various kinds of measurement. At first, the cable vibration responses will be recorded. Then it is necessary to clarify the effect of parametric factors such as the Scruton number and frequency dependence and so on. Second, the flow filed pattern near the wake of cable will be investigated. In this measurement, the axial flow, wake flow will be measured. Furthermore, different type of spiral surface will be examined to develop a better countermeasure for DG and rain wind induced vibration.

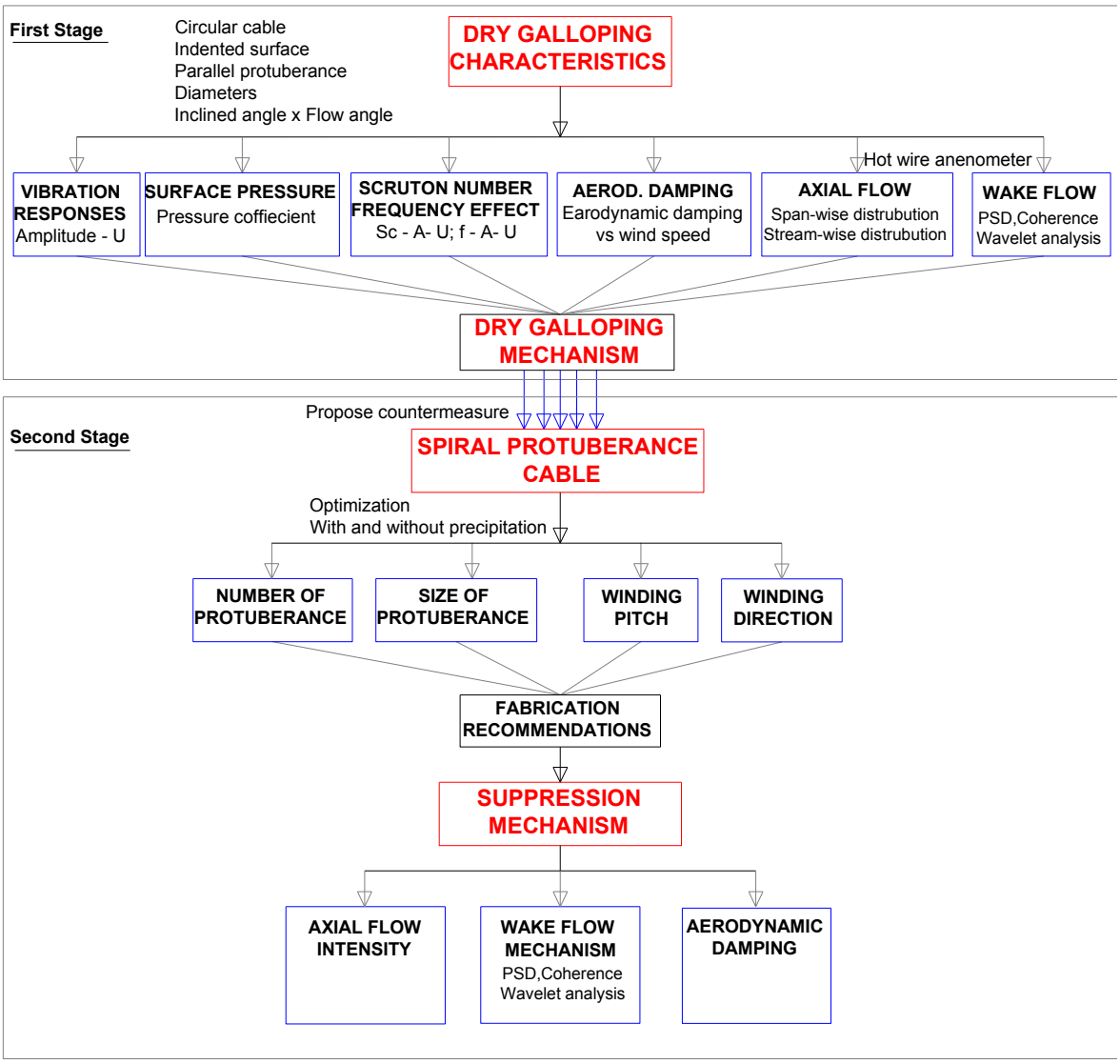

Figure 3-11 Wind tunnel test investigation procedure

3.4 Wind-induced vibrations parameters

3.4.1 Damping ratio

Logarithmic decrement method is used to compute damping ratio of the damped cable using the displacement time-history data collected in free vibration tests. The captured data need to be pre-processed before applying logarithmic decrement method. After pre-processing the data, only the 1st modal response is retained in the displacement time-history for determining 1st modal damping ratio. Logarithmic decrement is the natural logarithmic value of the ratio of two adjacent peak values of displacement time-history in free decay vibration. Then, the damping ratio is computed by:

$$\varsigma = \frac{\delta}{\sqrt{(2\pi)^2 + \delta^2}} \tag{3.6}$$

$$\text{where } \delta = \frac{1}{n}\left(\ln \frac{y_1}{y_{n+1}}\right) \tag{3.7}$$

Where δ is logarithmic decay; ς is the damping ratio of the modal cable; n is the number of cycle; y_1 and y_{n+1} are the displacement at the 1 st and the (n+1) th peak of the displacement time-history curve. In addition, from this free oscillation test the natural frequency already checked for comparing with the theory calculation. The logarithms decrement and damping ratio in current study will be addressed in next chapter.

3.4.2 Reduced Wind speed

Reduced velocity is non-dimensional velocity and can be defined as follows:

$$U_r = \frac{U}{fD} \tag{3.8}$$

Where: f = system natural frequency;

D = characteristic dimension (diameter)

U = velocity of the oncoming flow.

3.4.3 Reduced Amplitude (Non-dimensional Amplitude)

The non-dimensional amplitude is defined as follows:

$$A_r = \frac{A}{D} \tag{3.9}$$

Where: A = Vibration amplitude;

D = diameter of cable.

3.4.4 Scruton number

The Scruton number is an important parameter when considering vortex excitation, rain/wind-induced vibrations, wake galloping, and dry inclined cable galloping. Researchers use the Scruton number to relate wind tunnel tests of scale section models to full-scale cable behavior. The Scruton number is a non-dimensional parameter that characterizes the mass and damping properties of a flexible body. The Scruton number is defined as follows [6]:

$$S_c = \frac{2m\delta}{\rho D^2} \tag{3.10}$$

Where: m = unit-length mass of a cable model;

δ = logarithmic decrement

D = diameter of the cylinder; ρ = air density.

3.4.5 Reynolds Number

A key parameter in the description of compressible fluid flow around objects (such as wind around stay cables) is the Reynolds number. The Reynolds number is a measure of the ratio of the inertial forces of wind to the viscous forces and is given by equation 3.11:

$$Re = \frac{\rho V D}{\mu} \tag{3.11}$$

whereρ = air density (kg/m^3)

V= wind velocity (m/s),D= cable diameter (m) and μ = viscosity of air (g/m-s)

3.4.6 Strouhal number

The Strouhal number is a dimensionless parameter relevant to vortex excitation (equation 3.12):

$$S_t = \frac{f_s.D}{V} \tag{3.12}$$

f_s= frequency of vortex excitation

The Strouhal number remains constant over extended ranges of wind velocity. For circular cross section cables in the Reynolds number range 1×10^4 to 3×10^5, St is about 0.15-0.2.

3.5 Rain-wind induced vibration

3.5.1 Experimental conditions

To confirm the occurrence of RWIV for reference as well as to validate current WTT system, RWIV were examined with various cases. In this stage, experiment involves with two types of diameter, 158mm and 110mm respectively. Inclined angles are 9°, 25° and 40°. Whereas the flow angles will change by moving the supporting frame by 15° step from angle 0° to 60° as Table 3.5. In addition, Table 3.6 shows details of experiment parameters in which cable diameters are 110mm and 158mm with an effective model length of 1.5 m, the aspect ratio is 13.6 and 9.5, respectively.

Table 3.5 Wind tunnel test for circular cylinder

Diameter(mm)	Inclined angle α(°)	Flow angle β(°)	Surface type	Precipitation
D110, D158	9°, 25°, 40°	0°, 15°, 30°, 45°, 60°	Smooth	40-50mm/h

Table 3.6 Conditions of wind tunnel test

Diameter: D (mm)	110 and 158
Effective length (mm)	1,500
m (kg/m)	8.15 (110 mm); 9.86 (158 mm)
Natural frequency (Hz)	0.86 – 1.02 (α = 9°) 0.78 – 0.9 (α = 25°, 40°)
Logarithm decrement	0.005 - 0.014
Scruton number ($2m\delta/\rho D^2$)	3.26 – 3.95 (α = 9°) 5.83 – 11.22 (α = 25°, 40°)
Reynolds number	~ 2.1×10^5

Logarithmic decrement ranges from approximately 0.005 to 0.014. Natural frequency is around 0.78 - 1.02 Hz in considering typical value of actual stay cables. The Scruton number ranges from 3.26 to 11.22 depending on the unit mass of cable and logarithm

decrement. Rain volume at the cable model position was 40-50mm/h in the wind-speed range (around 8-15m/s), which was adjusted to create the critical RWIV amplitude. Because of the limitation of wind tunnel capacity, maximum wind speed is up to 20m/s equivalent to Reynolds number around 2.1×10^5 for non-yawed angle. When cable's orientation changed, the critical Reynolds can be also reduced. In addition, according to previous studies, DG of inclined cable could be observed in the subcritical Reynolds number regime [7-10] as well as in the transition and critical Reynolds number regime [11-13]. Therefore, above range of Reynolds number enable to reproduce the DG. The detail of wind Tunnel test parameter for circular cylinder is calculated as Appendix 1.

3.5.2 Rain-wind induced cable vibration

In this section, RWIV responses will be reproduced for validity and later references. As shown in Figures 3-12 to 3-16, experimental results agree with the former studies [14, 15] that RWIV only occurred in specific ranges of wind speed and relative angles to wind. In detail, large amplitude vibration with non-dimensional amplitude of more than 1.5*D* occurred in cases of the inclined angle 25°, and flow angle 30° and 45° for 110mm cable (Figure 3-11). It also occurred in cases of the inclined angle 25°, and flow angle 15-45° for 158mm cable (Figure 3-13). When RWIV occurs, cable can gallop rapidly and divergently. Due to the constraint of the supporting spring system, maximum amplitude can be recorded in this study is around 2*D*. According to the experiment results of Gu et al. [15], the range of inclined angles from 25-35° and flow angle from 30-35° was the critical region, which is consistent with current results.

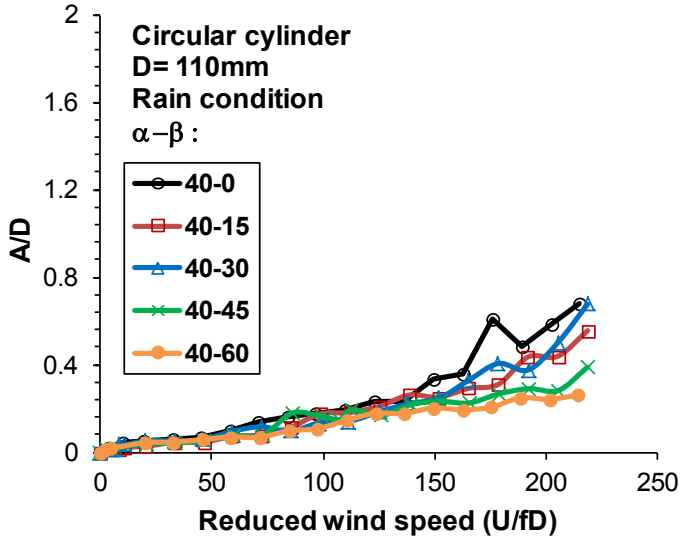

Figure 3-12 Rain wind induced vibration, D110 mm, Inclined angle 40°

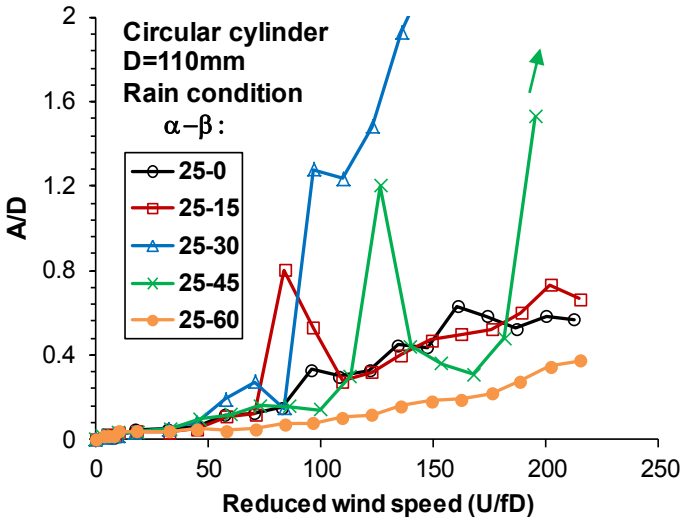

Figure 3-13 Rain wind induced vibration, D110 mm, Inclined angle 25°

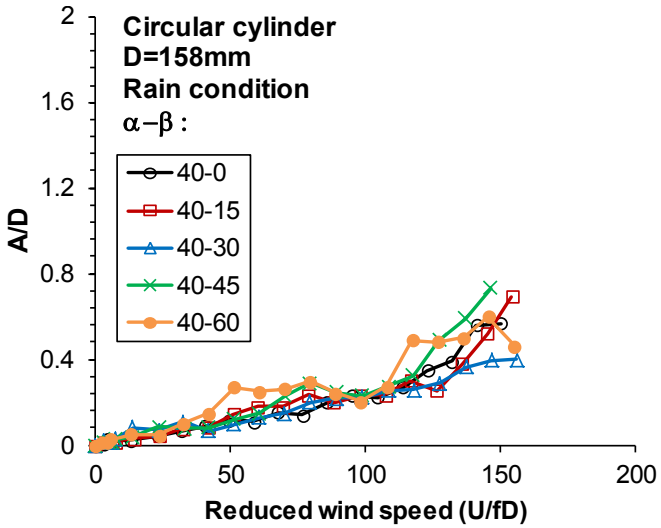

Figure 3-14 Rain wind induced vibration, D158 mm, Inclined angle 40°

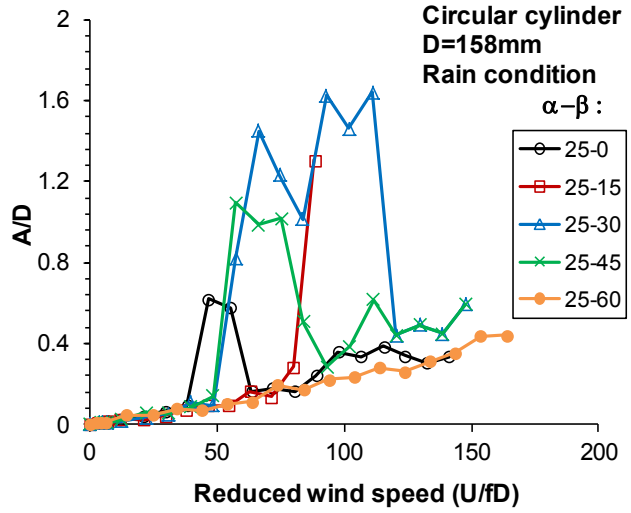

Figure 3-15 Rain wind induced vibration, D158 mm, Inclined angle 25°

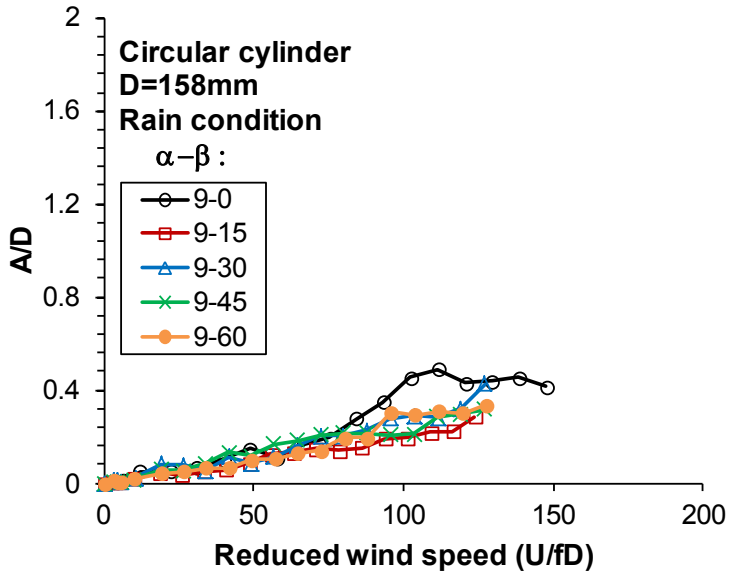

Figure 3-16 Rain wind induced vibration, D158 mm, Inclined angle 9°

Apart from that, Figure 3-17 and 3-18 elucidate the upper rain rivulet snaking down along the cable surface for the inclined angle 25° and the flow angle 30°, which are shown by the yellow dashed lines. These figures were snapshotted during cable vibration. Obviously, the shape of rivulet is relatively wide and located moderately at 70-80° from the stagnation point. When reduced wind speed reached 74.72 (10.18m/s), the water rivulet was located at around 70°-75°. As reduced wind speed increased to 107.89 (13.88m/s), it shifted a little to 75°-80°. According to the experiments by Matsumoto at el.[16], the critical position of the upper rivulet was 68-75°. This difference could be caused by dissimilar cable's attitude against wind between two studies. In addition, Matsumoto et al used artificial water rivulet for examining the effect of water rivulet position on cable response while current study used rain condition that is similar to nature. Moreover, by observing the upper and lower rivulet during cable vibration, it was understood that water rivulet vibrated harmoniously and synchronized with cable vibration frequency. This may show that large amplitude RWIV is caused by self-excited vibration mechanism between cable and rivulet motions. This should be further investigated. In addition, the experiment with the real rain simulation can capture the vibration characteristic of RWIV whereas we should be consider when use the artificial rivulet model to investigate the characteristic of this phenomenon. Finally, current test results confirm that rain-wind induced cable vibration is a dangerous vibration for stay cables that can cause divergent galloping with very large amplitude.

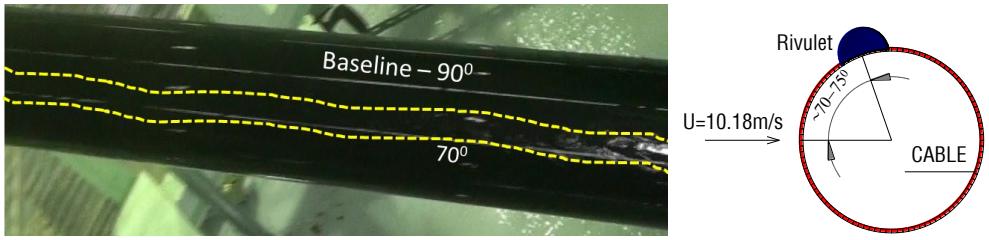

Figure 3-17 Upper rivulet (α = 25° and β = 30°, *U/fD* = 74.72 (10.18 m/s), D =158)

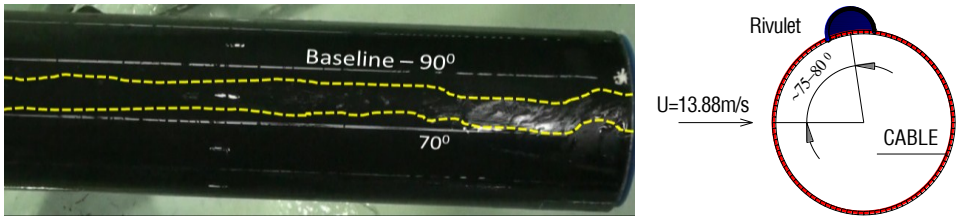

Figure 3-18 Upper rivulet (α = 25° and β = 30°, *U/fD* = 107.89 (13.88m/s), *D* =158)

3.5.3 Role of lower rivulet

Previous studies pointed out that the centerpiece of rain wind induced vibration is the forming of upper rivulet leading to change the aerodynamic characteristic of cable, then the vibration will be excited[14, 16, 17]. On the other hand, the lower rivulet was found to have a stabilizing effect, which would produce an aerodynamic damping force to suppress cable motion; whereas the upper rivulet would generate aerodynamic force to excite the cable motion. Generally, the lower rivulet used to be locate around 10°-40° depending on wind speed[14]. Due to the balance of wind force gravity force and friction force, lower rivulet could not go up to higher position. In some special conditions, like cable has a leading spiral protuberance on surface, lower rivulet can climb to higher position, say 45°, 60°, 135° or so on. Therefore checking the effect of lower rivulet is significant for understanding fully the rain wind induced vibration or countermeasure development.

According to previous study [18], it is found that the shapes of rivulet affected insignificantly to the cable response. Hence, the lower rain flow here was simulated by artificial rivulet which dimension was around 0.05Dx0.05D (as Figure 3-17). The rivulet was made of wood and mounted on lower side of cable. The position of lower rivulet on cable surface can be defined by the relative angle ϕ, which was changed from 0° to180° by every step of 15°, as the Figure 3-19. The experimental parameters are shown in Table 3-7 and the effect of lower rivulet to cable response can be referred to Figure 3-20. When lower rivulet was at 45° or 135°, cable vibrate divergently and reached amplitude 1D around 100 of reduced wind speed while the other cases exhibited only restricted responses. Obviously, at

some certain position, lower rivulet also play import role in exciting galloping. Therefore, it should pay attention that when fabricate the cable surface modification, we should take in to account how to suppress not only upper rivulet but also the lower one.

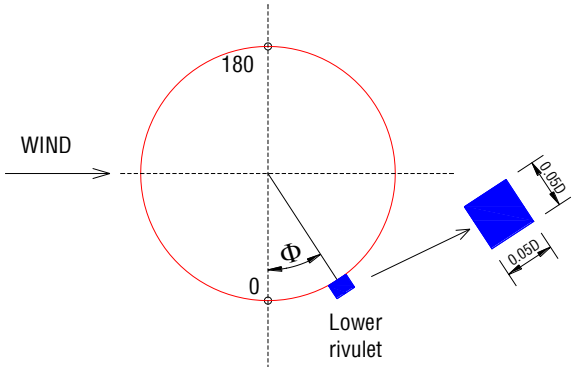

Figure 3-19 Location of rain rivulet

Table 3.7 Artificial rivulet test conditions

Parameters	Values
Diameter: D	110mm
Logarithms decrement	0.0068
Flow angles	45°
Inclination	25°
Mass of models (kg)	11.13
Natural frequency (Hertz)	0.946
Rain rivulet position	0°-180° by step 15°

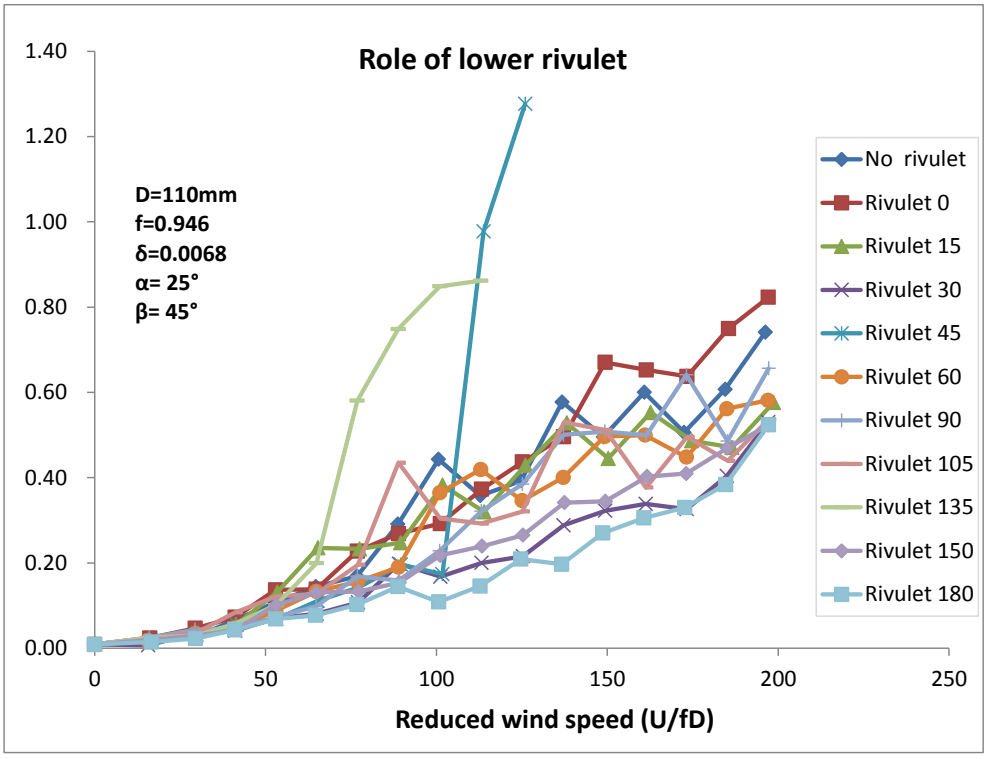

Figure 3-20 Effect of lower rivulet to cable galloping

3.6 Summary of Chapter 3

The detail of wind tunnel facilities and its parameters were illustrated in detail. Furthermore, the number of fabrication for different cable surfaces also addressed. In addition, several related wind parameters and wind tunnel test campaigned also were described. Moreover, the converting acceleration data to vibration amplitude also introduced. Besides that, RWIV has been reproduced successfully in various conditions. The test results give high agreement with previous studies. In the other expression, the current wind tunnel enable to carry out the test for rain wind induced vibration as well as dry galloping. The case of the inclined angle 25° and the flow angle 30° was the critical for rain-wind induced with vibration amplitude of more than 2D in case of a circular cable. Significantly, it should be taken in account the effect of lower rivulet, because when lower rivulet reached to some certain position on cable surface, it can excite galloping.

Bibliography

1. *Report of wind resistant committee*. 1993, Hoshu-shikoku Bridge Authority.

2. Delong, Z. and P.J. Nicholas, *Wind tunnel testing of yawed and inclined circular cylinders in the context of field observations of stay-cable vibrations.* J. Wind Eng. Ind. Aerodyn., 2009. **97** p. 219–227.

3. Dalton, C., *Allen and Vincenti Blockage Corrections in a Wind Tunnel. .* AIAA Journal, 1971. **9**(9): p. 1864-1865.

4. Matsumoto, M., M. Kitazawa, and H. Kanaji, *Wind tunnel test for stay cables of Higashi Kobe Ohashi Bridge -part 2 (in Japanese).* Proc. Of 44th Annual Conference of JSCE, 1989 p. 802-803.

5. Phelan, R., P. Sarkar, and K. Mehta, *Full-Scale Measurements to Investigate Rain-Wind Induced Cable-Stay Vibration and Its Mitigation.* Journal of Bridge Engineering, 2006. **11**(3): p. 293- 304.

6. 1991-1-4., E., *Eurocode 1:Actions on structures - Part 1-4: General actions - Wind actions.. p, .* 2005. p. 128.

7. Saito, T., M. Matsumoto, and M. Kitazawa. *Rain-wind Excitation of Cables on Cable-stayed Higashi-Kobe Bridge and Cable Vibration Control*. in *Proc. of Cable-stayed and Suspension Bridges*. 1994.

8. Honda, A., et al. *Wind tunnel test on rain-induced vibration of the stay cable*. in *Proceedings of International Symposium on Cable Dynamics*. 1995. Lie`ge, Belgium.

9. Matsumoto, M., et al., *Dry-galloping characteristics and its mechanism of inclined/yawed cables.* Journal of Wind Engineering and Industrial Aerodynamics, 2010. **98**: p. 317-327.

10. Miyata, T., H. Yamada, and T. Hojo. *Aerodynamic response of PE stay cables with pattern-indented surface*. in *International Conference on Cable-Stayed and Suspension Bridges (AFPC)*. 1994. Deauville, France.

11. Cheng, S., et al. *Aerodynamic instability of inclined cables*. in *The 5th ISCD*. 2003. Santa Margherita.

12. J.B. Jakobsen, et al., *Wind-induced response and excitation, characteristic of an inclined cable model in the critical Reynolds number range.* Journal of Wind Engineering and Industrial Aerodynamics, 2012. **110**: p. 100-112.

13. Nikitas, N. and J.H.G. Macdonald, *Aerodynamic forcing characteristics of dry cable galloping at critical Reynolds numbers.* European Journal of Mechanics B/Fluids, 2015. **49**: p. 243-249.

14. Hikami, Y. and N. Shiraishi, *Rain–wind induced vibrations of cables in cable-stayed bridges.* Journal of Wind Engineering and Industrial Aerodynamics, 1988. **29**: p. 409-418.

15. Gu, M. and X. Du, *Experimental investigation of rain-wind- induced vibration of cables in cable-stayed bridges and its mitigation.* Journal of Wind Engineering and Industrial Aerodynamics, 2005. **93**: p. 79-95.

16. Matsumoto, M., et al., *Response characteristics of rain-wind induced vibration of stay-cables of cable-stayed bridges.* Journal of Wind Engineering and Industrial Aerodynamics, 1995. **57**: p. 323-333.

17. Venviebe, C. *Rain-Wind-Induced Vibrations of Cables and Bars* in *Larsen, A. and Esdahl, S. (eds), "Bridge Aerodynamics"*. 1998. Balkema.

18. Bosdogianni, A. and D. Olivari, *Wind- and rain-induced oscillations of cables of stayed bridges.* J. Wind Eng. Ind. Aerodyn., 1996. **64**(2 - 3): p. 171 - 185.

Chapter 4: Characteristics of Dry Galloping and Its Generation Mechanism

As the discussion in previous chapters, rain-wind induced vibration (RWIV) and dry galloping (DG) can cause divergent vibration of cable. The mechanism of rain wind induced vibration has been clarified fully so far while DG mechanism still need more works to further elucidate. In the other aspect, aerodynamic control methods for RWIV have been developed by many manners. Nonetheless, it was pointed out that these methods are still defective in no rain condition. For example, indented surface type is effective for rain wind induced vibration but not for DG. Therefore, it is urgent to develop a control measure not only for DG but also for rain-wind interaction. In order to do that, it is important to confirm the generation mechanism of DG. Hence, the aim of this chapter is to confirm the Dry galloping phenomenon in wind tunnel. Further, the detail of DG characteristics and its generation mechanism will be investigated and discussed.

4.1.1 Reproduction of dry galloping

Wind tunnel test were carried out under no precipitation to investigate the cable dry galloping (DG). The test conditions are almost similar to Table 3.4 and 3.5 in chapter 3. The WTT results are summarized in Figure 4-1 to 4-2. Generally, divergent galloping took place in many cases. The arrows in below figures represent for the diverging characteristic at a constant wind speed. For 110 mm cable, divergent vibration occurred only at some wind attack angles such as the inclined angle (α) 40° with the flow angles (β) 15°, 30° and 45°, and (α) 25° with (β) 30° in the subcritical Reynolds number region (6×10^4 - 1.2×10^5). For

cable diameter of 158 mm, similar divergent vibration also recorded in most cases. This experimental result is consistent with previous studies [1, 2] that DG can occur at some specific cable orientations and wind speed range. As mentioned above, current experiment conduct with low Scruton number range from 3.26 to 11.22. In the other expression, current cable model is sensitive to external excitation. Therefore, DG seems to take place easily. From these results, it should pay attention that cable DG is one of large wind induced vibration, which can cause divergent galloping. Furthermore, due to various unknown characteristic of dry galloping and its control methods have not developed yet. Therefore, it needs more effort to clarify this phenomenon as well as develop its countermeasure.

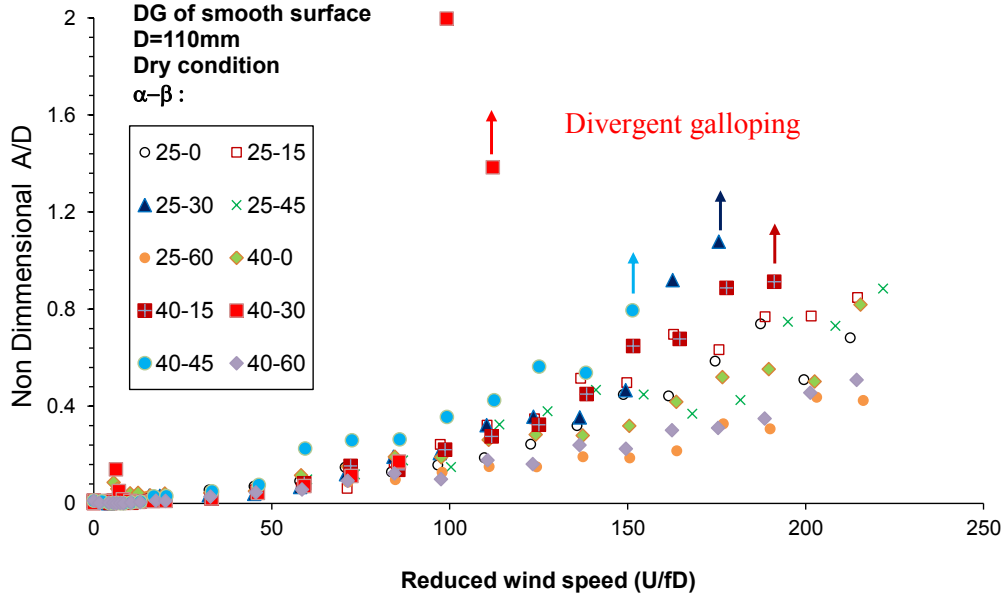

Figure 4-1 Dry galloping of smooth surface cylinder, D110mm

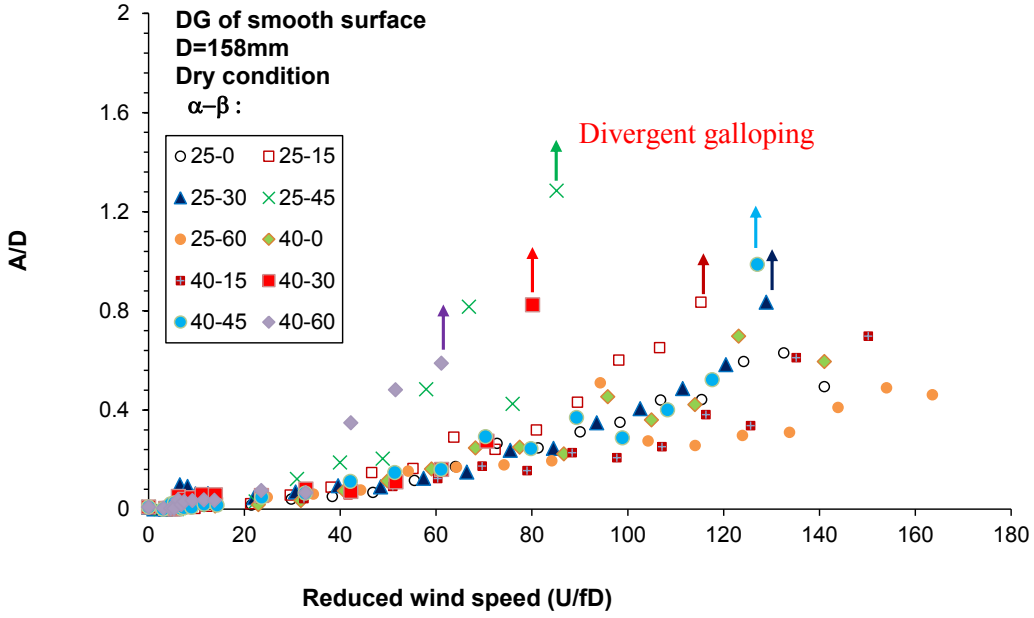

Figure 4-2 Dry galloping of smooth surface cylinder, D158mm

4.2 Characteristics of dry galloping

4.2.1 Sensitivity of dry galloping to Scruton number

Relating to the effect of Scruton number to DG, two criterions has been published by Saito et al. [3] and Federal Highway Administration (US)[4]. Nevertheless, there is a conflict between these criterions as Figure 4-3. According to Saito criterions, DG is less sensitive to Scruton number change while FHWA criterions showed that DG could be suppressed easily by adding more damping. Later, Matsumoto (2010) clarified this difference by classified the cable vibration into two types. The first is the divergent type galloping and the other is limited amplitude vibration. However, in order to propose a proper countermeasure for dry galloping, it is significant to confirm the effect of Scruton number (damping). Therefore, the aim of this section is to elucidate this difference.

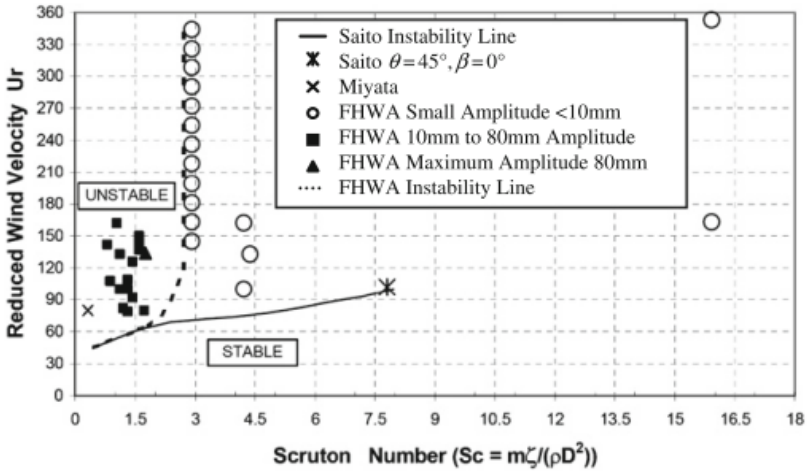

Figure 4-3 Comparison of wind velocity-damping relation[4]

In order to investigate sensibility of DG to Scruton number, wind tunnel test was measured with various cases. The Scruton number was change by increasing the mass of model. According to previous study [5], cable DG can occur horizontally in a range of yaw angle from 30°-60°, therefore current test will carried out with 50° of yawed angle. The conditions of wind tunnel test are illustrated at Table 4.1. The effect of Scruton number was estimated as Figure 4-4. Generally, cable DG is not so sensitive to Scruton number change. Even though when increases Sc to over 45, divergent galloping still occurred at approximate 15m/s where is the subcritical Reynolds region, around 8-9x10^5. However, when Scruton number was risen step by steps, the onset wind speed of DG a little bit increased. These outcomes totally agreed with Saito et al [3] that it is quite hard to eliminate DG of cable by adding more external damping or installing the external dampers. Therefore, the way to

increase the stability of stay cable should be change of the cable cover to harvest higher the aerodynamic damping so that suppress dry galloping.

Table 4.1 Experimental parameters for Scruton number effect

Frequency	f	Hz	1.75	1.7	1.65	1.583333	1.5
Logarithm decrement	Delta		0.0255	0.0350	0.0366	0.0375	0.0448
Damping ratio	ζ (zeta)	%	0.4057	0.5564	0.5818	0.5966	0.7136
Unit mass	m	kg/m	3.65	3.91	4.15	4.41	4.91
Air density	p	kg/m^3	1.2625	1.2625	1.2625	1.2625	1.2625
Diameter	D	m	0.086	0.086	0.086	0.086	0.086
Scruton number	Sc		19.95	29.24	32.47	34.98	46.39

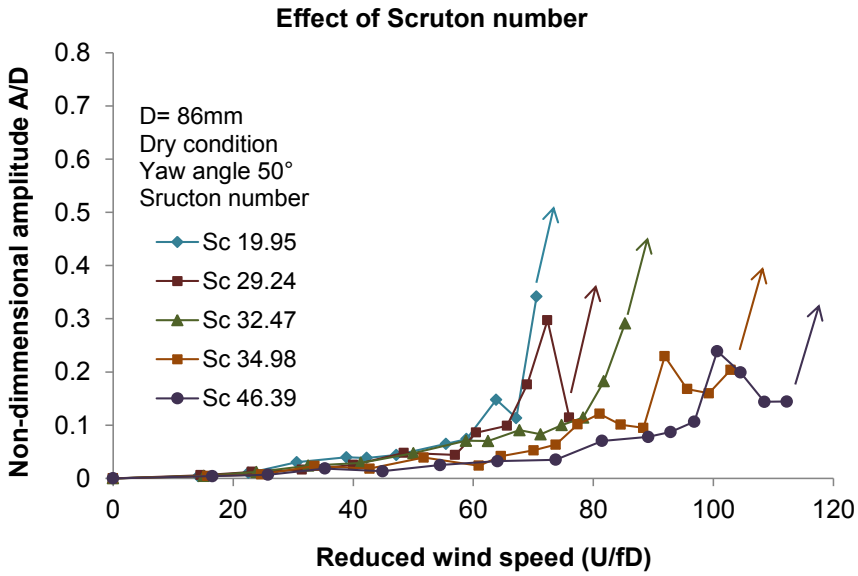

Figure 4-4 Estimated vibration amplitude with different Scruton numbers

4.2.2 Frequency dependence

The parameters of the these tests are wind yawed angle 50^0 and natural frequencies of the cable model of 1.567Hz, 1.717Hz, 2Hz, 2.233Hz and 2.433 Hz respectively. The frequency was change by increasing the stiffness of supported springs. Wind tunnel test parameters are shown in Table 4.2. Figure 4-5 illustrates the vibration amplitudes against wind speed under different natural frequencies. It is obvious that the increase of the natural frequency of the cable, the vibration amplitude decreases considerably. DG occurred at around 12-15m/s with the low natural frequency cases, say 1.567Hz, 1.717Hz and 2Hz. However, as natural frequency increased to 2.233Hz and 2.433Hz, DG was vanished up to 20m/s of wind speed equivalent to Reynolds number around $1.2x10^5$. In the other expression, increase natural frequency of stay cable can suppress dry galloping. In previous study [6], the effect of frequency on RWIV also confirmed that increase natural frequency and reduced

the RWIV, so current results highly agreed .Currently, crosstie system (Figure 2- 8) can be a good suggestion for dry galloping. Because it connects all cable by crosstie so that reduced the effective length of cable and therefore increase natural frequency of cable, then suppress the vibration. Nevertheless, the serious drawback of this countermeasure is that it only mitigate the in-plane galloping not for the out-plane one. In addition, its cost estimation for design and maintain is quite high. Therefore, it need more works on dry galloping countermeasures.

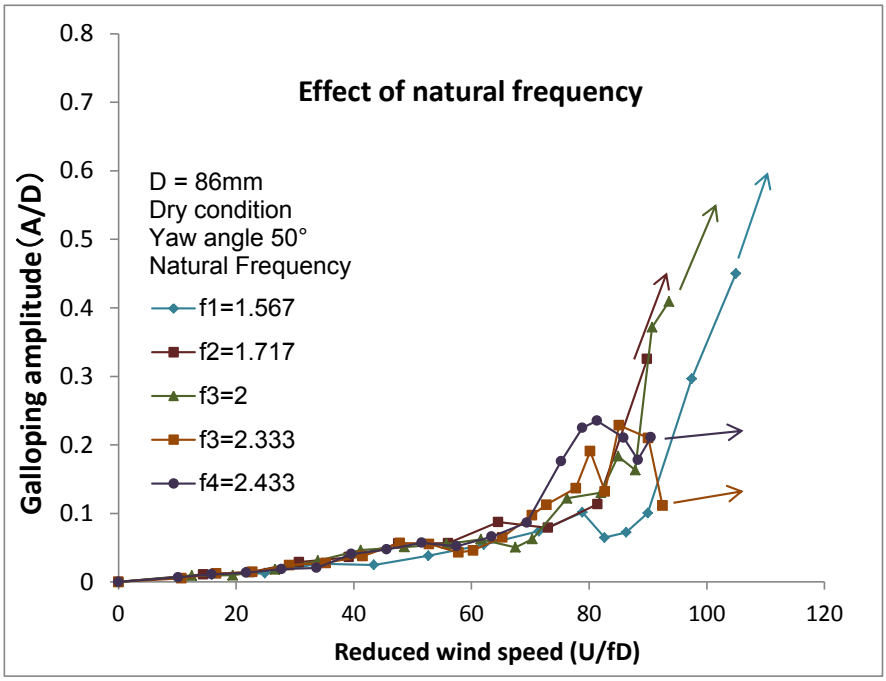

Figure 4-5 Vibration amplitudes versus natural frequencies

Table 4.2 Wind tunnel test parameter for frequency effect

Natural frequency	f	Hz	1.567	1.717	2.000	2.333	2.433
logarithm decrement	delta		0.016	0.009	0.017	0.021	0.016
Damping ratio	ζ (zeta)	%	0.254	0.144	0.270	0.327	0.247
Unit mass	m	kg/m	3.654	3.654	3.654	3.654	3.654
Air density	p	kg/m^3	1.26222	1.26222	1.26222	1.26222	1.26222
Diameter	D	m	0.086	0.086	0.086	0.086	0.086
Scruton number	Sc		12.492	7.067	13.267	16.101	12.139

4.2.3 Surface pressure distribution

4.2.3.1 Measurement set up

The overview of pressure measurement sketch up can be seen as Figure 4-6. Cable model was installed at the entrance of wind tunnel with single degree of freedom by spring-

supported system. Therefore, it enables to measure the surface pressure under dynamic condition. In order to capture the surface pressure characteristic, cable model was equipped the pressure rings and taps. Pressure rings are located at a distance from cable end of 1D, 2D, L/4 and L/2 and each ring has 24 pressure taps as shown in Figure 4-7. The experimental conditions for this WTT can be seen as Table 4.3. In this experiment, circumferential angle of the pressure holes is defined anti-clockwise from the stagnation point.

Table 4.3 Pressure measurement conditions

Parameters	values
Diameter: D	86 mm
Scruton number	28.2
Natural frequency (Hz)	1.717
Reynolds number	$0 – 10^5$
Wind yawed angle	50°
Inclination	0°

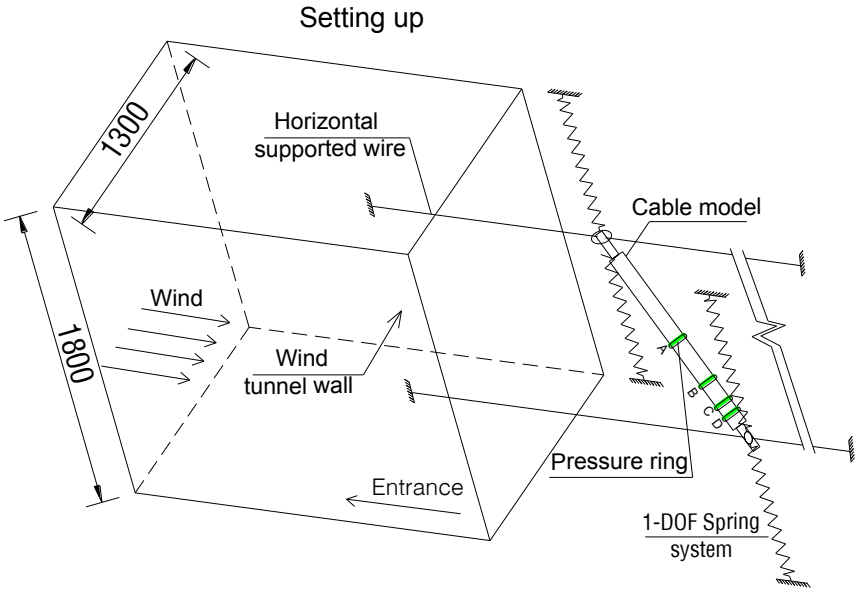

Figure 4-6 Pressure measurement set-up sketch

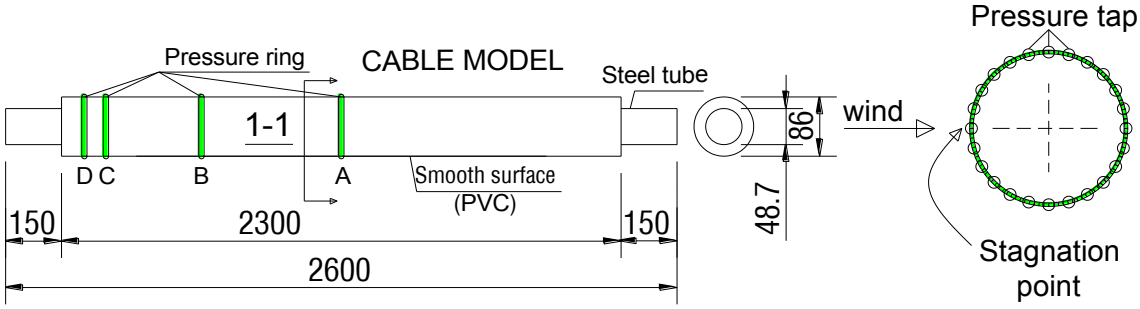

Figure 4-7 Cable model and pressure taps

4.2.3.2 Mean pressure coefficients

The surface pressure at Reynolds number $8.83x10^4$, $7.65x10^4$ and $5.6x10^4$ were measured respectively, in which the Reynolds number of $8.83x10^4$ took in to account the point before DG took place as Figure 4-8.

Pressures are usually measured with respect to the mean static pressure in the wind tunnel test section corresponding to the mean static pressure. Pressure coefficients are obtained by normalizing the measured pressures by the mean dynamic pressure measured. The mean pressure coefficients are thus defined as follows:

$$C_{\bar{p}} = \frac{\frac{1}{T}\int_0^T p(t).dt}{q} \tag{4.1}$$

where:

p(t) : is the instantaneous surface pressure measured with respect to the mean static reference pressure;

t : is time

T : is the sampling period

$q = \frac{1}{2}\rho\bar{U}^2$: is the reference mean dynamic pressure

ρ : is the air density

$\bar{U}$: is the mean wind speed

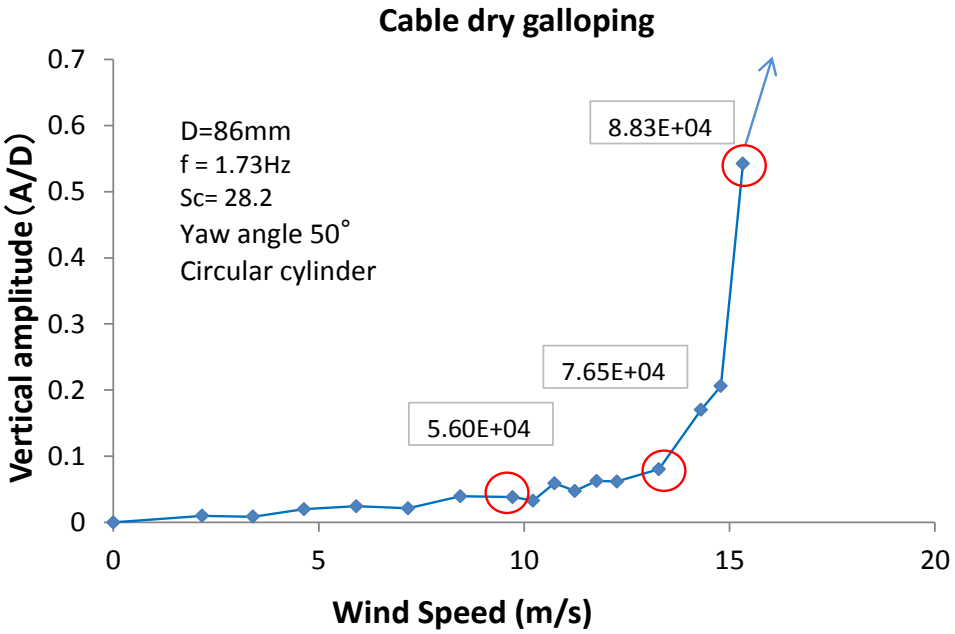

Figure 4-8 Pressure measurement points

The distribution of mean surface pressure (C_p) around the cable surface at different sections shows as Figures 4-9, 4-10, 4-11 and 4-12. Generally, large negative pressure can be seen at around flow separation points and the small recovery of the pressure in the leeward surface for plain cable. Especially, when wind speed was around 15.32m/s equivalent to Reynolds number around $8.83x10^4$, there was a stronger recovery compare to the case of 9.72 and 13.38m/s. The forces coefficients at the center position (section A) were obtained by integration of the surface pressure around the cable model. The drag force coefficient at yaw angle around 50° tended to go down with increase of Reynolds numbers as Figure 4-13. It reached the value of 0.4 where the point before DG occurred. At the same time, there is a little change of the lift force coefficient as Figure 4-14. Moreover, the pressure distribution in presence of spiral protuberance can be referred as Appendix 2.

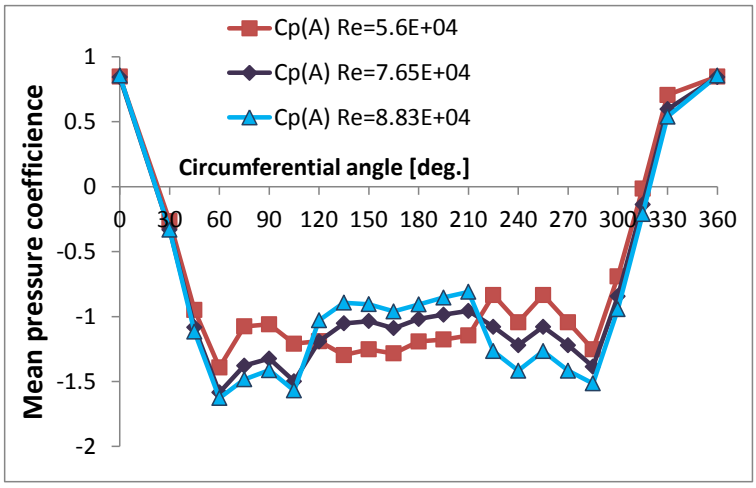

Figure 4-9 Pressure distribution at center section, (circular cable, yawed angle 50°)

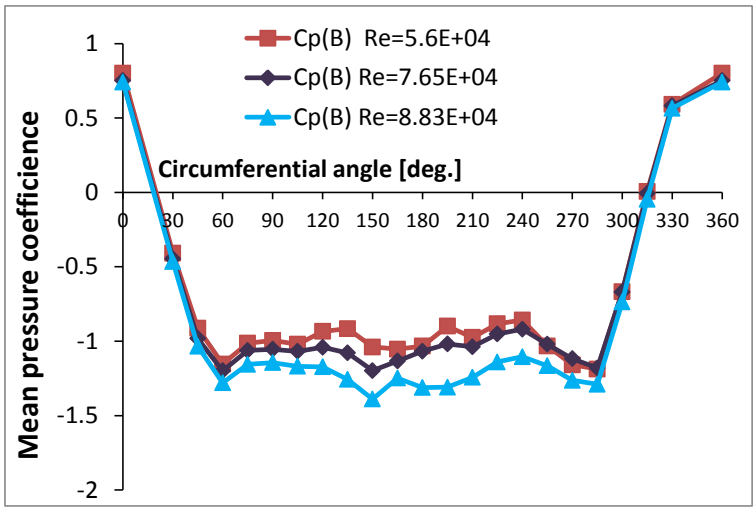

Figure 4-10 Pressure distribution at quarter section (circular cable, yawed angle 50°)

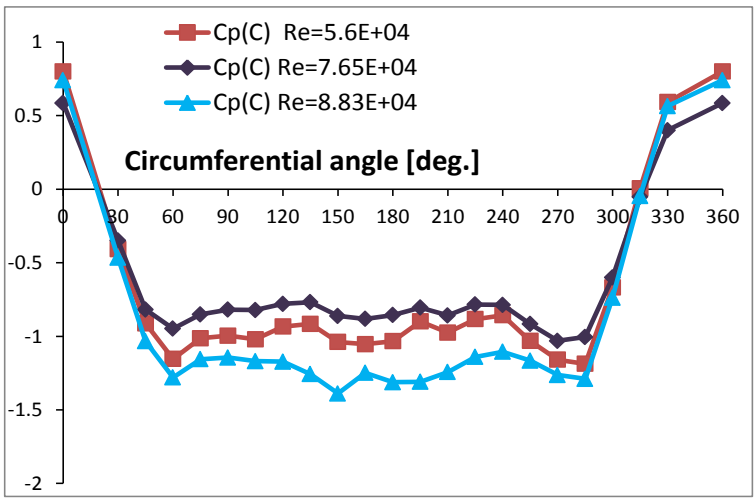

Figure 4-11 Pressure distribution at section C (circular cable, yawed angle 50°)

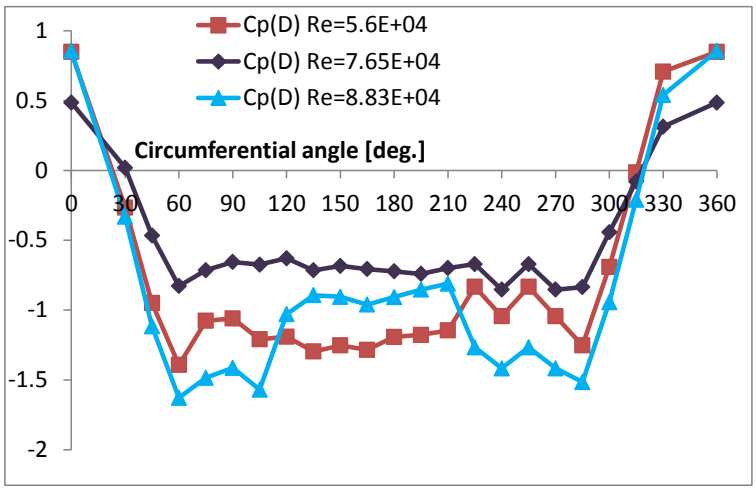

Figure 4-12 Pressure distribution at section D (circular cable, yawed angle 50°)

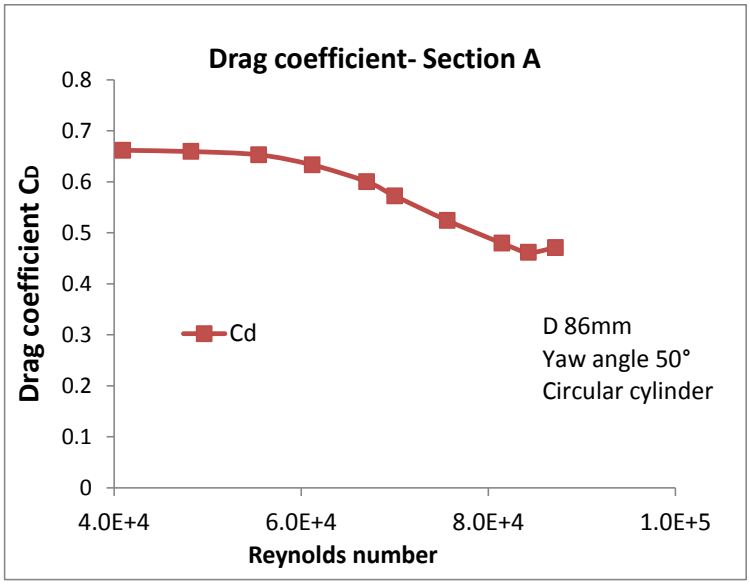

Figure 4-13 Drag force coefficient with Reynolds number

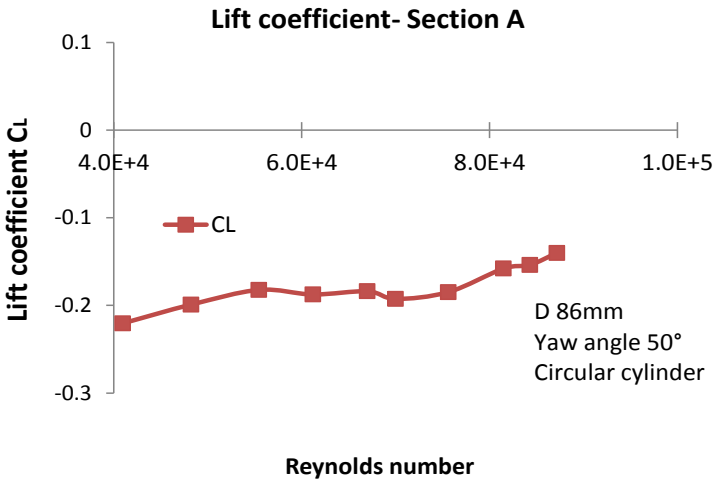

Figure 4-14 Lift force coefficient with Reynolds number

4.2.4 Role of axial flow

It is pointed out that axial flow in a wake of cable plays a role in exciting galloping in dry condition[1]. However, the detail of mechanism of axial flow still unknown. To confirm this characteristic, the axial flow velocity (*Va*) was measured by anemometer with smooth surface. The static model was installed at inclined angle 25° and flow angle 30° that was the case of DG took place. Diameter of 158mm was used in this experiment. The axial flow velocity was measured in span-wise direction and stream-wise direction. The measurement plan is illustrated in Figure 4-15a. For measuring the span-wise axial flow velocity, anemometer was located 0.2D from the wake of cable. The measured wind speeds are 5, 10, 15 and 20m/s as Table 4.4. Figure 4-16 elucidates that axial flow velocity distributes non-uniformly and decrease gradually from the upstream cable end to the downstream one. In the upstream cable end, axial flow velocity was around 70-85% of incoming velocity whereas it was 30-40% in the downstream cable end. The distribution pattern seems to be similar to every incoming velocity. In addition, the stream-wise axial flow distribution was also recorded. In this measurement, the anemometer was located at centerline from 0.2D to 2D with steps as Figure 4-15b. According to Figure 4-17, velocity intensity of axial flow in the range from 0.2D to 0.8D seems to be unchanged with high intensity around 60-80%. According to Nakamura [7], the galloping generation mechanism is interruption of communication between upper and lower separated flows. Because communication of two separated flows can tend to make pressure difference on upper and lower surfaces of cylinder zero. Therefore, this strong channel can play the role as a “splitter plate” in the rear side of cable, which can stop the communication between upper and lower flows or suppressing the Karman vortex shedding. In addition, the increasing of wind speed also contributes to improve the separation of lower and upper flows. Consequently, this can excite galloping.

Current finding is consistent with the conclusions of previous study [1, 7]. The dimension of "splitter plate" is illustrated as the red line area in Figure 4-18. The role of axial flow will be discussed more in next sections.

Table 4.4 Axial flow measurement

No.	Location	Wind Speed (m/s)	Inclination	Flow angles	Apparatus	Cable surface
1	2D	5, 10, 15, 20	25	30	Hot wire anemometer	Normal cable
2	3D	5, 10, 15, 20				
3	4D	5, 10, 15, 20				
4	5D	5, 10, 15, 20				
5	6D	5, 10, 15, 20				
6	7D	5, 10, 15, 20				
7	8D	5, 10, 15, 20				

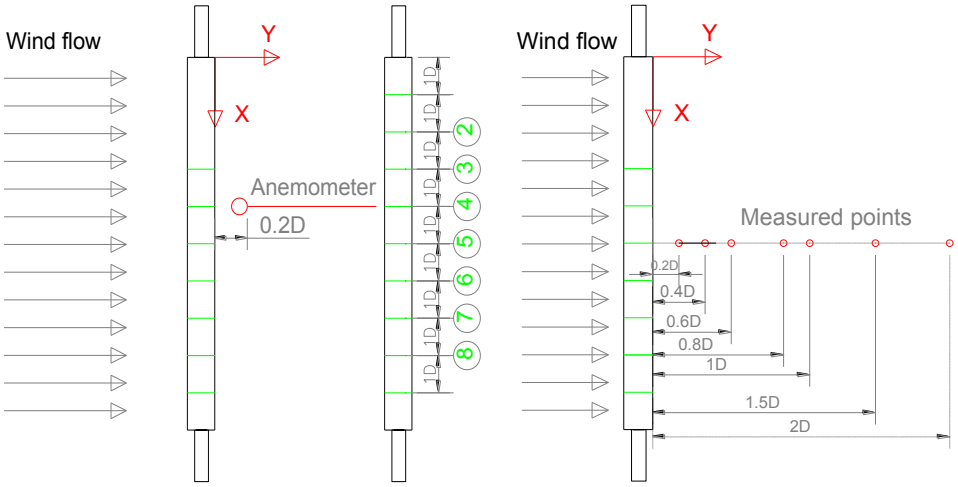

a. Span-wise measurement b. Stream-wise measurement

Figure 4-15 Measurement arrangement for axial flow intensity

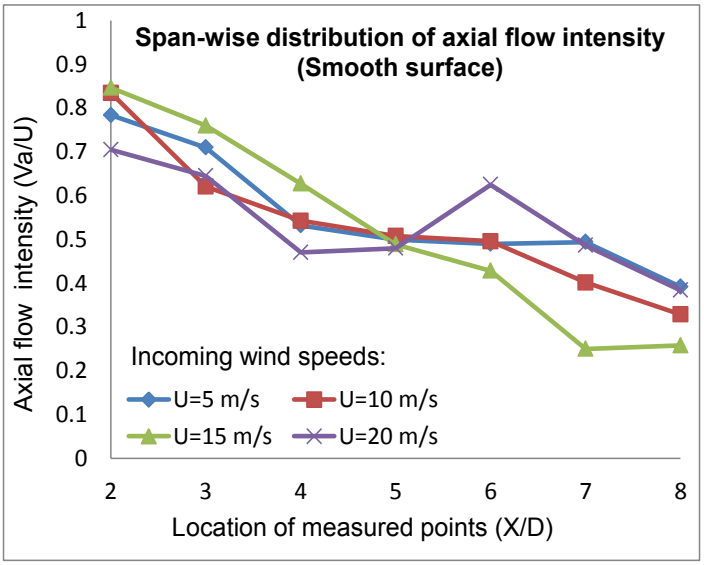

Figure 4-16 Span-wise velocity distribution of axial flow

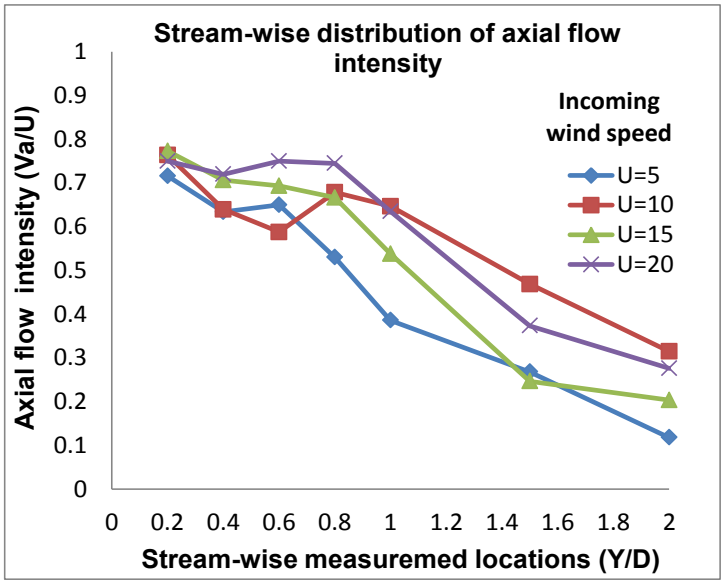

Figure 4-17 Stream-wise velocity distribution of axial flow

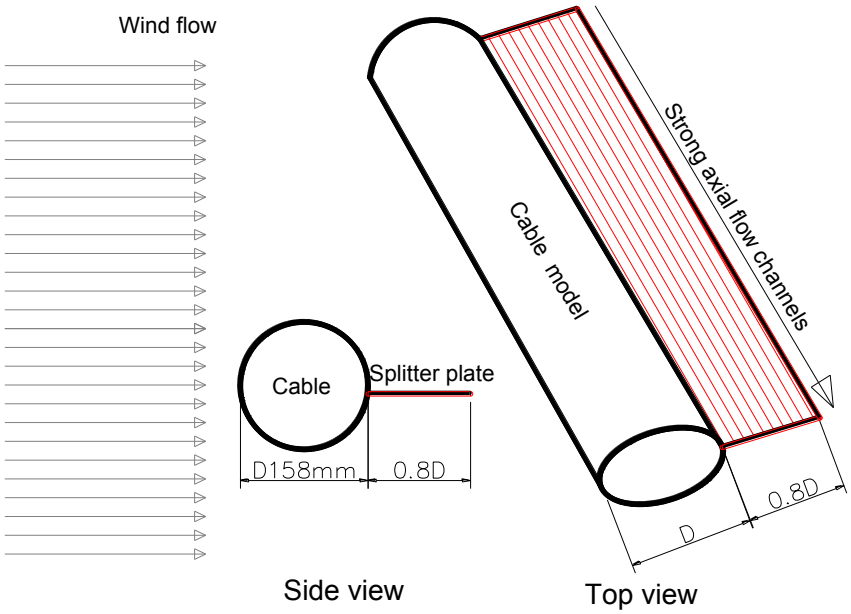

Figure 4-18 Splitter plate dimension

4.2.5 Wake flow mechanism

4.2.5.1 Excitation force from latent low frequency

The fluctuating of wind velocity in the wake of the inclined cable model was recorded along the model. The circular cylinder was mounted in the wind tunnel with flow angle β=30° and inclined angle α= 25°. The hot-wire anemometer was set at 2D from the cable wake and 0.5D from cable axis as shown in Figure 4-19 and its position along the cable direction was varied from the upstream side to the downstream side at the distances

from 2D to 7D. From this set up, fluctuation of wind speed in spatial and time will be measured at different wind speeds.

The power spectrum density (PSD) diagrams of fluctuating wind velocity in vertical direction near the wake along the cable direction are shown in Figure 4-20, 4-21 and 4-22. The mean wind velocities in the wind tunnel are fixed as 5/s 10m/s and 15 m/s respectively. When wind speed at around 5m/s Karman vortex frequency with Strouhal number around 0.2 seem to be dominant. However, as wind speed increase to U=10m/s, the low frequency components, which may be supposed as axial vortex components [8], are observed through span-wise direction. Especially at the downstream side corresponding to 6D and 7D locations, theses low frequency components are extremely dominant. These frequency components correspond to reduced wind velocity around U/f_vD= 110; where f_v is the dominating frequency of fluctuating velocity. This kind of pattern also detected more clearly at wind speed U=15m/s. Further, there are two dominant frequency components: one corresponds to U/f_vD= 110 which probably driven force of dry galloping phenomenon and the other is U/f_vD=60 where supposed for vortex induced vibration at high reduced wind speed[8]. Because both the vibrations apparently differ from the conventional Karman vortex-excited vibration because of the appearance of vibration at much higher reduced wind velocity. Furthermore, this kind of trend also appeared in case of flow angle β=45° and inclined angle α= 25° or β=0° and inclined angle α= 25° as Figure 4-23 and 4-24. In this figure, the wind speed is 20m/s and the low dominant frequency component around U/f_vD= 110. Moreover, the dominant frequency is around 0.6-2Hz, which is close to fundamental frequency of cable, so the vibration can easily occur. This finding is consistent with the DG occurrence range in previous section.

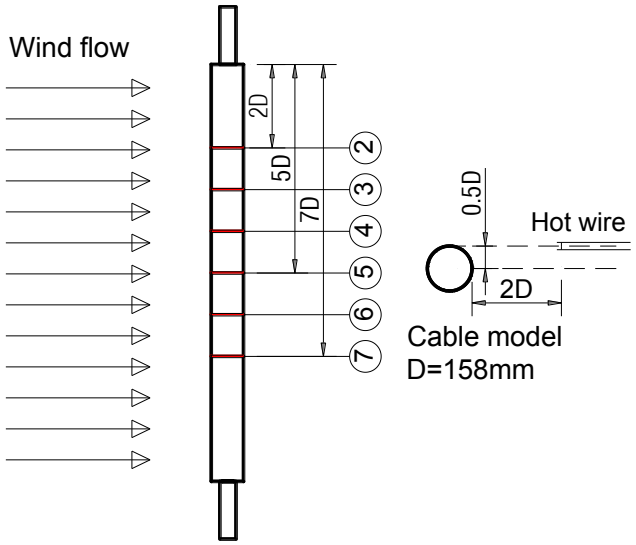

Figure 4-19 Arrangement for measurement wake flow fluctuation

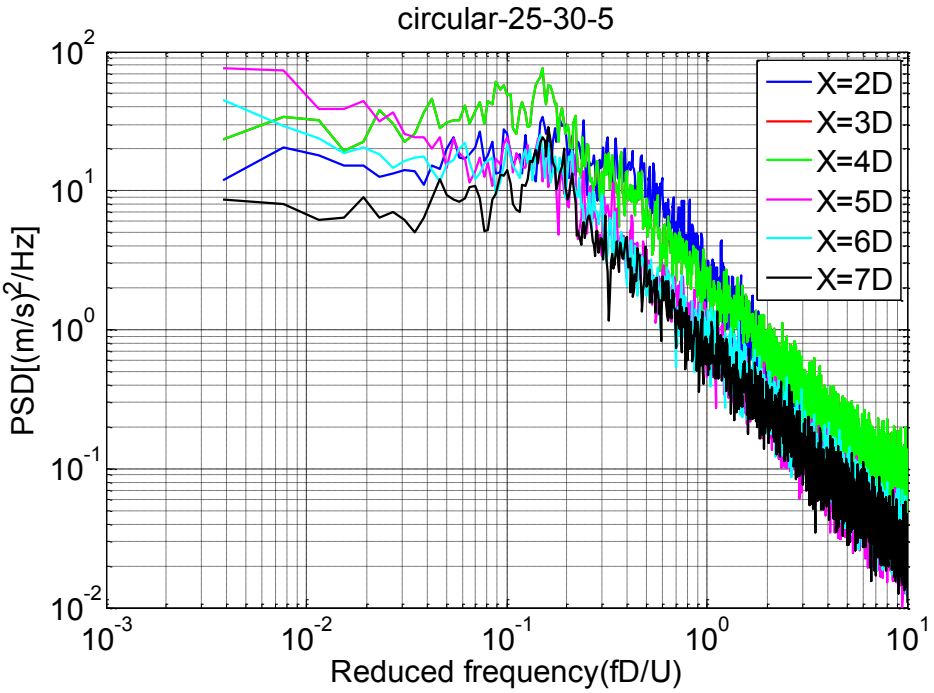

Figure 4-20 PSD of fluctuating wind velocity in the wake of stationary inclined cable. (Smooth flow. U=5m/s, β=30° and α= 25°)

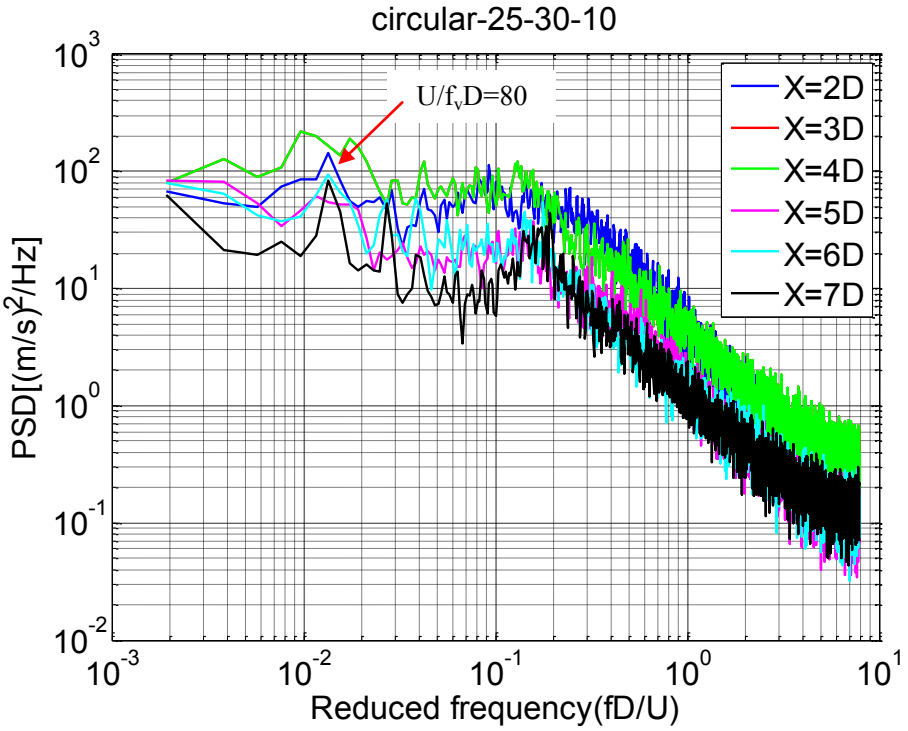

Figure 4-21 PSD of fluctuating wind velocity in the wake of stationary inclined cable. (Smooth flow. U=10m/s, β=30° and α= 25°)

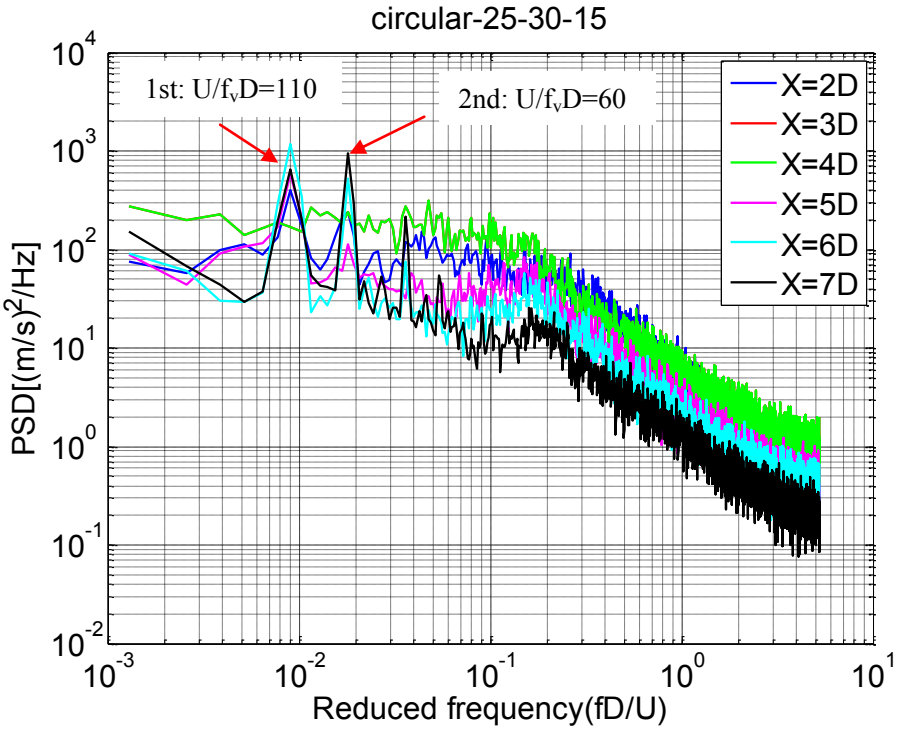

Figure 4-22 PSD of fluctuating wind velocity in the wake of stationary inclined cable. (Smooth flow. U=15m/s, β=30° and α= 25°)

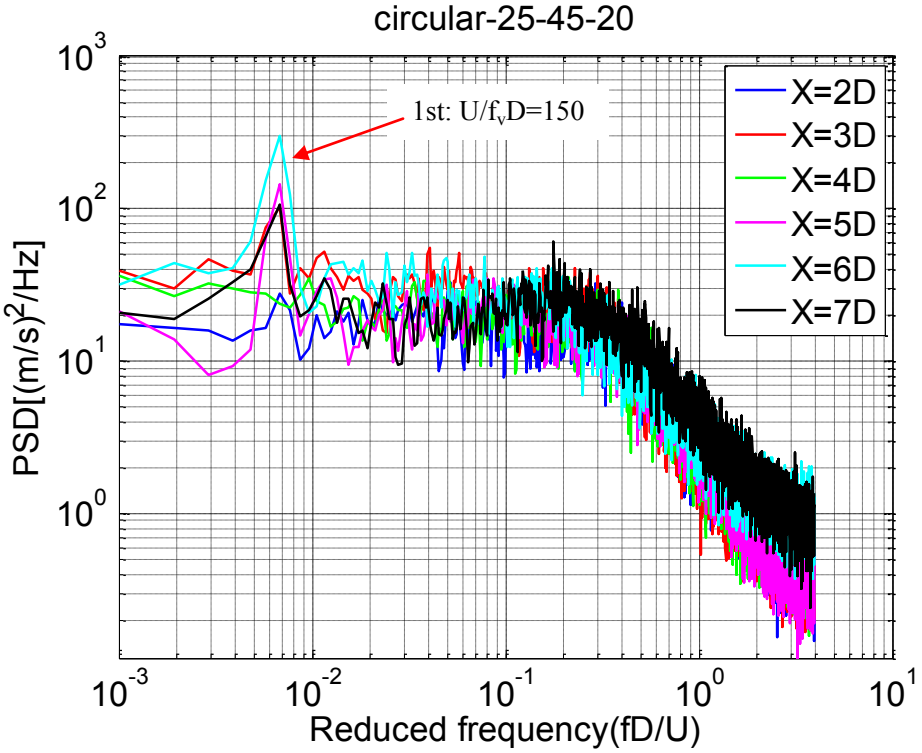

Figure 4-23 PSD of fluctuating wind velocity in the wake of stationary inclined cable. (Smooth flow. U=20m/s, β=45° and α= 25°)

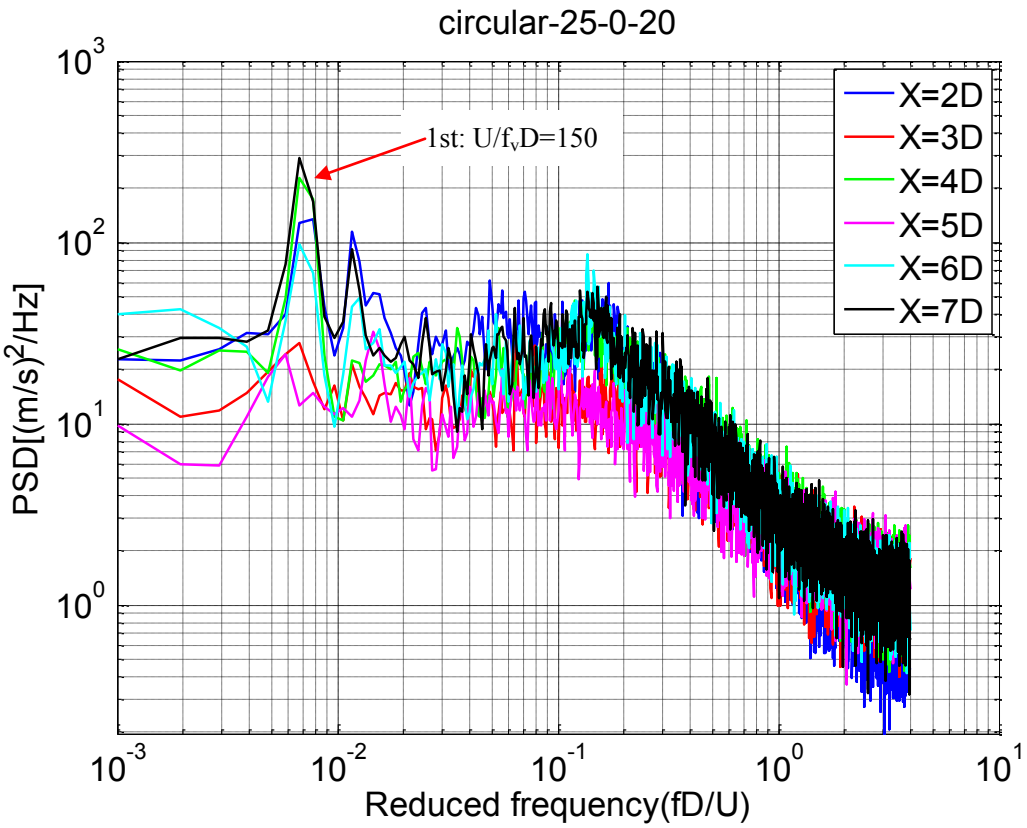

Figure 4-24 PSD of fluctuating wind velocity in the wake of stationary inclined cable. (Smooth flow, D=158mm, U=20m/s, β=0° and α= 25°)

In addition, the wavelet analysis was carried out to observe the variation of the velocity against time as well as the excitation mode, in which Morlet wavelet is mother function. The results are plotted in Figure 4-25 and 4-26. Two peaks for first mode and second mode keep their shapes and magnitude almost unchanged along the time. In addition, the low peak frequency can be observed clearly. Similar trends were found at 2D, 3D, 4D and 5D in Figure 4-27 to 4-30. In addition, there are some frequency peaks with much shorter period region. Since the reduced velocity for these peak is calculated around U/f_vD=5-8, it can be the conventional Karman vortex induced vibration. PSD and wavelet analysis of other wind angles and wind speeds can be seen at Appendix 3 and Appendix 4 respectively. In short, the wake flow fluctuation with very low frequency and it combine with axial flow play important role in DG mechanism. It is obviously that there are many latent low frequencies at high wind speed and they will only appear at high range of wind velocity with high energy. In addition, the wavelet analysis results for the other wind attack angles are showed as Figure 4-31 to 4-34.

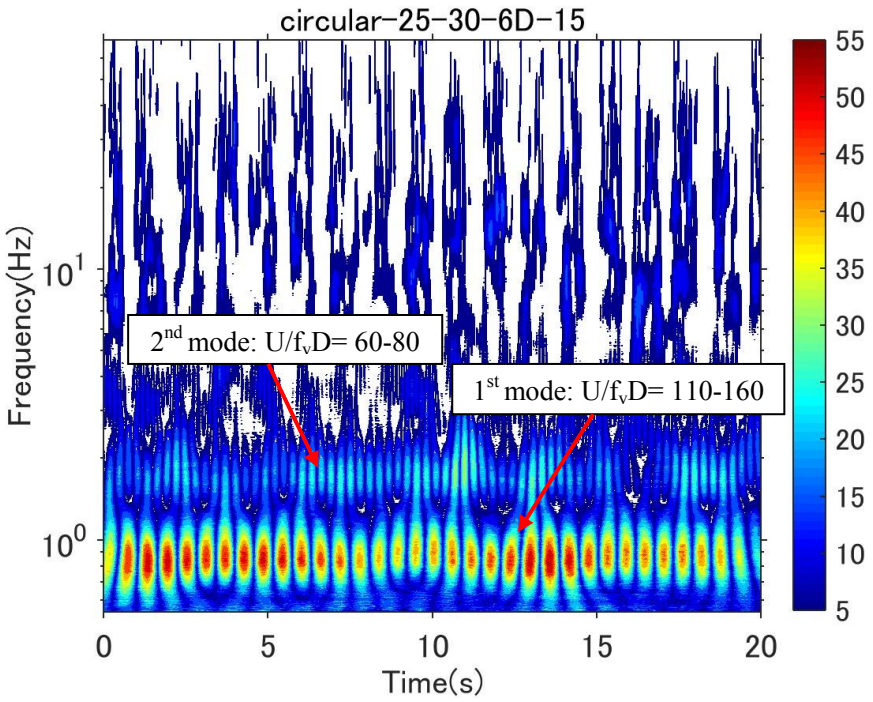

Figure 4-25 Wavelet analysis (WA) of fluctuating wind velocity in the wake of stationary inclined circular cylinder (Smooth flow, Location= 6D, U=15m/s, β=30° and α= 25°)

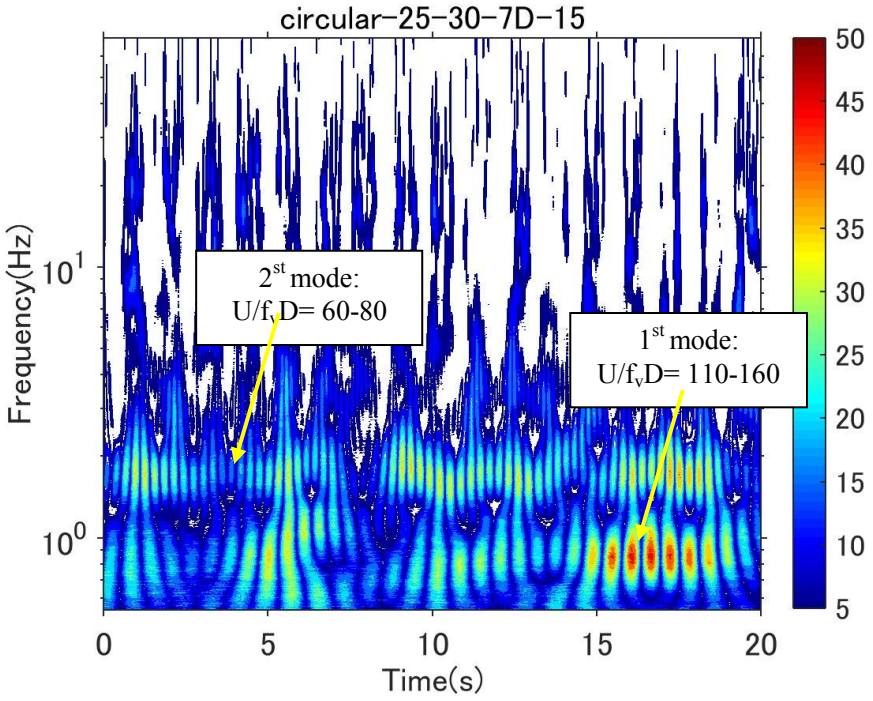

Figure 4-26 Wavelet analysis (WA) of fluctuating wind velocity in the wake of stationary inclined circular cylinder (Smooth flow, Location= 7D, U=15m/s, β=30° and α= 25°)

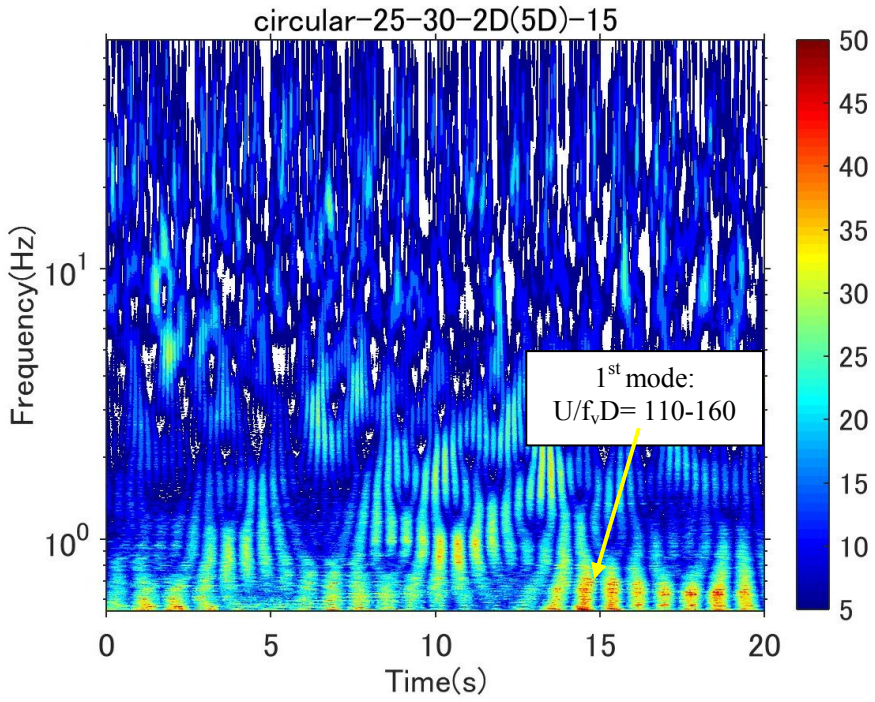

Figure 4-27 Wavelet analysis of fluctuating wind velocity in the wake of stationary inclined circular cylinder (Smooth flow, Location= 2D, U=15m/s, β=30° and α= 25°)

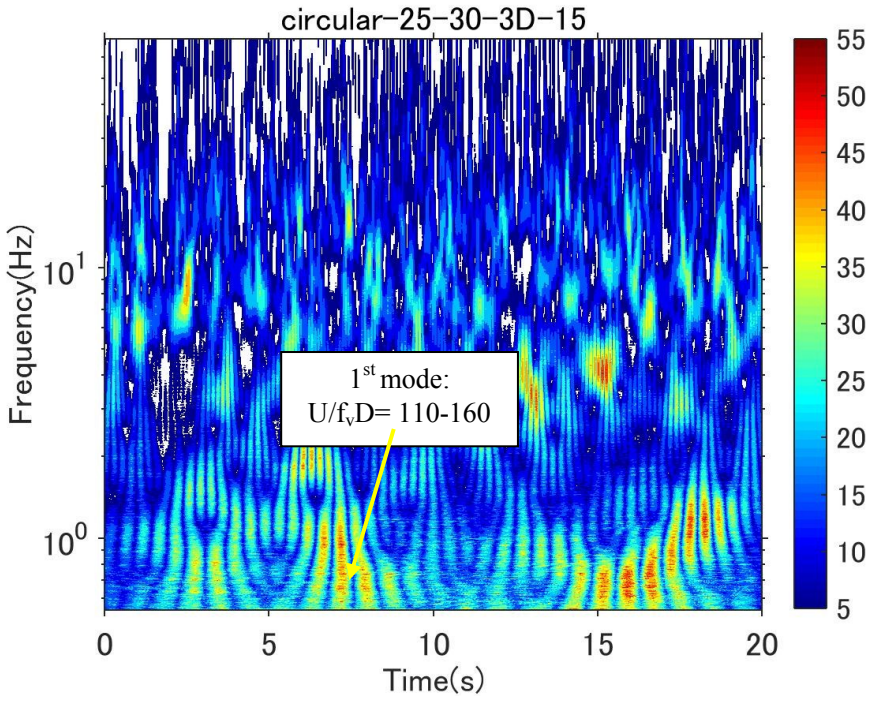

Figure 4-28 Wavelet analysis of fluctuating wind velocity in the wake of inclined circular cylinder (Smooth flow, Location= 3D, U=15m/s, β=30° and α= 25°)

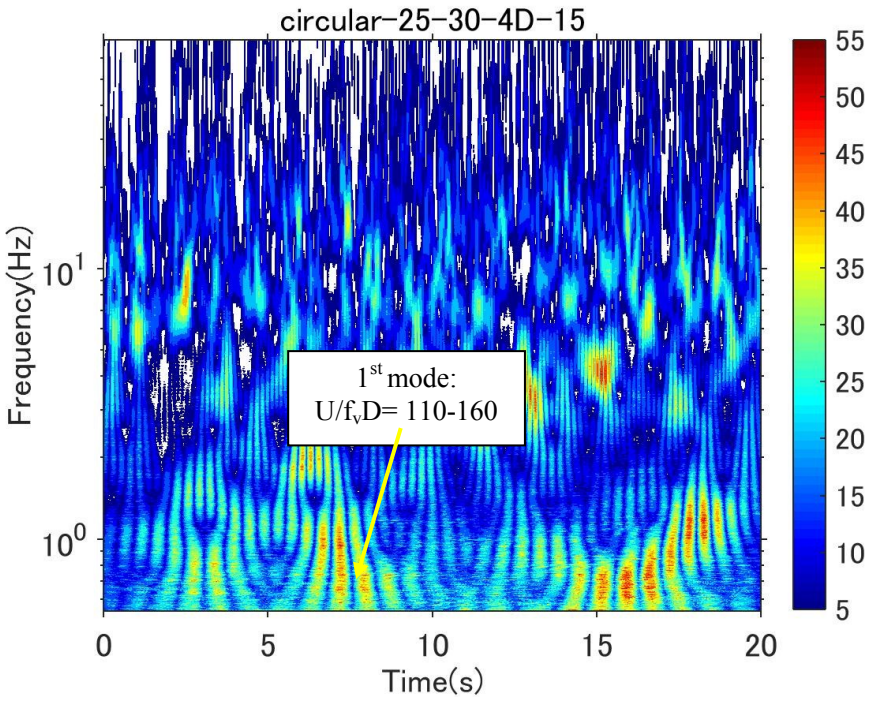

Figure 4-29 Wavelet analysis of fluctuating wind velocity in the wake of inclined circular cylinder (Smooth flow, Location= 4D, U=15m/s, β=30° and α= 25°)

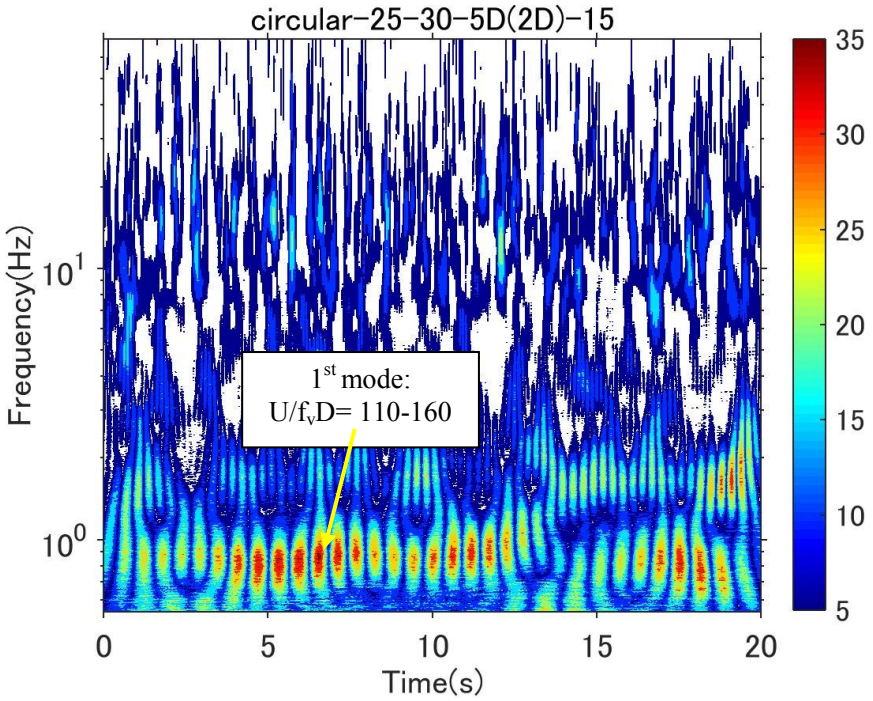

Figure 4-30 Wavelet analysis of fluctuating wind velocity in the wake of inclined circular cylinder (Smooth flow, Location= 4D, U=15m/s, β=30° and α= 25°)

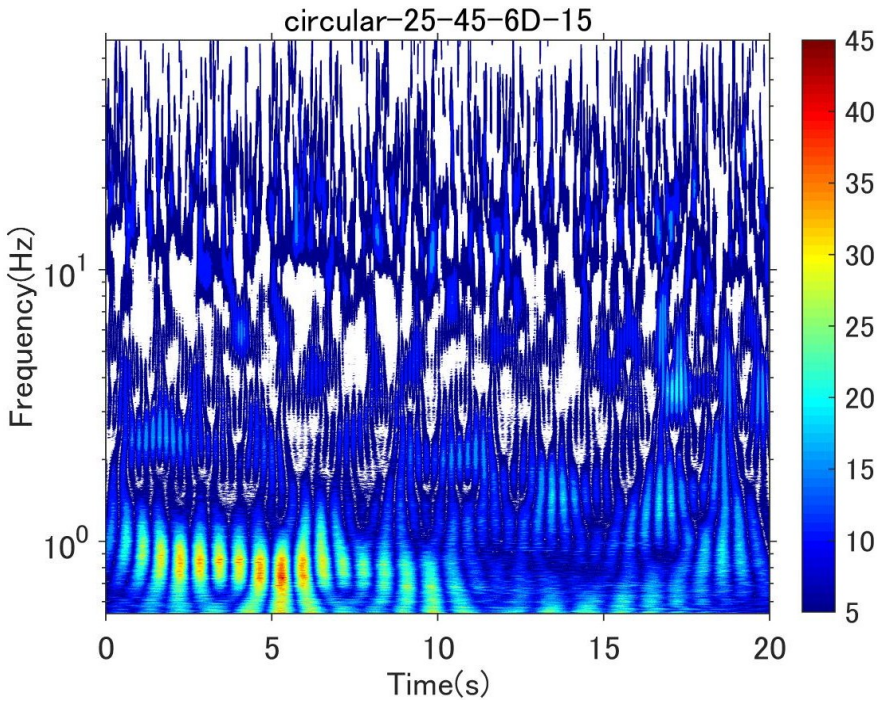

Figure 4-31 Wavelet analysis of fluctuating wind velocity in the wake of inclined circular cylinder (Smooth flow, Location= 6D, U=15m/s, β=45° and α= 25°)

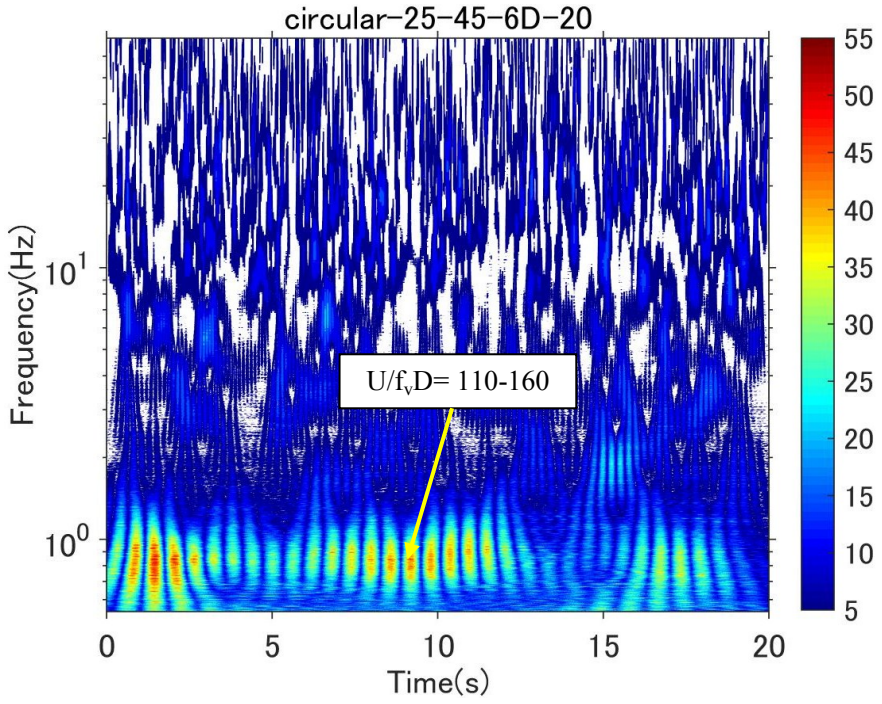

Figure 4-32 Wavelet analysis of fluctuating wind velocity in the wake of inclined circular cylinder (Smooth flow, Location= 6D, U=20m/s, β=45° and α= 25°)

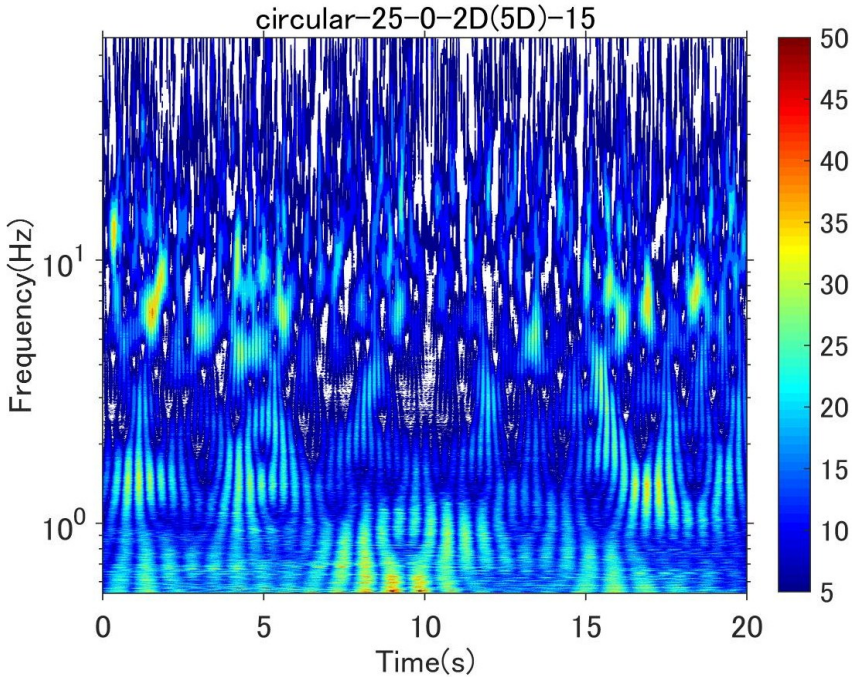

Figure 4-33 Wavelet analysis of fluctuating wind velocity in the wake of inclined circular cylinder (Smooth flow, Location= 2D, U=15m/s, β=0° and α= 25°)

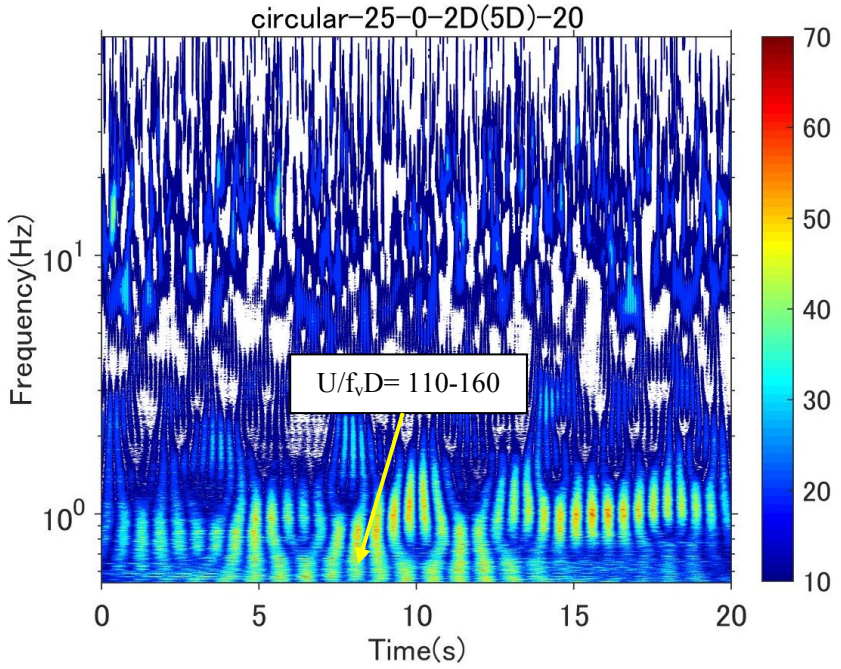

Figure 4-34 Wavelet analysis of fluctuating wind velocity in the wake of inclined circular cylinder (Smooth flow, Location= 2D, U=20m/s, β=0° and α= 25°)

4.2.5.2 Dry galloping generation mechanism

To investigate generation mechanism of dry galloping, normalized power spectrum density at different wind speeds were analyzed. Generally, normalized PSD is obtained by PSD multiplied with frequency and divided by standard deviation. However, frequency

multiplied form is difficult to compare different frequency region, so normalized PSD will be calculated by PSD divide the standard deviation of fluctuating wind speed. According to Figures 4-35 and 4-36, Karman vortex (KV) is mitigated gradually when wind speed went up. In detail, the normalized PSD was around 0.17 at wind speed 5m/s and reduced to nearly a half at U=10m/s, and then it reached around zero at 15m/s. Typically, Karman vortex Strouhal number (fD/U) of circular is around 0.2. When cable normal to the wind and this value a little decrease when cable orientation is yawed and inclined to the wind. In this figure, the Strouhal number was approximate 0.18, which is in normal range. According to former literature, it was pointed out that the generation mechanism of galloping is interruption of communication between upper and lower separated flows. Because the communication of two separated flows can tend to cancel pressure difference on upper and lower surfaces of cylinder. In addition, Karman vortex would be produced by communication of upper and lower separated flows, in another expression, the Karman vortex shedding should promote the communication between two separated flows, the interruption of this communication between two separated flows should be identical to the interruption of Karman vortex shedding. Therefore, it can be explained that mitigation of Karman vortex can excite galloping instability[1, 7]. In parallel with KV interruption found here, low frequency component started dominating when incoming wind increased. Low frequency component contains much of energy can create high excitation force. There was a relationship between forming of low frequency component and interruption of Karman vortex, when Karman vortex decreased, low frequency increased. That means wake flow itself content various latent frequency (Strouhal number), as Karman vortex frequency suppressed, the other Strouhal component will be dominant. The suppression of Karman vortex component can be caused by the effect of “axial flow- splitter plate” or effect of critical Reynolds number or combination of both. According to previous studies [1], as flow reaches to critical Reynolds number, the Karman Vortex is suppressed. This relation of Karman vortex and low dominant frequency also were confirm by different locations along cable and different cable orientations as shown in Figures 4-37and 4-38.

In summary, possible dry galloping’s generation mechanism can be summarized as follow: when wind speed is high enough, Karman vortex will be interrupted by effect of axial flow and the flow will enter critical Reynolds regime. At this time, flow pattern will becomes unstable and its regularity will be lost. It leads to the flow separation will not synchronize periodically at some locations. Consequently, low frequency flow/vortices will be appeared with high energy, which can excite dry galloping.

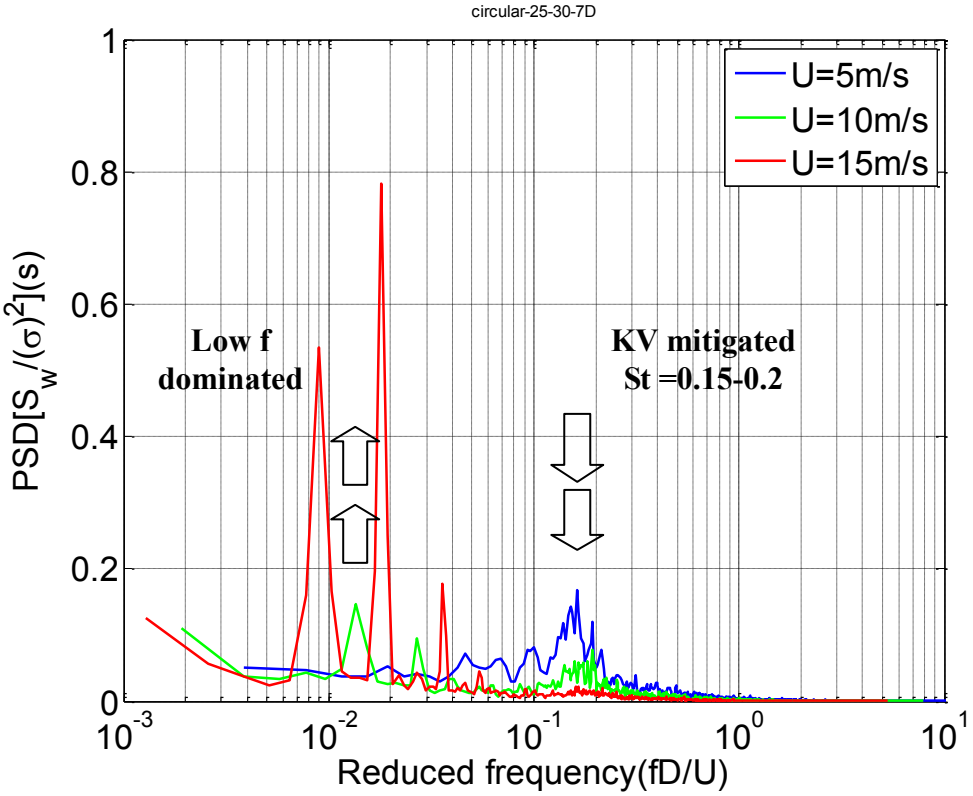

Figure 4-35 Normalized PSD (Location 7D, D=158mm, β=30° and α= 25°)

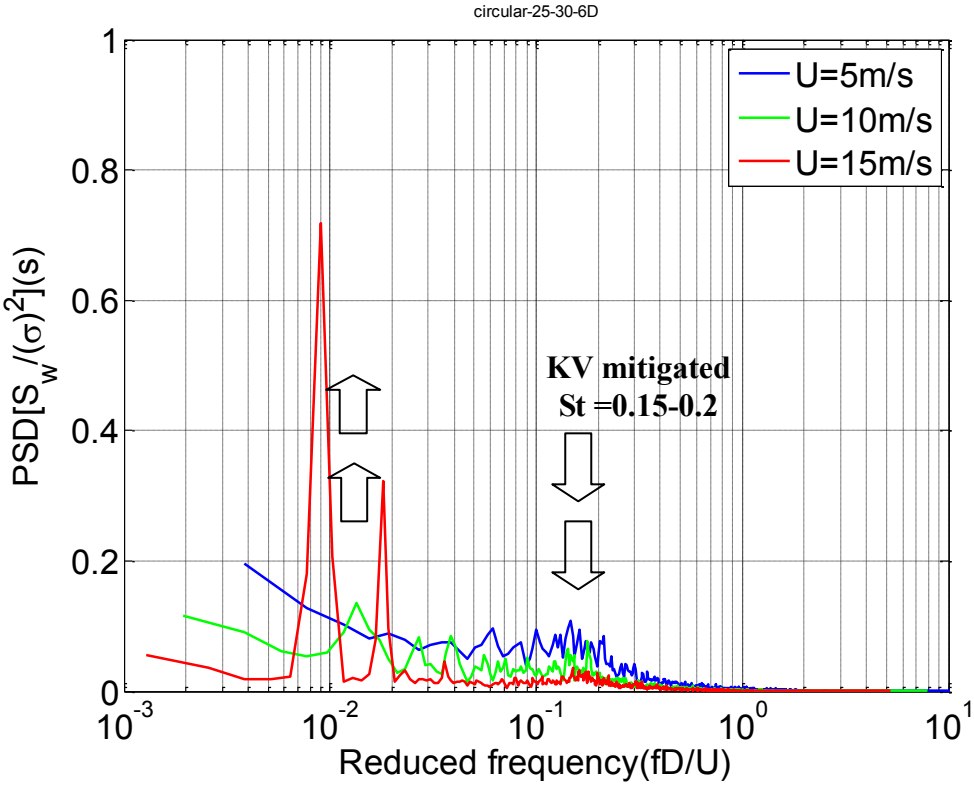

Figure 4-36 Normalized PSD (Location 6D, D=158mm, β=30° and α= 25°)

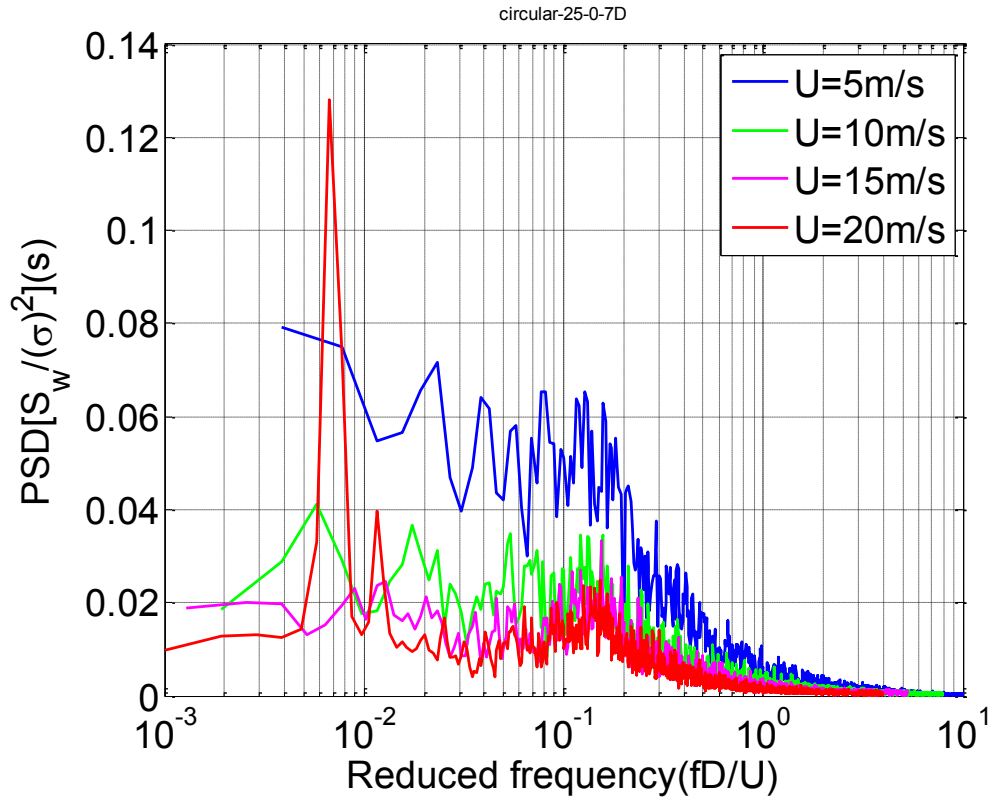

Figure 4-37 Normalized PSD (Location 7D, D=158mm, β=0° and α= 25°)

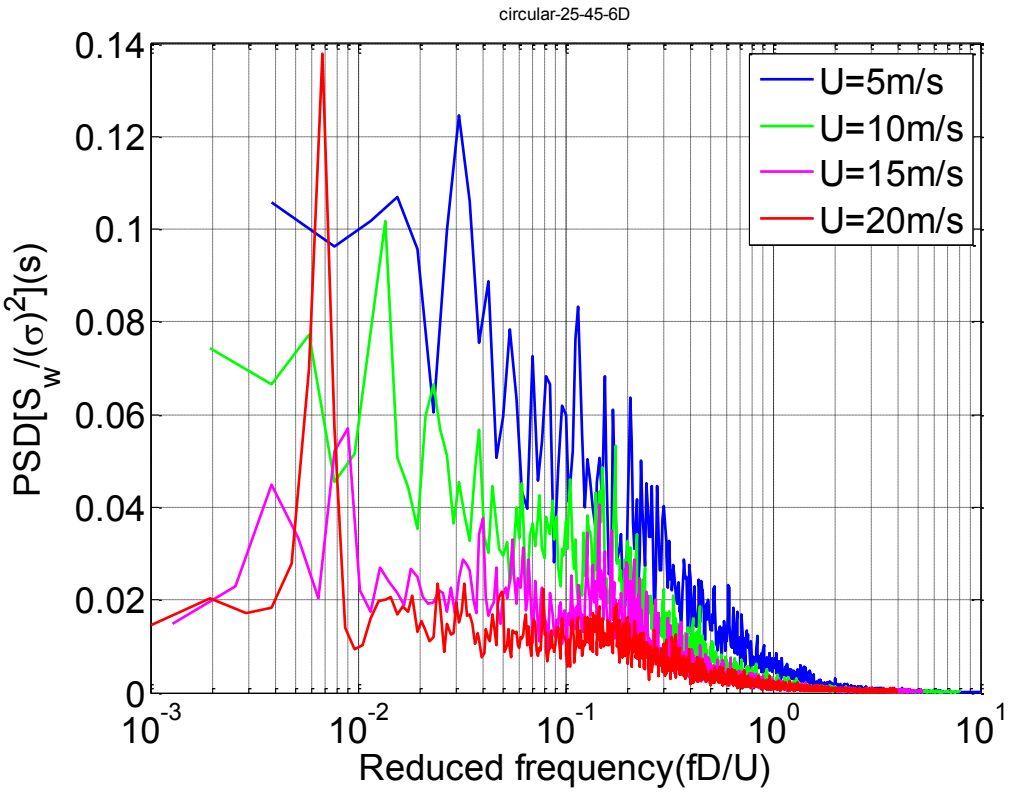

Figure 4-38 Normalized PSD (Location 6D, D=158mm, β=45° and α= 25°)

4.2.5.3 High shedding ccorrelation of low frequency component

In order to clarify the correlation of wind speed fluctuation, the coherence of each two locations at the cable wake were measured with two hot wire anemometers (as Figure 4-23). Coherence, γ^2 , is a non-dimensional form of the cross-spectral density and is denoted by:

$$\gamma^2_{u_1u_2}(f) = \frac{\left|S_{u_1u_2}(f)\right|^2}{S_{u_1u_1}(f) \times S_{u_2u_2}(f)} \leq 1 \tag{4.2}$$

If $\gamma^2_{u1u2}(f) = 0$ at a particular frequency, then $u_1(t)$ and $u_2(t)$ are incoherent or uncorrelated at that frequency). If $u_1(t)$ and $u_2(t)$ are independent random signals, then $\gamma^2_{u1u2}(f) = 0$ for all frequencies. This function shows the same decay behavior as the autocorrelation and cross-correlation coefficients. Besides that, the cross spectral density is the frequency domain equivalent of the cross-covariance function. It contains the same information about correlation, frequency content and relative phases of the same frequencies in the two signals. The coherence can therefore be used to define a region where the two signals are significantly related [9]. The correlation of wake flow are illustrated in Figure 4-39, 4-40 and 4- 41. It is obviously that the correlation of at low frequency (Strouhal number <<0.2) was high at wind speed around 15m/s in case of orientation β=30° and α= 25°. This correlation was very low at wind speed 5m/s and 10m/s. Besides that, this kind of result is consistent with Wavelet analysis and PSD results. In case of 15m/s of wind speed, the low reduced frequency band (fD/U) from 0.006-0.01 equivalent to U/fD=100-165 exhibited very high correlation with coherence (γ^2) more than 0.5 between 2D and 6D or 2D and 7D. In addition, the correlation at vortex induced vibration frequency also high around 0.6 for case 4D-5D. Furthermore, this kind of tendency also found at the wind angle β=0°&45° and α= 25° as Figures 4-42, 4-43 and 4-44. In conclusion, the fluctuation of wind speed with low band frequency with high energy, shedding with high correlation can cause much of excitation force and it therefore can trigger the cable galloping. This kind of tendency only appeared at high wind speed around 15m/s, 20m/s or higher. The existence of this fact is consistent with the cable response at relative high wind speed. The correlation of wake flow in span-wise direction of the other wind angle such as (β=45° x α= 25°) and (β=0; α= 25°) can be referred in Appendix 5.

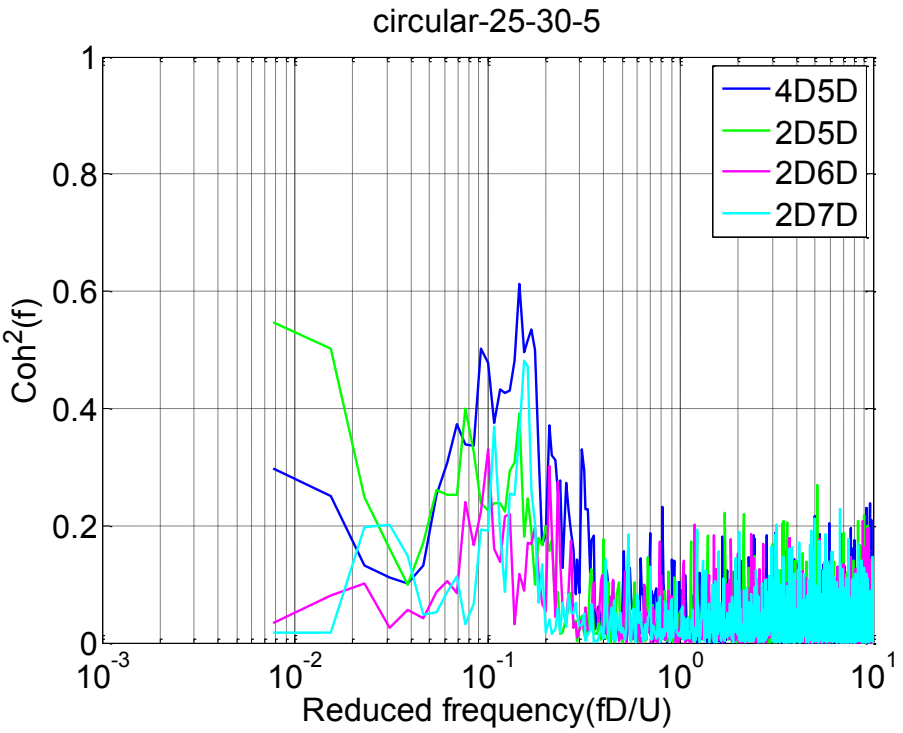

Figure 4-39 Correlation of wake flow (Smooth flow, U=5m/s, β=30° and α= 25°)

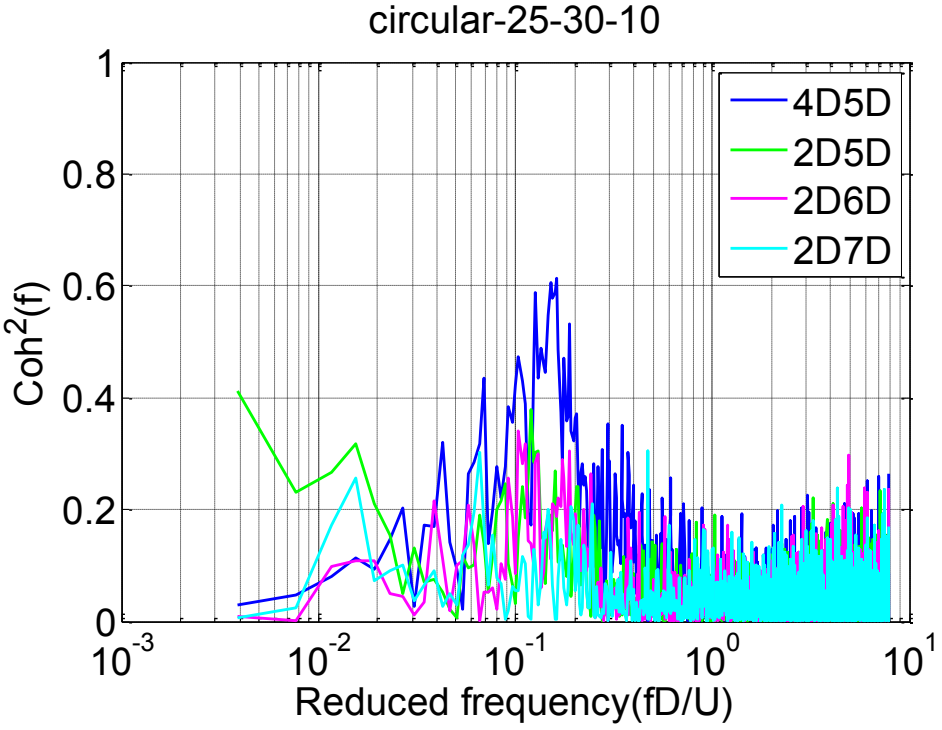

Figure 4-40 Correlation of wake flow (Smooth flow, U=10m/s, β=30° and α= 25°)

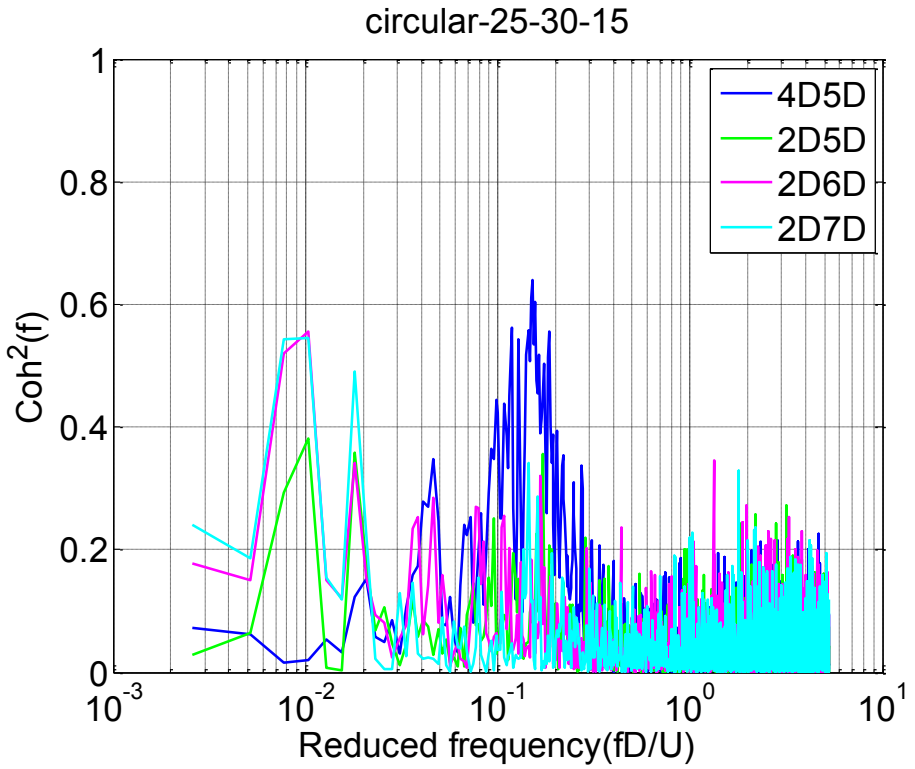

Figure 4-41 Correlation of wake flow (Smooth flow, U=15m/s, β=30° and α= 25°)

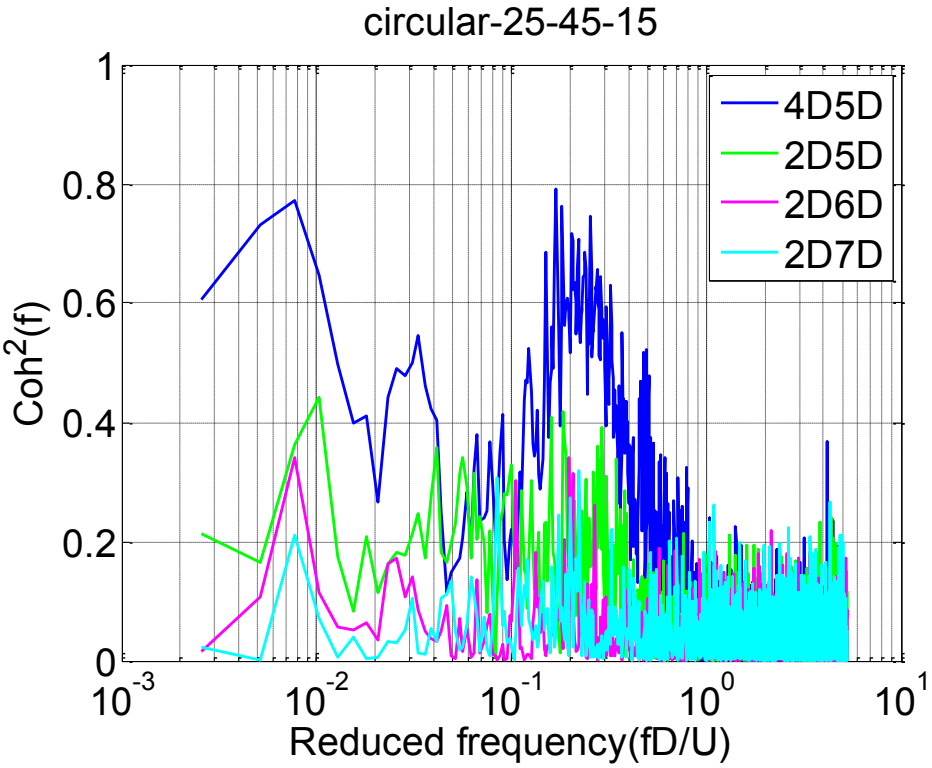

Figure 4-42 Correlation of wake flow (Smooth flow, U=15m/s, β=30° and α= 25°)

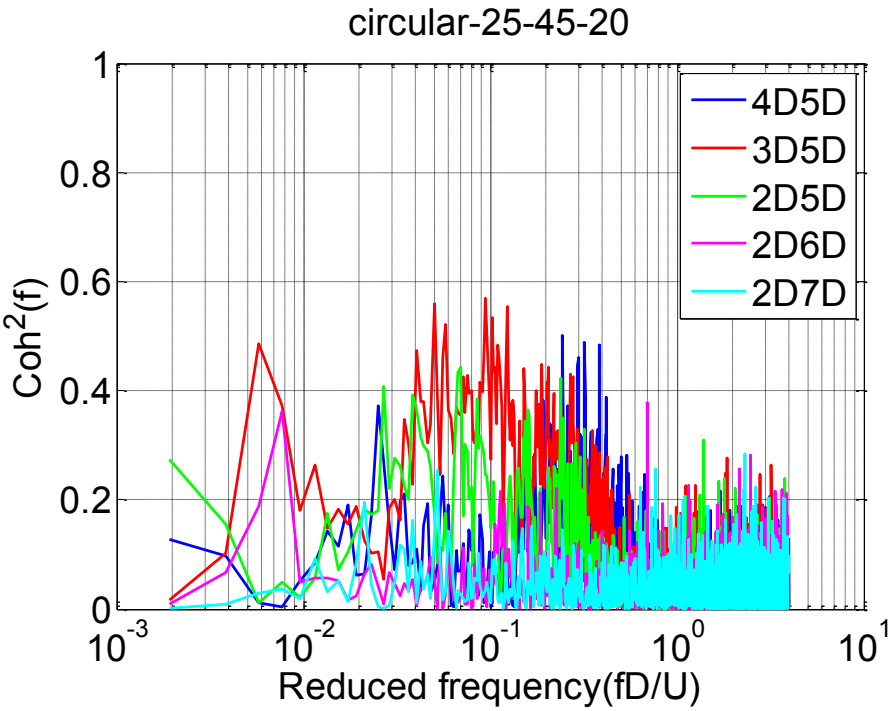

Figure 4-43 Correlation of wake flow (Smooth flow, U=20m/s, β=45° and α= 25°)

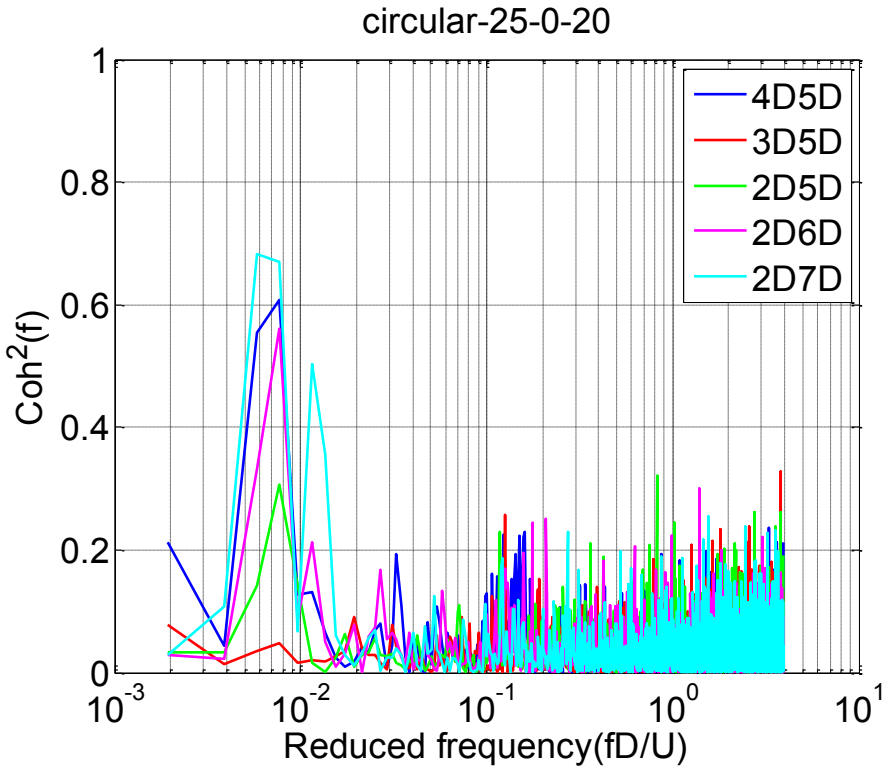

Figure 4-44 Correlation of wake flow (Smooth flow, U=20m/s, β=0° and α= 25°)

4.2.6 Aerodynamic damping characteristic of DG

Divergent galloping of a stay cable is associated with the occurrence of negative aerodynamic damping. As aerodynamic damping significant enough to overcome the positive structural damping, it will result in negative effective damping of the cable. However, actual structural damping for limited amplitude vibrations was only approximate 0.03% [10]. Moreover**,** it was found that for a certain cable-wind attack angle region, the symmetry and the characteristics of the flow field are altered and negative aerodynamic damping may occur [11]. To evaluate the aerodynamic damping ratio in dry condition, the model was manually excited and the free-vibration decay recorded using two accelerators at cable ends. The tests were performed in-plane directions for various steps in velocity, ranging from U=0-20m/s with around 0.5-1m/s intervals. The aerodynamic damping ratio of the cable model (ζ_a) was determined by subtracting the damping of the rig measured at zero wind velocity (ζ_s) from the total measured damping (ζ) as equation (4.2). The detail of aerodynamic damping calculation can refer at Table 4.5 and Table 4.6.

$$\zeta_a = \zeta - \zeta_s \tag{4.3}$$

Figure 4-45 and 4-46 illustrates the aerodynamic damping ratio of circular cable model with diameter 110mm and 158mm at inclined angle 25° and flow angle 30°. Generally, aerodynamic damping fluctuated from 0% to 0.3%. The maximum value is at around 100 of reduced wind speed. Further, it tends to reduce when reach to the dry galloping occurrence area. The negative damping (around -0.02% and -0.12%) was found at 208 of reduced wind speed for 110mm and at reduce wind speed 146 for 158mm case, this wind speed is where coincides with the area that dry galloping started occurring. In addition, low aerodynamic damping value (less than 0.03%) were found in several cases, so this proved that why limited amplitude vibration occurred for many cases. It means that dry galloping is one of dangerous vibration because the negative damping type galloping always associated with divergent type galloping.

Table 4.5 Aerodynamic damping in dry condition, D110mm

No.	U (m/s)	Ur	Total δ	Total ζ	ζa
1	0	0.00	0.008	0.12%	0.00%
2	3.07	33.13	0.015	0.24%	0.12%
3	3.56	38.38	0.016	0.25%	0.13%
4	4.05	43.66	0.016	0.25%	0.14%
5	4.54	48.93	0.015	0.24%	0.12%
6	5.53	59.58	0.019	0.30%	0.18%
7	6.03	64.97	0.024	0.38%	0.26%
8	6.52	70.24	0.022	0.35%	0.23%
9	7.02	75.67	0.023	0.37%	0.25%
10	7.52	81.03	0.022	0.35%	0.23%
11	8.52	91.83	0.018	0.29%	0.17%
12	9.53	102.67	0.025	0.40%	0.28%
13	10.53	113.44	0.020	0.31%	0.19%
14	11.04	118.99	0.025	0.40%	0.28%
15	12.53	135.00	0.016	0.25%	0.14%
16	13.54	145.94	0.010	0.16%	0.04%
17	14.54	156.64	0.009	0.14%	0.02%
18	16.03	172.70	0.010	0.15%	0.03%
19	16.77	180.70	0.008	0.13%	0.01%
20	19.36	208.67	0.007	0.10%	-0.02%

Table 4.6 Aerodynamic damping in dry condition, D158mm

No.	U (m/s)	Ur	Total δ	Total ζ	ζa
1	0	0.00	0.009	0.14%	0.00%
2	4.31	30.85	0.015	0.24%	0.10%
3	5.55	39.67	0.018	0.29%	0.15%
4	7.04	50.36	0.018	0.29%	0.15%
5	8.04	57.48	0.015	0.24%	0.10%
6	10.06	71.92	0.020	0.32%	0.18%
7	11.06	79.13	0.018	0.29%	0.15%
8	12.08	86.37	0.018	0.29%	0.15%
9	13.07	93.50	0.017	0.27%	0.13%
10	14.06	100.52	0.020	0.32%	0.18%
11	15.08	107.82	0.012	0.19%	0.05%
12	16.05	114.79	0.011	0.18%	0.04%
13	16.83	120.39	0.014	0.22%	0.09%
14	18.02	128.85	0.010	0.15%	0.01%
15	19.26	137.74	0.010	0.16%	0.02%
16	20.51	146.64	0.001	0.02%	-0.12%

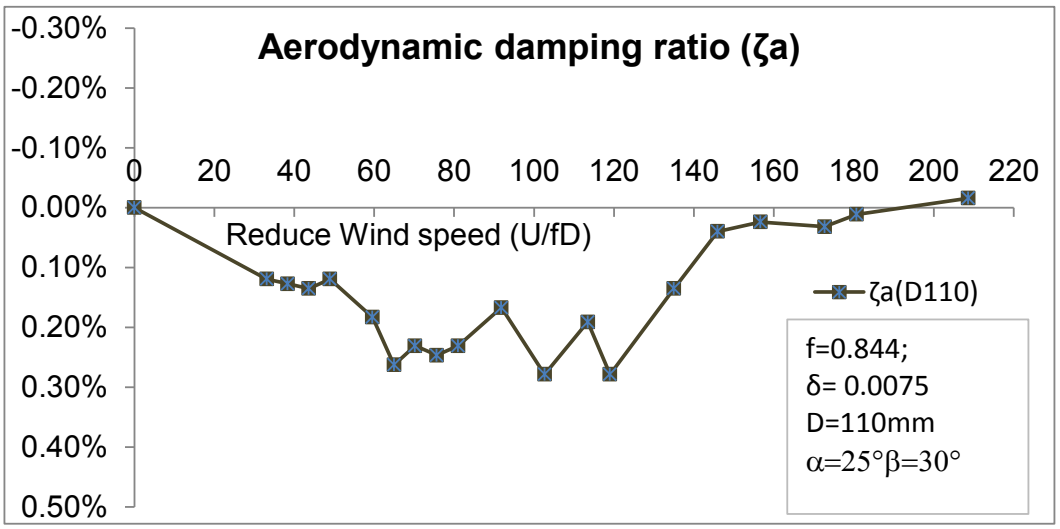

Figure 4-45 Aerodynamic damping ratio at 25° x 30°, D110mm

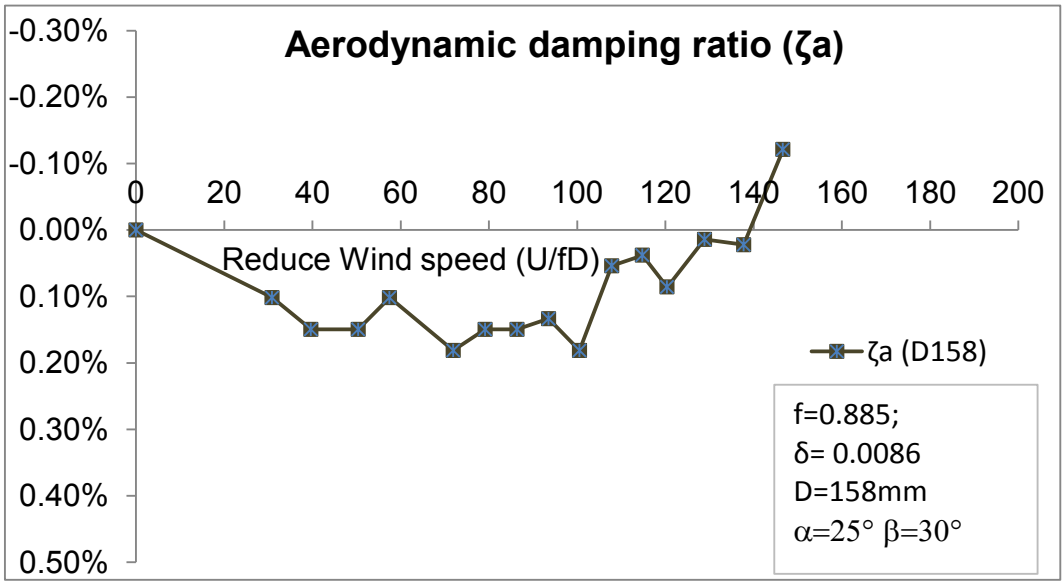

Figure 4-46 Aerodynamic damping ratio at 25° x 30°, D158mm

4.3 Effect of Indented surface and parallel protuberances in low Scruton number

After the RWIV was figured out as a dangerous vibration, which can cause the harmfulness of cable attachment and bridge deck, wind-resistant design of stay cables always requires a countermeasure versus rain-wind induce vibration. Indented surface and parallel protuberance cables used to develop for this aim. The main purpose of these countermeasures is rain rivulet destruction, leading to the suppression of rain-wind induce vibration. Indented surface was the first applied to Tatara Cable-stayed Bridge and later to

the Sutong Bridge and Stonecutters Bridges. This control method was initially proposed by Miyata et al.[12]. In order to eliminate the rain rivulet, dimples were made on the cable surface with a specific scale and arrangement. It has been also found to improve the stabilization of cable under rain-wind interaction with low drag force, around 0.6. In the similar scenario, parallel protuberances initially applied in Higashi Kobe Bridge. This countermeasure uses twelve of fillets along cable to control the forming of upper and lower rivulets, and then it can stop rain-wind induce vibration. The main defectiveness of parallel protuberance is that drag force is very high compare to indented surface. When compared the characteristics of dry-galloping between normal and indented cable surface, Katsuchi and Yamada [13] found that the indented cable could not mitigate the dry-galloping effectively, in which large amplitude vibration still occurred. In addition, Hojo et al [14] also carried out experiment for indented cables with Scruton number around 21, they concluded that large amplitude vibration continued appearing. Moreover, it was also reported that very large amplitude vibration, approximately 30cm, still occurred for parallel protuberance cable as Figure 2-17 in chapter 2[15]. This kind of vibration could not blame for rain wind induced vibration due to the rivulet could not form on the cable surface. On the other hand, the aerodynamic responses in low Scruton number of these modifications have not been clarified fully yet. In this section, aerodynamic responses of indented surface and parallel protuberances will be clarified with various conditions. Then, the axial flow in the wake of cables will be measured and discussed.

4.3.1 Material and method

4.3.1.1 Experiment

The setting up of wind tunnel tetst were as Figure 4-47. The model was fabricated same type with prototype cable with diameters 110mm and 158mm respectively. The flow conditions were measured at cable model position by hot wire anemometer and turbulence intensities of 0.48–0.62% were recorded for 25%, 50% and 100% of maximum wind speed. The supporting system and experimental facilities were similar to the describes in previous section.

Figure 4-47 Test for Indented surface

4.3.1.2 Models fabrication

Two models were investigated, included a HDPE cylinder with parallel protuberances and a HDPE cylinder with indented surface. The model samples were fabricated with same scale to prototype one. Cable diameters are 110mm and 158mm with an effective model length of 1.5 m, the aspect ratio is 13.6 and 9.5, respectively. The indented surface was fabricated same pattern of stayed-cables of Tatara stayed cable Bridge while a parallel protuberance cable was fabricated similarly to Higashi Kobe Bridge cables by adding the twelve rubber fillets. The detail of surface modification can be seen as Figure 4-48 and 4-49.

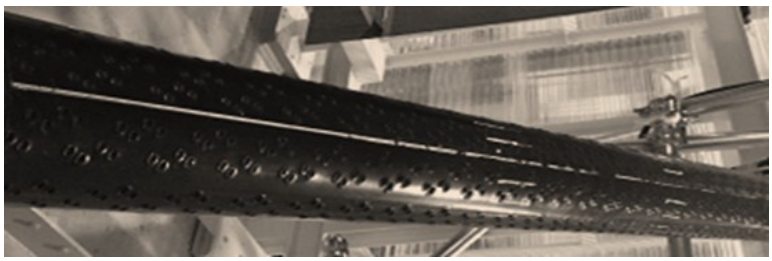

Figure 4-48 Indented surface cable

Figure 4-49 Parallel protuberance cable

4.3.1.3 Test parameters

Table 4.7 shows the detail of experiment parameters in which cable diameters are 110mm and 158mm. Logarithm decrement ranges from approximately 0.005 to 0.012 and natural frequency is around 0.77 - 1.01 Hz in considering typical stay cables values of prototype bridges. Due to the limitation of wind tunnel capacity, maximum wind speed is up to 20m/s, equivalent to Reynolds number around 2.1×10^5. Nevertheless, according to previous studies DG of inclined cable could be observed in the subcritical Reynolds number regime as well as in the transition and critical Reynolds number regime. Moreover, Scruton number ($2m\delta/\rho D^2$) is a non-dimensional parameter that characterizes the mass and damping properties of a flexible body. In this study, Scruton number range from 3.26 to 15.57 where is quite low damping region. The further detail of parameters can be seen in Appendix 6.

Table 4.7 Conditions of experiment

Diameter: D (mm)	110 and 158
Effective length (mm)	1,500
m (kg/m)	8.18 – 8.84 (D110 mm); 9.86 – 10.89 (D158 mm)
Natural frequency (Hz)	0.77 – 1.01
Logarithm decrement	0.005-0.012
Scruton number ($2m\delta/\rho D^2$)	3.26 – 15.57
Reynolds number	0- 2.1×10^5

4.3.2 Unstable vibration in low Scruton number range

4.3.2.1 Indented surface cable

Indented surface has been applied for some cable-stayed bridges in Japan and East Asia. Tatara cable stayed Bridge that connects the islands of Honshu and Shikoku was the first case applying the indented surface cable. Nevertheless, it is pointed out that this modification type could not suppress well DG particularly in a low Scruton number condition [13, 14]. Hence, the main purpose of the present test is to examine mitigation efficiency for wind induced cable vibration with and without precipitation. Figure 4-50 and 4-51 illustrate the aerodynamic responses of indented surface in dry condition. Generally, mostly divergent vibration was mitigated, except unexpected cases of the inclined angle (α) 25° with the flow angle (β) 45° of diameter 158mm. In addition, limited vibration still

appeared for many cases with amplitude around 0.5D-1D. This may be due to the inherent unstable characteristic of stayed cables in small Scruton number range. It is also observed that cable with 158nn diameter tended to be more unstable rather than 110 mm cable at a same wind speed. This could be due to the higher Reynolds number of 158mm cable. Large vibration mostly started at the reduced wind speed (*U*/*fD*) of approximately 70 with amplitude of around 1.2D in case of α 25°and β 45°. In range of low Scruton number, indented surface is still defective in eliminating DG.

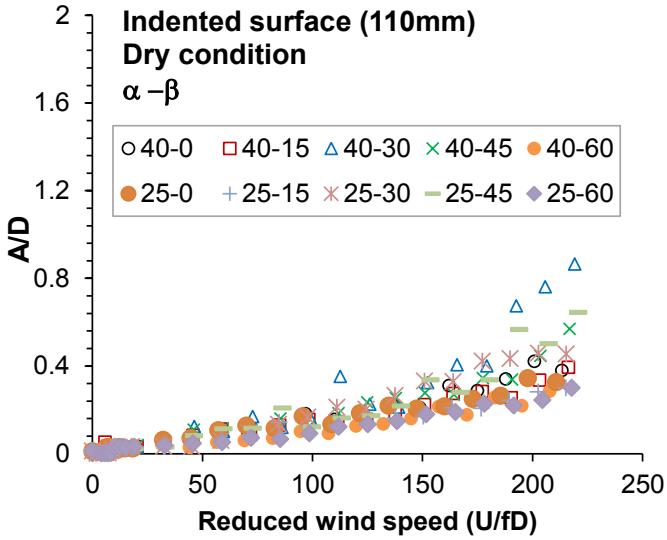

Figure 4-50 DG of indented surface cable

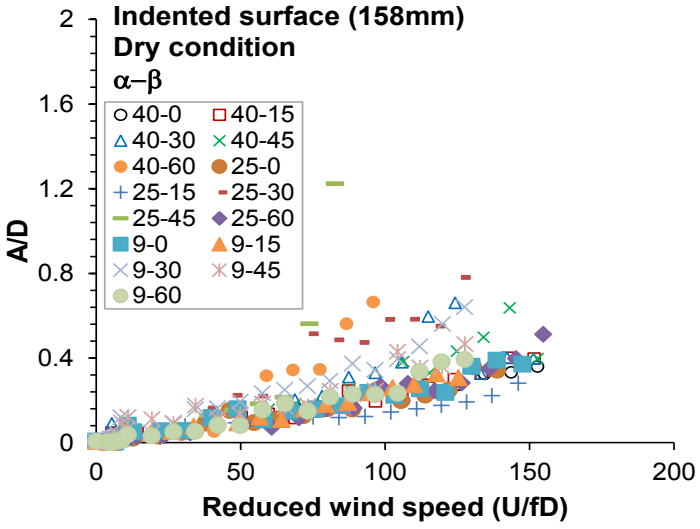

Figure 4-51 DG of indented surface cable

On the other hand, the wind tunnel test also carried out in precipitation condition. The summarized results are shown as Figure 4-52 and 4-53. Generally, most of large RWIV

was suppressed, except case 25°-45° and 40°- 45° of 158mm cable diameter. The large amplitude vibration started at around 70-90 of reduced wind speed where are in the subcritical Reynolds number region. However, it should pay attention that a thin upper rain rivulet still appeared on the surface as Figure 4-54 and Scruton number was quite low in this experiment.

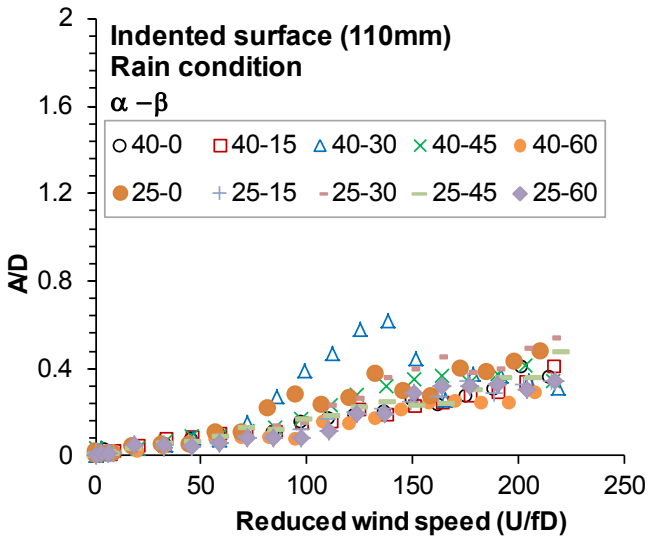

Figure 4-52 Vibration of indented surface cable in rain condition

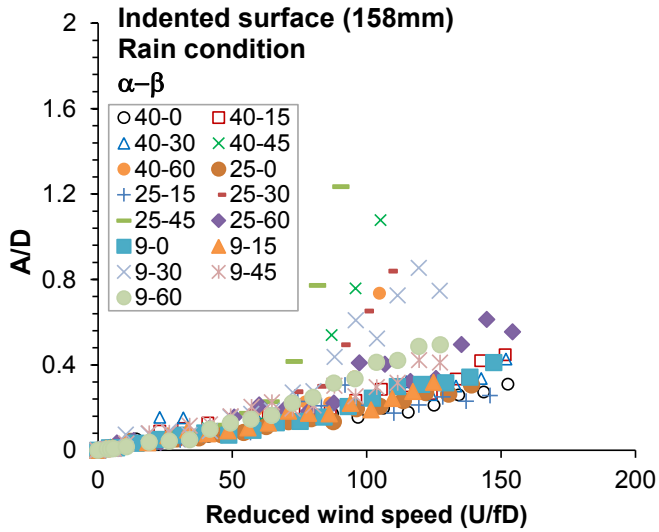

Figure 4-53 Vibration of indented surface cable in rain condition

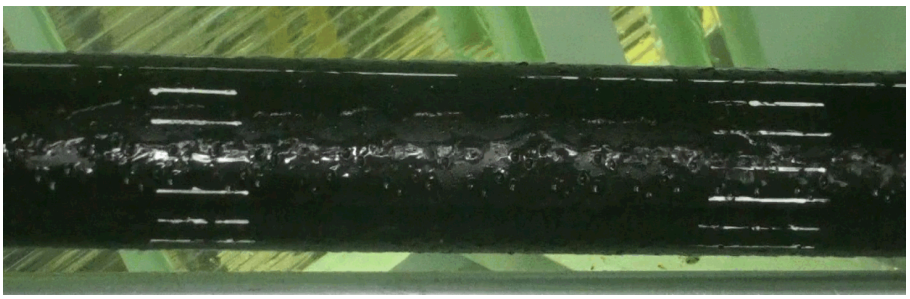

Figure 4-54 Small upper rivulet still remained on indented cable surface

4.3.2.2 Wind and rain-wind induced vibration for parallel protuberance

For confirmation the effectiveness, same extensive wind tunnel tests were carried out for the parallel-protuberance countermeasure in both rain and no rain condition. In dry condition, parallel protuberance can mitigate cable vibration to some extent as shown in Figure 4-55 and Figure 4-56. Nevertheless, divergent type vibration still appeared. The largest amplitude is approximately 1.4*D* in the case of the inclined angle 25° with the flow angle 15° for 110 mm cable. Large vibration started occurring at reduced wind speed around 100-170 in cases of wind angles 40°-30°, 25°-45° and 25°-15°. In case of D158, divergent galloping appeared at wind angles 25°-45° and 25°-45 whereas the remained cases still exhibited the large amplitude vibration. In addition, when cable model was rotated around its axis to check the effect of protuberances location, vibration response was almost similar. This result totally agreed with the WTT result of Higashi Kobe Ohashi Bridge [16]. In precipitation condition, RWIV almost disappeared with some exceptional cases shown at Figure 4-57 and 4-58. Cases with the inclined and flow angles of 40° and 30° (110mm), 25° and 15°, 25° and 45°, and 40° and 30° (158mm) respectively exhibited large amplitude vibration. It should be mentioned that under the presence of parallel protuberance, upper and lower rivulets along the cable vanished thoroughly but vibration still occurred. The inherent instability of an inclined cable with low damping might cause these vibrations.

Above discussions suggest that one should be careful when applying the indented surface and parallel protuberance for suppressing rain wind induced vibration and DG for low Scruton number cable. It is therefore imperative to develop an innovative cable surface that can mitigate both rain-wind induced cable vibration and DG, especially for low damping cable.

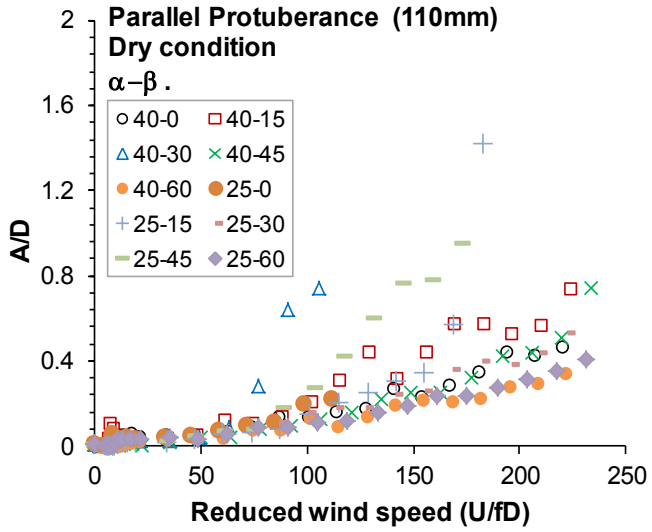

Figure 4-55 DG of Parallel protuberance cable, D110

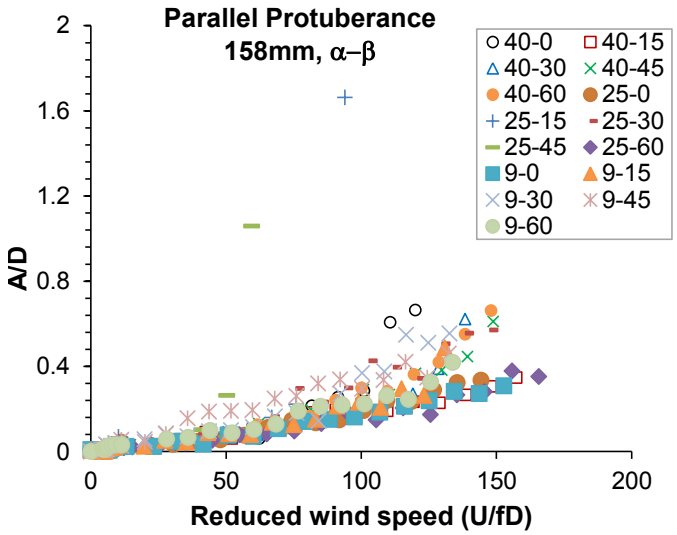

Figure 4-56 DG of Parallel protuberance cable, D158

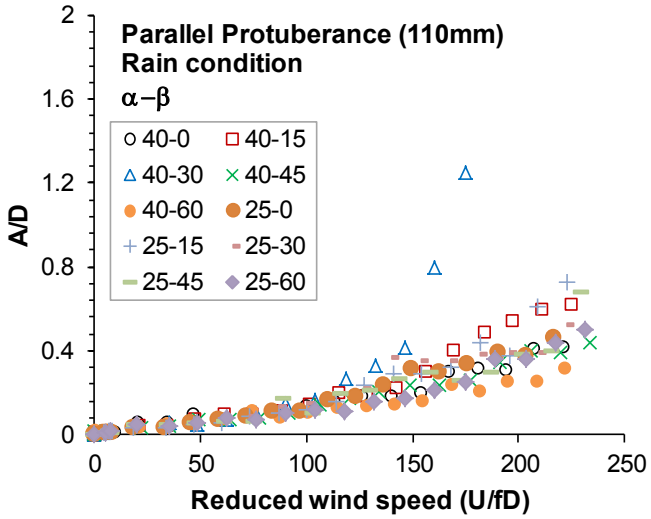

Figure 4-57 Parallel protuberance cable under precipitation, D=110mm

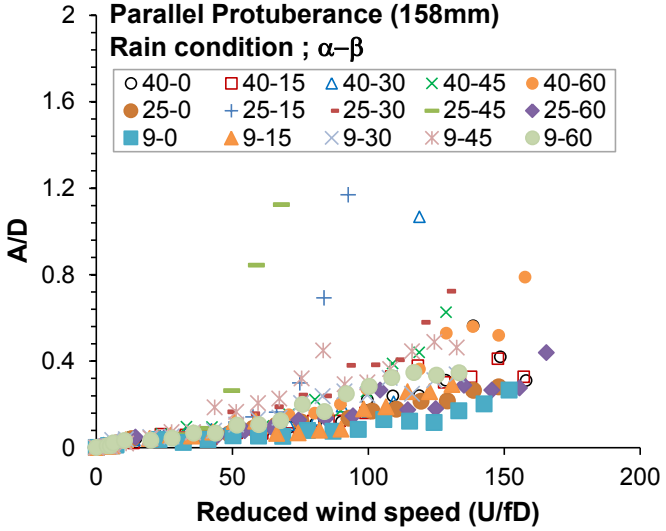

Figure 4-58 Parallel protuberance cable under precipitation, D=158mm

4.3.2.3 Axial flow near the wake of modification cable

It is pointed out that axial flow in a wake of cable plays significant role for galloping instability in dry condition[1]. To confirm whether axial flow will occur or not for modification cable, the measurement will be carried out by anemometer for indented surface and parallel protuberances. The static model was installed at inclined angle 25° and flow angle 30° where is one of critical case. Diameter of 158mm was used in this experiment.

The distribution of axial flow velocity near wake of indented surface and parallel protuberance cables can be seen in Figure 4-59 and Figure 4-60. Obviously, strong channel of axial flow still existed with intensity above 50% of coming flow. Upper cable end still exhibited higher velocity intensity compare to lower side. Axial flow patterns are quite similar for both cable types. However, the difference between upper end and lower ends of cable is smaller compare to smooth surface case. In addition, the comparison between smooth surface, indented surface and parallel protuberances can be seen in Figure 4-61. In this figure, incoming wind speed is 15m/s in order to take in to account the occurrence range where DG occurred. Generally, the axial flow distributions of three cables were quite similar for all cases. In the other expression, it seems to be that the axial flow is one of inherent characteristic of inclined cable again wind incoming wind and it does not depends on the cable surface much.

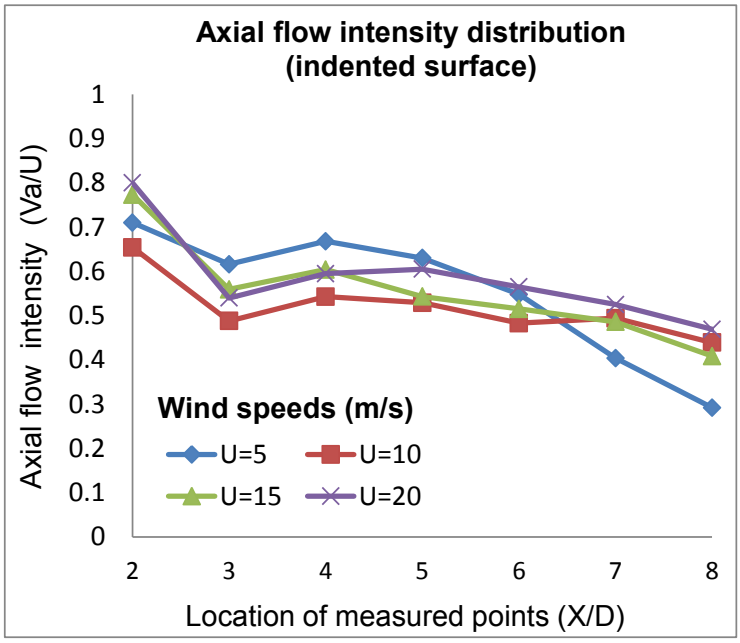

Figure 4-59 Span-wise distribution of axial flow of indented cable

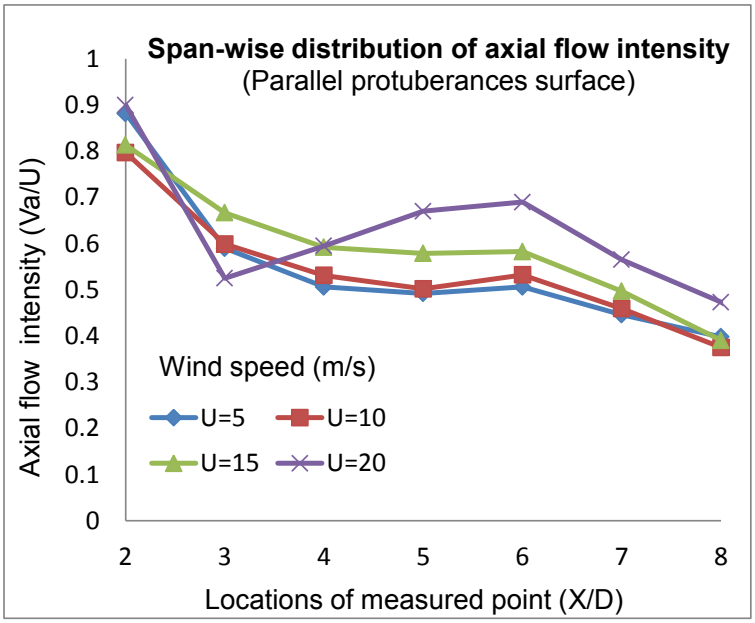

Figure 4-60 Span-wise distribution of axial flow of parallel protuberance cable

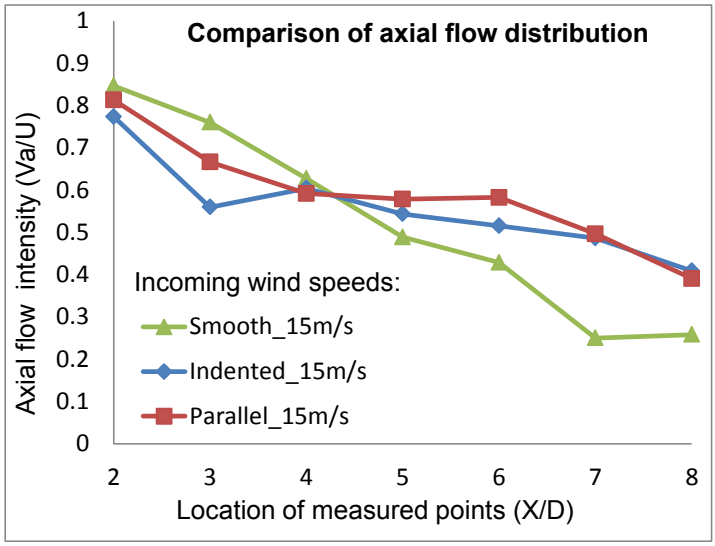

Figure 4-61 Comparison between different surfaces

4.4 Summary of Chapter 4

To reproduce Dry galloping of stay cable and to elucidate the characteristics of dry galloping and its mechanism, an extensive wind tunnel test campaign was carried out carefully. Under each case, responses of cable were different and it depended on wind attack angle, surface modification. The current results allow the following conclusions to be drawn:

1. Dry galloping has been reproduced successfully in various conditions. Both restricted response and divergent type galloping were recorded with large amplitude vibration.

2. Dry galloping is less sensitive to the cable damping rather than frequency. Therefore, it is hard to suppress the dry galloping by installing the external damper. There is a strong recovery of surface pressure in leeward side during DG occurred.

3. A strong axial flow channel also found near the wake of cable in current experiment with intensity around 60-80% of incoming wind flow. It located around 0.2-0.6D from cable wake. This strong channel of axial flow can contribute to mitigate the Karman vortex shedding near the wake of cable. Then contribute to excite galloping.

4. Dry galloping and Rain-wind induced vibration of indented surface and parallel protuberances was examined thoroughly. The experimental results exhibited that indented surface and parallel protuberances used to apply for RWIV; however, it could not eliminate DG well. Large amplitude vibration still occurred for many cases in low Scruton number range. On the other hand, there is existence of axial flow with high intensity near wake of smooth cable, which can excite galloping. These flow channels remained in case of indented surface and parallel protuberance cable. Therefore, axial flow is one of inherent characteristic of inclined cable against wind incoming and it does not depends on the cable surface much.

5. The mechanism of dry galloping strongly relates to the forming of low dominant frequency components and interruption of Karman vortex near the wake of cable. When wind speed increase to a critical value, under the effect of axial flow or high wind speed, the Karman vortex will be interrupted. At the same time, low frequency flow becomes dominant. Low frequency flow/vortices exhibited high energy, high correlation and it sheds continuously and constantly by time. Therefore, it can create high excitation force. Consequently, cable will be excited.

6. The existence of dry galloping with large amplitude vibration for smooth cable, indented surface and parallel protuberances leads to the fact that it is imperative to develop a better countermeasure for this phenomenon. To suppress dry galloping, it is important to suppress the effect from low frequency flow excitation through destroying the shedding correlation and reducing its energy or by improve the Karman vortex shedding.

Bibliography

1. Matsumoto, M., et al., *Dry-galloping characteristics and its mechanism of inclined/yawed cables.* Journal of Wind Engineering and Industrial Aerodynamics, 2010. **98**: p. 317-327.

2. J.B. Jakobsen, et al., *Wind-induced response and excitation, characteristic of an inclined cable model in the critical Reynolds number range.* Journal of Wind Engineering and Industrial Aerodynamics, 2012. **110**: p. 100-112.

3. Saito, T., M. Matsumoto, and M. Kitazawa. *Rain-wind excitation of cables on cable-stayed Higashi-Kobe bridge and cable vibration control*. in *The International Conference on Cable-Stayed and Suspension Bridges*. 1994. Deauville.

4. FHWA/HNTB, *Wind induced vibration of stay cables. Interim final report, RDT 05-004.* 2005.

5. VO, D., et al., *Experimental study on dry-state galloping with various wind relative angles and its countermeasures.* Journal of Structural Engineering (JSCE), 2014. **60A**: p. 428-436.

6. Gu, M. and X. Du, *Experimental investigation of rain-wind- induced vibration of cables in cable-stayed bridges and its mitigation.* Journal of Wind Engineering and Industrial Aerodynamics, 2005. **93**: p. 79-95.

7. Nakamura, Y., K. Hirata, and T. Urabe, *Galloping of rectangular cylinders in the presence of a splitter plate.* Journal of Fluids and Structures, 1991. **5**: p. 521-549.

8. Matsumoto, M., et al., *Vortex-induced cable vibration of cable-stayed bridges at high reduced wind velocity.* Journal of Wind Engineering and Industrial Aerodynamics 2001. **89**: p. 633–647.

9. Barltrop N. D. P. and A.A. J., *Dynamic of fixed marine structures*. Third edition 1991.

10. Cheng, S., et al., *Aerodynamic behaviour of an inclined circular cylinder.* Wind and Structures, 2003. **6**(3): p. 197-208.

11. Raeesi, A., S. Cheng, and D.S.K. Ting, *Some Insight into the Wind-Induced Vibration of Stay Cables in the Context of Rigid Static Inclined Circular Cylinder.* Journal of Applied Fluid Mechanics, 2012. **5**(2): p. 99 -112.

12. Miyata, T., H. Yamada, and T. Hojo. *Aerodynamic response of PE stay cables with pattern-indented surface*. in *International Conference on Cable-Stayed and Suspension Bridges (AFPC)*. 1994. Deauville, France.

13. Katsuchi, H. and H. Yamada. *Wind-tunnel Study on Dry-galloping of Indented-surface Stay Cable*. in *11th Americas conference on wind engineering*. 2009. Puerto Rico.

14. Hojo, T., S. Yamazaki, and H. Okada, *Development of low drag aerodynamically stable cable with indented processing*. 2000.

15. Matsumoto, M. *Review of Bridge Cable Vibrations in Japan*. in *Wind Induced Vibration of Cable Stay Bridges Workshop*. 2006. Kyoto, Japan.

16. Matsumoto, M., M. Kitazawa, and H. Kanaji, *Wind tunnel test for stay cables of Higashi Kobe Ohashi Bridge -part 2 (in Japanese)*. Proc. Of 44th Annual Conference of JSCE, 1989 p. 802-803.

Chapter 5: Aerodynamic Countermeasure for Cable Dry Galloping by Spiral Protuberances

Aerodynamic control methods for rain wind induced vibration have been developed for 30 years. However, those countermeasures are effective for rain-wind induced vibration but not for dry galloping. To assist developing an aerodynamically stable stay cable under dry galloping, an extensive wind tunnel test campaign was carried out carefully. Spiral protuberance cable with different number of fillets, sizes and pitches will be examined to find optimum range for mitigating rain wind induced vibration and DG. Furthermore, some of aerodynamic stability mechanisms of spiral protuberance cable will be shed a light on.

5.1 Need of new aerodynamic stable cable

As discussion on chapter 4, dry galloping related to low frequency peak component with high energy and high correlation in wake flow and the interruption of Karman vortex shedding. Therefore, to mitigate dry galloping, it is significant to either disrupt the low frequency flow shedding correlation or reduced the wake energy or improve the Karman Vortex component. According to previous studies [1-8], spiral protuberance of sharp-edged rectangular section works on the principle of disrupting the coherence of vortex/flow formation, helps avoiding the rain induced vibrations by preventing the generation of upper

or lower rivulets and they also introduce a three-dimensional disturbance in the flow, which can help suppressing wind flow induced vibrations. In addition, the application of spiral protuberance can also reduce the wake flow energy. Therefore, it is also believed that suitable type of spiral type of protuberance can mitigate dry galloping.

Nowadays, spiral protuberance type cable is widely applied in foreign countries and some hangers of suspension bridges in Japan. Table 5.1 presents a list of helical fillet geometries that have been installed on bridge stay cables in Europe and North America for control RWIV[9]. Field measurement showed that installing a spiral wire could mitigate wind-induced vibration of stay cables to some extent. Due to this fact, many WTTs have been carried out to optimize the spiral pitch and spiral wire size. However, an optimized innovative countermeasure has not been proposed yet. In addition, recent full-scale monitoring at Øresund Bridge revealed that they were not effective as initially expected[10]. They pointed out that stay cables with small diameter helical fillets still exhibited large amplitude vibration. Besides that, Gu et al. concluded [11] that only proper spiral pitch could mitigate RWIV of cables, however their development was for RWIV. Recently, Yagi et al.[12] used twelve spiral protuberances with the winding angle of 27° to control RWIV with harvesting lower drag force compared to the parallel-protuberances type. They found that the drag force coefficient was around 0.8 and remained for wide range of wind speed. Recently, Larose et al (2013) indicated that helical fillet could not suppressed dry galloping well, large amplitude vibration still recorded. Especially for low Scruton region as the Figure 5-1 [9]. We should pay attention that the Scruton number in Figure 5-1 is that S_{c1}=1.6 and S_{c2}=5.1, these values are equipvalent to approximate 20 and 64 when scruton number calculated by equation 3.7 in current study.

Table 5.1 Typical helical fillet geometries (all double helix)

Bridge	Cable diameter (mm)	Pitch (mm)	Helix angle (degrees)	Pitch to diameter ratio	Helical fillet (mm)	Cross-section helical fillet
Normandie	170	600	41.7	3.5	1.3 dia.	round
Öresund	250	550	55.0	2.2	2.1 high x 3.0 wide	rectang.
Charles River	178	610	42.5	3.4	1.5 high x 3.3 wide	rectang.
Generic 1	200	600	46.3	3.0	2.0 dia.	round
Generic 2	160	490	45.7	3.1	4.0 dia.	round
Generic 3	200	620	45.4	3.1	2.0 dia x 4.0 wide	round
Generic 4	200	630	45.0	3.1	2.0 dia x 4.0 wide	round
Present study	162	520	44.4	3.2	2.3 high x 2.4 wide	rectang.

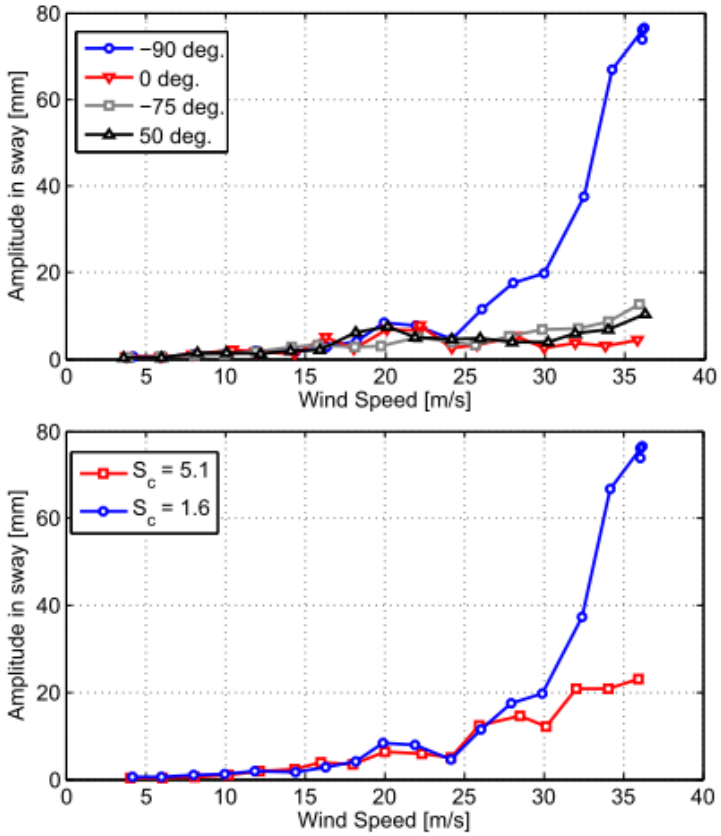

Figure 5-1 Amplitude of motion for inclined cable at 60° with a helical fillet

Furthermore, it is also pointed out that a single helical fillet wound with 2D-3D pitch can suppress DG for some yawed angles [13]. Nevertheless, the effects for RWIV and DG in low Scruton number have not been examined yet and they carried out with 75mm diameter cable. Therefore, larger diameter needs to be tested to check the efficiency in different types of diameter and higher Reynolds number region. Currently, the experiment with single helical fillet also was carried out in low damping area (ζ <1%) as Figure 5-2 and Figure 5-3. Generally, the divergent galloping of RWIV and DG has been eliminated. In case of D110mm, amplitude decreased considerably in both dry and wet conditions. However, the large amplitude vibration around 0.8D appeared in case of diameter D158mm. Therefore, it is necessary to continue optimizing spiral protuberance type to develop a better countermeasure for DG and RWIV, especially for low Scruton number region where unstable vibration often occurs. Above discussion revealed that the current countermeasures still have some drawbacks, especially for restricted amplitude in dry condition. Therefore, the spiral protuberance should be improved more to adapt not only with RWIV but also dry galloping at low Scruton number range.

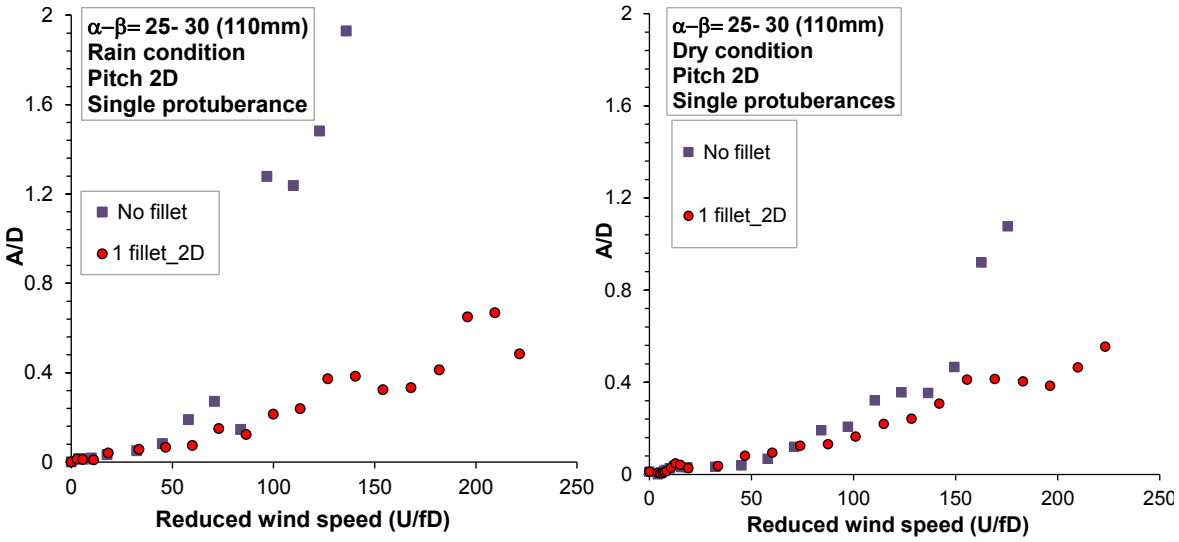

Figure 5-2 Effectiveness of single spiral protuberances, (f=0.817, ζ=0.088%)

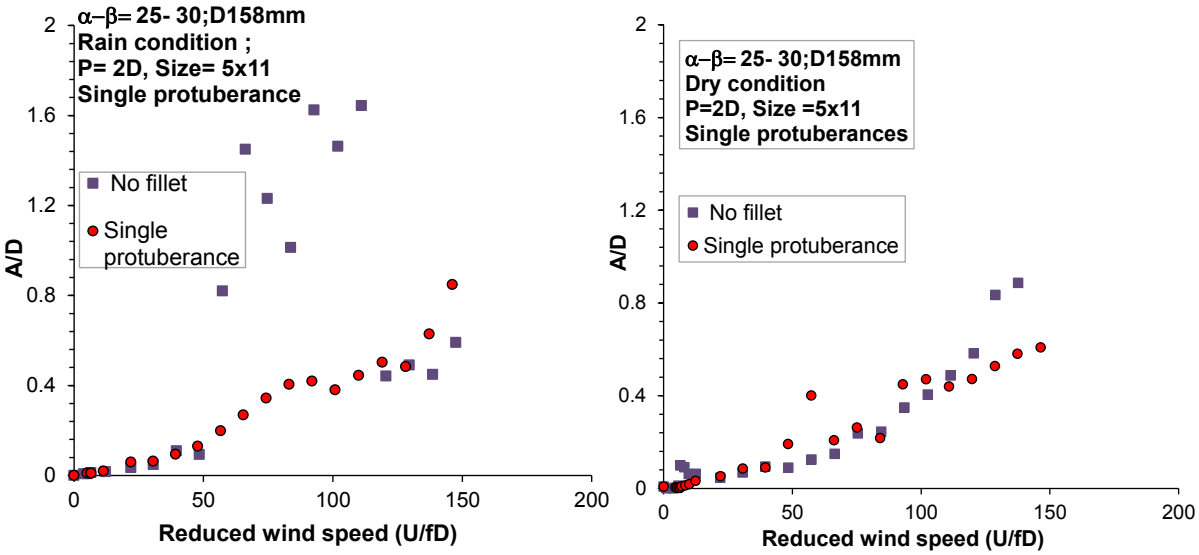

Figure 5-3 Effectiveness of single spiral protuberances (f=0.87, ζ=0.095%)

5.2 Optimization for Spiral protuberance cable

5.2.1 Wind tunnel test campaign

Table 5.2 illustrates the scope of wind tunnel test campaign. First, to ensure the suppression not only DG but also RWIV, each experiment was carried out under rain and dry condition. From chapter 4, the case of 25° of inclination and 30° of flow angle was one of critical wind attack direction of rain-wind induced vibration and dry galloping, therefore, this angle was selected for current experiments. Two kinds of cable diameter also tested in parallel, 110 and 158mm respectively. To optimize the range for suppressing DG and RWIV,

various kind of spiral protuberances are examined. In Table 5.2, number of spiral protuberances of 02, 04, 06, and 12 are checked for their mitigation effectiveness. There are two winding directions, original and reverse direction. The original direction is anti-clockwise winding whereas reverse direction is clockwise winding. The protuberance sizes also change by 2mm × 6mm (height × width), 4mm × 6mm, 5mm× 7.5mm, 2mm × 7.5mm, 3mm × 7.5mm respectively. The requirement of protuberance size is that it should be larger enough to destroy rain rivulet as well as enhance stability in dry condition. Furthermore, it is pointed out that the spiral with 27° exhibited smaller drag force compare to the other winding angle [12]. Therefore, the winding pitch at 3.86D, which is equivalent to 27° of winding angle, was selected for basic case. In addition, the effect of pitch also was examined by 2.95D, 3.86D and 4.378D respectively. By comparing winding directions, winding pitches and protuberance sizes, optimization range for spiral-protuberance countermeasure can be proposed.

Table 5.2 Spiral protuberances optimization

Diameter D	Wind angles	No. of protuberance	Winding direction	Sizes S (mm)	Winding pitch P (mm)	Rain
110 mm	Inclined angle 25° and Flow angle 30°	12	Reverse direction	4 (H) × 6 (W)	425 (3.86D)	w · w/o
		2, 4, 6, 12	Original direction	4 × 6	425 (3.86D)	
		12	Original direction	5 × 7.5	425 (3.86D)	
				4 × 6	325 (2.95D)	
					525 (4.78D)	
158 mm	Inclined angle 25° and Flow angle 30°	12	Reverse direction	5 × 7.5	610 (3.86D)	w · w/o
		2, 4, 6, 12	Original direction	2 × 7.5	610 (3.86D)	
				3 × 7.5	610 (3.86D)	
				5 × 7.5	610 (3.86D)	
		12	Original direction	5 × 7.5	610 (3.86D)	
					465 (2.95D)	
					755 (4.78D)	

5.2.2 Spiral protuberances model

A spiral protuberance cable is composed from HPDE tube and rubber fillets. The winding direction, pitch and size of protuberances follow the information in Table 5.1. The

rubber fillets were adhered on cable surface by two-sides tapes which strong enough during strong wind and rain-wind interaction. The length and diameter are same as previous chapter. The Figure 5-4 shows the spiral protuberance model.

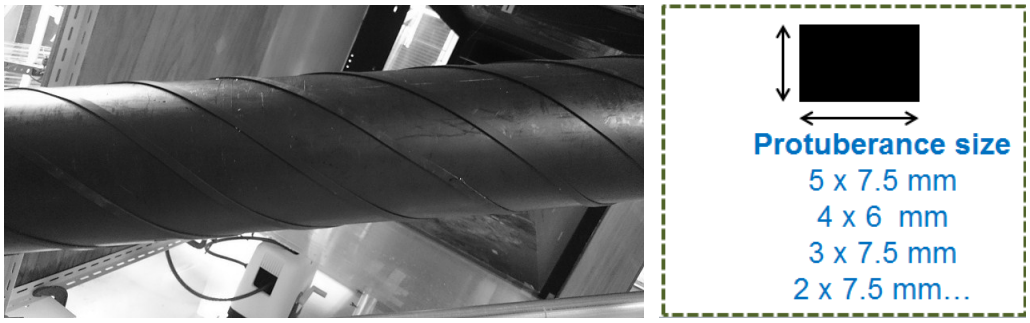

Figure 5-4 Spiral protuberance model

5.2.3 Test parameters

In this experiment, cable diameters were same as previous section includes 110mm and 158mm. Fundamental frequency is around 0.8Hz. Maximum and minimum damping ratio were 0.16% and 0.08% that are similar to low damping stay cables of real bridges. Nevertheless, these values are quite low region compared to the damping value of prototype stay cables when they were installed damper. In correlation, maximum Scruton number is 9.6 while minimum value is 3.31. The detail of experiment parameters for spiral optimization experiment is illustrated in Appendix 7.

5.3 Aerodynamic responses of spiral protuberance cable

5.3.1 Number of protuberances effect

To clarify the effect of protuberances number, various types of model were fabricated as Figure 5-5. The effect of number of spiral protuberances to DG and RWIV are illustrated in Figures 5-6, 5-7, 5-8 and 5-9. The cases of 02, 04, 06 and 12 protuberances at pitch of 3.86D with size 5x7.5 were tested. In addition, the single protuberance with 2D pitch also examined for comparison. Generally, cases of 04, 06 and 12 protuberances suppressed RWIV and DG totally, while one and two protuberances exhibited slightly larger vibration with around 0.6-0.8*D* of amplitude as Figure 5-7.

Furthermore, the effect of number of protuberances with different sizes can be seen in Figure 5-10, 5-11, 5-12 and 5-13. When the protuberance size decreased from 5x7.5 to 3x7.5, the mitigation effectiveness was still conservative. In the case of size 5x7.5, the efficiency is generally similar between 4, 6 and 12 protuberances. However, there is a gap in effectiveness level in case of size 3x7.5mm. In detail, the twelve spiral protuberances exhibited the optimum countermeasure. Remained cases also suppressed vibration to some extent. When protuberances size reduced to 2x7.5, all cases exhibited low level in destroying DG and RWIV. Hence, there is a strong relationship between number of protuberance and protuberance size.

Figure 5-5 Spiral protuberance models with 2, 4, 6, and 12 protuberances

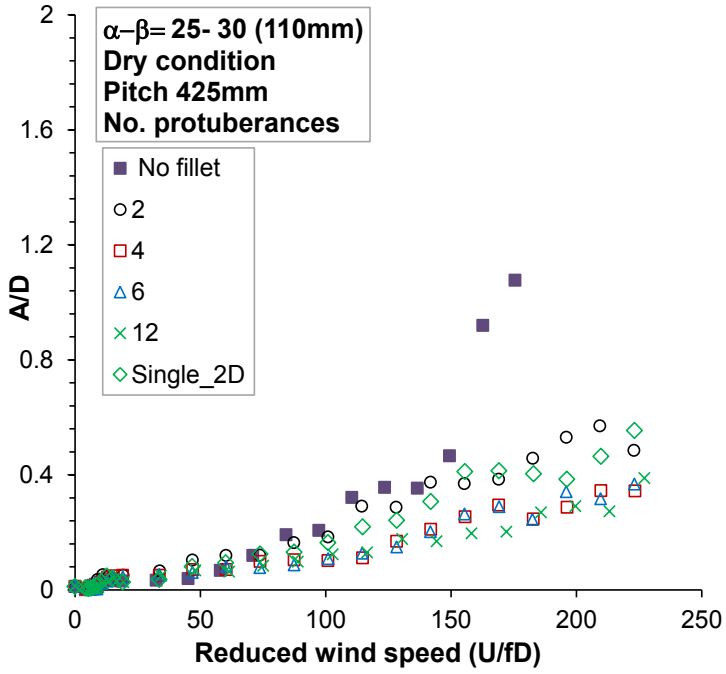

Figure 5-6 Effect of number of spiral (Dry, S=4mm×6mm and original direction)

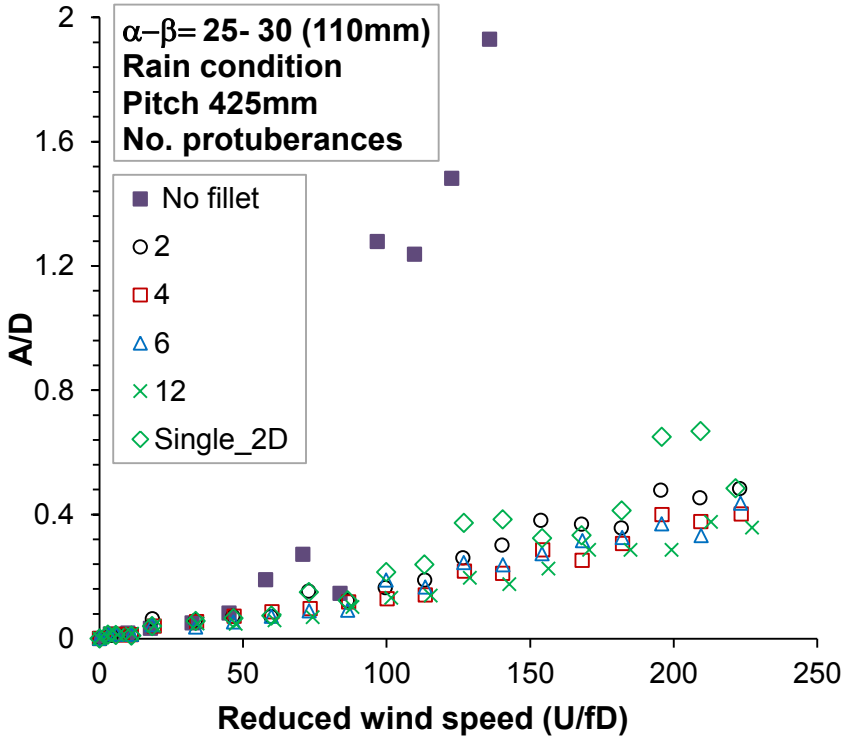

Figure 5-7 Effect of number of spiral (Rain, S=4mm×6mm and original direction)

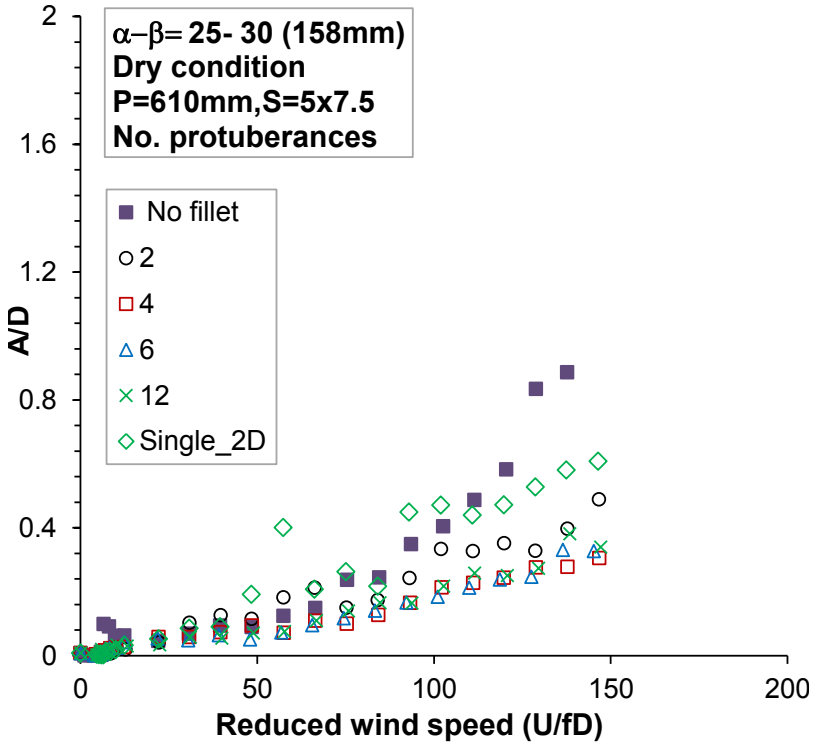

Figure 5-8 Effect of number of spiral (Dry, S =5×7.5 and original direction)

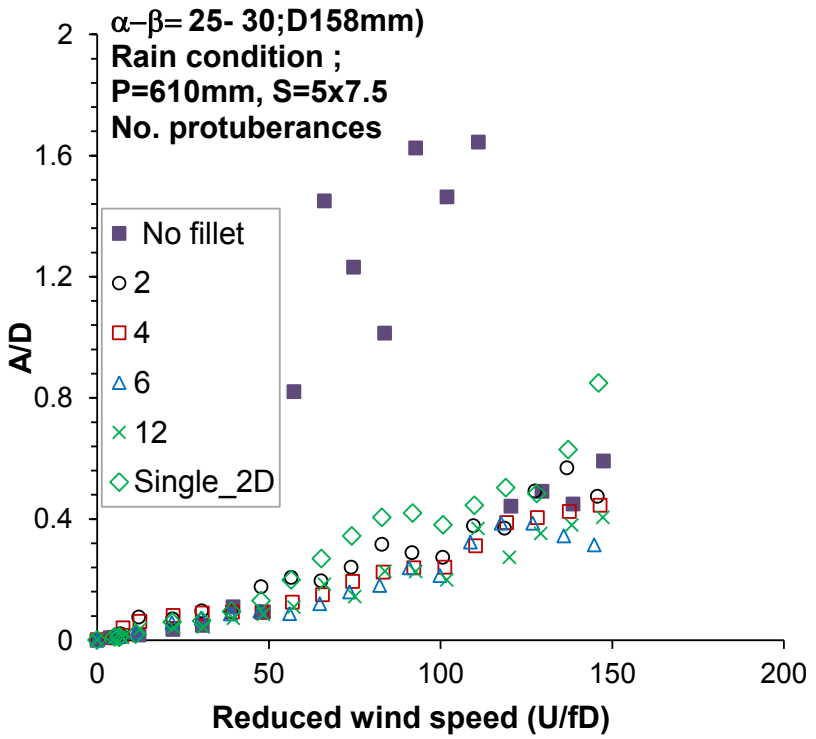

Figure 5-9 Effect of number of spiral (Rain, S =5×7.5 and original direction)

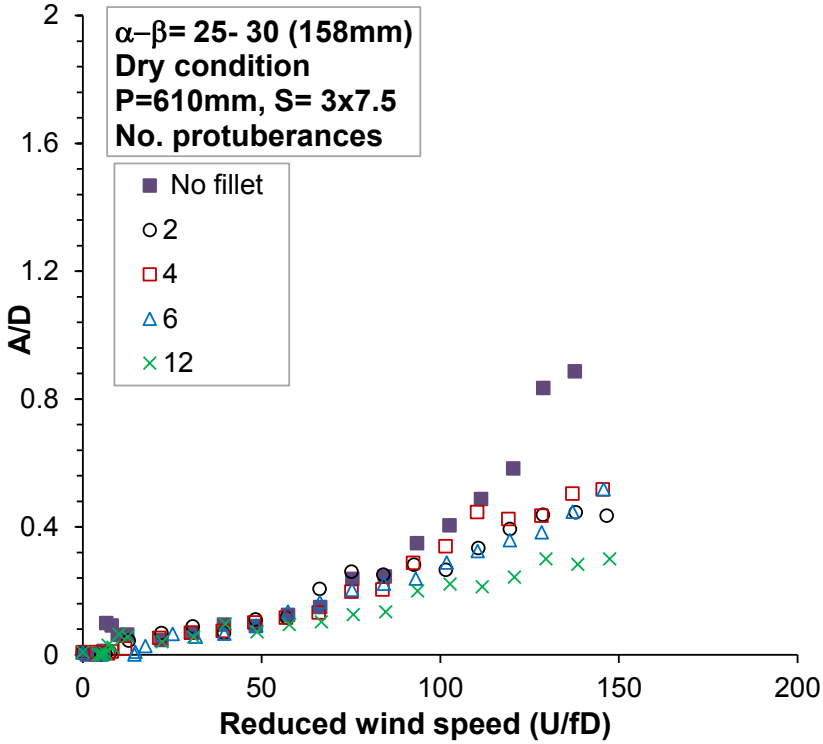

Figure 5-10 Effect of number of spiral (Dry, S =3×7.5 and original direction)

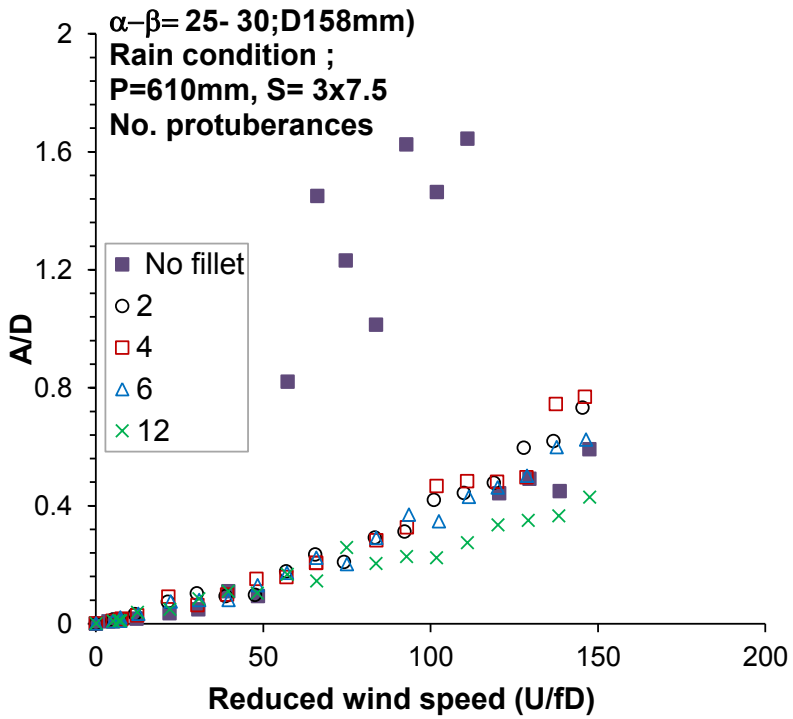

Figure 5-11 Effect of number of spiral (Rain, S =3×7.5 and original direction)

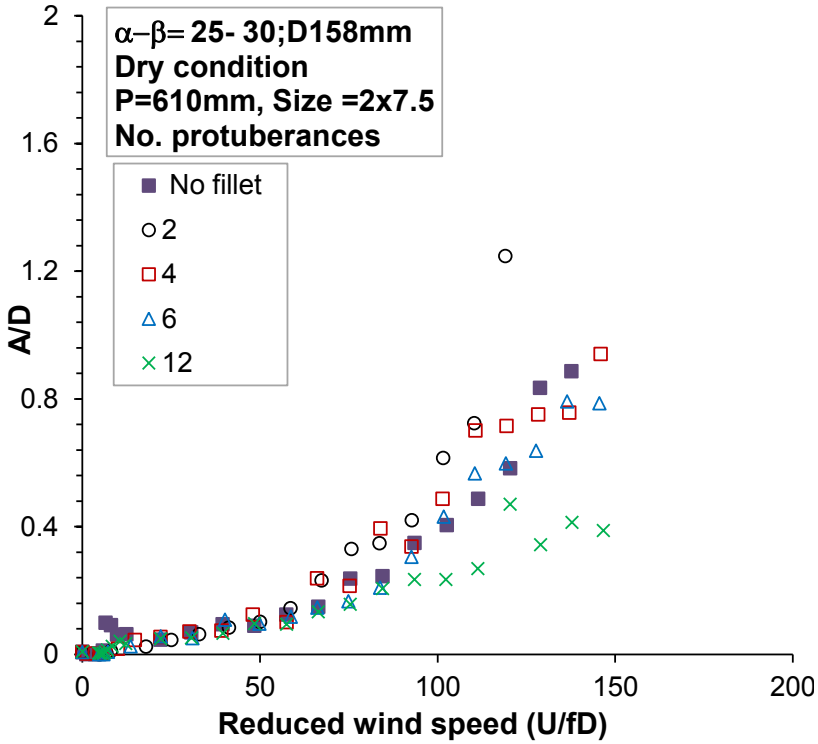

Figure 5-12 Effect of number of spiral (Dry, S =2×7.5 and original direction)

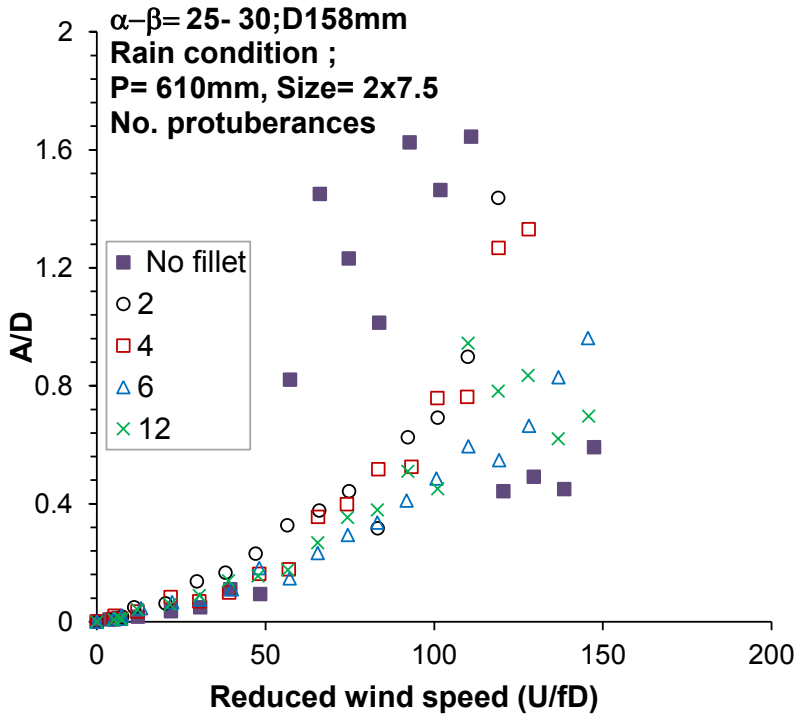

Figure 5-13 Effect of number of spiral (Rain, S =2×7.5 and original direction)

5.3.2 Winding pitches effect

According to previous studies, winding pitch is one of an important parameter when optimize the spiral protuberance. Its effect is not only on mitigation effect but also on the cable aerodynamic force. In this experiment, to check the effect of pitch to aerodynamic responses, several pitches were examined. The pitches 250mm, 325mm, 425mm and 525mm were used for 110mm diameter while the 158mm diameter was checked at pitches of 465mm, 610m and 755mm respectively. Furthermore, the number of protuberances was unchanged at 12 fillets. Generally, the winding pitches also have a modest effect to the mitigation effectiveness as shown in Figure 5-14, 5-15, 5-16 and 5-17. All current pitches exhibited high effectiveness in eliminating galloping amplitude through the experiment. The large amplitude vibration was suppressed totally in both dry and rain condition even though the Scruton number was very small in these tests. Significantly, the largest pitch also showed high effectiveness. It is therefore the pitch do not play the vital role in efficiency level. Nevertheless, it should pay attention that the pitch at 425mm and 610mm (3.86D) are strong recommendation because they have lower drag force than other according to previous study [12].

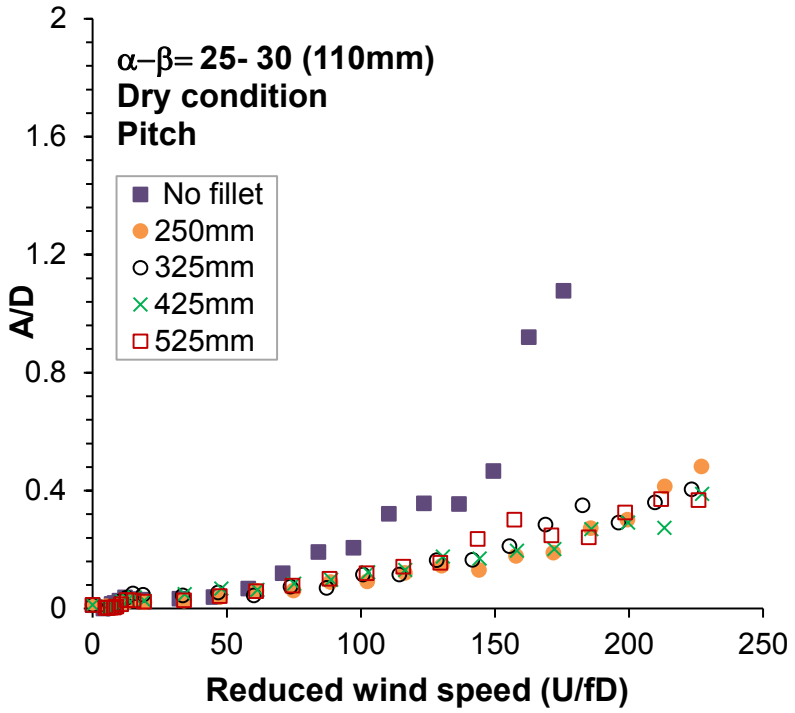

Figure 5-14 Effect of pitches (Dry, S= 4×6mm and original winding direction)

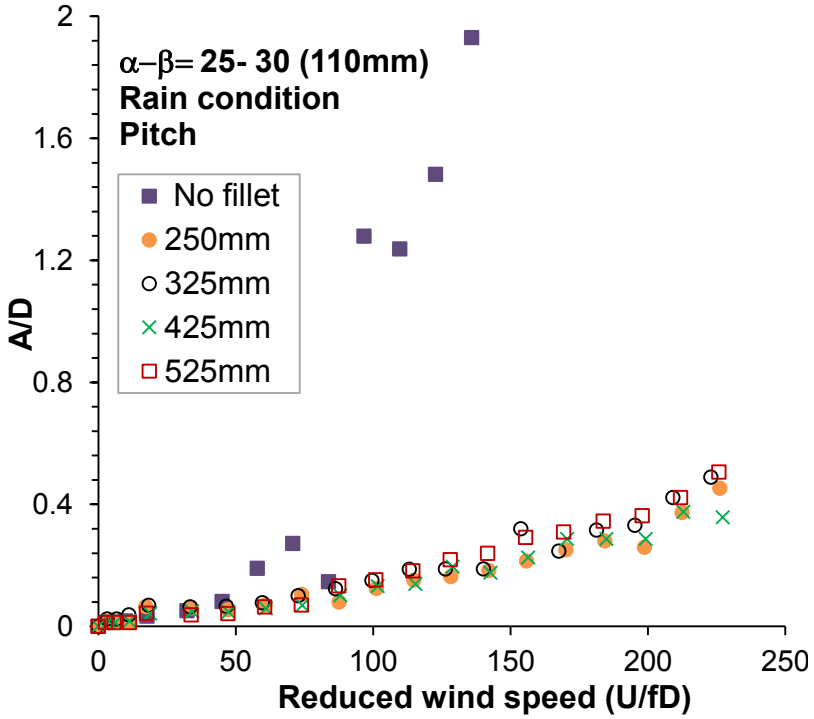

Figure 5-15 Effect of pitches (Rain, S= 4×6mm and original direction)

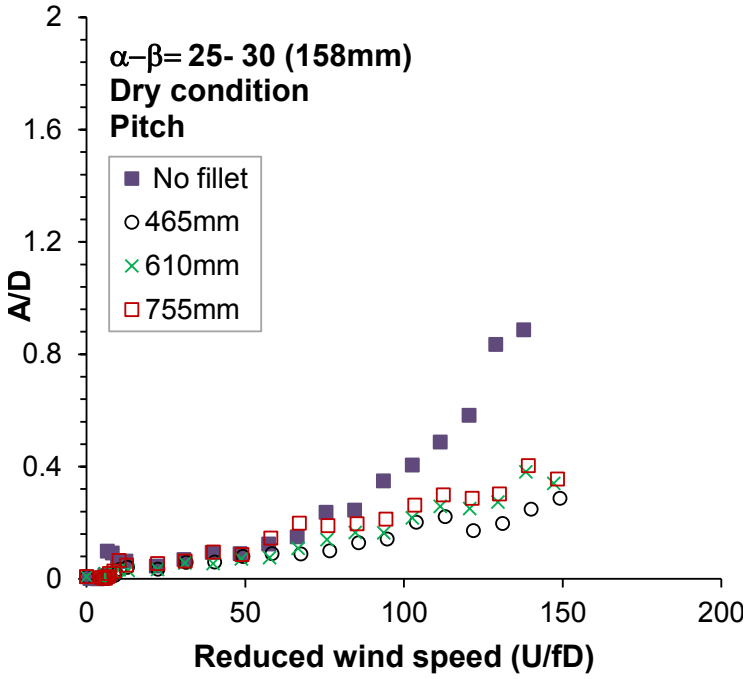

Figure 5-16 Effect of pitches (Dry, 12 spirals, S= 5×7.5mm and original direction)

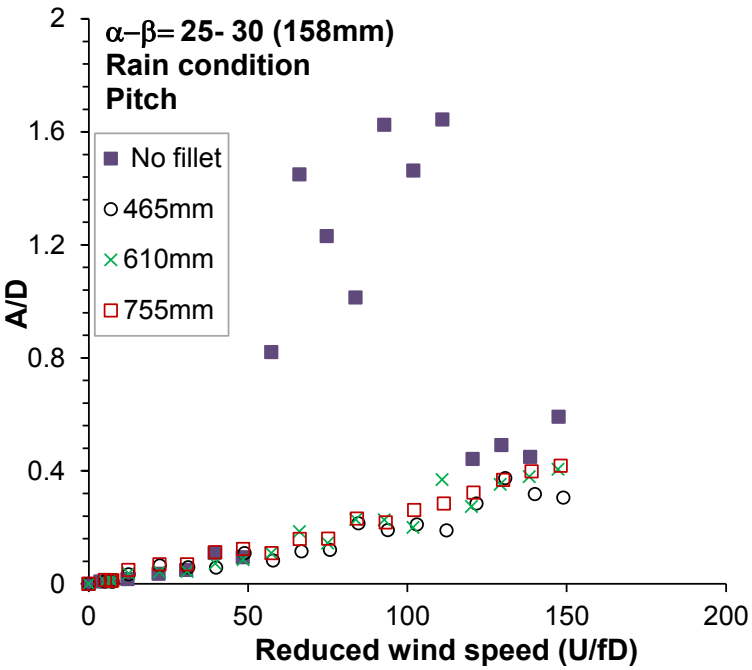

Figure 5-17 Effect of pitches (Rain, 12 spirals, S= 5×7.5mm and original direction)

5.3.3 Protuberances size effect

As the discussion in section 5.3.1, the numbers of protuberances and protuberance size have close relationship. To clarify deeper in size effect, various type of protuberances were checked with same twelve protuberances. Figures 5-18, 5-19, 5-20 and 5-21 displays the effectiveness of protuberances sizes. RWIV and DG were eliminated thoroughly under

all cases except 2×7.5 mm size for 158 mm cable. Observation showed that 2 mm thickness of protuberance could not prevent upper rain rivulet and some amount of water climbed over the protuberance. This might lead to changing the aerodynamic characteristic of cable and therefore its response is larger than other cases. On the other hand, winding direction did not affect RWIV. Similar efficiency level was recorded when winding direction was reverse compare to original one.

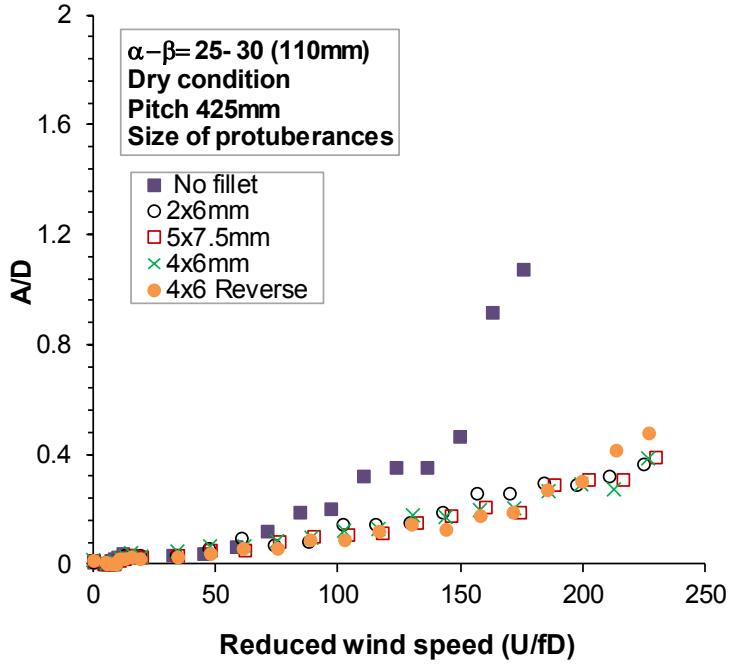

Figure 5-18 Effect of size (Dry, 12 protuberances, original and reserve direction)

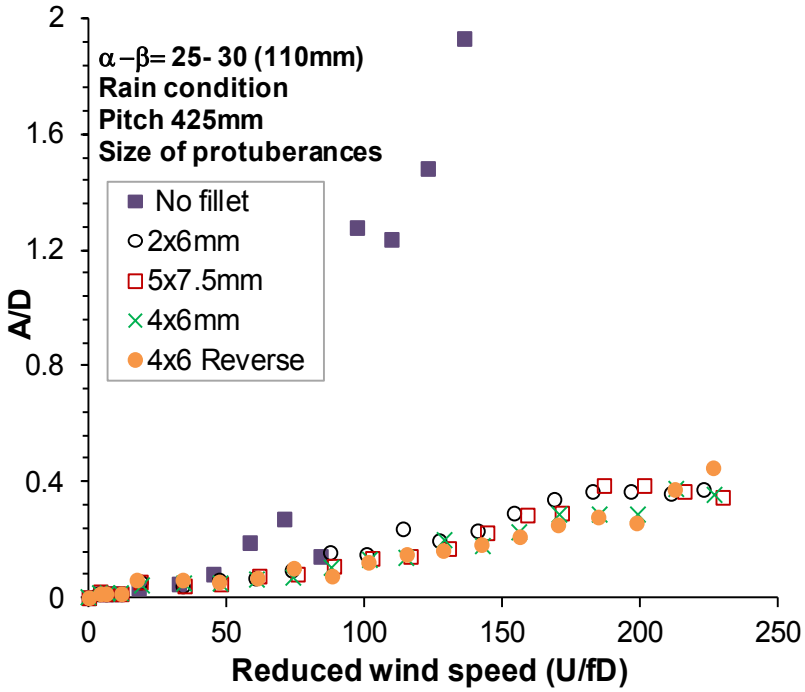

Figure 5-19 Effect of size (Rain, 12 protuberances, original and reserve direction)

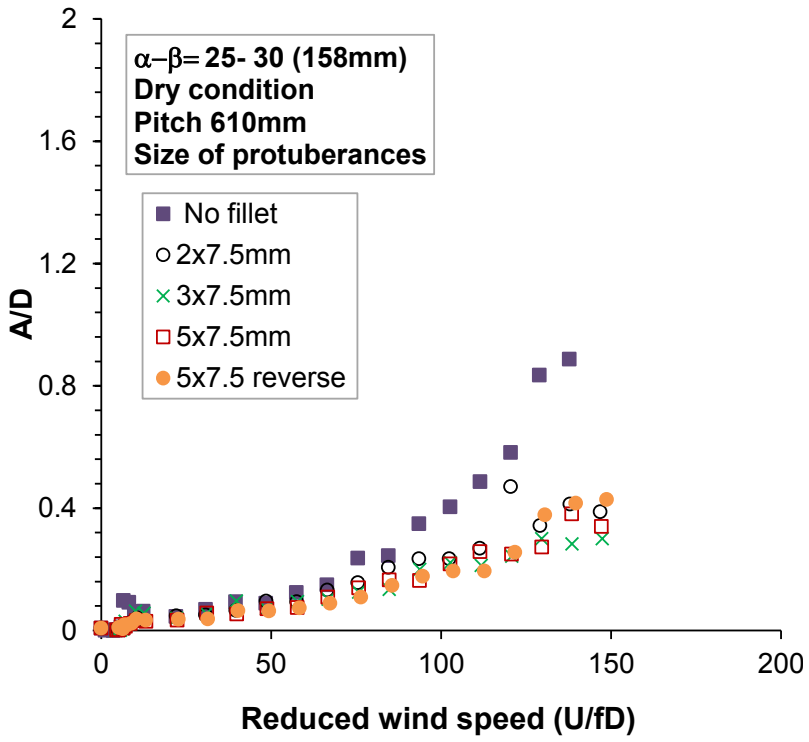

Figure 5-20 Effect of size (Dry, 12 protuberances, original and reserve winding)

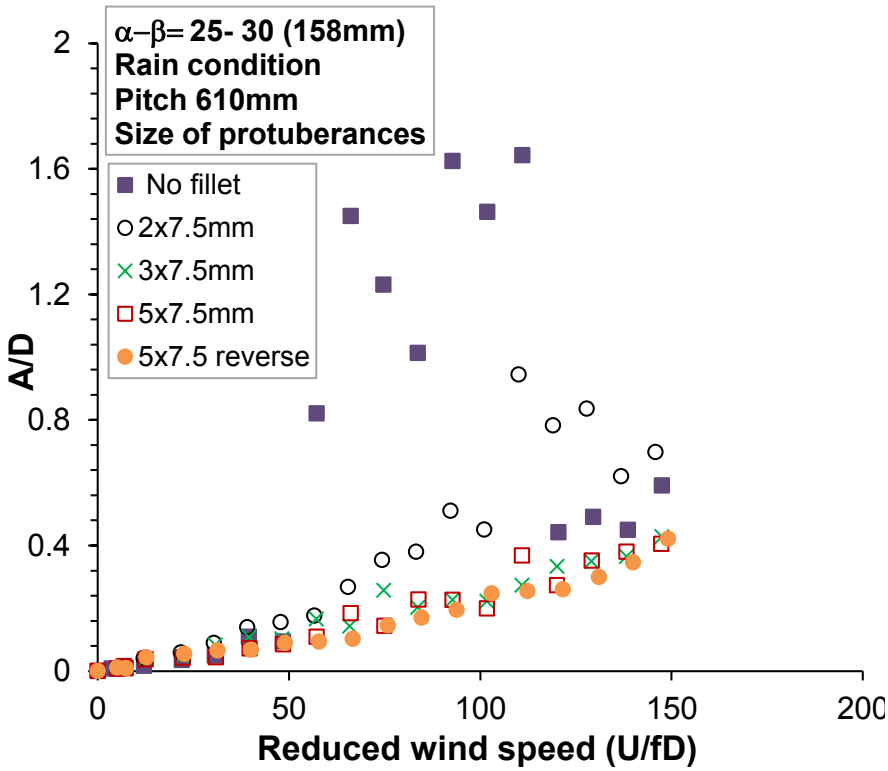

Figure 5-21 Effect of size (Rain, 12 protuberances, original and reserve winding)

5.3.4 Aerodynamic responses of spiral protuberance cable

To examine the effectiveness in various conditions, variety of wind attack angles, diameter and precipitation conditions were simulated. In detail, inclined angle (α) of 40°, 25° and 9° combined with flow angle of 60°, 45°, 30°, 15°, and 0° to create a wide range of wind attack angle. Cable diameters are 110 and 158mm respectively. Additionally, experiment was conducted in both rain and dry weathers. Scruton number ranged from 3.54 to 15.28. The more detail of experimental parameters can be seen in Appendix 8. Rough comparison between normal cable and 12 spiral-protuberances can be seen in Figure 5-22 and 5-23 Obviously, large amplitudes were suppressed by spiral-protuberances. It should be paid attention that current experiment deals with low Scruton number range. Therefore, if spiral protuberances could suppress DG and RIWV in this region, it will be effective to higher damping area. Moreover, the general comparison among spiral protuberances, indented surface and parallel protuberances is illustrated as Figure 5-24. In this figure, cable responses were investigated in same conditions for three types of cable modifications. Obviously, spiral protuberances exhibited its superiority in suppressing cable vibration. To the contrary, cable still vibrated with large amplitude in cases of indented surface and parallel protuberances. Therefore, it can be concluded that in the same condition, spiral-protuberance cable is the most stable even with small Scruton number.

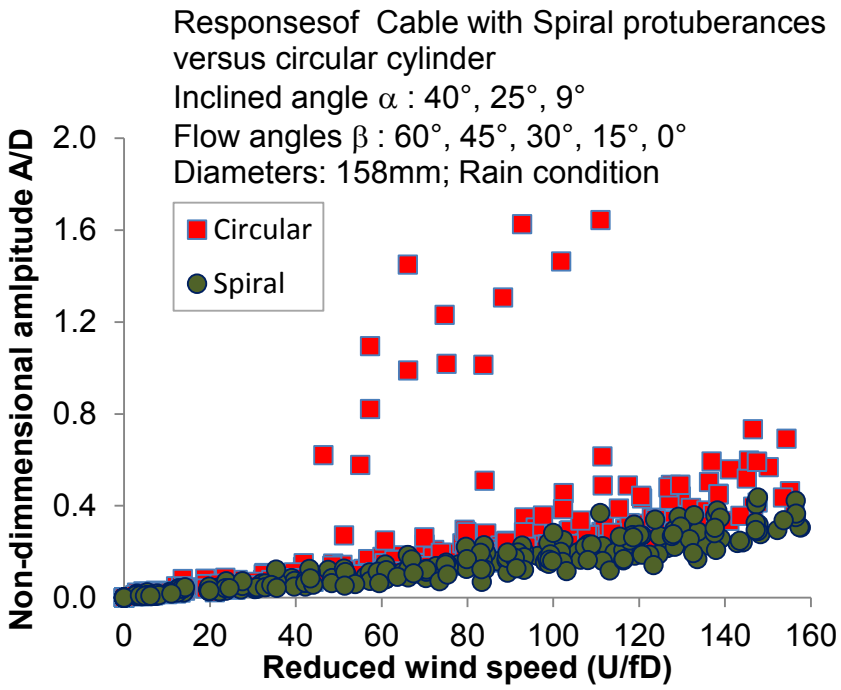

Figure 5-22 Spiral cable versus smooth cable under precipitation

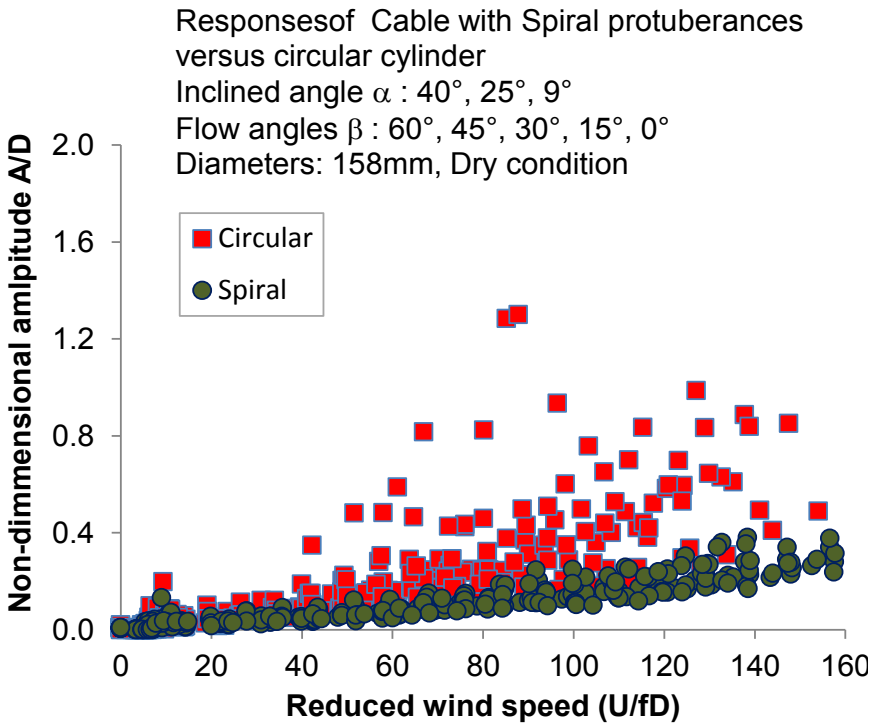

Figure 5-23 Spiral cable versus smooth cable under dry condition

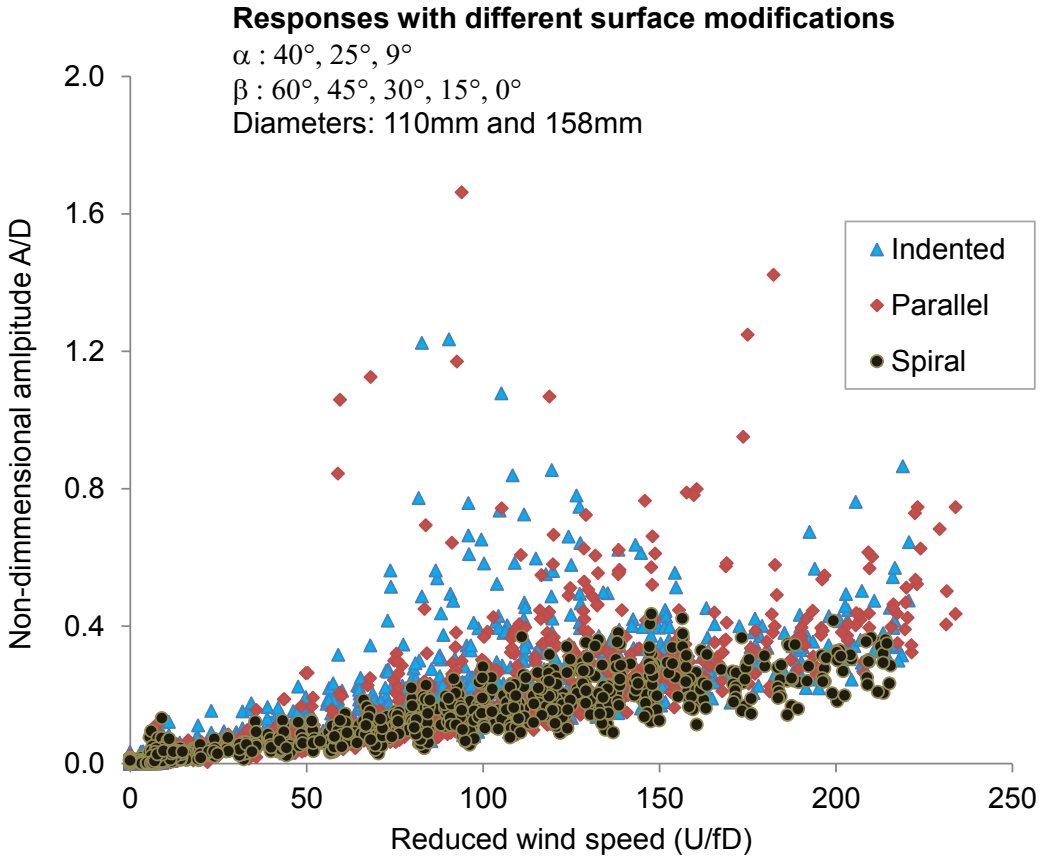

Figure 5-24 Overall comparisons among different cable's modifications

5.3.5 Recommendations for fabricating spiral protuberances

Wind tunnel test results showed that spiral protuberance cable could suppress both dry galloping and rain-wind induced vibration when it is well fabricated with a reasonable range of number protuberances, winding pitch and protuberance size. Based on the above discussion, the design recommendations for fabricating the spiral protuberance cable are summarized as Table 5.3. In this table, four, six and twelve protuberances with sized from 3x7.5 to 5x7.5 at the pitch of 2.95D to 4.78D are recommended.

Table 5.3 Fabrication recommendations for spiral protuberance cable

	No. of protuberance	**Winding direction**	**Protuberance Sizes S (mm)**	**Winding pitch P (mm)**
Diameter D	4 6 12	Original or Reverse direction	From 3mm × 7.5mm To 5mm × 7.5mm	From 2.95D To 4.78D

5.4 Stabilization characteristic of spiral protuberance cable

5.4.1 The elimination of low frequency band

Wake flow velocity of inclined spiral protuberance cable model was recorded along the model. The cable with twelve spiral protuberances was mounted in the wind tunnel with flow angle β=30° and inclined angle α= 25°. The experimental set up was same to measurement of circular cable in chapter 4. The power spectrum density (PSD) diagrams of fluctuating wind velocity in the wake along the spiral protuberance cable direction are shown in Figure 5-25, 5-26, and its comparison with circular cable can be seen at Figure 5-27 and 5-28. Significantly, the low frequency flows/vortices were vanished through span-wise direction. In comparison with circular cable, spiral one have much lower power in low frequency component band. In the other expression, the spiral protuberances mitigated the energy of wake flow considerably and made it becomes weaker. In addition, the normalized PSD also were plotted as the Figures 5-29, 5-30 and 5-31. In presence of spiral protuberance, Karman vortex (St=0.15-0.2) is most dominant flow, which contained higher energy. Moreover, The Karman vortex flow also decreased as wind speed increased, and it is nearly suppressed at high wind speed, say 15m/s or 20m/s. In this cases, there were some low frequency peak but the excitation energy is negligible. Furthermore, there was no large

amplitude vibration occurred in these cases. It means that the interruption of Karman vortex is only necessary condition , not the sufficient condition for dry galloping. The sufficient conditions for generation dry galloping are both interruption of Karman vortex and forming of low frequency flow/vortices. This kind of pattern also confirmed with different wind attack angle, said yawed angles 0, 30°, 45° and inclined angle 25°.

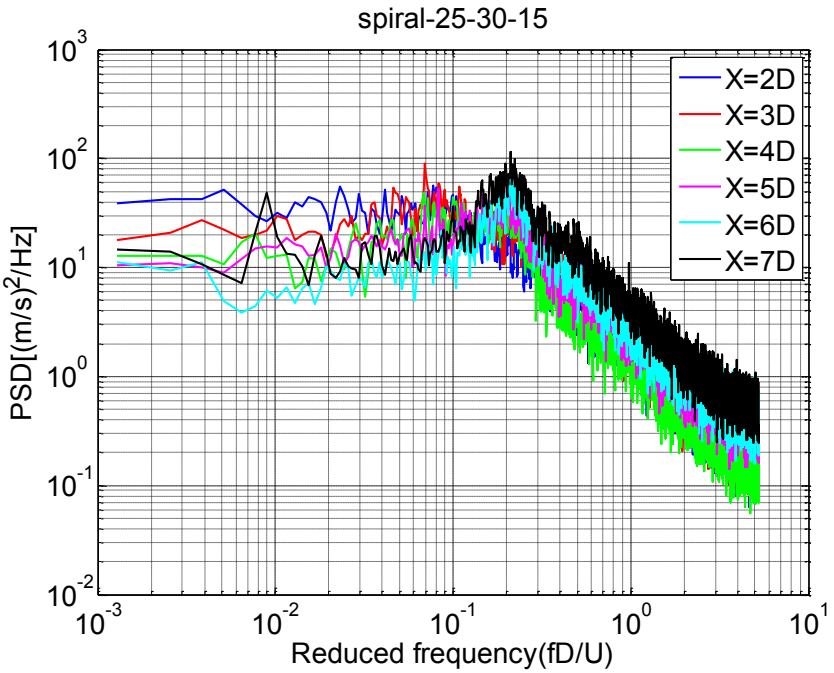

Figure 5-25 PSD of U fluctuating (U=15m/s, β=30° and α= 25°)

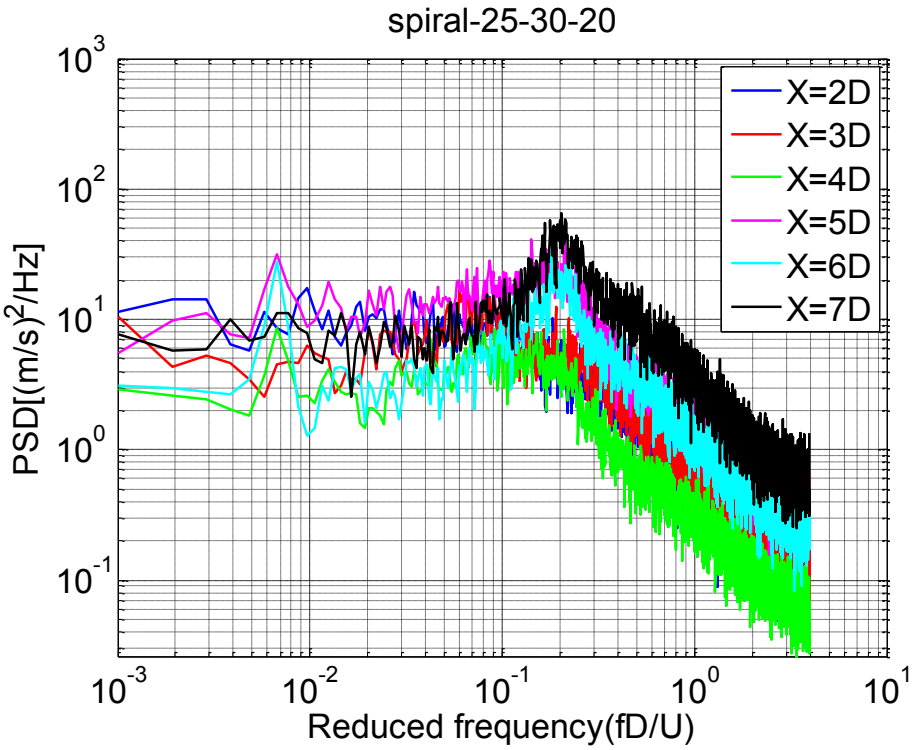

Figure 5-26 PSD of U fluctuating (U=20m/s, β=30° and α= 25°)

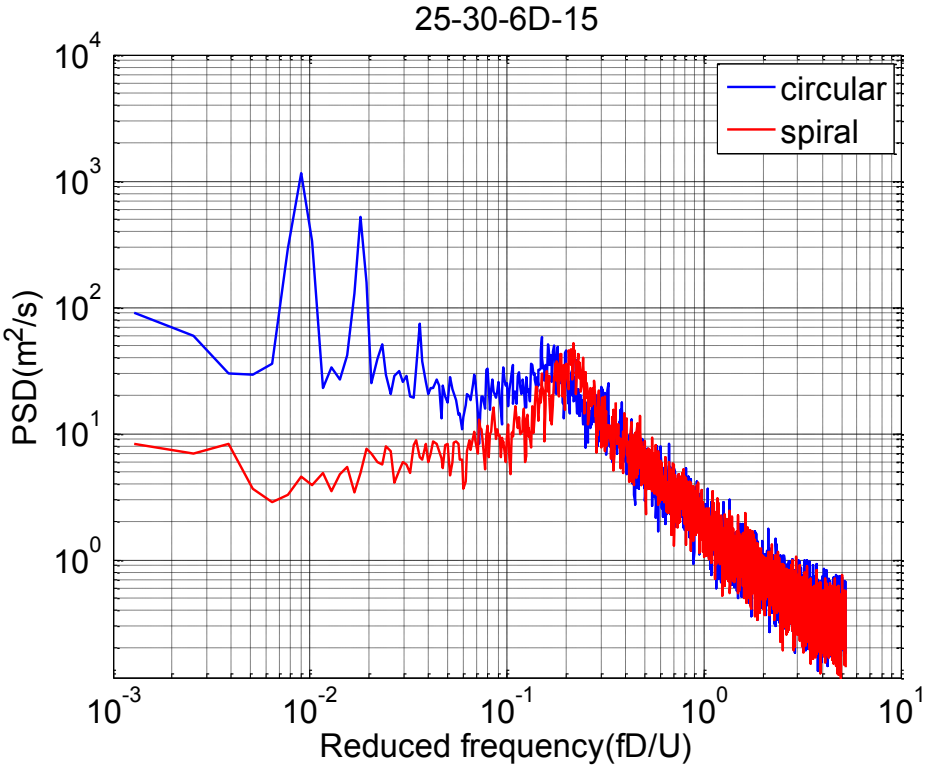

Figure 5-27 PSD of fluctuating wind velocity: circular cable versus spiral protuberance cable. (Smooth flow, location 6D, U=15m/s, β=30° and α= 25°)

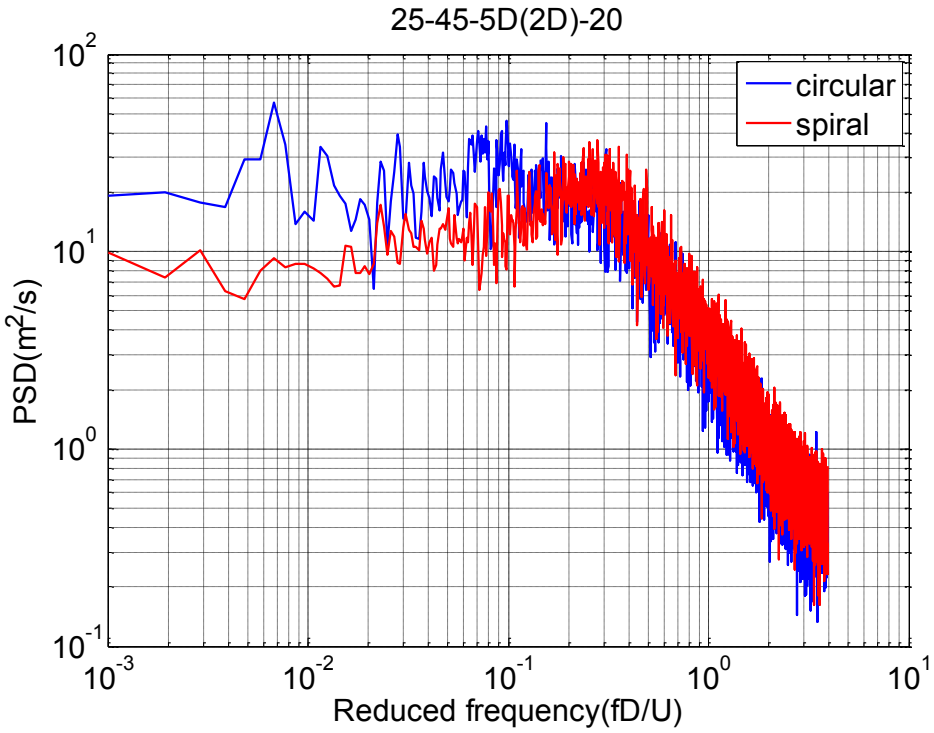

Figure 5-28 PSD of fluctuating wind velocity: circular cable versus spiral protuberance cable. (Smooth flow, location 5D, U=20m/s, β=45° and α= 25°)

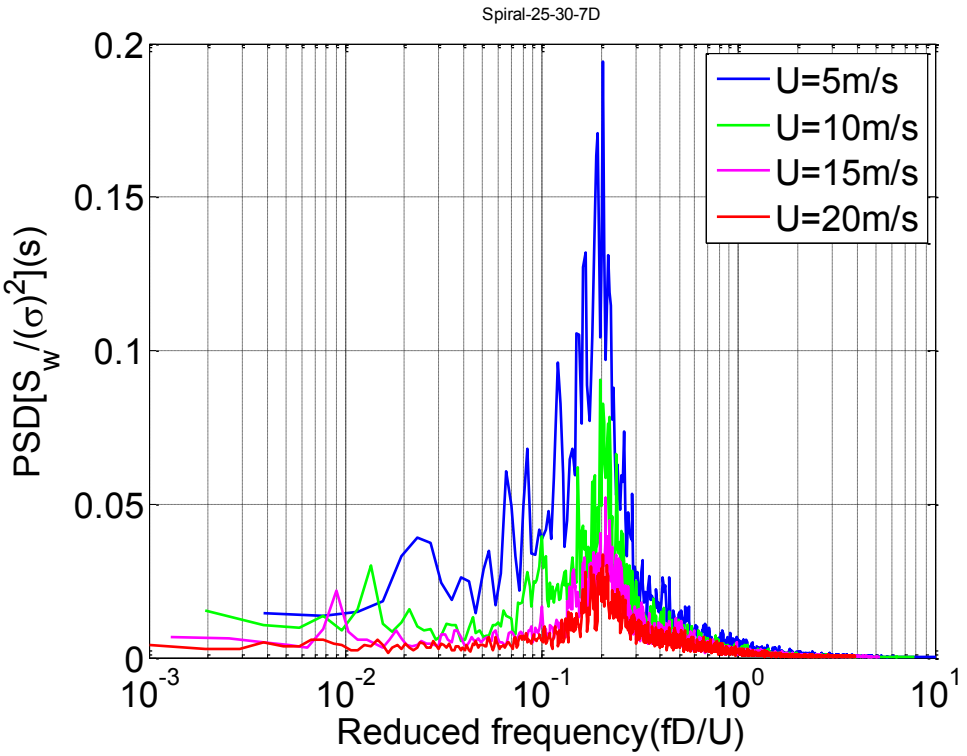

Figure 5-29 Normalized PSD of fluctuating wind velocity of spiral cable (Smooth flow, β=30° and α= 25°)

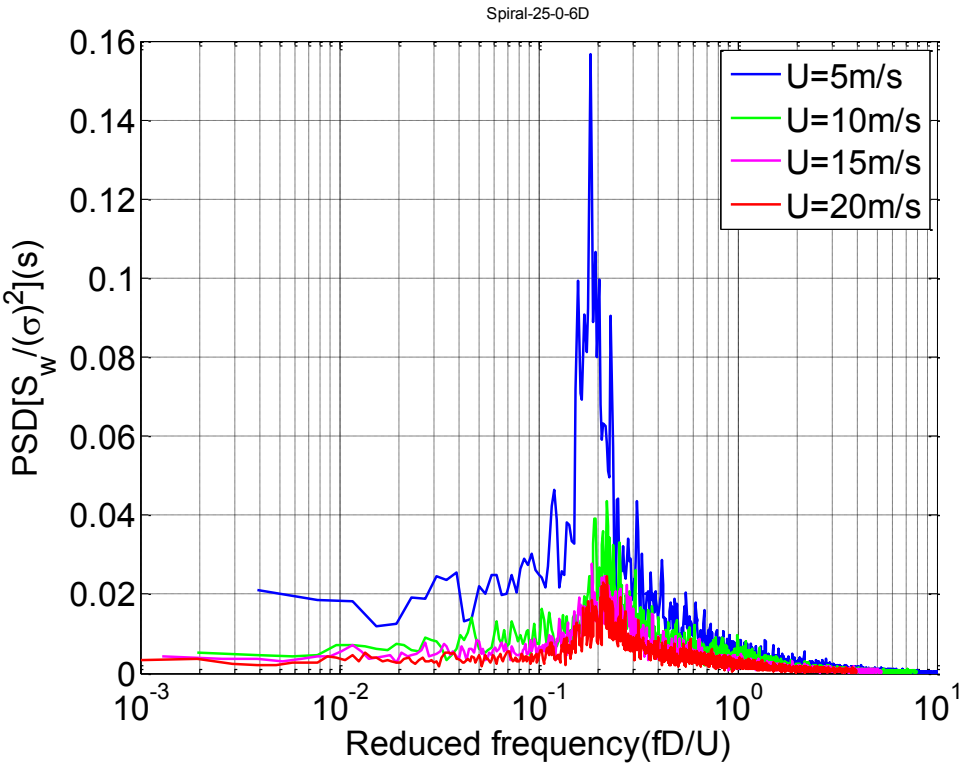

Figure 5-30 Normalized PSD of fluctuating wind velocity of spiral cable (Smooth flow, β=0° and α= 25°)

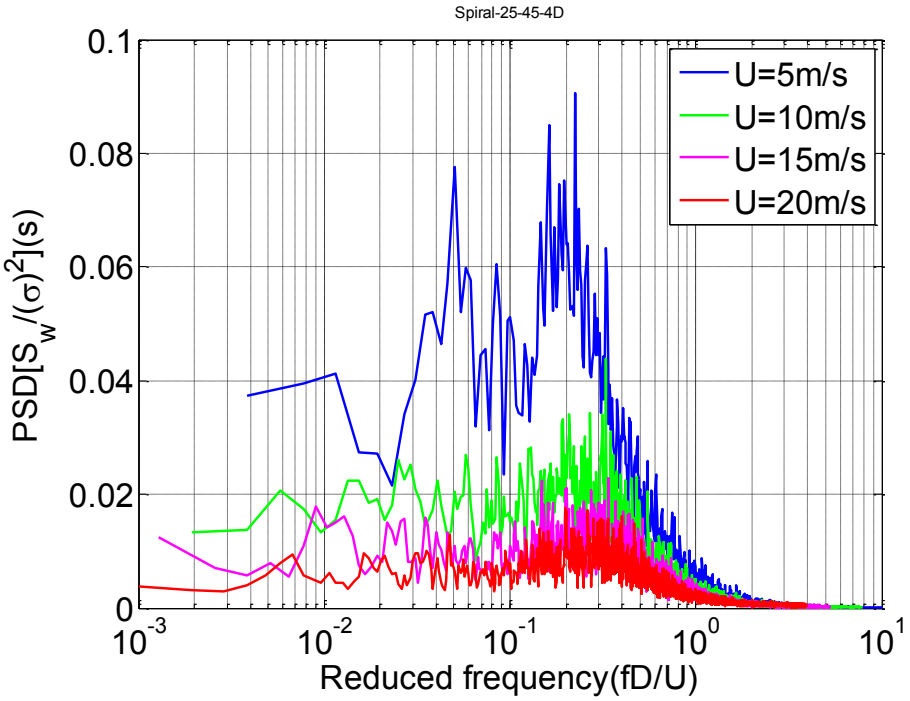

Figure 5-31 Normalized PSD of fluctuating wind velocity of spiral cable (Smooth flow, , β=45° and α= 25°)

Besides that, according to the wavelet analysis in Figure 5-32, 5-33, 5-34 and 5-35, there was a shift of frequency from low range in case of circular cable to high frequency components in presence of spiral protuberances. In particular, the total energy of wake flow reduced considerably. Frequency component from 1-10Hz seem to be suppressed and the power of other component were also reduced. In another expression, spiral protuberance changed the wale flow pattern from unstable pattern to the stable one. In addition, the low frequency peak vortices with reduced wind speed (U/f_vD=110-160) which was found in circular cable, also was vanished. Currently, there are high non-stationary frequency peaks correspond to reduced wind velocity around U/f_vD= 4-6. This range of reduced wind speed is equivalent to Strouhal number around 0.15-0.25, which is conventional Karman vortex. According to previous publications[14], when Karman vortex shed, amplitude become small. Because the Karman vortex would come from the communication of two separation flows and this communication make the pressure difference of upper and lower sides of cable become zero. As a result, it can reduce galloping. Furthermore, the Karman vortex-induced oscillation for stay cables is not so dangerous and it is easy to suppress by increase structural damping. Above findings proved that spiral protuberances destroyed the low frequency component, which may cause cable vibration at high wind speed. The results of PSD and wavelet analysis for spiral protuberances at remained wind angles can be found at Appendix

9 and Appendix 10. In short, the presence of spiral protuberances suppressed the low frequency component as well as reduced the energy of wake flow.

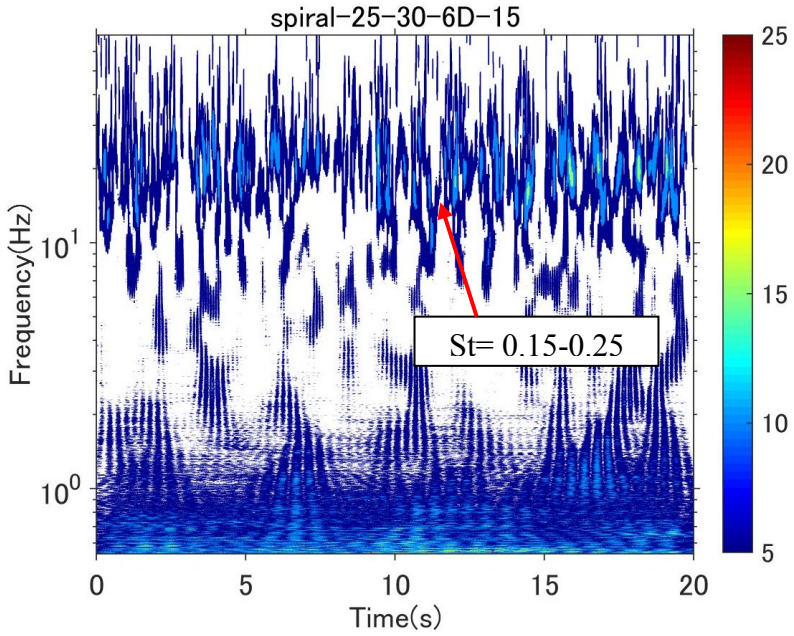

Figure 5-32 Wavelet analysis of fluctuating wind velocity in the wake (Smooth flow, Location= 6D, U=15 m/s, β=30° and α= 25°)

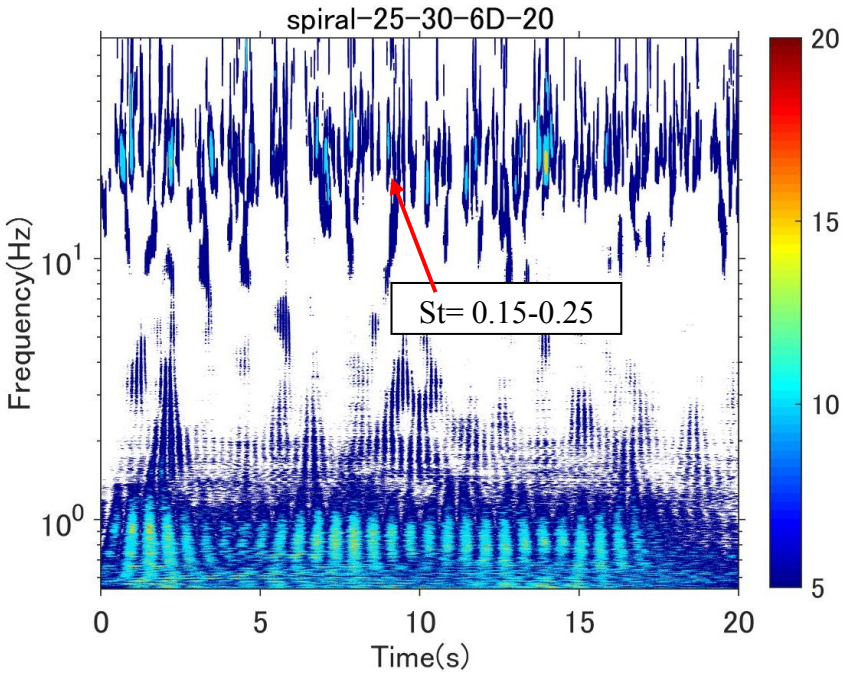

Figure 5-33 Wavelet analysis of fluctuating wind velocity in the wake of stationary spiral protuberance cable (Smooth flow, Location= 6D, U= 20m/s, β=30° and α= 25°)

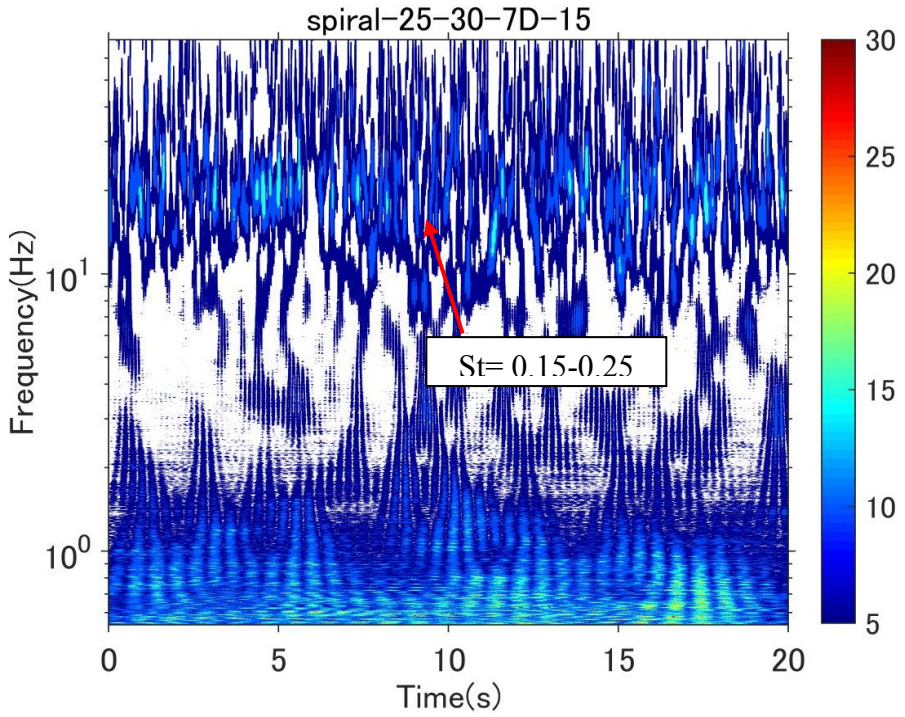

Figure 5-34 Wavelet analysis of fluctuating wind velocity in the wake of stationary spiral protuberance cable (Smooth flow, Location= 7D, U=15 and 20m/s, β=30° and α= 25°)

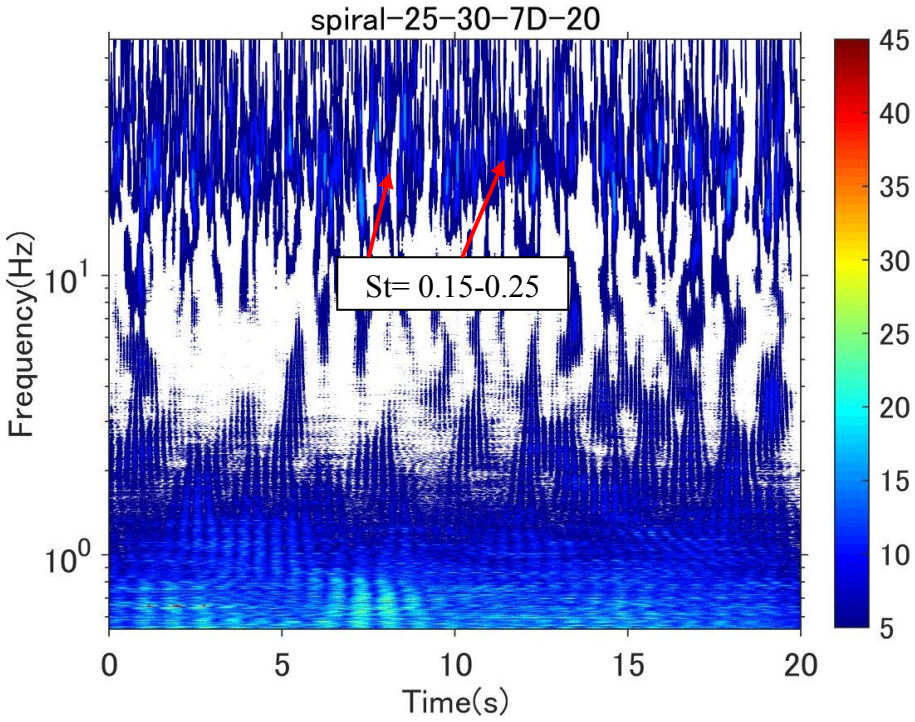

Figure 5-35 Wavelet analysis of fluctuating wind velocity in the wake of stationary spiral protuberance cable (Smooth flow, Location= 7D, U=15 and 20m/s, β=30° and α= 25°)

5.4.1.1 Interruption of shedding correlation

In case of circular cylinder, it was found that the low frequency has a high correlation with high energy; therefore, it can create strong excitation force. Currently, coherence also

used for assessing the correlation of wake flow in span-wise direction of spiral protuberance cable. The correlation of wake flow of flow angel 30° and inclination 25° can be seen at Figure 5-36 and 5-37. Under comparison with circular cable, it is found that spiral cable has higher correlation at Strouhal number (fD/U) around ~0.2 which corresponding to Karman vortex component. In the other expression, owning to spiral protuberance, shedding correlation of low frequency flow was mitigated while the Karman vortex shedding correlation increased again. According to previous studies, when KV shed, amplitude becomes small [14, 15]. At low frequency flow band, spiral protuberance exhibited very low correlation compare to circular surface. Similar trends also found for different wind attack angles at flow angle 45° and inclination 25° or flow angle 0° and inclination 25° as Figure 5-38, 5-39 and 5-40. The further correlation analysis can be referred more at Appendix 11. In conclusion, the suppression mechanism procedure is as following: In presence of spiral, flow separation point is fixed, the regularity of flow shedding will be maintained even though the Karman Vortex is suppressed in this case. Then, the vortex continue shedding regularly. Consequently, low frequency vortices does not be generated and its spatial correlation also disrupted. It leads to no excitation force created. Consequently, the dry galloping will be mitigated.

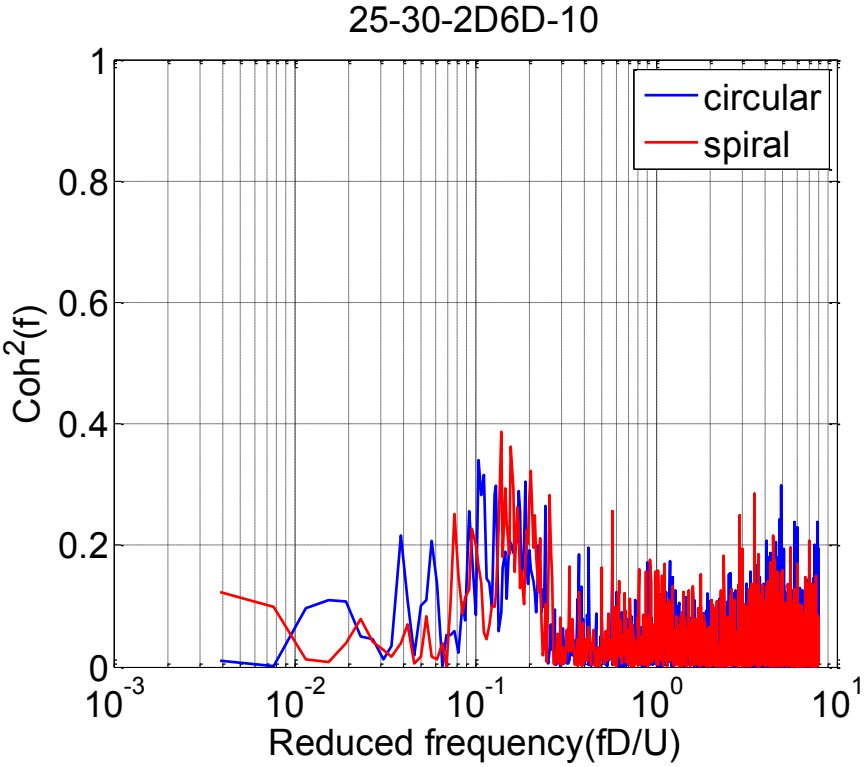

Figure 5-36 Coherence of fluctuating wind velocity in the wake (Smooth flow, Location= 6D, U=15 m/s, β=30° and α= 25°)

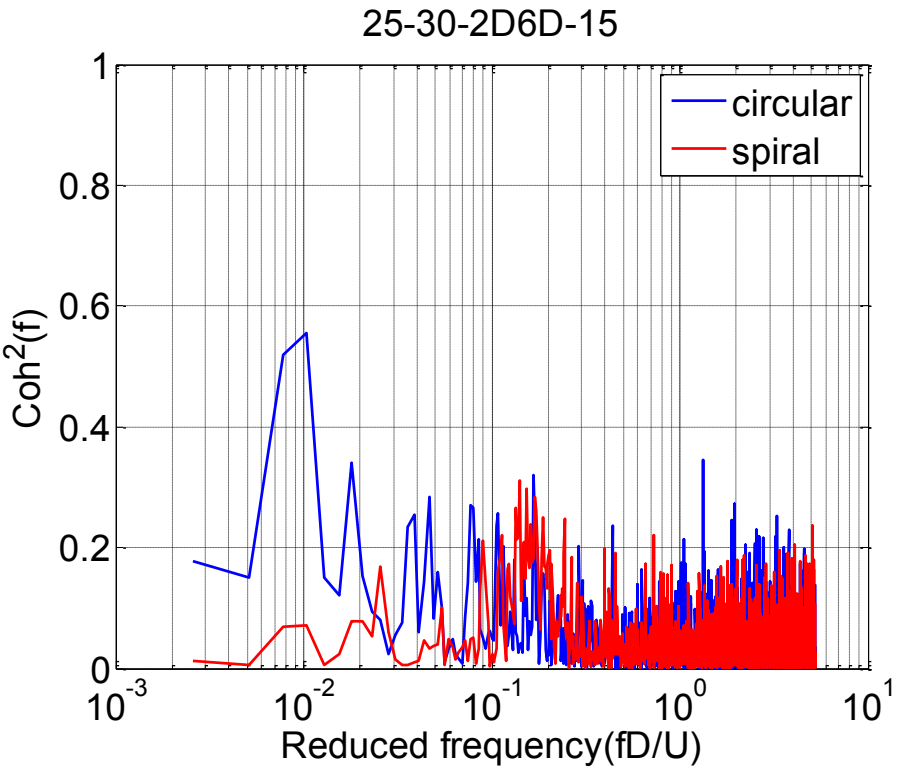

Figure 5-37 Coherence of fluctuating wind velocity in the wake (Smooth flow, Location= 6D, U=15 m/s, β=30° and α= 25°)

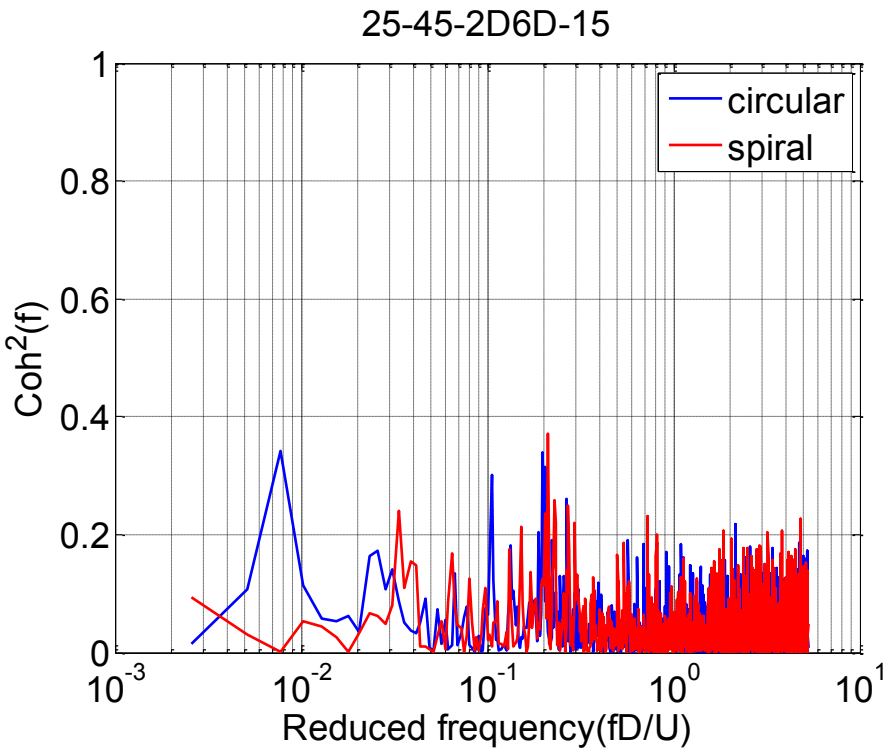

Figure 5-38 Coherence of fluctuating wind velocity in the wake (Smooth flow, Location= 6D, U=15, β=30° and α= 25°)

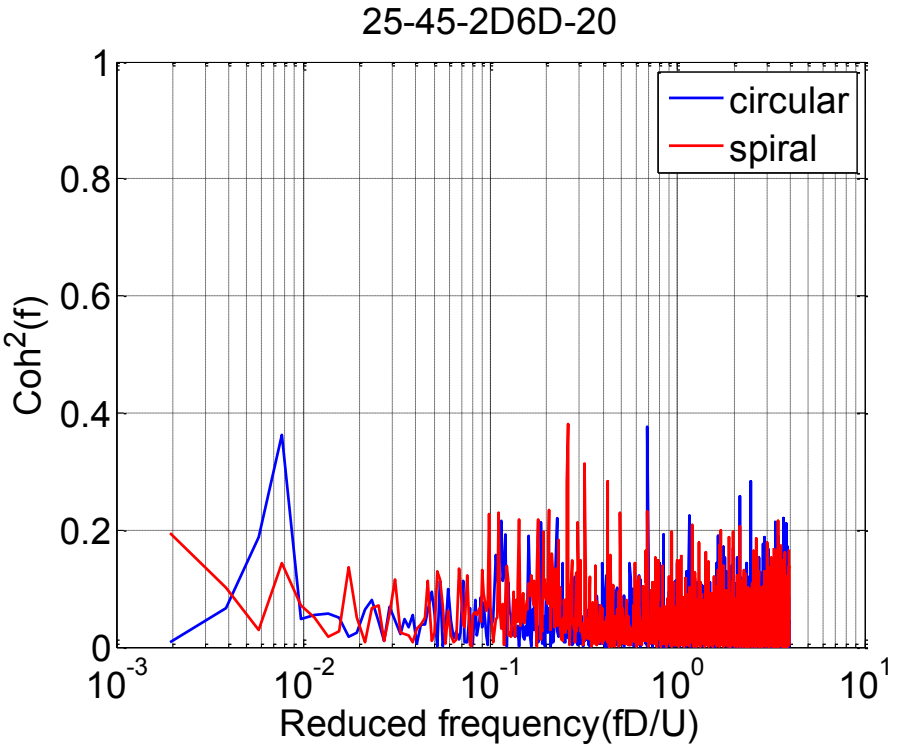

Figure 5-39 Coherence of fluctuating wind velocity in the wake (Smooth flow, Location= 6D, U=15 m/s, β=30° and α= 25°)

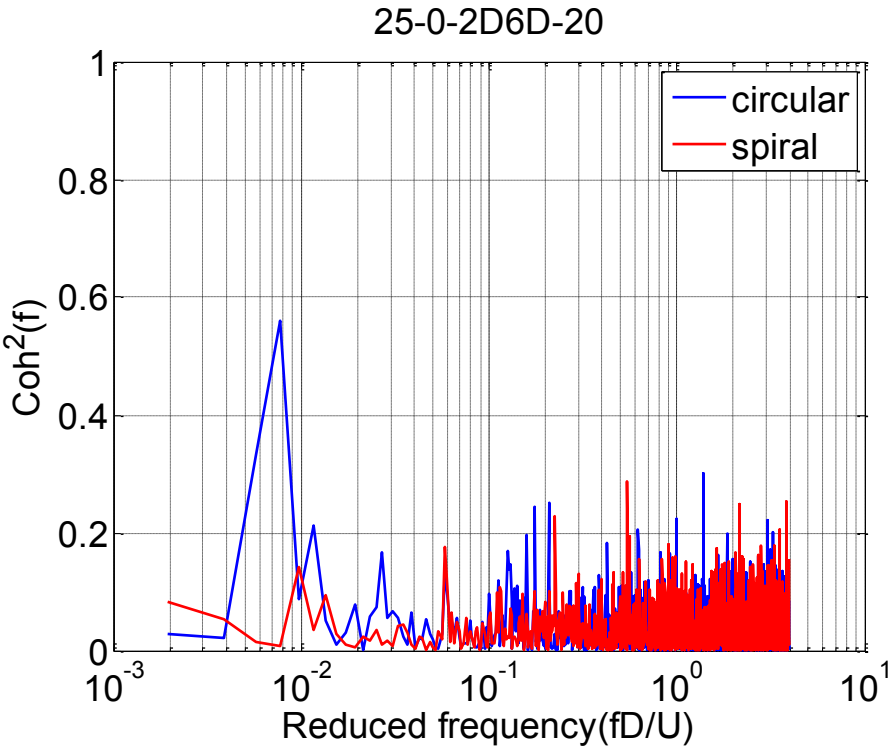

Figure 5-40 Coherence of fluctuating wind velocity in the wake (Smooth flow, Location= 6D, U=15 m/s, β=30° and α= 25°)

5.4.2 Further understanding on axial flow role

Figures 5-41 and 5-42 illustrate the comparison of axial flow distribution between spiral protuberance cable and circular cable. The wind attack angle was 25° of inclination and 30° of flow angle. Cable diameter was 158mm. The wind speed of 10 and 15m/s where the large amplitude vibration occurred, will be measured. Generally, the intensity of axial flow is high for both cable types. In presence of spiral protuberances, axial flow tend to decrease from upstream cable end to the centerline of cable, then it was approximately level off to downstream end. This kind of pattern is far different from the tendency of circular one. In the upstream cable end, axial flow velocity was around 60-70% of incoming velocity whereas it was 40-50% from center to downstream cable end. In addition, the stream-wise axial flow distribution was also recorded. In this measurement, the anemometer was located at centerline from 0.2D to 2D with steps same to measurement for circular cable. According to Figure 5-26, axial flow was fluctuated frequently and different trends compare to smooth surface cable but intensity still high. There are some a suppression of axial flow in location around 0.6D near the wake of cable. The intensity at 0.6D was around 30%-50% at 0.6D and increase to 50-90% at 0.8D-1D, and then it leveled off until the end of cable. In this case, the existence of axial flow also detected with the high intensity and no large amplitude vibration was recorded. It is therefore obviously that axial flow is the inherence characteristic of yawed/inclined cable to the wind, it can contribute partly in exciting galloping but not the centerpiece of this phenomenon. In addition, the existence of axial flow confirmed that why Karman vortex also suppressed in case of spiral protuberances.

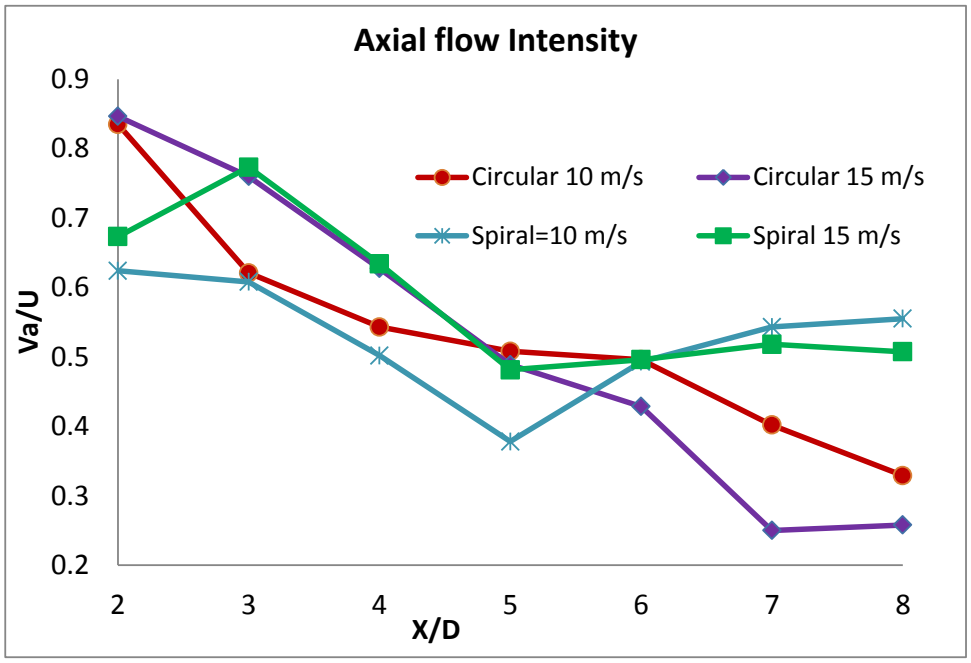

Figure 5-41 Comparison of spiral cable and circular cable (span-wise direction)

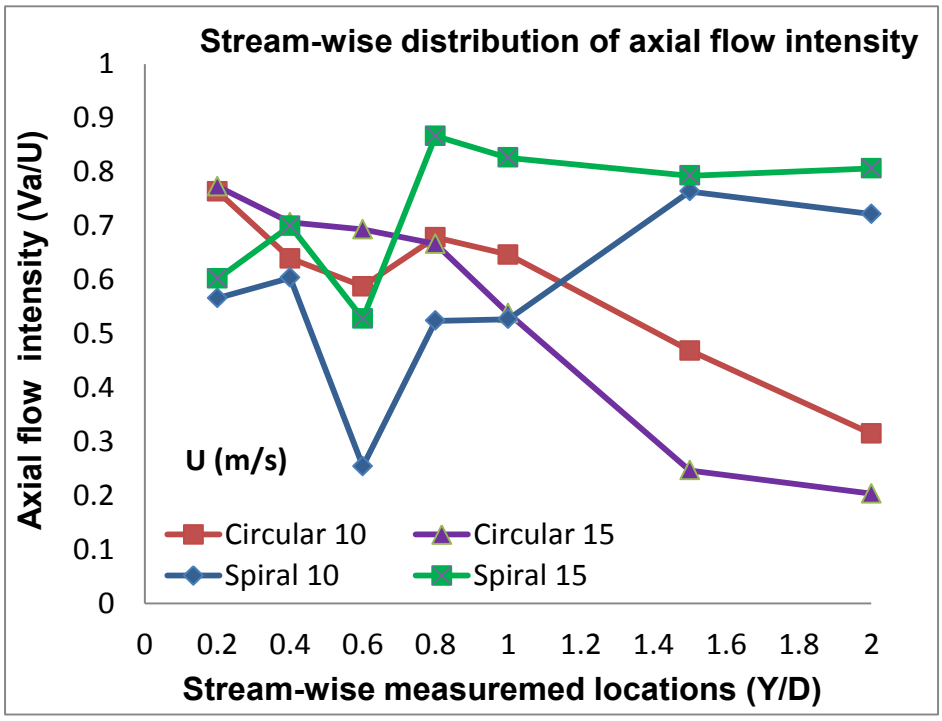

Figure 5-42 Comparison between spiral cable and circular cable (Stream-wise)

5.4.3 High aerodynamic damping of spiral protuberance cable

According to discussion in chapter 4, dry galloping of a stay cable was associated with the occurrence of negative aerodynamic damping. To evaluate the aerodynamic damping ratio in dry condition for spiral protuberance cable, the model was also manually excited and the free-vibration decay recorded using two accelerators at cable ends. The tests were carried out with the same condition to the experiment of circular cylinder test in section 4.2.6. The aerodynamic damping ratio (ζ_a) was determined by same equation (4.2). The twelve-spiral protuberance cable with diameter 110 and 158mm was measured in this section, respectively.

Figure 5-43 illustrates the aerodynamic damping ratio of 110 mm spiral protuberance cable at inclined angle 25° and flow angle 30°. Generally, there was no negative aerodynamic damping was recorded. Aerodynamic damping increased direct proportionally with the wind speed and reached the maximum value around 0.64% at reduced wind speed 200. This is very high damping level because the cable after installing dampers, its damping is approximate under 0.6% [16]. Besides that, in case of circular cylinder, low aerodynamic damping less than 0.03% occurred in many wind speeds. Nevertheless, this kind of low damping level could not be seen in case of spiral one. The same trend and characteristic were found when cable diameter changed to 158mm as Figure 5-44. In comparison with circular

cylinder, spiral protuberances exhibited extremely higher aerodynamic damping ratio, especially for medium and high wind speed, that is reason why spiral protuberance was stable under wind attack.

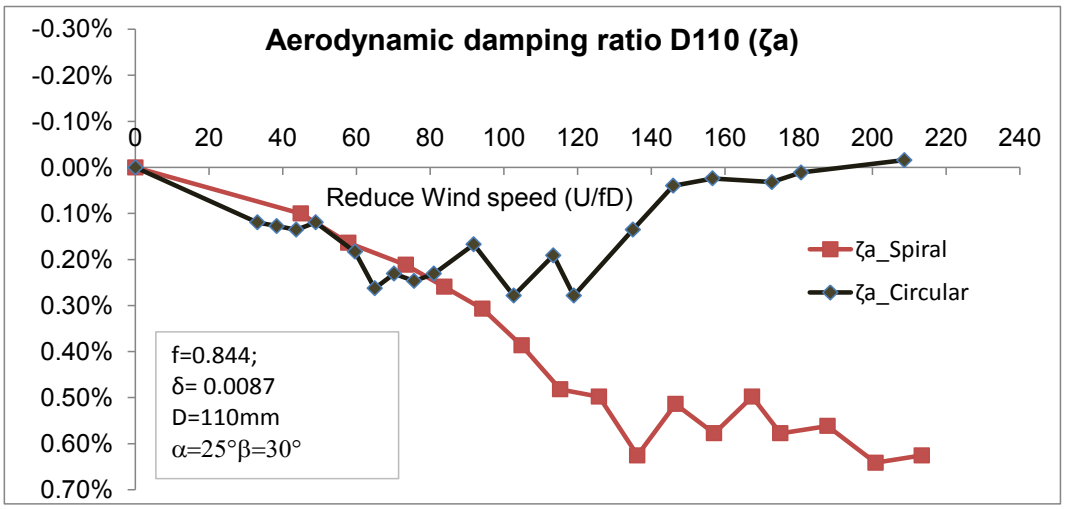

Figure 5-43 Effect of spiral protuberances on aerodynamic damping (D110mm)

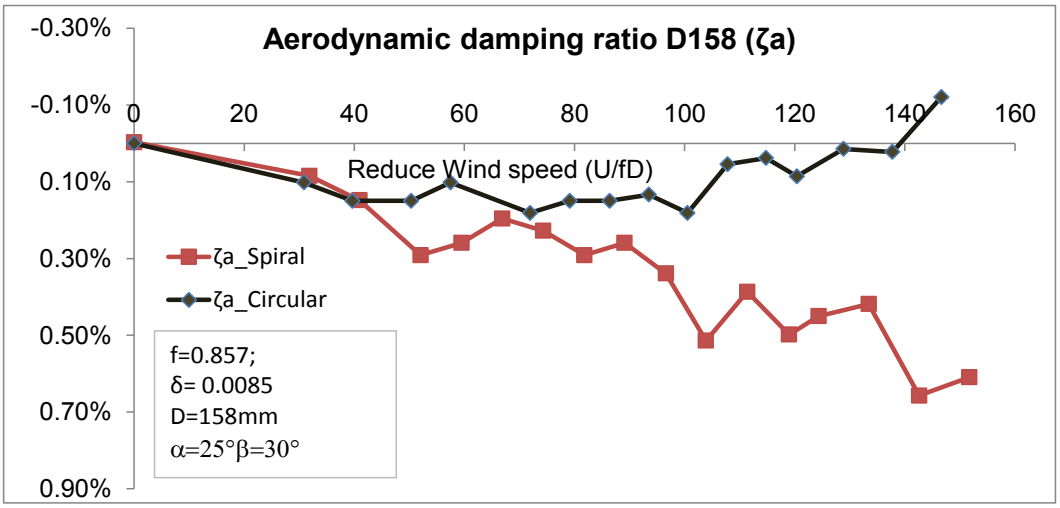

Figure 5-44 Effect of spiral protuberances on aerodynamic damping (D158mm)

5.5 Summary of chapter 5

Under above results and discussions, it is obviously that spiral protuberance cable could stop both dry galloping and rain-wind induced vibration when it is well fabricated under a reasonable range of number protuberances, winding pitch and protuberance size. The fabrication recommendation for spiral protuberance type was proposed.

In presence of spiral protuberances, axial flow tend to reduce from upstream cable end to the centerline of cable, then it was approximately level off to downstream end. This kind of pattern is far different from the tendency of circular one. However, the intensity of axial flow was still high. That mean axial flow can contribute partly to excite galloping as previous study figured out but it cannot be the main factor of galloping excitation.

Furthermore, the mitigation mechanism of spiral protuberances were shed the light on. The suppression mechanism involved three main facts: the mitigation of the wake flow energy and the suppression of low frequency component and the shedding correlation destruction. In addition, the spiral protuberances can increased much of aerodynamic damping of cable, especially at high wind speed. Aerodynamic damping increased proportionally with the wind speed and reached a value more than 0.6% at high-reduced wind speed.

Bibliography

1. Poulin, S. and A. Larsen, *Drag loading of circular cylinder inclined in the along-wind direction.* J. Wind Eng. Ind. Aerodyn., 2007(95): p. 1350-1363.

2. Watkins, B.J.V.a.R.D. *Flow-induced vibrations of cylindrical structures*. 1964. Proceedings Hydraulics and Fluid Mechanics.

3. Walshe, D.E. and L.R. Wootton. *Preventing wind-induced oscillations of structures of circular section*. in *Proc. Inst. Civ. Eng., .* 1970.

4. Cowdrey, C.F. and J.A. Lawes, *Drag Measurements at High Reynolds Numbers of a Circular Cylinder Fitted with Three Helical Strakes.*, in *Aero Report 384*. 1959, National Physical Laboratory.

5. Ruscheweyh , H., *Tip effect on vortex excited oscillation of a model stack with and without ellfux stream.* Symp. on Flow Induced Structural Vibrations, Karlsruhe, Germany, 1972: p. 101-103.

6. L., W. and J.F.M. Maybrey, *Further Experiments on the Use of Helical Strakes for Avoiding Wind Excited Oscillations of structures of circular or nearly circular section.* National Physical Laboratory, 1959(Aero Report 381).

7. Scruton, C. and D.E.J. Walshe, *A means for avoiding wind-excited oscillations of structures with circular or nearly circular cross section.* . National Physical Laboratory, Aero Report 335, 1957.

8. Wong, H.Y., *An aerodynamic means of up pressing vortex excited oscillation.* Proc. Inst. Ar. Eng., 1997. **Part 2 (1977)**(Paper 1030.).

9. Larose , G., et al. *Wind-tunnel investigations of an inclined stay cable with a helical fillet*. in *6th European and African Wind Engineering Conference*. 2013.

10. K. Kleissl and C.T. Georgakis, *Comparison of the aerodynamics of bridge cables with helical fillets and a pattern-indented surface.* Journal of Wind Engineering and Industrial Aerodynamics, 2012. **104-106**: p. 166-175.

11. Gu, M. and X. Du, *Experimental investigation of rain-wind- induced vibration of cables in cable-stayed bridges and its mitigation.* Journal of Wind Engineering and Industrial Aerodynamics, 2005. **93**: p. 79-95.

12. Yagi, T.O., et al. *Modification of surface configurations of stay cables for drag force reduction and aerodynamic stabilization*. in *The 13th International Conference on Wind Engineering*. 2011. Amsterdam.

13. VO, D., et al., *Experimental study on dry-state galloping with various wind relative angles and its countermeasures.* Journal of Structural Engineering (JSCE), 2014. **60A**: p. 428-436.

14. Nakamura, Y., K. Hirata, and T. Urabe, *Galloping of rectangular cylinders in the presence of a splitter plate.* Journal of Fluids and Structures, 1991. **5**: p. 521-549.

15. Matsumoto, M., et al., *Dry-galloping characteristics and its mechanism of inclined/yawed cables.* Journal of Wind Engineering and Industrial Aerodynamics, 2010. **98**: p. 317-327.

16. FHWA/HNTB, *Wind induced vibration of stay cables. Interim final report, RDT 05-004.* 2005.

Chapter 6: Conclusions and Recommendations

On the basis of experimental study conducted on the stay cables WTT and data analysis, various aspects were considered, the following conclusions are established.

1. Dry galloping was a dangerous vibration with large amplitude vibration at some specific wind attack angles. The divergent type galloping was also recorded for dry galloping.

2. Dry galloping is less sensitive to the Scruton number change rather than frequency. Therefore, it is hard to suppress this type of vibration by increase damping of structure. Occurrence of DG associated with a strong recovery of surface pressure in leeward side and negative aerodynamic damping in high wind speed. There is an existence of a strong axial flow channel located at 0.2D to 0.8D with intensity around 60-80% of incoming wind flow can contribute in mitigation of Karman vortex shedding.

3. The mechanism of dry galloping strongly relates to the forming of low dominant frequency components and interruption of Karman vortex near the wake of cable. Low frequency wake flow exhibited high energy and high correlation, which can create large forces to excite galloping. The appearance of low frequency component was coupled with interruption of Karman vortex. The occurrence procedure of dry galloping can be summarized as follow: Due to the effect of axial flow, the Karman Vortex will be interrupted. Flow regime will be unstable and it will enter the critical Reynolds regime. Low frequency flow/vortices become dominant with high excitation force. Consequently, stayed-cable will be excited.

4. Indented surface and parallel protuberances used to apply for RWIV; however, it could not eliminate DG well in low Scruton number range.

5. Spiral protuberance cable could stop both dry galloping and rain-wind induced vibration when it is well fabricated under a reasonable range of number protuberances, winding pitch and protuberance size. Currently, the 04, 06 and 12 spiral protuberances with protuberance size from 3x7.5 to 5x7.5 associated with winding pitch from 2.95D to 4.78D are strongly recommended for spiral cable fabrication.

6. The spiral protuberances can enhance much of aerodynamic damping of cable. Its aerodynamic damping increased directs proportionally with the wind speed and can reach very high value of damping.

7. In presence of spiral protuberances, axial flow tend to reduce from upstream cable end to the centerline of cable, then it was approximately level off to downstream end. This kind of pattern is different from the tendency of circular one. However, the intensity quite same for various case of surface modifications, therefore axial flow does not depend on cable surface, it is inherent characteristic of yawed/inclined angle. It can interrupt Karman Vortex shedding but not the centerpiece of dry galloping. The suppression of Karman vortex shedding is only necessary condition**,** not the sufficient condition for dry galloping.

8. The mitigation mechanism of spiral protuberances strongly relates to suppression of the low frequency flows/vortices and its shedding correlation. In detail, the presence of spiral protuberance will disrupt thoroughly the shedding correlation or it will not generate the low frequency flows/vortices. Therefore it can mitigate the excitation force of wake flow, leading to reduce the excitation force. Consequently, the dry galloping will be suppressed.

Appendix 1: Experimental parameters of circular cylinder

Diameter	Inclined angle	Flow angle	Cross section	Rain	Natural frequency (Hz)	Logarithm decrement	Cable mass (kg)	Spring mass (kg)	Rings mass (kg)	Unit mass (kg/m)	D (m)	ρ (with rain) (kg/m3)	ρ (without rain) (kg/m3)	Sc (with rain)	Sc (No rain)
φ110	40°	60°	circular	w・w/o	0.87	0.009	11.98	0.34	0.38	8.15	0.110	1.240	1.240	9.77	9.77
		45°	circular	w・w/o	0.85	0.009	11.98	0.34	0.38	8.15	0.110	1.200	1.220	10.10	9.93
		30°	circular	w・w/o	0.85	0.010	11.98	0.34	0.38	8.15	0.110	1.200	1.220	11.22	11.04
		15°	circular	w・w/o	0.85	0.010	11.98	0.34	0.38	8.15	0.110	1.220	1.240	11.04	10.86
		0°	circular	w・w/o	0.85	0.010	11.98	0.34	0.38	8.15	0.110	1.220	1.210	11.04	11.13
φ158		0°	circular	w・w/o	0.85	0.010	14.55	0.28	0.38	9.86	0.158	1.210	1.210	6.53	6.53
		15°	circular	w・w/o	0.83	0.014	14.55	0.28	0.38	9.86	0.158	1.200	1.210	9.22	9.14
		30°	circular	w・w/o	0.82	0.012	14.55	0.28	0.38	9.86	0.158	1.200	1.200	7.90	7.90
		45°	circular	w・w/o	0.82	0.012	14.55	0.28	0.38	9.86	0.158	1.200	1.220	7.90	7.77
		60°	circular	w・w/o	0.82	0.012	14.55	0.28	0.38	9.86	0.158	1.220	1.210	7.77	7.83
φ110	25°	60°	circular	w・w/o	0.85	0.010	11.98	0.34	0.38	8.15	0.110	1.210	1.200	11.13	11.22
		45°	circular	w・w/o	0.82	0.008	11.98	0.34	0.38	8.15	0.110	1.210	1.210	8.90	8.90
		30°	circular	w・w/o	0.84	0.009	11.98	0.34	0.38	8.15	0.110	1.200	1.210	10.10	10.02
		15°	circular	w・w/o	0.84	0.008	11.98	0.34	0.38	8.15	0.110	1.200	1.200	8.98	8.98
		0°	circular	w・w/o	0.86	0.008	11.98	0.34	0.38	8.15	0.110	1.200	1.210	8.98	8.90
φ158		0°	circular	w・w/o	0.90	0.010	14.55	0.28	0.38	9.86	0.158	1.210	1.210	6.53	6.53
		15°	circular	w・w/o	0.90	0.009	14.55	0.28	0.38	9.86	0.158	1.220	1.220	5.83	5.83
		30°	circular	w・w/o	0.86	0.010	14.55	0.28	0.38	9.86	0.158	1.190	1.190	6.64	6.64
		45°	circular	w・w/o	0.86	0.010	14.55	0.28	0.38	9.86	0.158	1.190	1.180	6.64	6.69
		60°	circular	w・w/o	0.78	0.014	14.55	0.28	0.38	9.86	0.158	1.200	1.200	9.22	9.22
φ158	9°	60°	circular	w・w/o	0.99	0.005	14.55	0.25	0.38	9.86	0.158	1.200	1.200	3.29	3.29
		45°	circular	w・w/o	1.00	0.006	14.55	0.25	0.38	9.86	0.158	1.200	1.210	3.95	3.92
		30°	circular	w・w/o	1.00	0.006	14.55	0.25	0.38	9.86	0.158	1.210	1.210	3.92	3.92

		15°	circular	w・w/o	1.02	0.006	14.55	0.25	0.38	9.86	0.158	1.200	1.200	3.95	3.95
		0°	circular	w・w/o	0.86	0.005	14.55	0.25	0.38	9.86	0.158	1.210	1.210	3.26	3.26
Summary					Natural frequency	Logarithm decrement				Damping ratio				Scruton number	Scruton number
				Max	1.02	0.014	-	-	-	0.22%	-	-	Max	11.22	11.22
				Min	0.78	0.005	-	-	-	0.08%	-	-	Min	3.26	3.26

Appendix 2: Redistribution of surface pressure in presence of single spiral protuberance

Single spiral fillet (single spiral protuberances) is much effective to mitigate DG at a yaw angle when installed at proper twined spacing with selected wire diameter. The vibration suppression of single spiral protuberances shows in Figure A-2.1. The relative position of spiral protuberances to the pressure measurement section shows at Figure A-2.2. The mean pressure coefficient distribution is illustrated at Figures from A-2.3 to A-2.6. Generally, the mean surface pressure coefficient divided in two zones which positive pressure in the upper half part of cable and negative value in the lower part. The surface pressure patterns are quite similar at four sections even though the location of fillet is different. Further, it decreased dramatically in lower side in presence of single helical fillet at 2D. That mean surface pressure redistributed when cable was wound with single helical fillet (single spiral protuberances) compare to circular cable as discussed above.

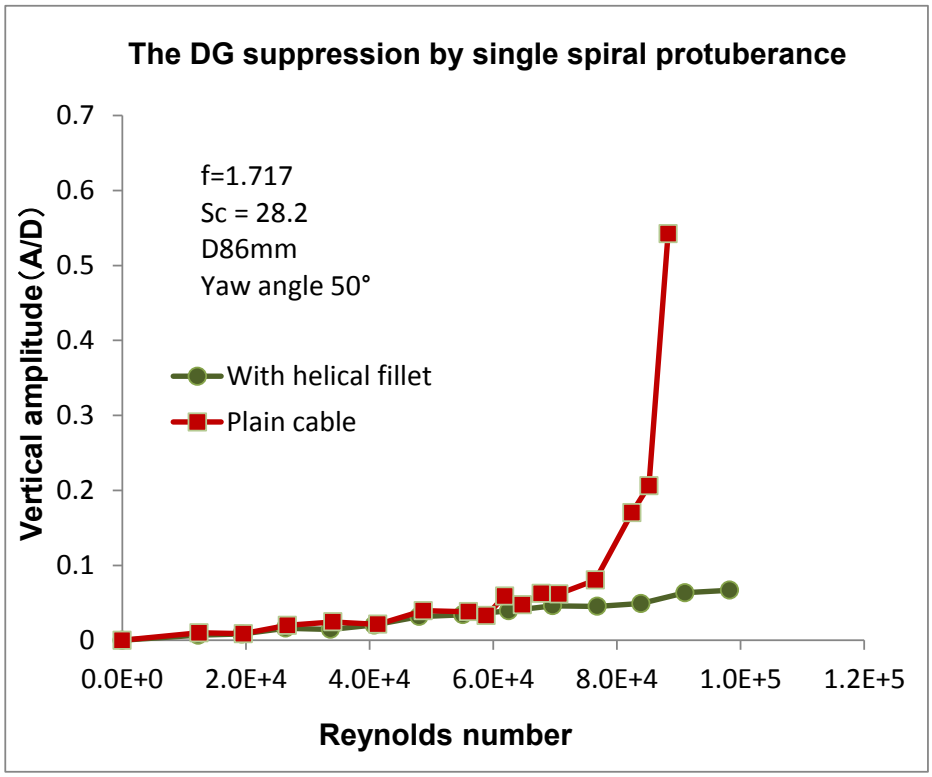

Figure A-2. 1 Response of cable at yawed angle 50° with single spiral protuberances

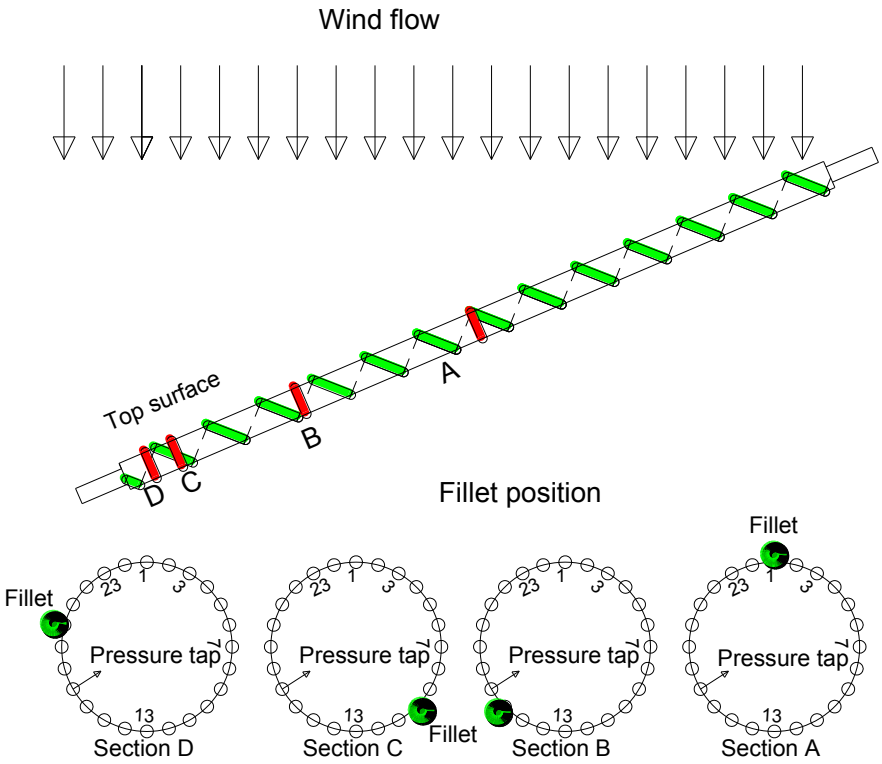

Figure A-2. 2 Relative position of protuberances to the Pressure measurement section

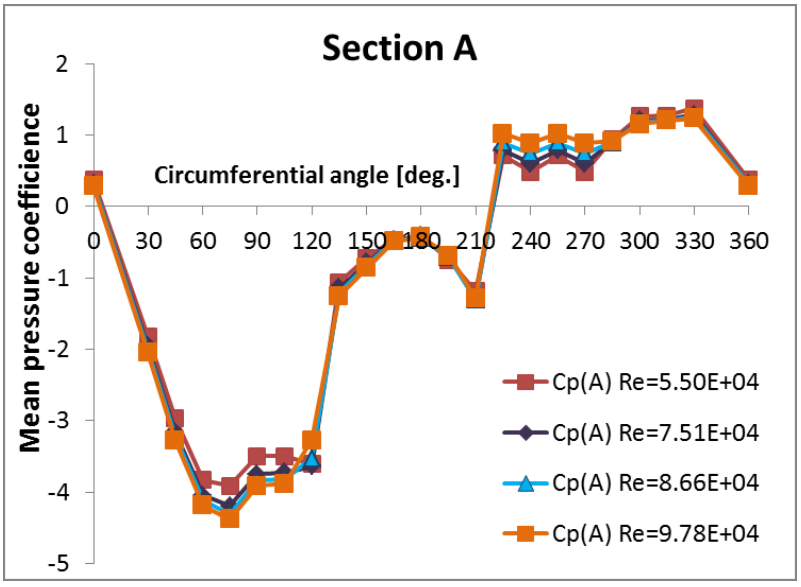

Figure A-2. 3 Pressure distribution at section A (Single helical fillet, yawed angle 50°)

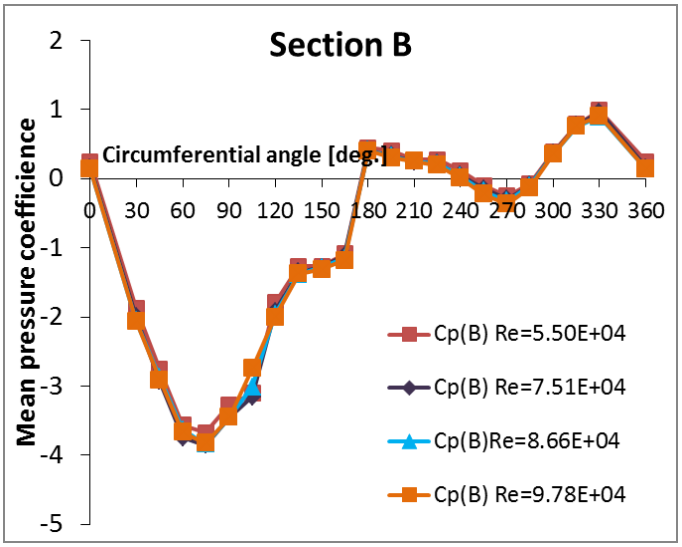

Figure A-2. 4 Pressure distribution at section B (Single helical fillet, yawed angle 50°)

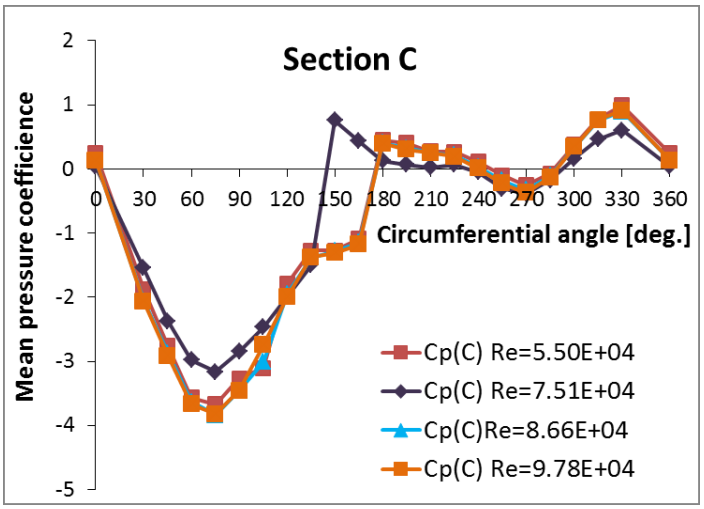

Figure A-2. 5 Pressure distribution at section C (Single helical fillet, yawed angle 50°)

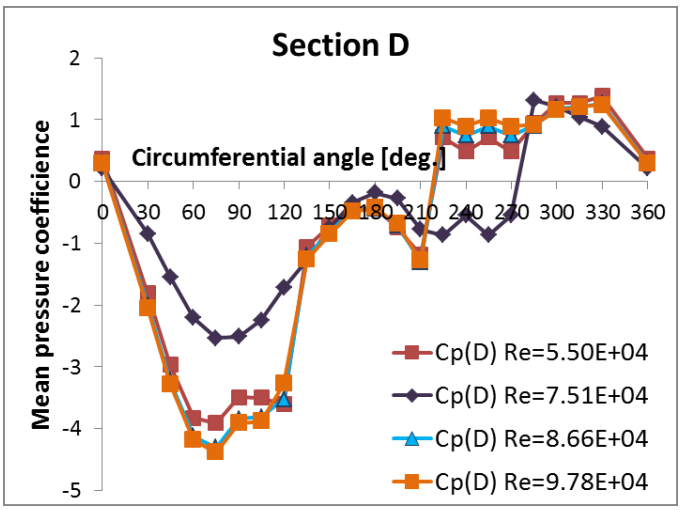

Figure A-2. 6 Pressure distribution at section D (Single helical fillet, yawed angle 50°)

Appendix 3: Power spectrum density of fluctuating wind velocity in the circular cable wake

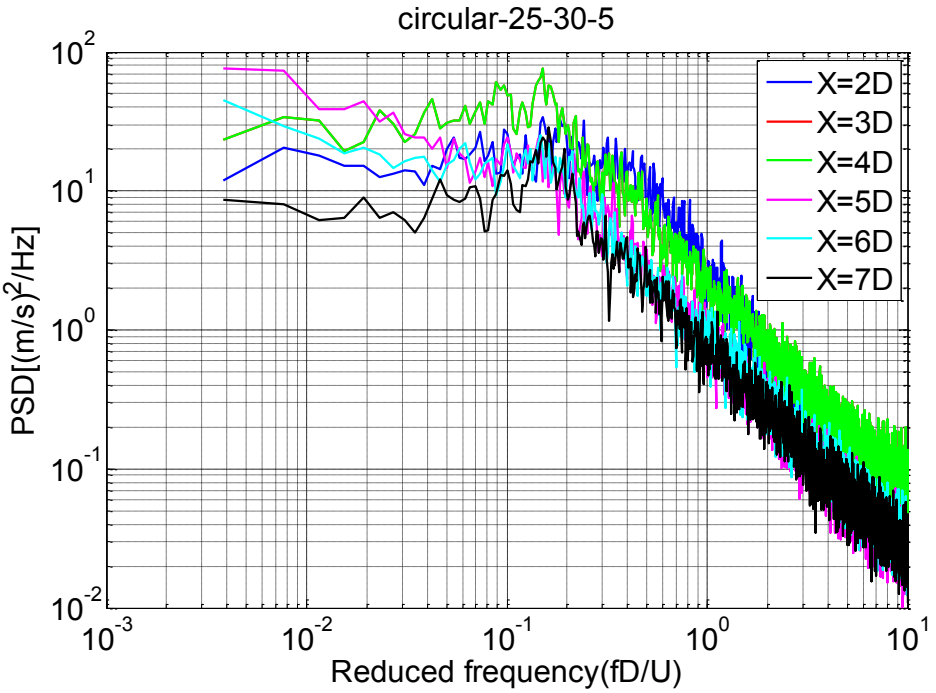

Figure A-3. 1 PSD of circular cylinder (U=5m/s, β=30° and α= 25°)

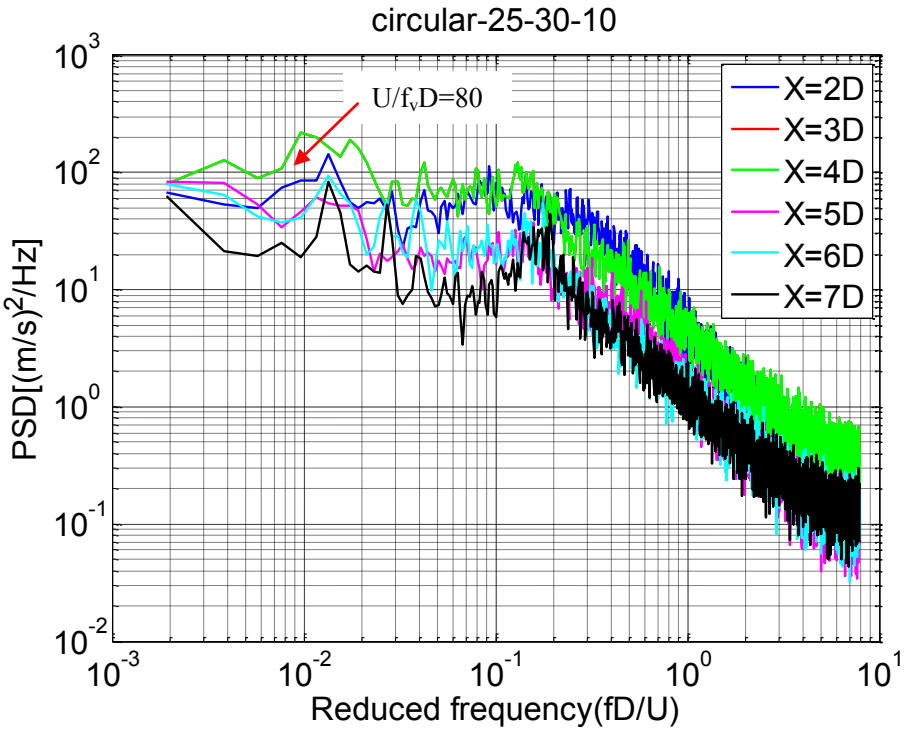

Figure A-3. 2 PSD of circular cylinder (U=10m/s, β=30° and α= 25°)

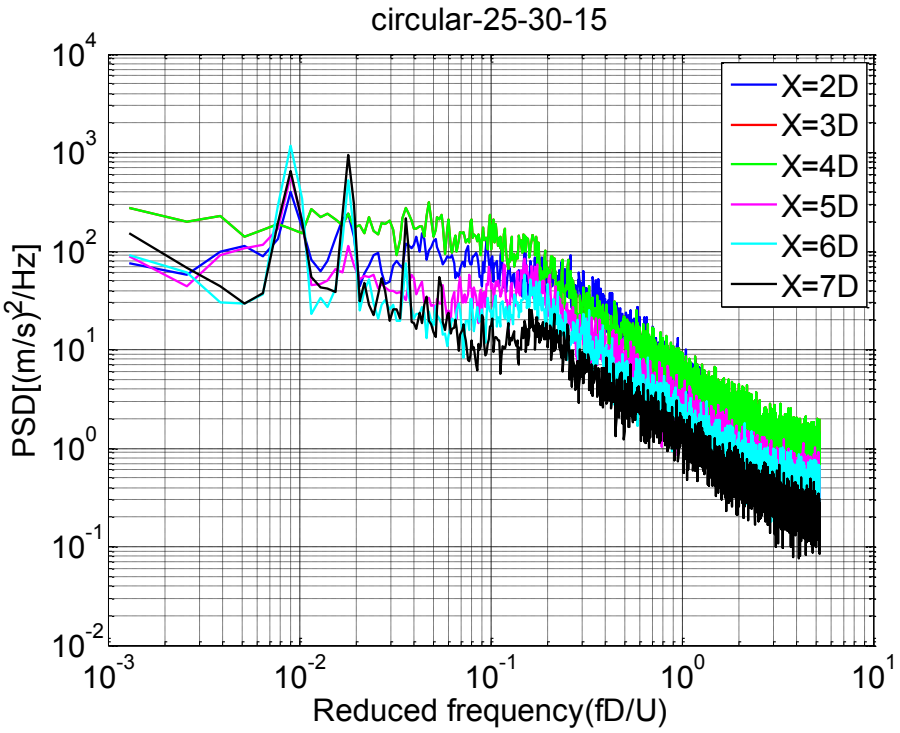

Figure A-3. 3 PSD of circular cylinder (U=15m/s, β=30° and α= 25°)

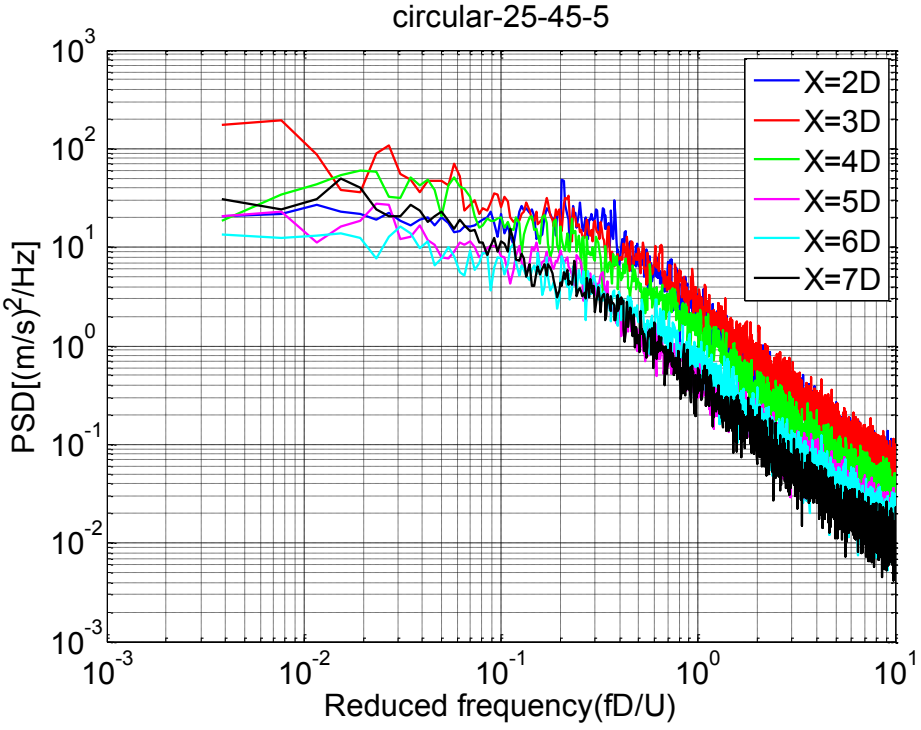

Figure A-3. 4 PSD of circular cylinder, D=158mm U=5m/s, β=45° and α= 25°

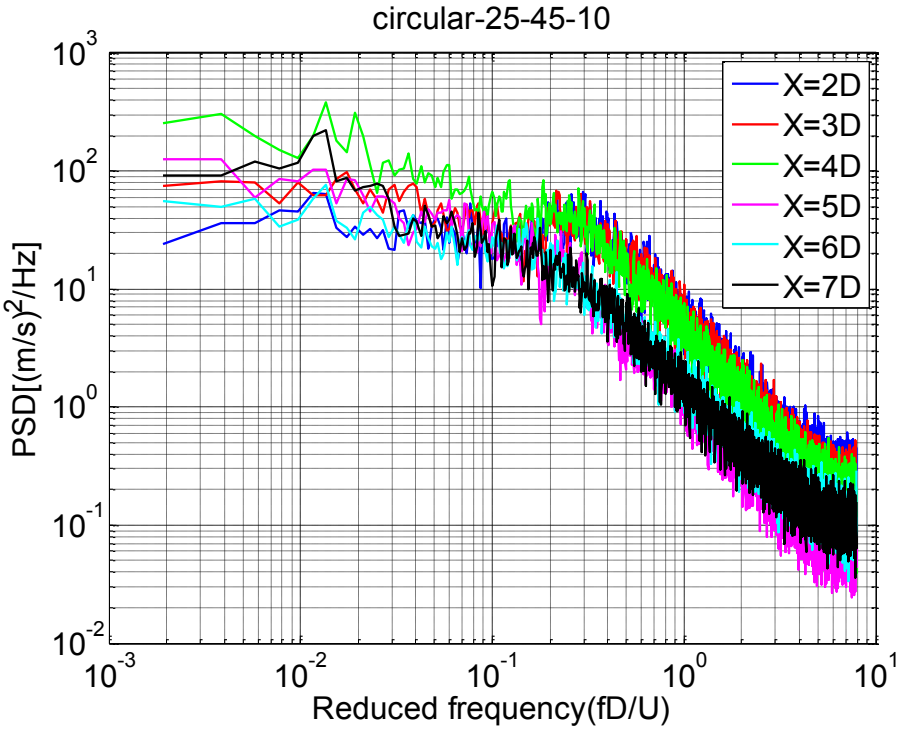

Figure A-3. 5 PSD of circular cylinder, D=158mm U=10m/s, β=45° and α= 25°

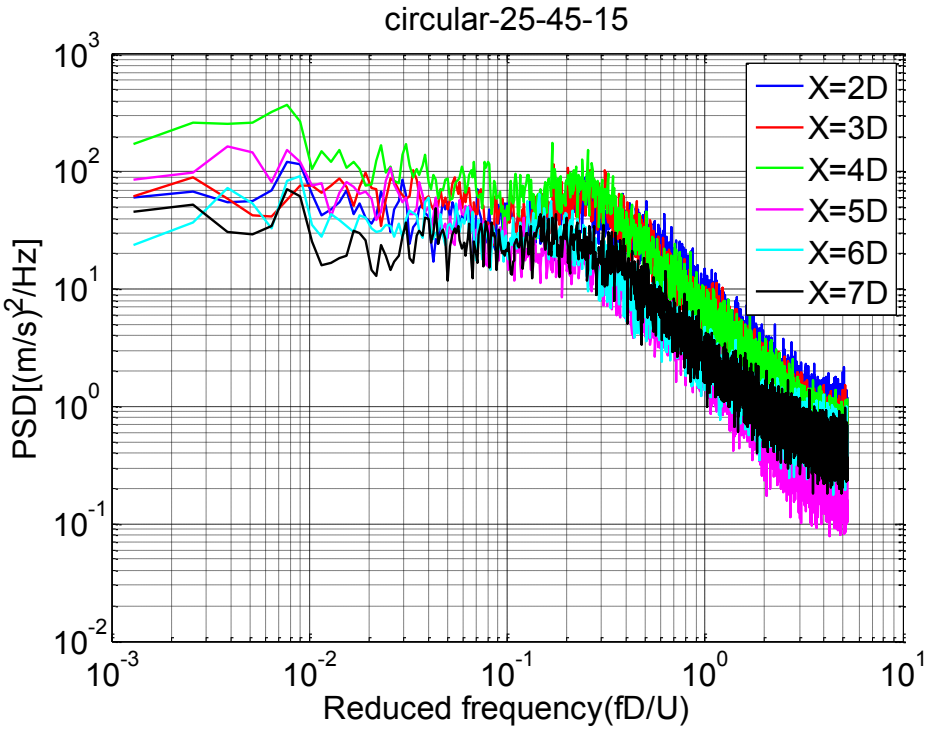

Figure A-3. 6 PSD of circular cylinder, D=158mm U=15m/s, β=45° and α= 25°

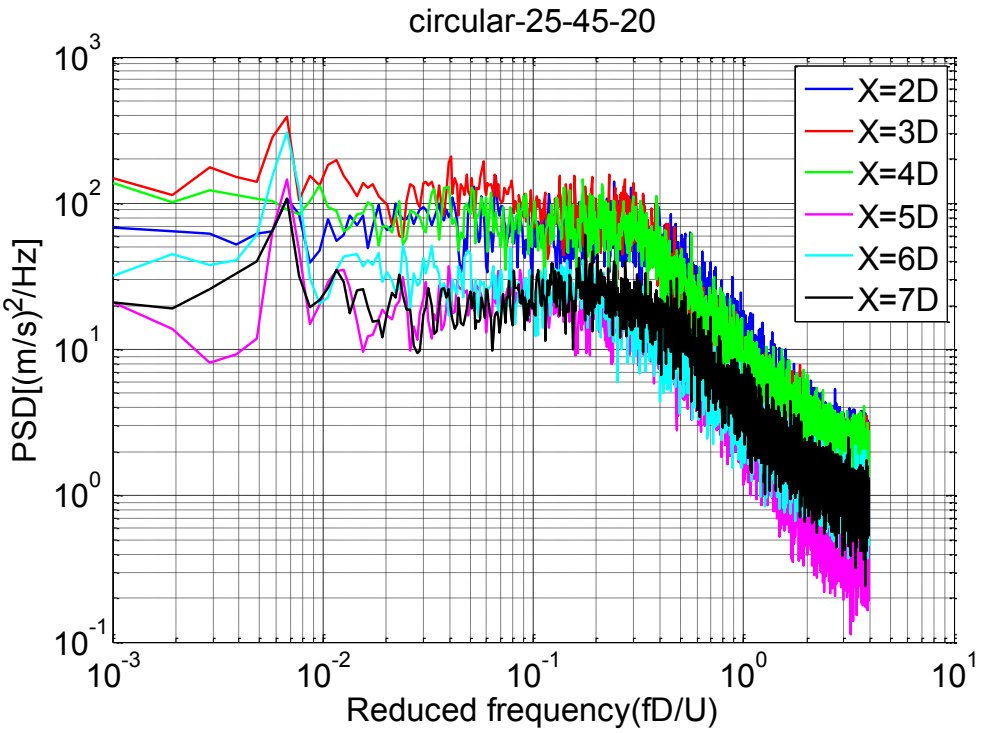

Figure A-3. 7 PSD of circular cylinder, D=158mm U=20m/s, β=45° and α= 25°

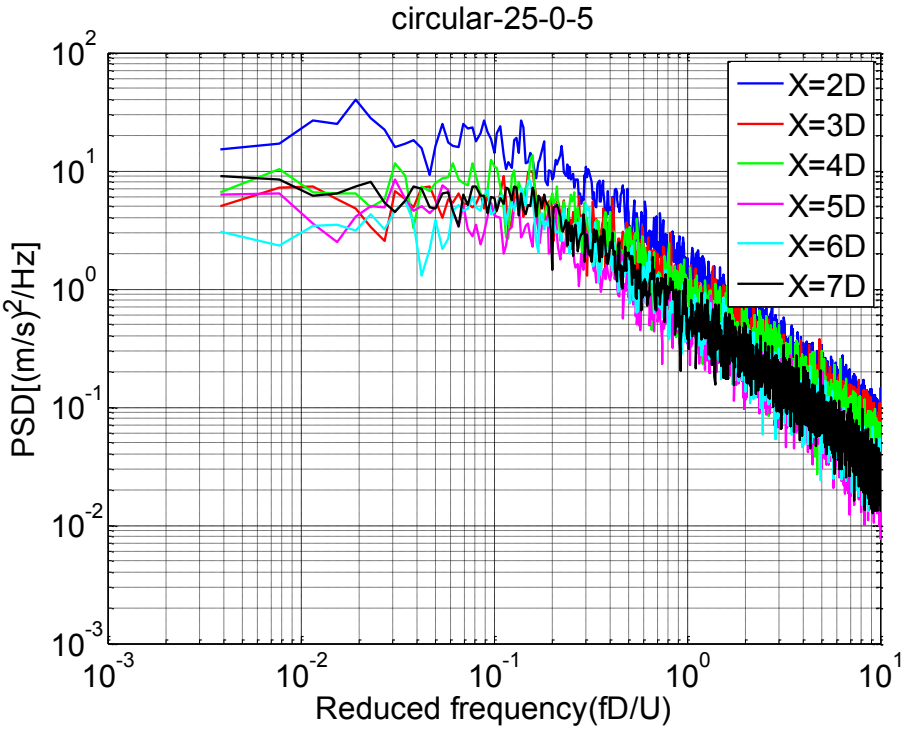

Figure A-3. 8 PSD of circular cylinder, D=158mm U=5m/s, β=0° and α= 25°

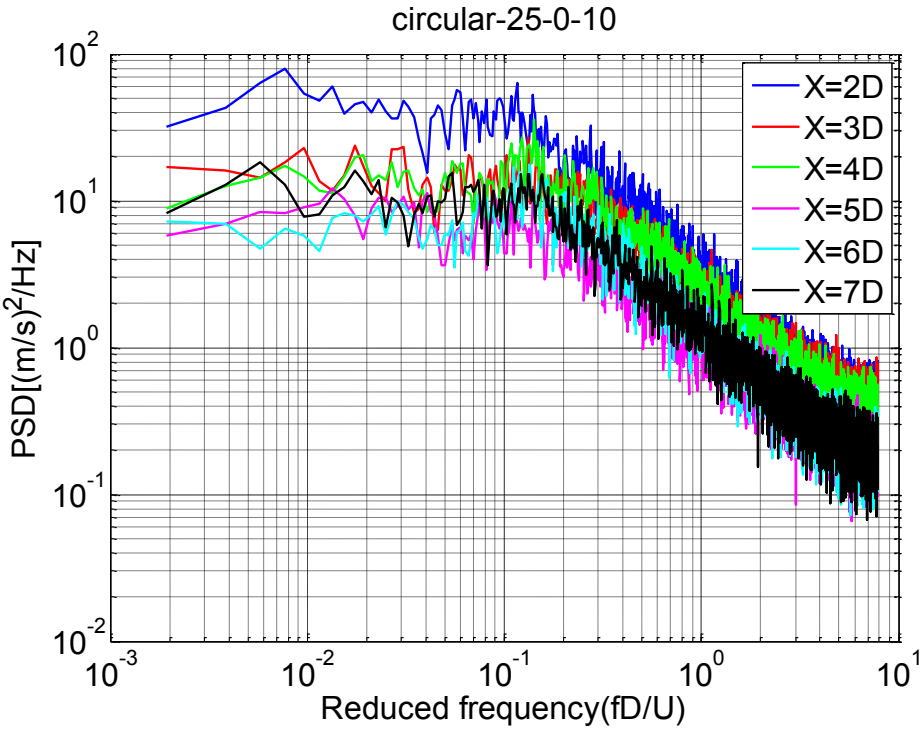

Figure A-3. 9 PSD of circular cylinder, D=158mm U=10m/s, β=0° and α= 25°

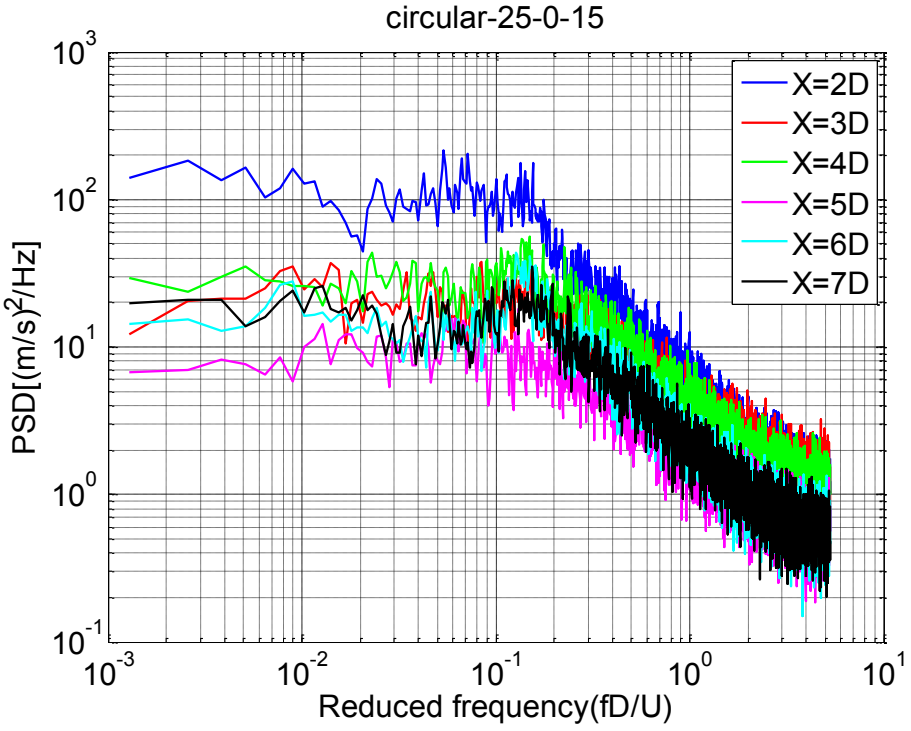

Figure A-3. 10 PSD of circular cylinder, D=158mm U=15m/s, β=0° and α= 25°

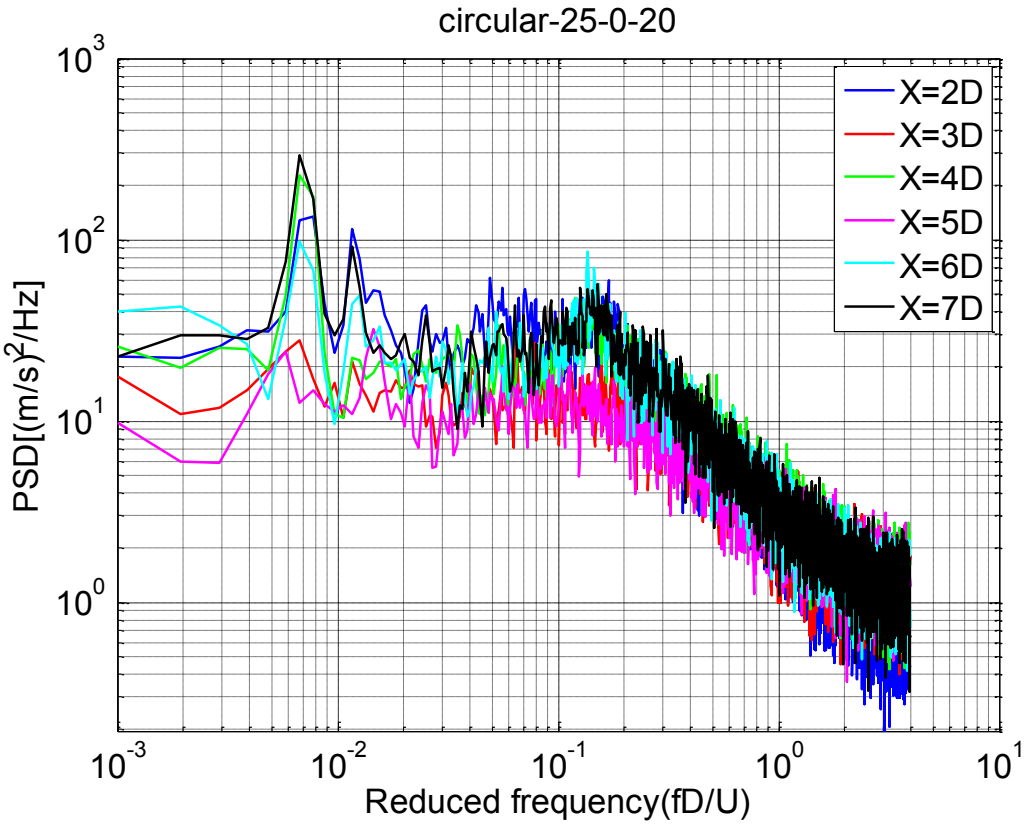

Figure A-3. 11 PSD of circular cylinder (U=20m/s, β=0° and α= 25°)

Appendix 4: Wavelet analysis of U fluctuating near circular cable wake

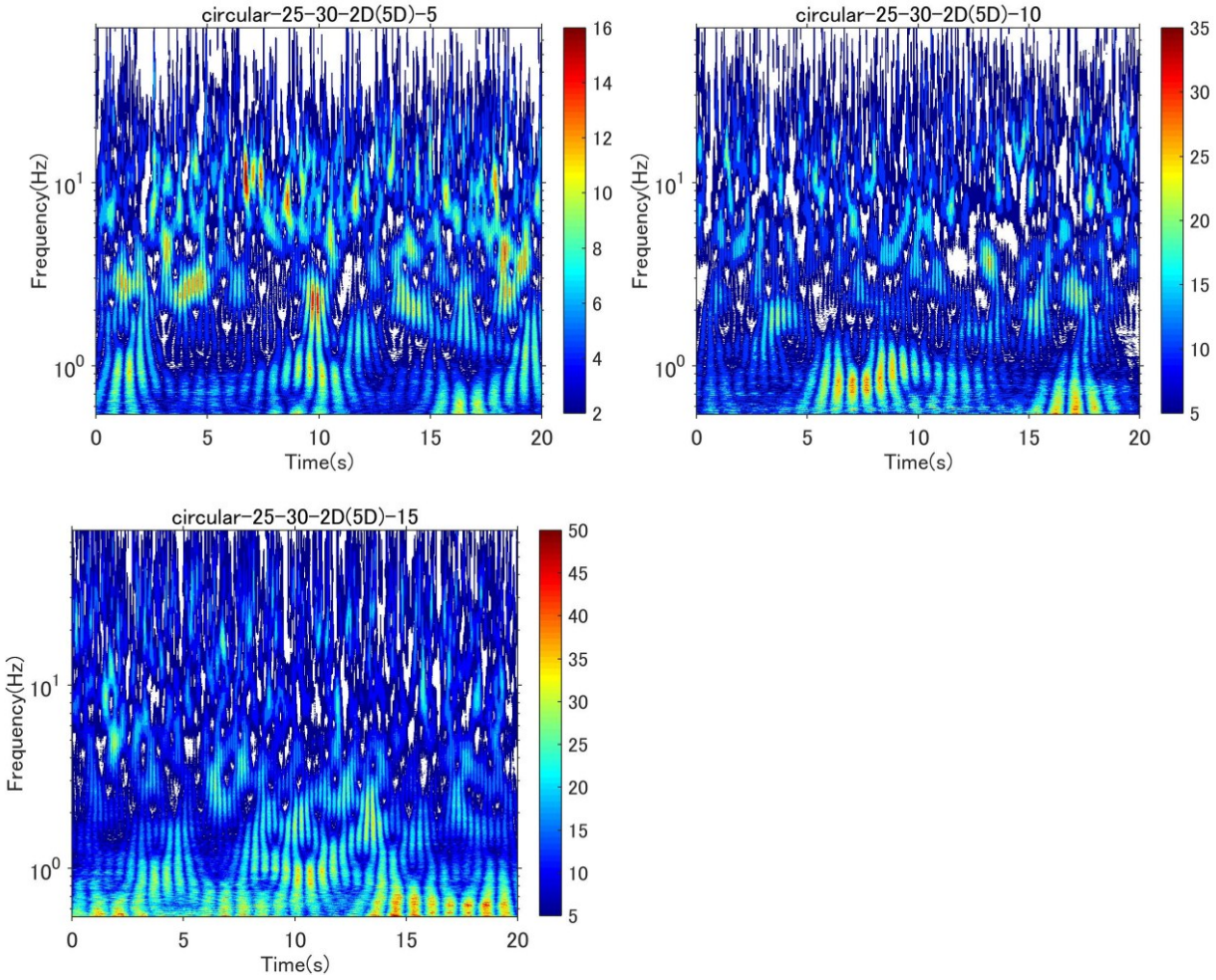

Figure A-4.1 Wavelet analysis (WA), Circular, 2D, U=5 -10-15m/s, β=30° and α= 25°

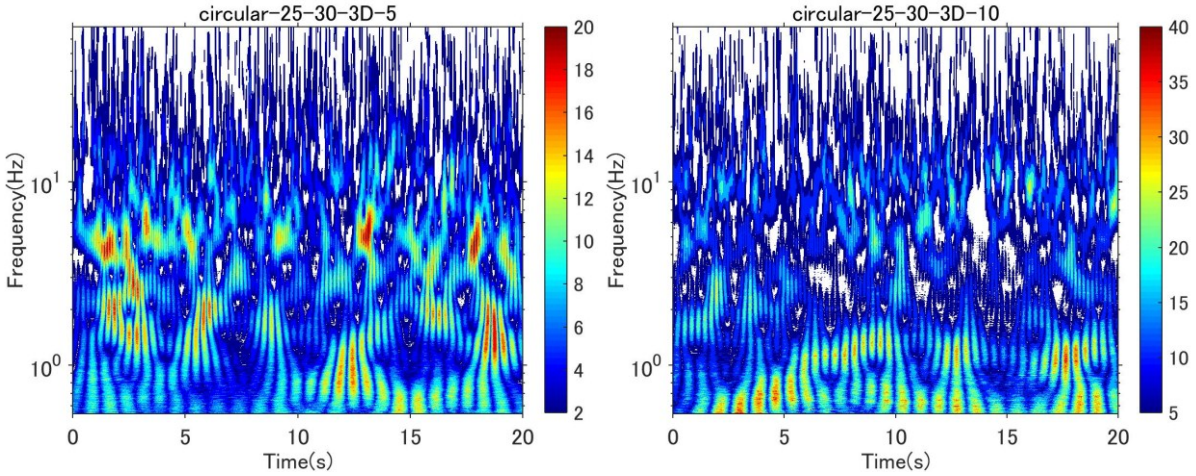

Figure A-4.2 WA of circular cylinder, L= 3D, U=5m/s - 10m/s, β=30° and α= 25°

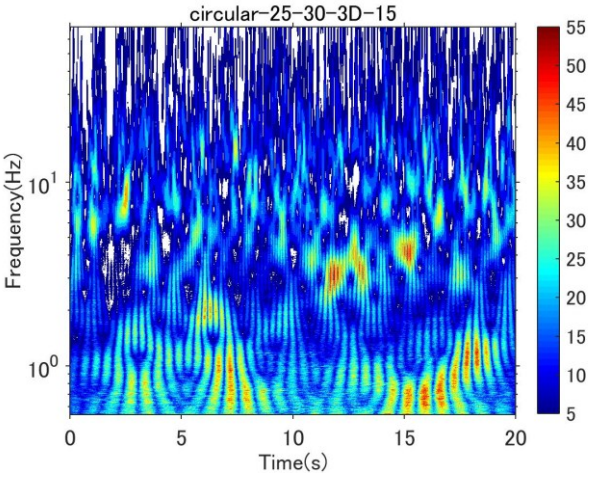

Figure A-4.3 WA of circular cylinder, L= 3D, U=15m/s, β=30° and α= 25°

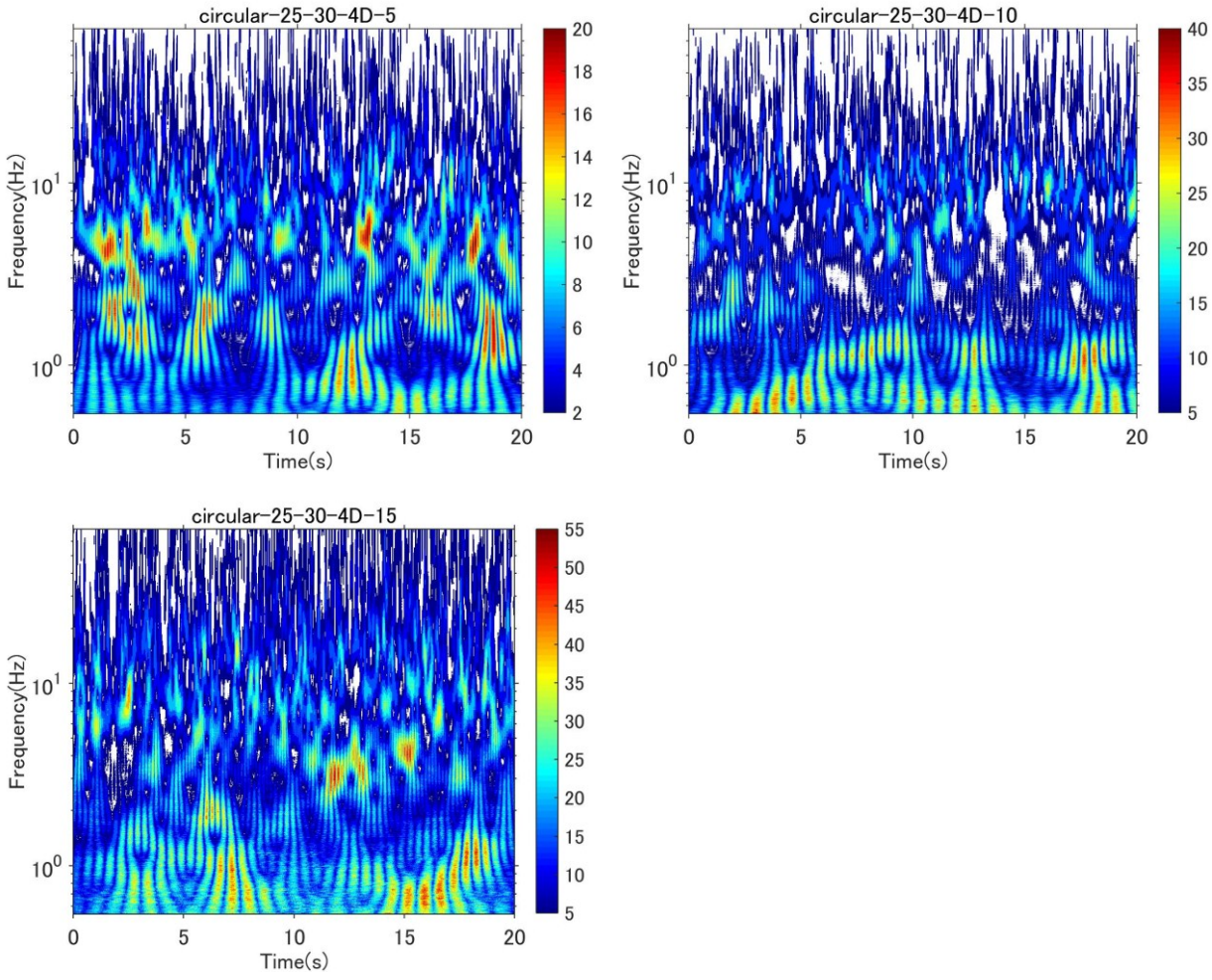

Figure A-4.4 W.A of circular cylinder, L= 4D, U=5-10 and 15m/s, β=30° and α= 25°

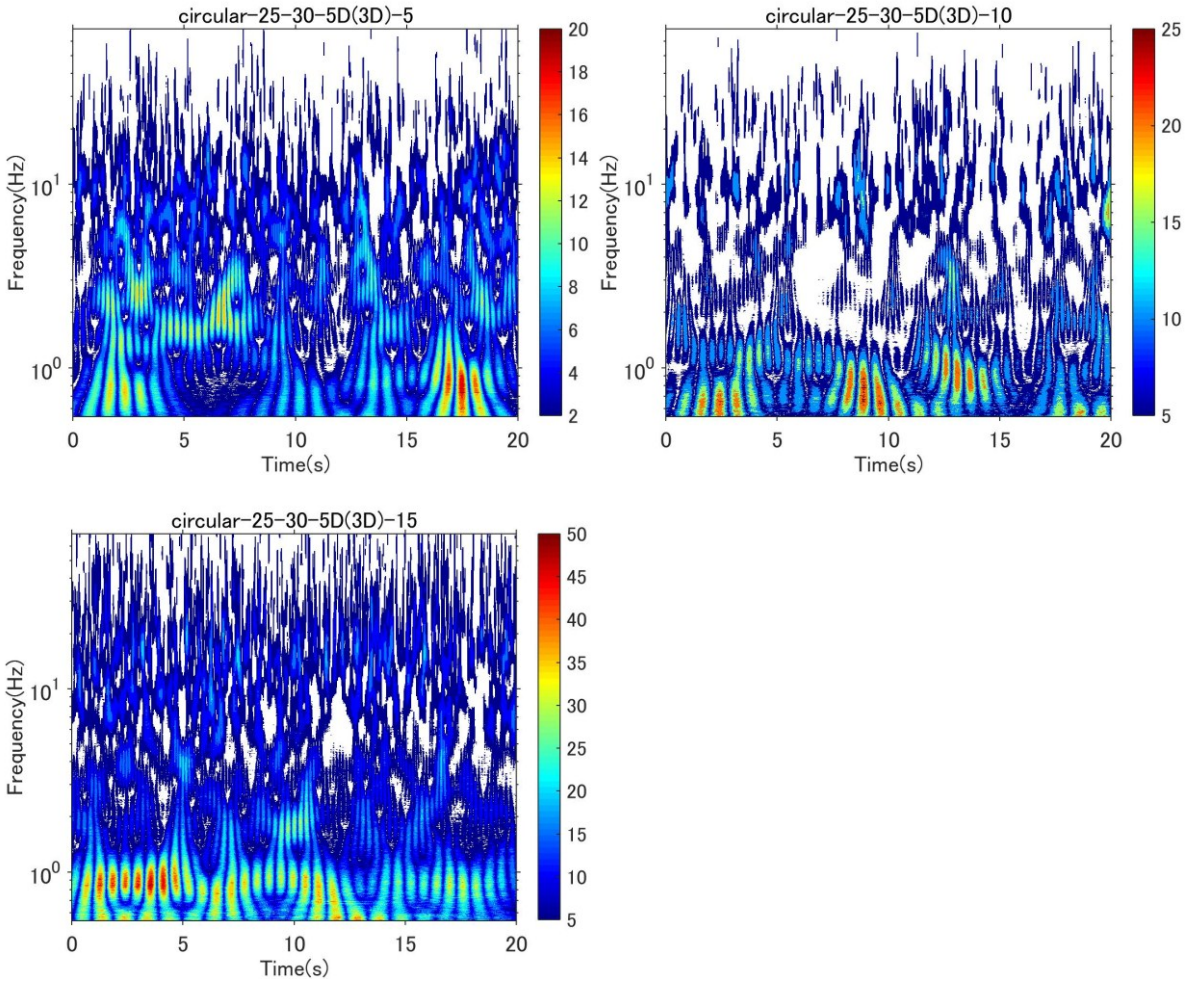

Figure A-4.5 W.A of circular cylinder, L= 5D, U=5-10 and 15m/s, β=30° and α= 25°

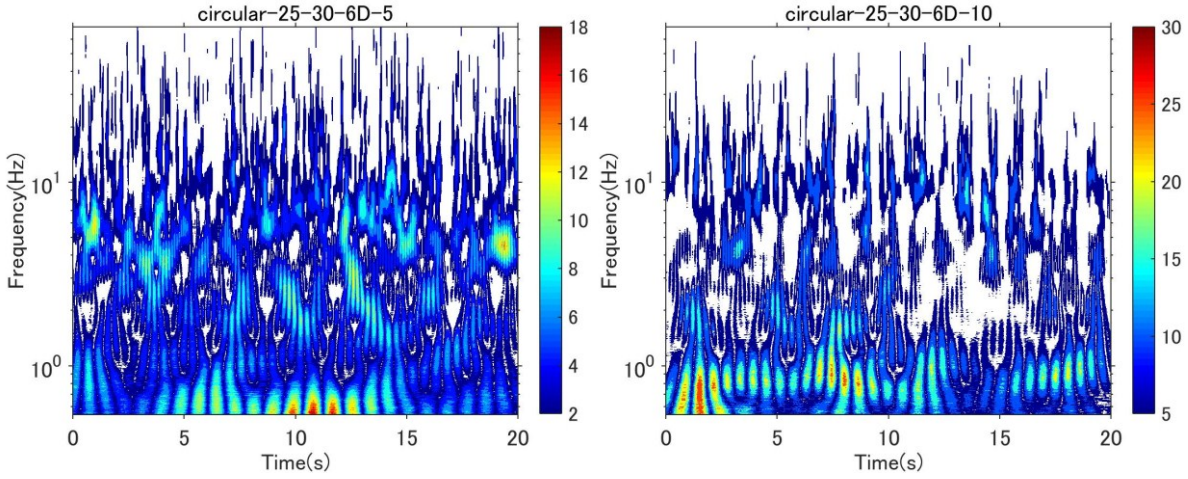

Figure A-4.6 W.A of circular cylinder, L= 6D, U=5m/s - 10m/s, β=30° and α= 25°

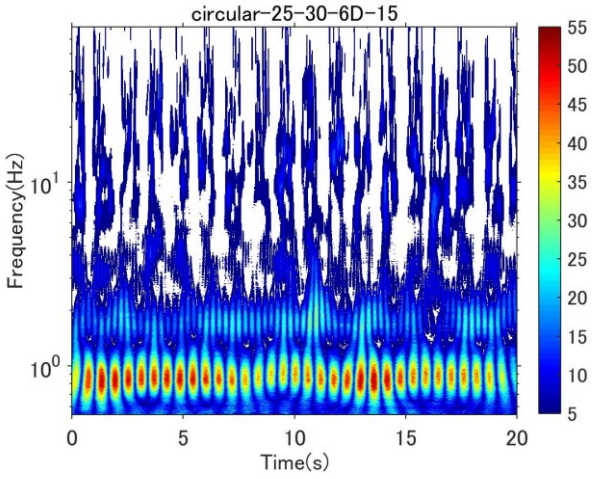

Figure A-4.7 W.A of circular cylinder, L= 6D, U=15m/s, β=30° and α= 25°

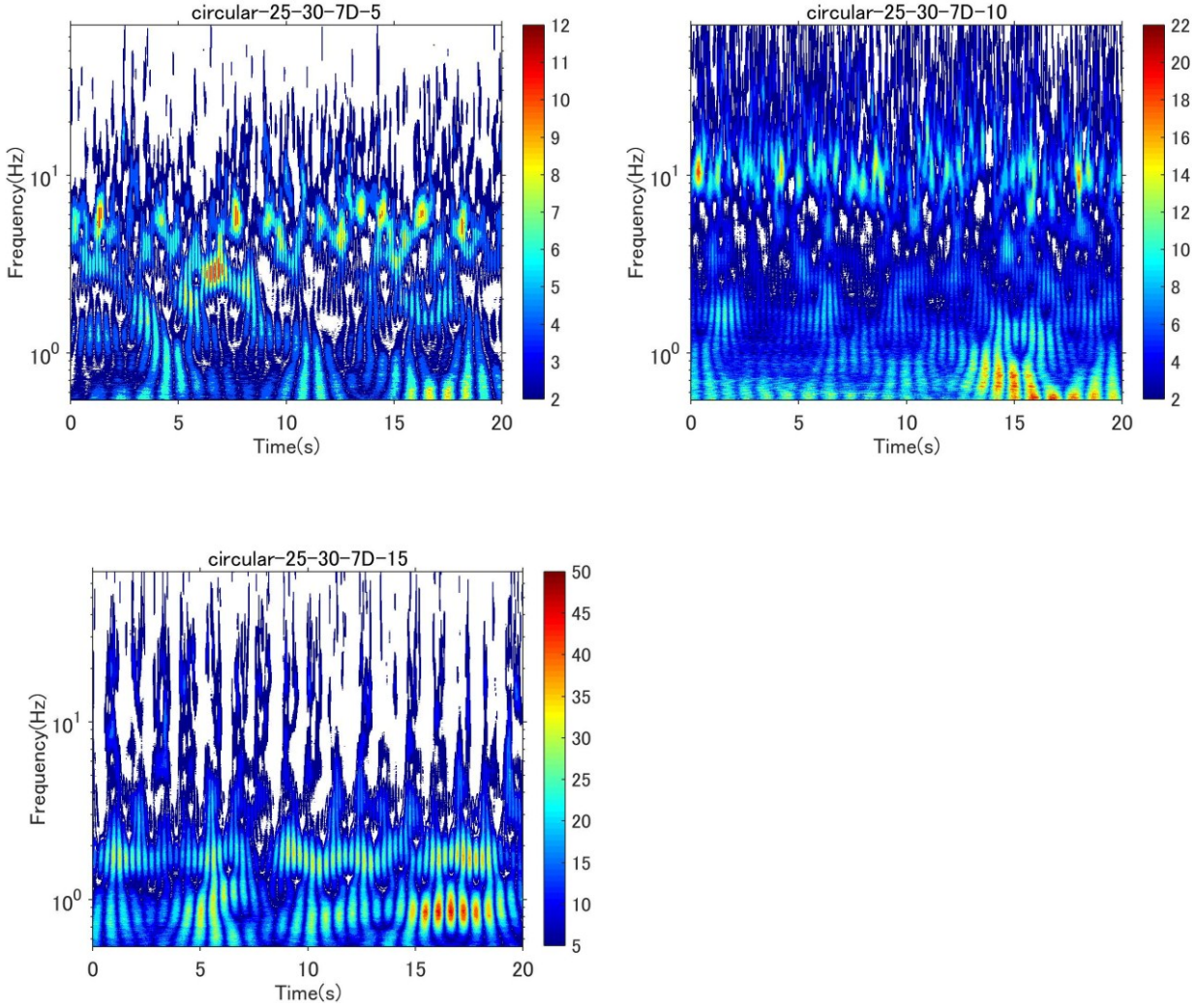

Figure A-4.8 W.A of circular cylinder, L= 7D, U=5 – 10 and 15m/s, β=30° and α= 25°

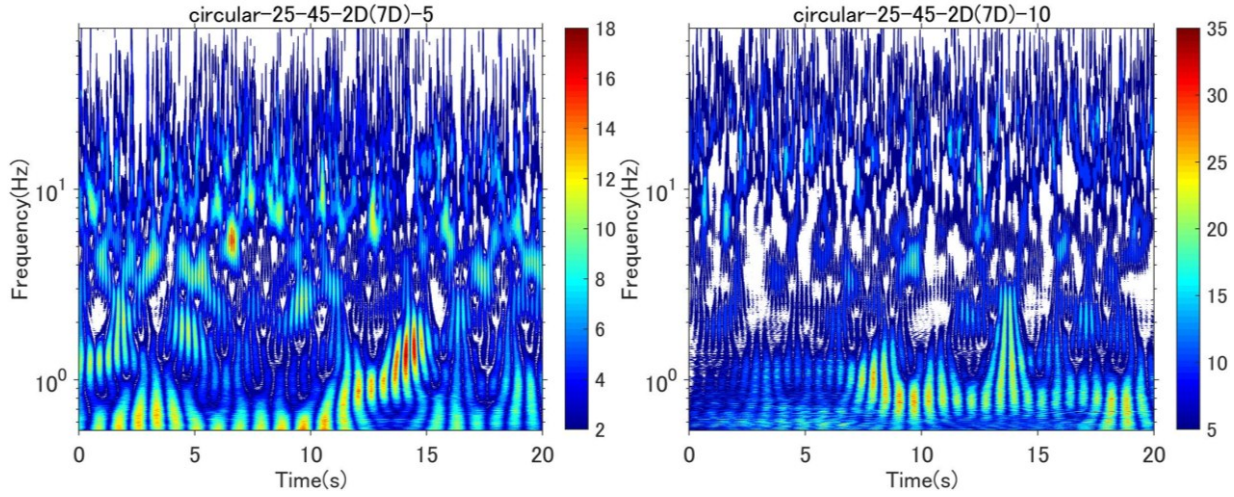

Figure A-4.9 W.A of circular cylinder, L= 2D, U=5m/s - 10m/s, β=45° and α= 25°

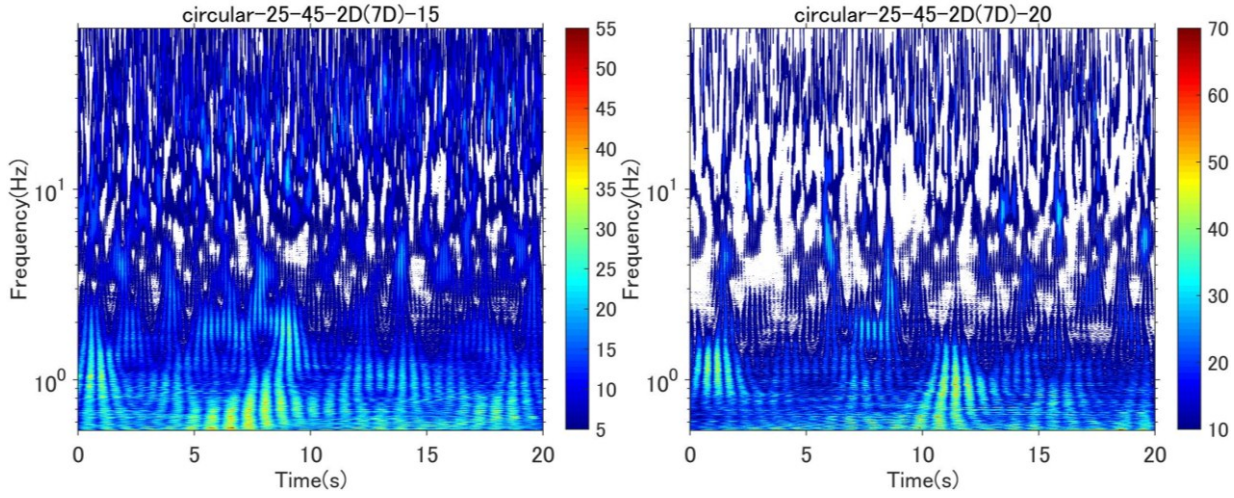

Figure A-4.10 W.A of circular cylinder, L= 2D, U=15m/s - 20m/s, β=45° and α= 25°

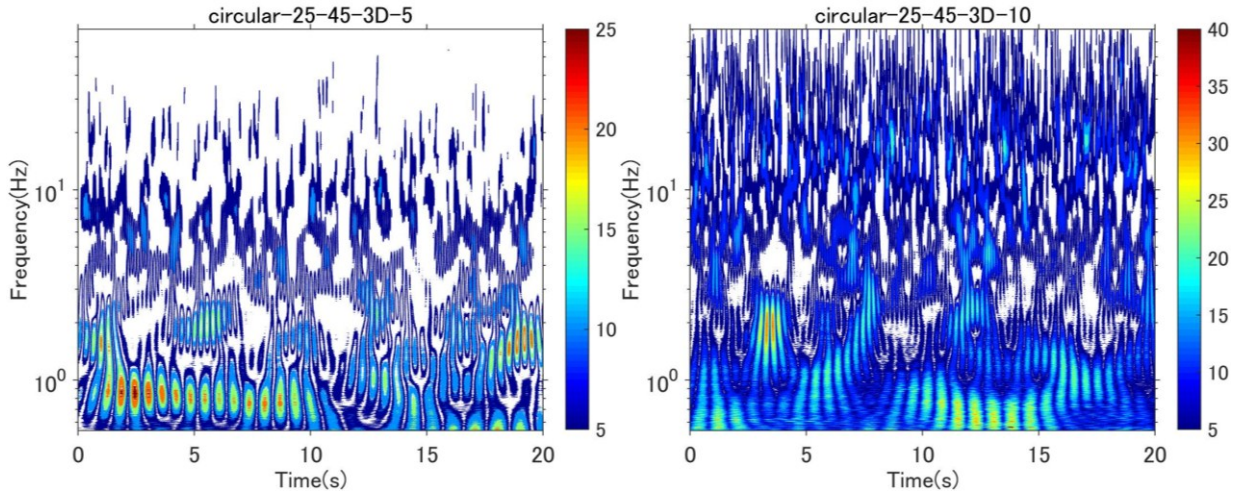

Figure A-4.11 W.A of circular cylinder, L= 3D, U=5m/s - 10m/s, β=45° and α= 25°

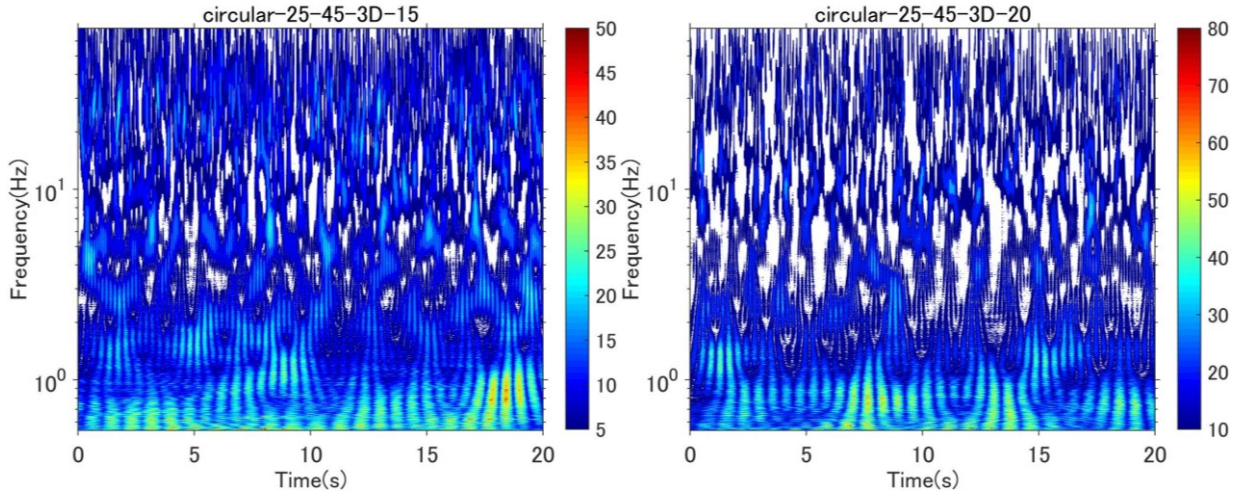

Figure A-4.12 W.A of circular cylinder, L= 3D, U=15m/s - 20m/s, β=45° and α= 25°

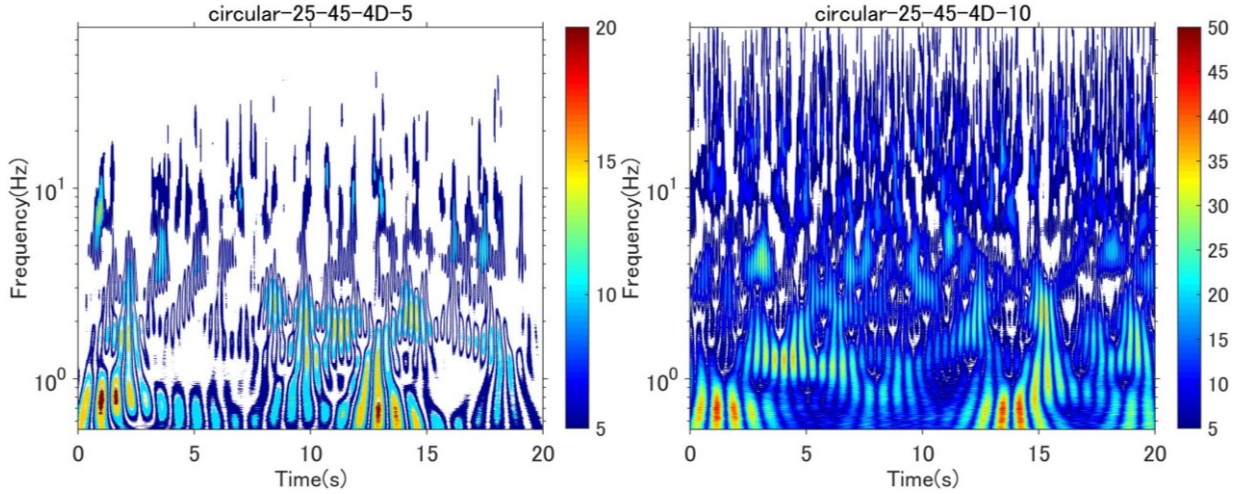

Figure A-4.13 W.A of Circular cylinder, L= 4D, U=5m/s - 10m/s, β=45° and α= 25°

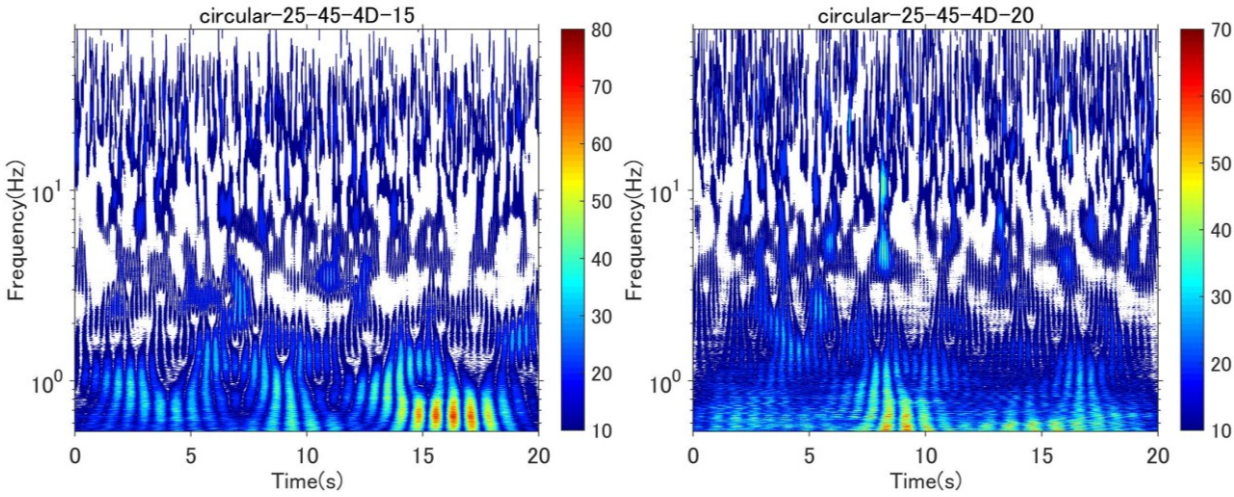

Figure A-4.14 W.A of Circular cylinder, L= 4D, U=15m/s - 20m/s, β=45° and α= 25°

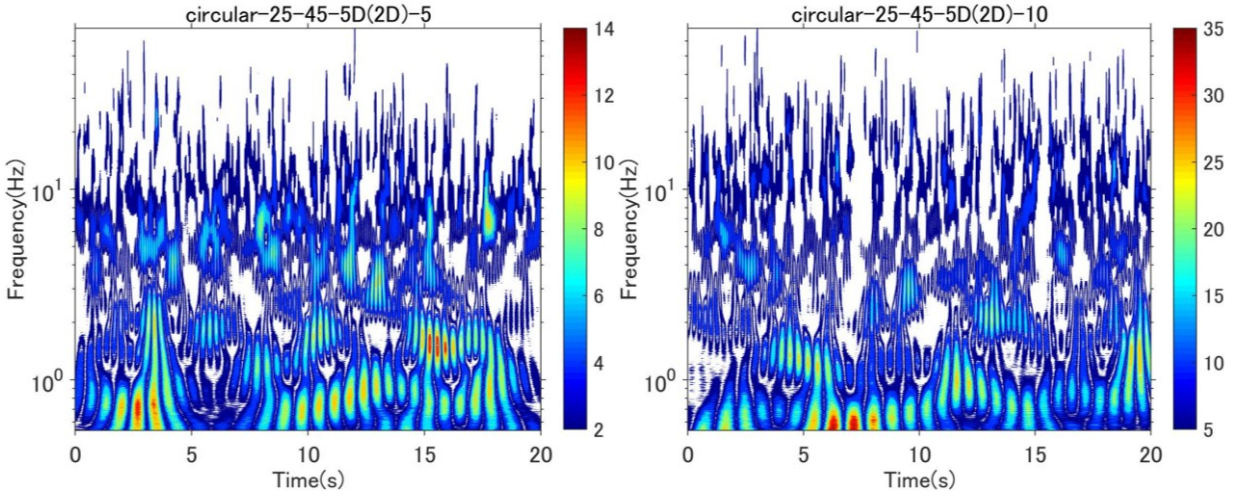

Figure A-4.15 W.A of Circular cylinder, L= 5D, U=5m/s - 10m/s, β=45° and α= 25°

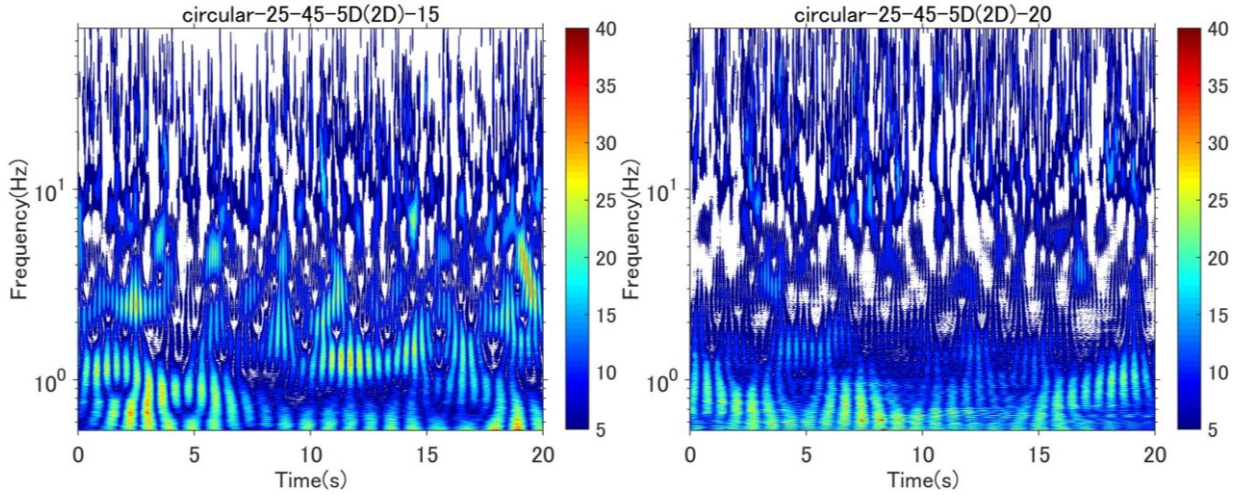

Figure A-4.16 W.A of Circular cylinder, L= 5D, U=15m/s - 20m/s, β=45° and α= 25°

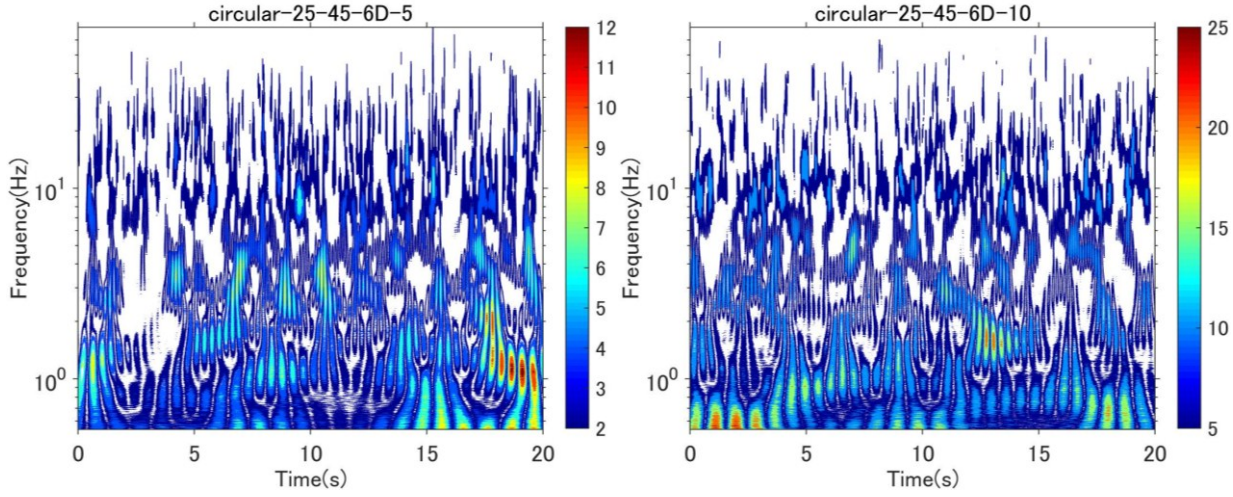

Figure A-4.17 W.A of Circular cylinder, L= 6D, U=5m/s - 10m/s, β=45° and α= 25°

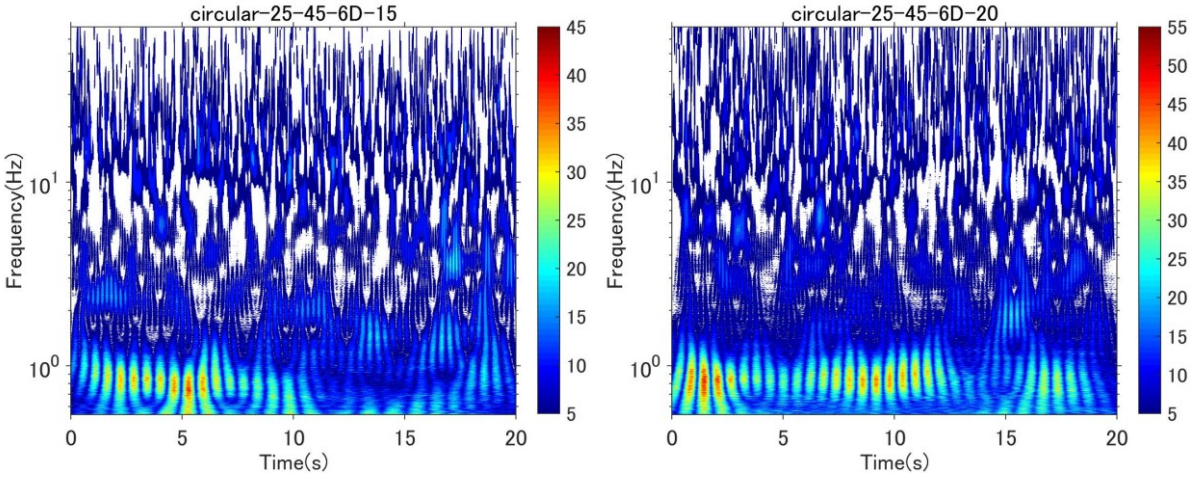

Figure A-4.18 W.A of Circular cylinder, L= 6D, U=15m/s - 20m/s, β=45° and α= 25°

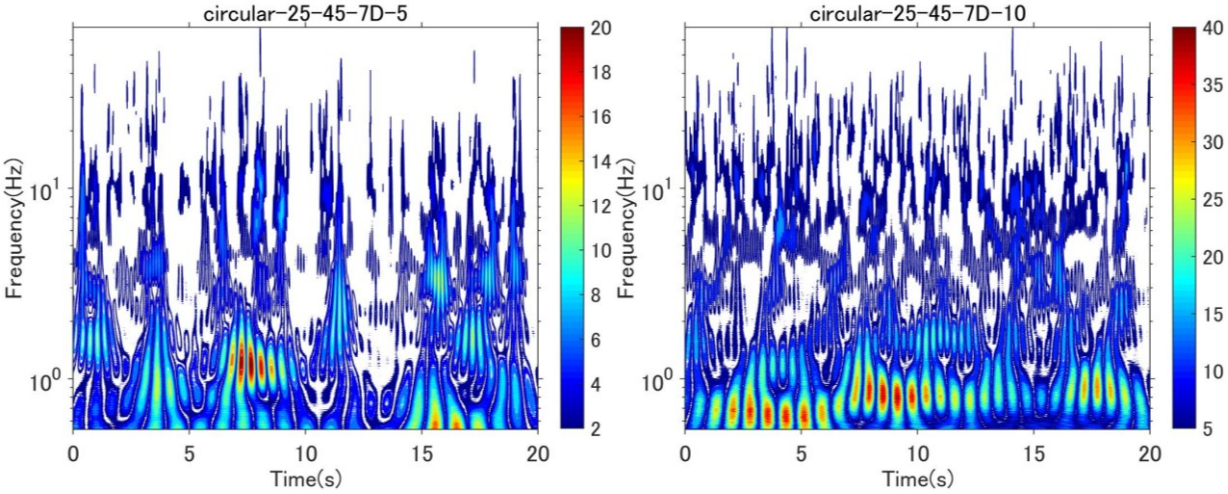

Figure A-4.19 W.A of Circular cylinder, L= 7D, U=5m/s - 10m/s, β=45° and α= 25°

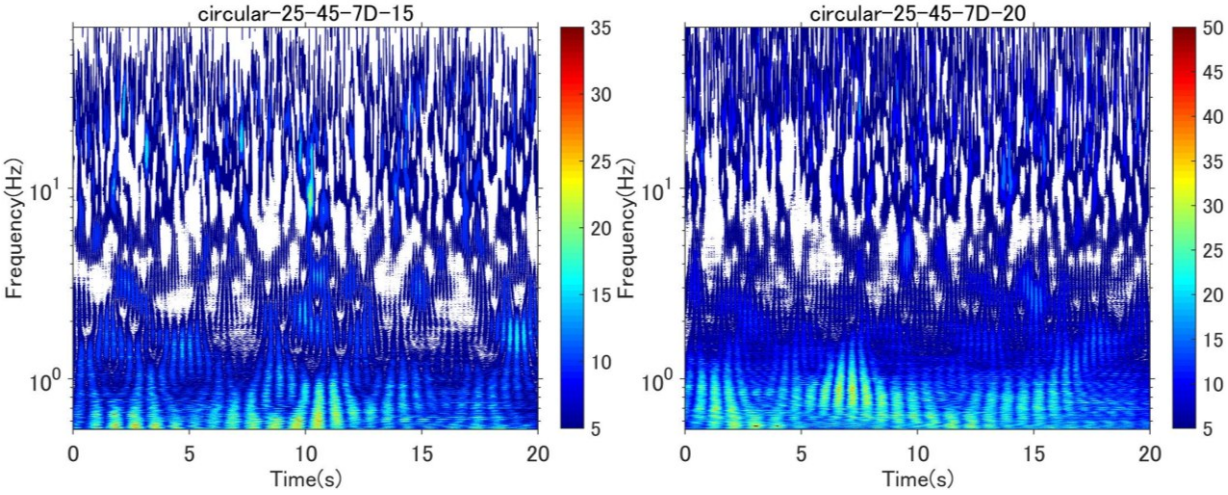

Figure A-4.20 W.A of Circular cylinder, L= 7D, U=15m/s - 20m/s, β=45° and α= 25°

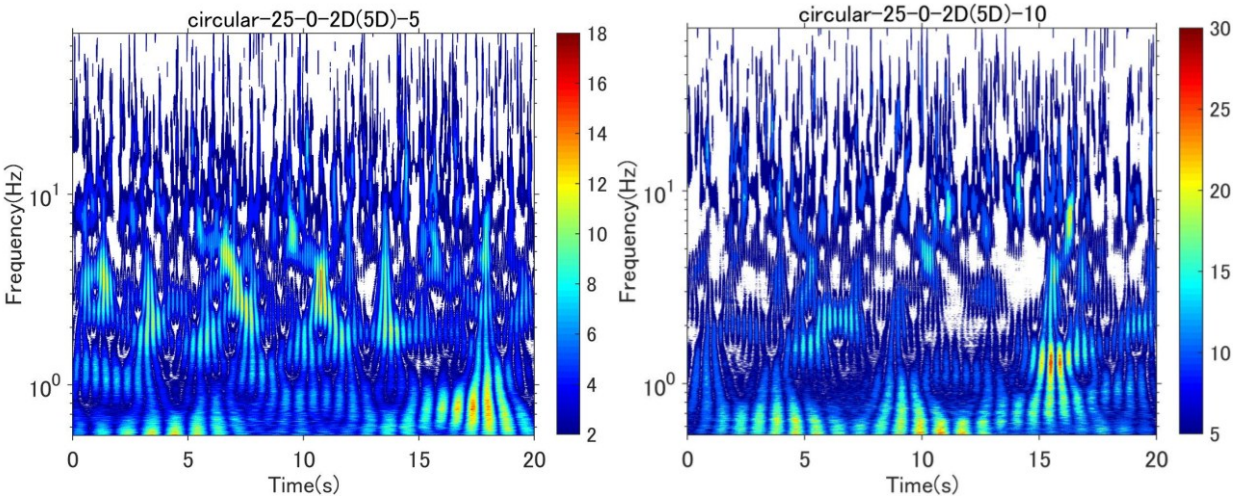

Figure A-4.21 W.A of Circular cylinder, L= 2D, U=5m/s - 10m/s, β=0° and α= 25°

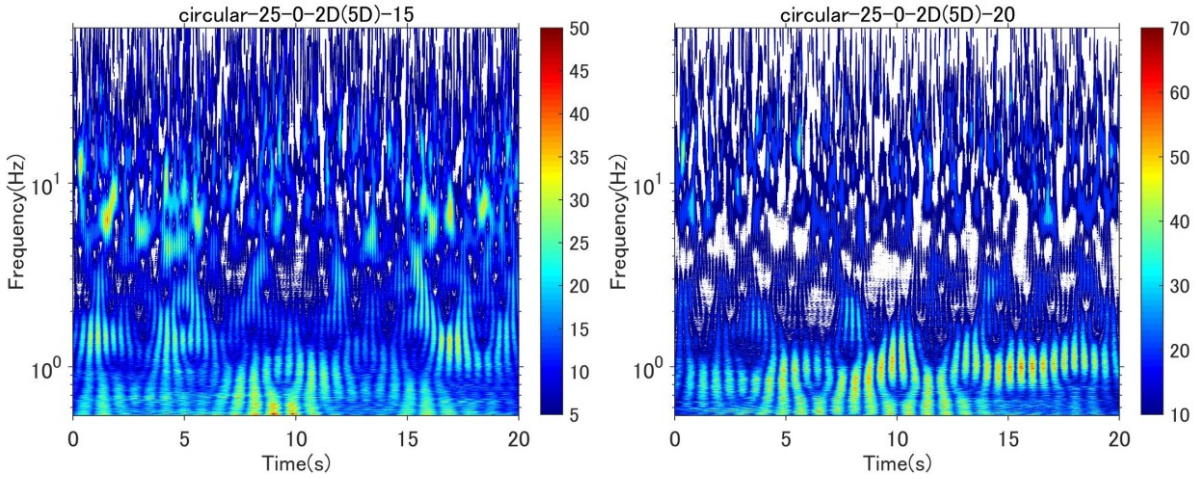

Figure A-4.22 W.A of Circular cylinder, L= 2D, U=15m/s - 20m/s, β=0° and α= 25°

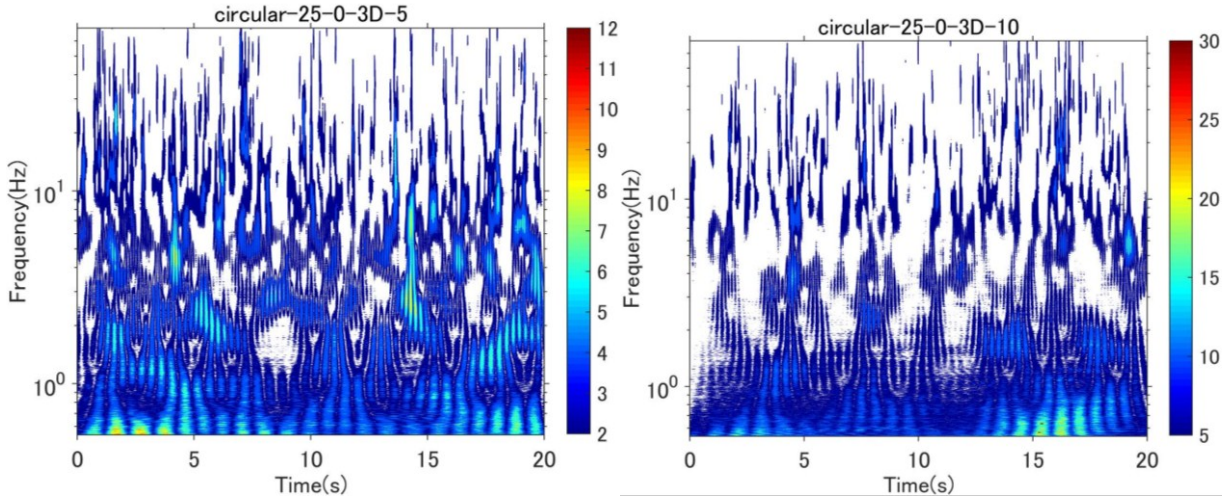

Figure A-4.23 W.A of Circular cylinder, L= 3D, U=5m/s and 10m/s, β=0° and α= 25°

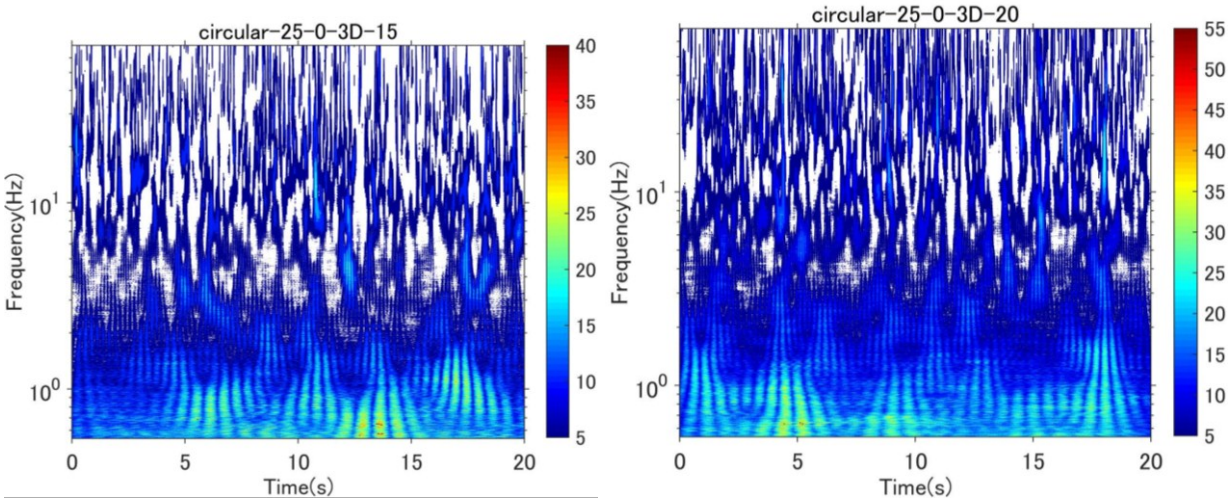

Figure A-4.24 W.A of Circular cylinder, L= 3D, U=15m/s - 20m/s, β=0° and α= 25°

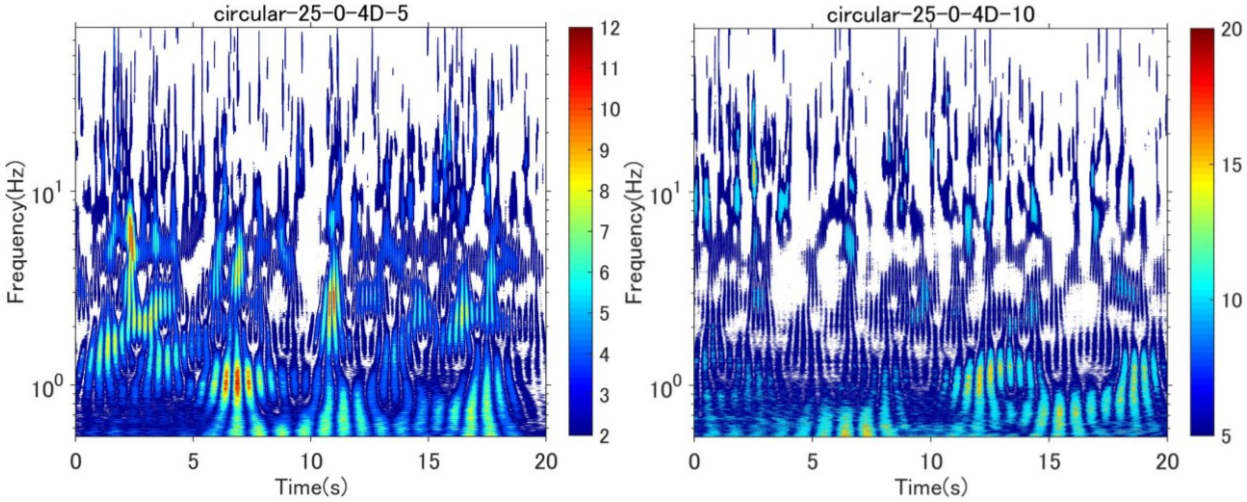

Figure A-4.25 W.A of Circular cylinder, L= 4D, U=5m/s - 10m/s, β=0° and α= 25°

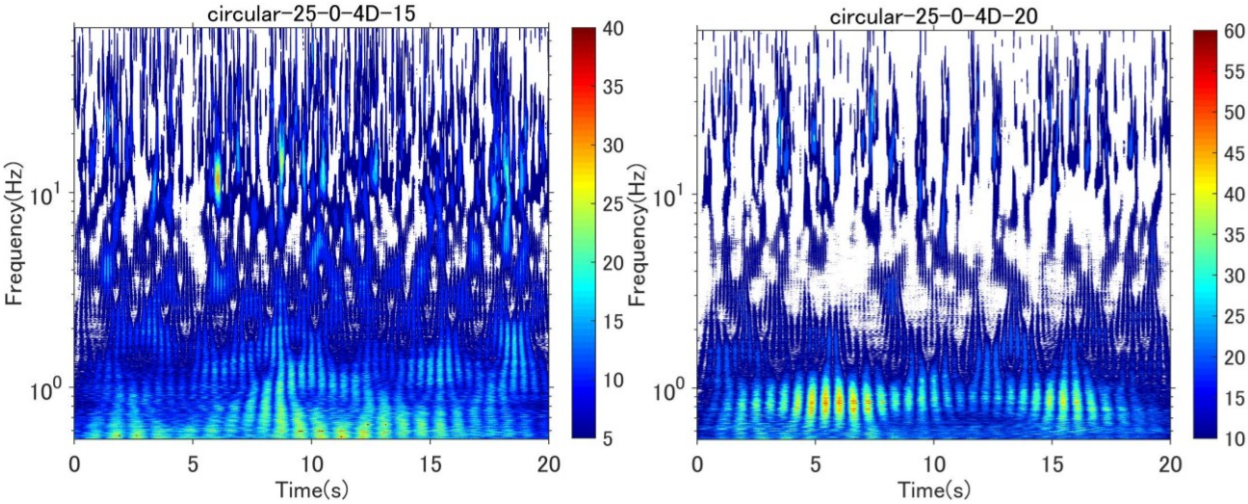

Figure A-4.26 W.A of Circular cylinder, L= 4D, U=15m/s - 20m/s, β=0° and α= 25°

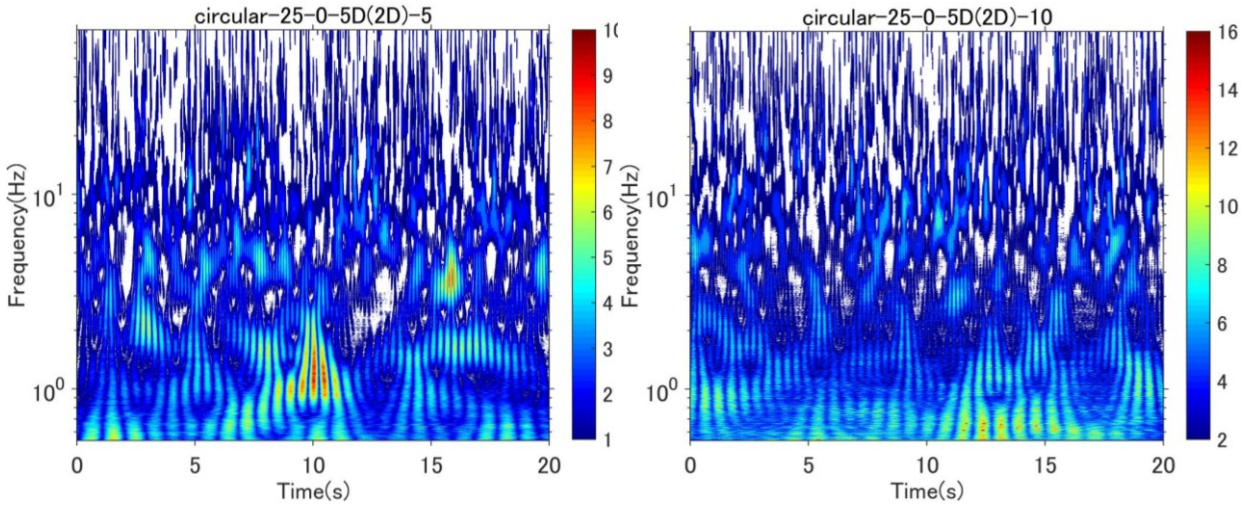

Figure A-4.27 W.A of Circular cylinder, L= 5D, U=5m/s - 10m/s, β=0° and α= 25°

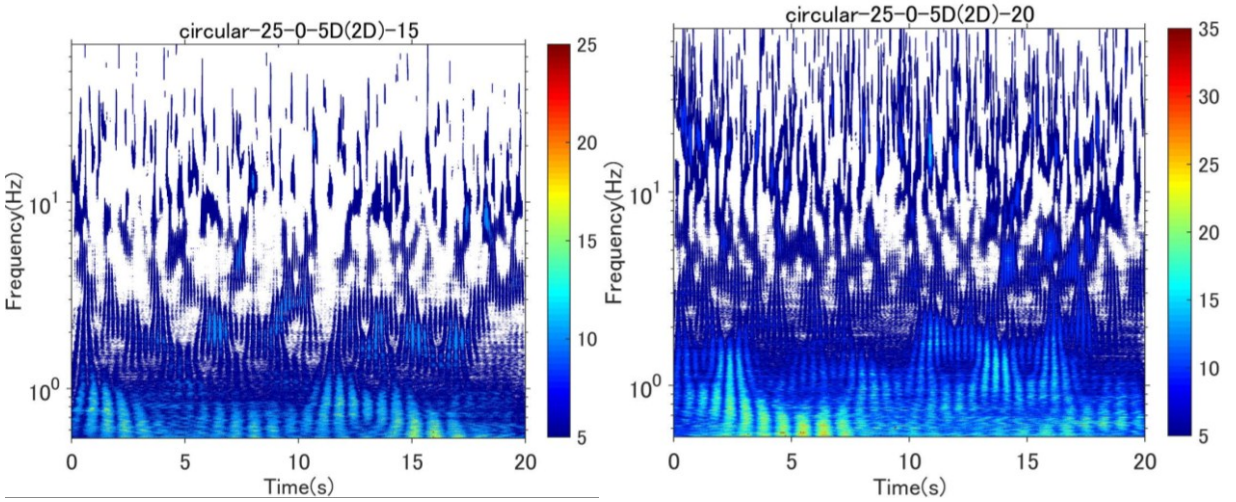

Figure A-4.28 W.A of Circular cylinder, L= 5D, U=15m/s - 20m/s, β=0° and α= 25°

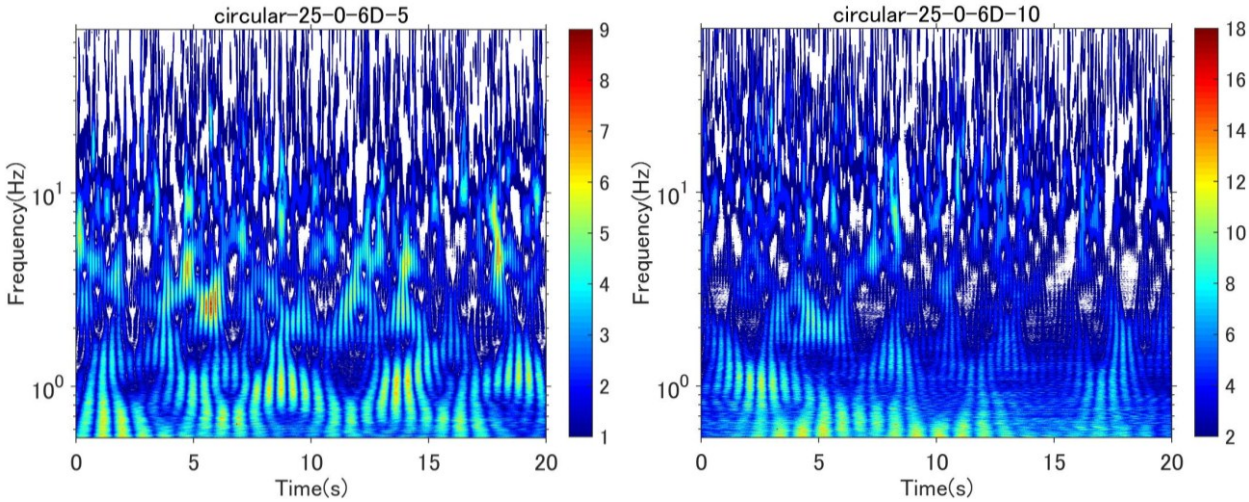

Figure A-4.29 W.A of Circular cylinder, L= 6D, U=5m/s - 10m/s, β=0° and α= 25°

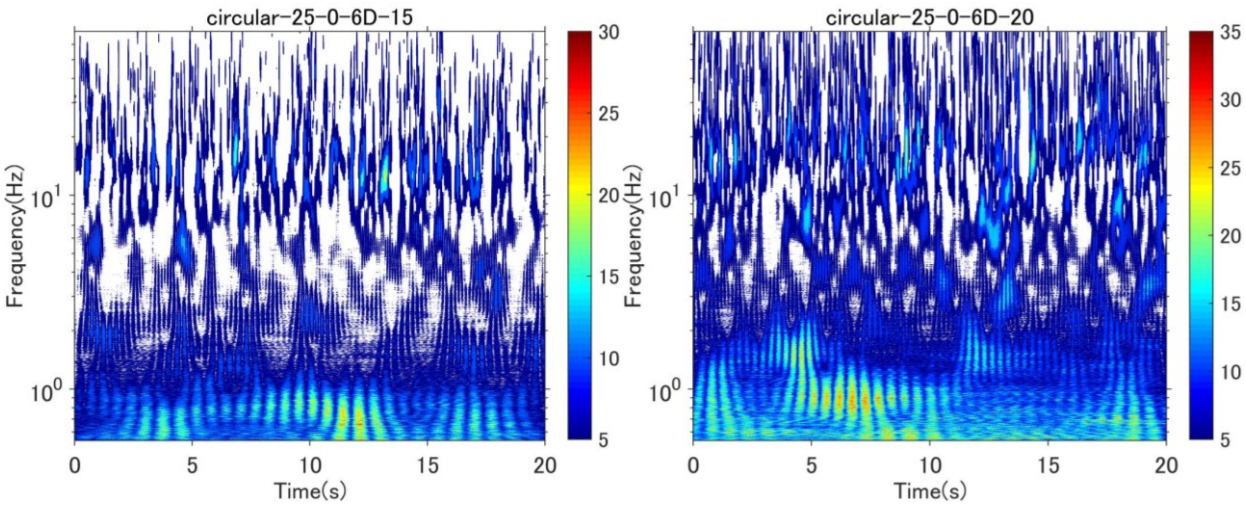

Figure A-4.30 W.A of Circular cylinder, L= 6D, U=15m/s - 20m/s, β=0° and α= 25°

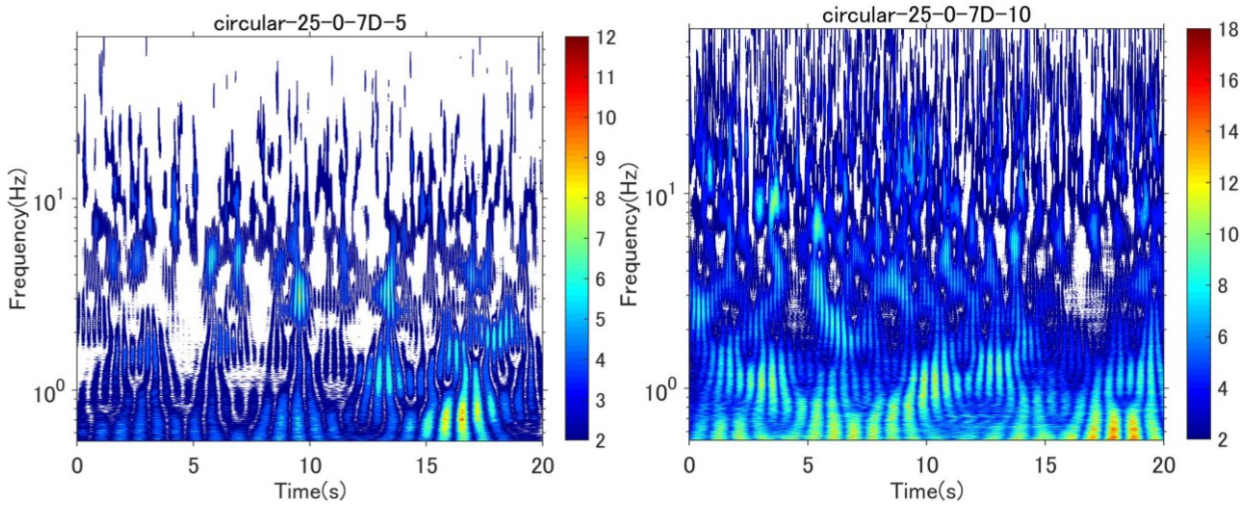

Figure A-4.31 W.A of Circular cylinder, L= 7D, U=5m/s - 10m/s, β=0° and α= 25°

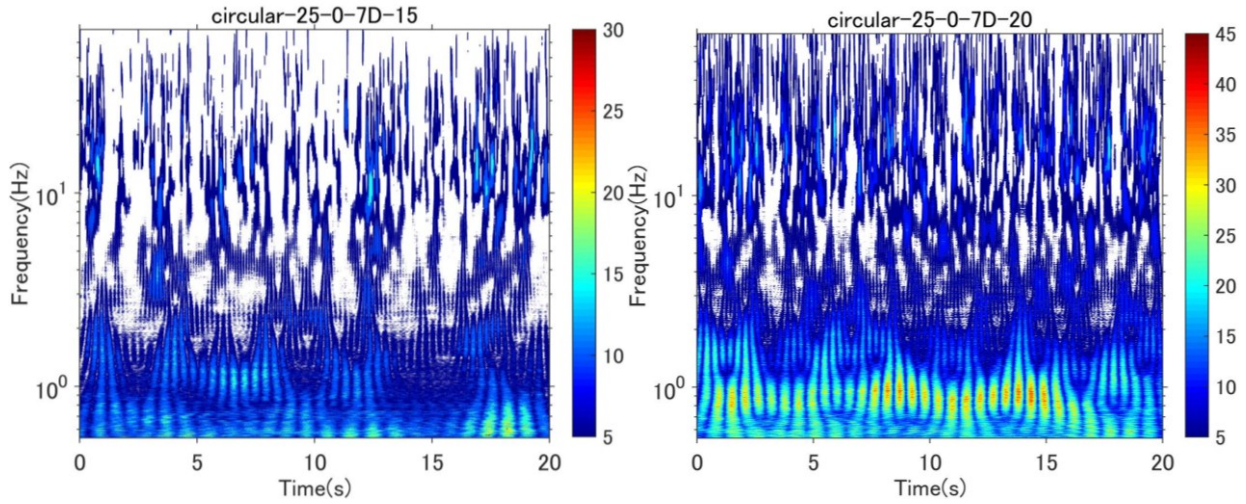

Figure A-4.32 W.A of Circular cylinder, L= 5D, U=15m/s - 20m/s, β=0° and α= 25°

Appendix 5: Coherence estimation for wake flow near circular cylinder wake in span-wise direction

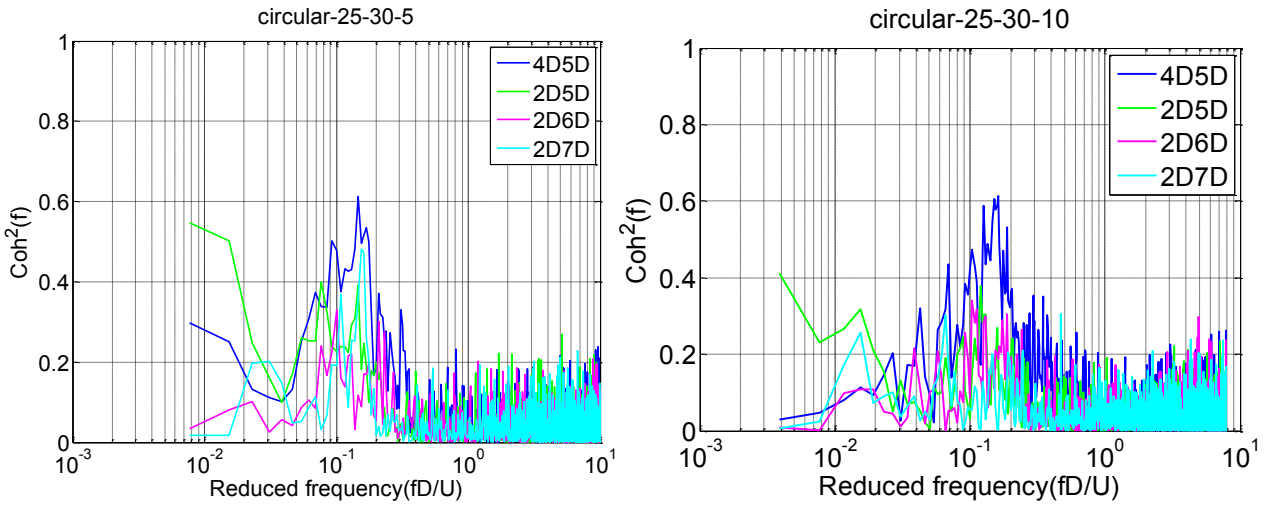

Figure A-5.1 Correlation of wake flow (Smooth flow, U=5m/s-10m/s, β=30° and α= 25°)

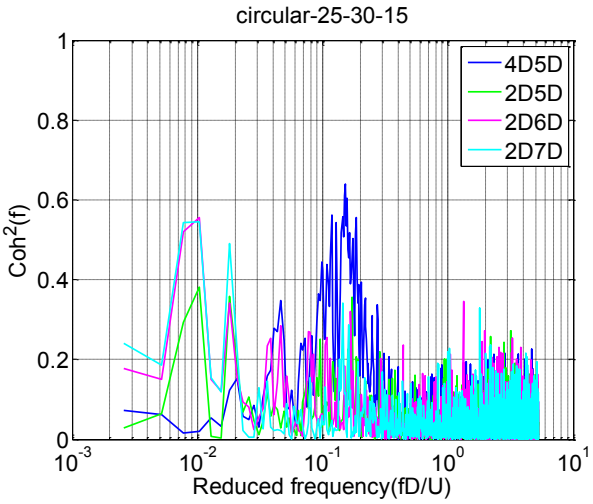

Figure A-5.2 Correlation of wake flow (Smooth flow, U=15m/s- 20m/s, β=30° and α= 25°)

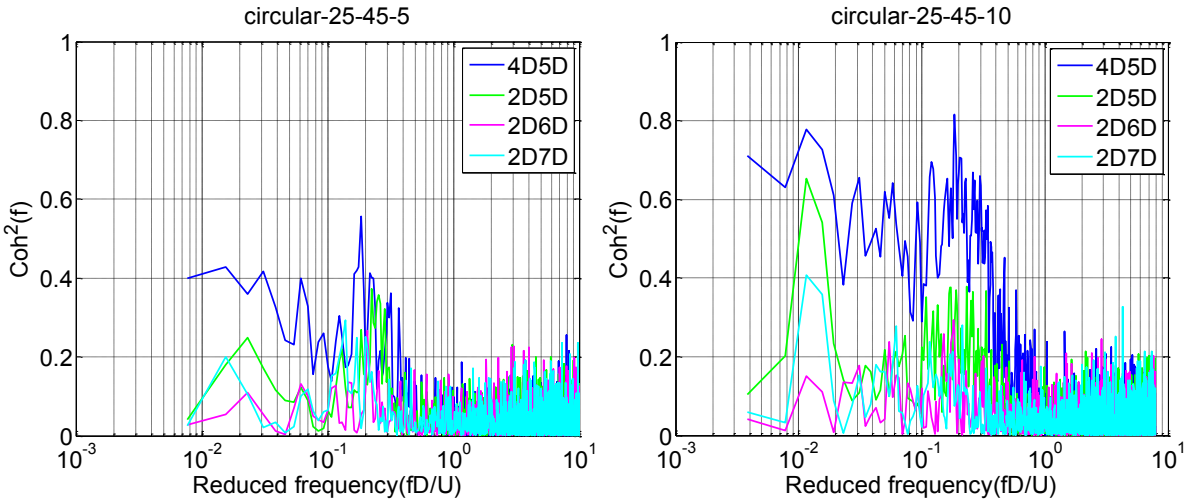

Figure A-5.3 Coherence analysis, Circular cylinder, U=5m/s and 10m/s, β=45° and α= 25°

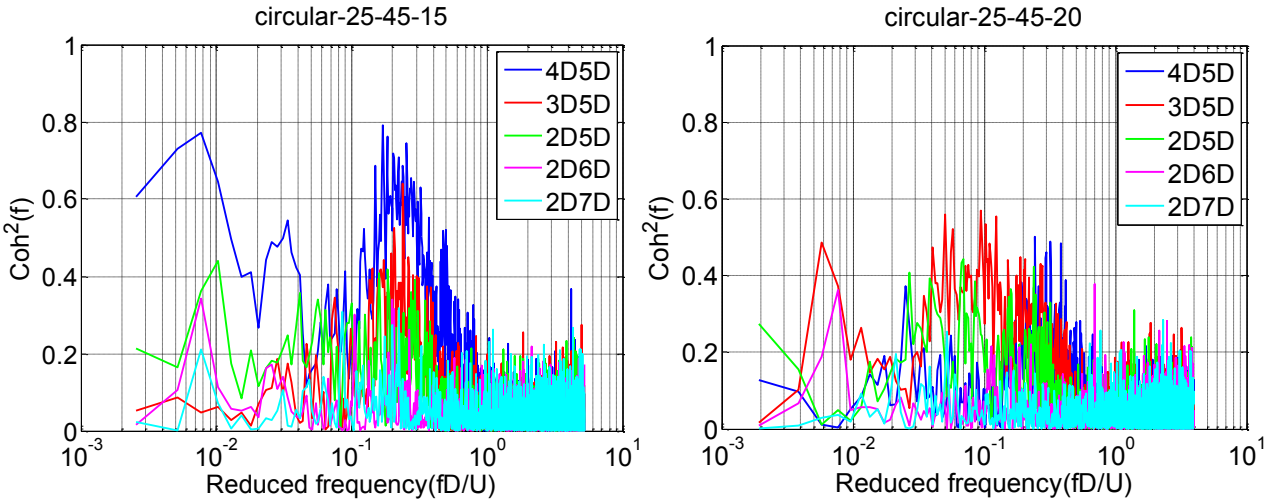

Figure A-5.4 Coherence analysis, circular cylinder, U=15m/s and 20m/s, β=45° and α= 25°

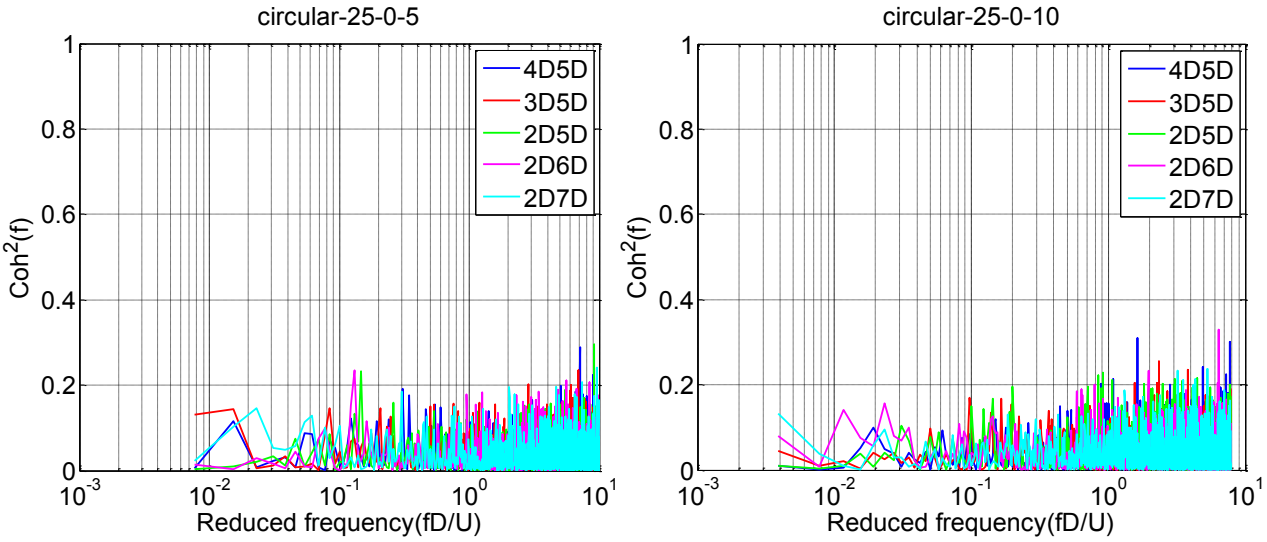

Figure A-5.5 Coherence analysis, circular cylinder, U=5m/s and 10m/s, β=0° and α= 25°

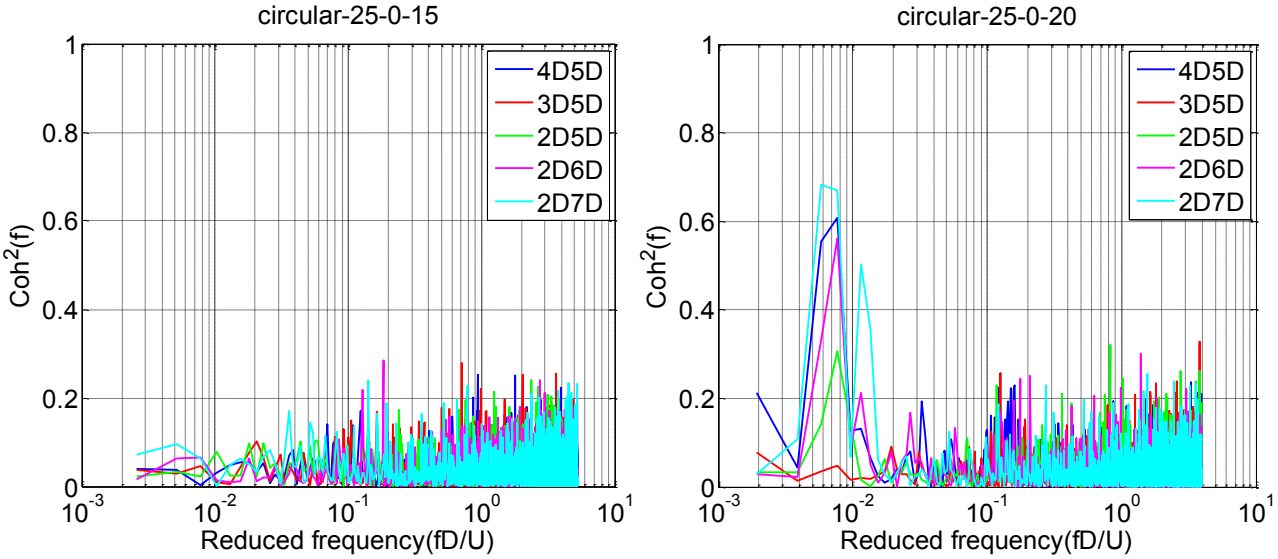

Figure A-5.6 Coherence analysis, circular cylinder, U=15m/s and 20m/s, β=0° and α= 25°

Appendix 6: Experiment parameters of indented surface and parallel protuberances

Diameter	Inclined angle	Flow angle	Cross section	No. of protuberance	Dimension of protuberance	Rain	Natural frequency（Hz）	Logarithm decrement	Unit mass (kg/m)	Sc (with rain)	Sc (No rain)
φ110	**40°**	60°	Indented surface			w・w/o	0.89	0.010	8.180	10.90	10.90
		60°	Parallel protuberances	12	4x9		0.84	0.013	8.840	15.57	15.57
		45°	Indented surface				0.86	0.010	8.180	11.08	11.08
		45°	Parallel protuberances	12	4x9		0.79	0.006	8.840	7.13	7.13
		30°	Indented surface				0.85	0.010	8.180	11.08	11.08
		30°	Parallel protuberances	12	4x9		0.80	0.010	8.840	12.08	12.18
		15°	Indented surface				0.86	0.011	8.180	12.19	12.19
		15°	Parallel protuberances	12	4x9		0.83	0.011	8.840	13.07	13.07
		0°	Indented surface				0.86	0.011	8.180	12.39	12.39
		0°	Parallel protuberances	12	5x11		0.83	0.010	8.840	11.88	11.88
φ158	**40°**	0°	Indented surface			w・w/o	0.84	0.014	9.867	9.15	9.15
		0°	Parallel protuberances	12	5x11		0.81	0.011	10.900	7.81	7.81
		15°	Indented surface				0.84	0.012	9.867	7.84	7.84
		15°	Parallel protuberances	12	5x11		0.81	0.011	10.900	7.94	7.94
		30°	Indented surface				0.84	0.012	9.867	7.78	7.78
		30°	Parallel protuberances	12	5x11		0.81	0.013	10.900	9.38	9.46
		45°	Indented surface				0.84	0.012	9.867	7.90	7.97
		45°	Parallel protuberances	12	5x11		0.81	0.012	10.900	8.81	8.81
		60°	Indented surface				0.84	0.012	9.867	7.84	7.84
		60°	Parallel protuberances	12	5x11		0.81	0.013	10.900	9.54	9.54
φ110	**25°**	60°	Indented surface			w・w/o	0.84	0.010	8.180	11.27	11.27
		60°	Parallel protuberances	12	4x9		0.79	0.010	8.840	12.08	12.08
		45°	Indented surface				0.87	0.009	8.180	10.23	10.23
		45°	Parallel protuberances	12	4x9		0.79	0.009	8.840	10.96	10.96
		30°	Indented surface				0.84	0.011	8.180	12.39	12.39

		30°	Parallel protuberances	12	4x9		0.82	0.011	8.840	13.39	13.39
		15°	Indented surface				0.84	0.009	8.180	10.14	10.14
		15°	Parallel protuberances	12	4x9		0.82	0.012	8.840	14.61	14.61
		0°	Indented surface				0.86	0.009	8.180	10.14	10.14
		0°	Parallel protuberances	12	4x9		0.84	0.009	8.840	10.78	10.78
φ158	**25°**	0°	Indented surface			w・w/o	0.91	0.009	9.867	5.83	5.83
		0°	Parallel protuberances	12	5x11		0.88	0.010	10.900	7.16	7.16
		15°	Indented surface				0.87	0.008	9.867	5.23	5.23
		15°	Parallel protuberances	12	5x11		0.86	0.008	10.900	5.73	5.73
		30°	Indented surface				0.88	0.010	9.867	6.48	6.48
		30°	Parallel protuberances	12	5x11		0.86	0.010	10.900	7.22	7.22
		45°	Indented surface				0.88	0.008	9.867	5.23	5.23
		45°	Parallel protuberances	12	5x11		0.84	0.007	10.900	5.14	5.18
		60°	Indented surface				0.83	0.013	9.867	8.49	8.49
		60°	Parallel protuberances	12	5x11		0.77	0.014	10.900	10.02	10.02
φ158	**9°**	60°	Indented surface			w・w/o	0.99	0.005	9.860	3.26	3.26
		60°	Parallel protuberances	12	5x11		0.95	0.006	10.893	4.40	4.40
		45°	Indented surface				1.00	0.005	9.860	3.32	3.32
		45°	Parallel protuberances	12	5x11		0.96	0.005	10.893	3.67	3.64
		30°	Indented surface				1.00	0.006	9.860	4.02	4.02
		30°	Parallel protuberances	12	5x11		0.96	0.005	10.893	3.61	3.61
		15°	Indented surface				1.01	0.005	9.860	3.29	3.29
		15°	Parallel protuberances	12	5x11		0.97	0.006	10.893	4.36	4.36
		0°	Indented surface				0.86	0.006	9.860	3.92	3.92
		0°	Parallel protuberances	12	5x11		0.82	0.01	10.893	5.72	5.72
Summary							Natural frequency	Logarithm decrement	Unit mass	Scruton number	Scruton number
						Max	1.01	0.014	10.90	15.57	15.57
						Min	0.77	0.005	8.18	3.26	3.26

Appendix 7: Experimental parameter for spiral protuberance optimization

Diameter	Inclined angle	Flow angle	Cross section	No. of protuberance	Winding direction	Size of protuberance	Winding pitch	Rain	Natural frequency (Hz)	Logarithm decrement	Unit mass (kg/m)	Sc (with rain)	Sc (No rain)
φ110	25°	30°	Spiral	12	Reverse	4×6 (original)	425 mm (original)	w・w/o	0.80	0.008	8.71	9.60	9.52
	25°	30°	Spiral	12	Original				0.80	0.007	8.71	8.54	8.54
	25°	30°	Spiral	6					0.81	0.007	8.43	8.13	8.06
	25°	30°	Spiral	4					0.81	0.007	8.33	8.10	8.10
	25°	30°	Spiral	2					0.82	0.006	8.24	6.87	6.87
	25°	30°	Spiral	12		5×7.5			0.79	0.007	9.11	8.79	8.79
	25°	30°	Spiral			2×6			0.81	0.006	8.44	7.09	7.09
	25°	30°	Spiral			4×6 (original)	325 mm		0.80	0.007	8.82	8.50	8.43
	25°	30°	Spiral				525 mm		0.80	0.007	8.67	8.29	8.29
φ158	25°	30°	Spiral	12	Reverse	5×7.5 (original)	610 mm (original)	w・w/o	0.85	0.006	10.77	4.32	4.24
	25°	30°	Spiral	12	Original				0.86	0.010	10.77	7.13	7.13
	25°	30°	Spiral	6					0.86	0.005	10.31	3.41	3.41
	25°	30°	Spiral	4					0.87	0.006	10.15	4.07	4.07
	25°	30°	Spiral	2					0.87	0.005	10.01	3.31	3.34
	25°	30°	Spiral	12		2×7.5			0.86	0.006	10.23	4.06	4.13
	25°	30°	Spiral	6					0.88	0.006	10.03	4.12	4.12
	25°	30°	Spiral	4					0.88	0.006	9.97	4.12	4.12
	25°	30°	Spiral	2					0.88	0.006	9.91	3.84	3.84
	25°	30°	Spiral	2		3×7.5			0.88	0.007	9.93	4.74	4.74
	25°	30°	Spiral	4					0.88	0.006	10.02	3.95	3.95
	25°	30°	Spiral	6					0.87	0.006	10.11	3.98	3.98
	25°	30°	Spiral	12					0.86	0.006	10.38	3.78	3.78
	25°	30°	Spiral	12		5×7.5	465 mm		0.85	0.006	10.89	4.32	4.32

	25°	30°	Spiral	12		(original)	755 mm		0.85	0.006	10.70	4.25	4.25
Summary									Natural frequency	Logarithm decrement	Damping ratio	Scruton number	Scruton number
								Min	0.79	0.005	0.08%	3.31	3.34
								Max	0.882	0.01	0.16%	9.60	9.52

Appendix 8: Experimental parameter for spiral protuberance in different wind attack angles

Diameter	Inclined angle	Flow angle	Cross section	No. of protuberance	Winding direction	Size of protuberance	Winding pitch	Rain	Natural frequency (Hz)	Logarithm decrement	Unit mass (kg/m)	Sc (with rain)	Sc (No rain)
ϕ 110	40°	60°	Spiral protuberances	12	Original	4×6	425	w・w/o	0.89	0.015	7.580	15.28	15.28
ϕ 110	40°	45°	Spiral protuberances	12	Original	4×6	425	w・w/o	0.87	0.007	7.580	7.19	7.19
ϕ 110	40°	30°	Spiral protuberances	12	Original	4×6	425	w・w/o	0.87	0.009	7.580	9.32	9.32
ϕ 110	40°	15°	Spiral protuberances	12	Original	4×6	425	w・w/o	0.90	0.010	7.580	10.27	10.27
ϕ 110	40°	0°	Spiral protuberances	12	Original	4×6	425	w・w/o	0.87	0.008	7.580	8.22	8.22
ϕ 158	40°	0°	Spiral protuberances	12	Original	5×7.5	610	w・w/o	0.81	0.012	10.773	8.56	8.56
ϕ 158	40°	15°	Spiral protuberances	12	Original	5×7.5	610	w・w/o	0.81	0.012	10.773	8.56	8.49
ϕ 158	40°	30°	Spiral protuberances	12	Original	5×7.5	610	w・w/o	0.81	0.012	10.773	8.56	8.63
ϕ 158	40°	45°	Spiral protuberances	12	Original	5×7.5	610	w・w/o	0.81	0.012	10.773	8.56	8.70
ϕ 158	40°	60°	Spiral protuberances	12	Original	5×7.5	610	w・w/o	0.81	0.012	10.773	8.70	8.70
ϕ 110	25°	60°	Spiral protuberances	12	Original	4×6	425	w・w/o	0.85	0.010	7.580	10.35	10.35
ϕ 110	25°	45°	Spiral protuberances	12	Original	4×6	425	w・w/o	0.86	0.011	7.580	11.58	11.58
ϕ 110	25°	30°	Spiral protuberances	12	Original	4×6	425	w・w/o	0.87	0.012	7.580	12.63	12.63

ϕ 110	25°	15°	Spiral protuberances	12	Original	4×6	425	w・w/o	0.87	0.010	7.580	10.53	10.53
ϕ 110	25°	0°	Spiral protuberances	12	Original	4×6	425	w・w/o	0.89	0.008	7.580	8.35	8.28
ϕ 158	25°	0°	Spiral protuberances	12	Original	5×7.5	610	w・w/o	0.88	0.009	10.773	6.37	6.37
ϕ 158	25°	15°	Spiral protuberances	12	Original	5×7.5	610	w・w/o	0.86	0.007	10.773	5.08	5.08
ϕ 158	25°	30°	Spiral protuberances	12	Original	5×7.5	610	w・w/o	0.86	0.010	10.773	7.13	7.13
ϕ 158	25°	45°	Spiral protuberances	12	Original	5×7.5	610	w・w/o	0.86	0.009	10.773	6.42	6.42
ϕ 158	25°	60°	Spiral protuberances	12	Original	5×7.5	610	w・w/o	0.78	0.016	10.773	11.51	11.41
ϕ 158	9°	60°	Spiral protuberances	12	Original	5×7.5	610	w・w/o	0.96	0.005	10.767	3.56	3.56
ϕ 158	9°	45°	Spiral protuberances	12	Original	5×7.5	610	w・w/o	0.97	0.005	10.767	3.62	3.62
ϕ 158	9°	30°	Spiral protuberances	12	Original	5×7.5	610	w・w/o	0.96	0.006	10.767	4.31	4.35
ϕ 158	9°	15°	Spiral protuberances	12	Original	5×7.5	610	w・w/o	0.97	0.005	10.767	3.56	3.56
ϕ 158	9°	0°	Spiral protuberances	12	Original	5×7.5	610	w・w/o	0.83	0.005	10.767	3.54	3.54
Summary									Natural frequency	Logarithm decrement	Damping ratio	Scruton number	Scruton number
								Min	0.78	0.005	0.08%	3.54	3.54
								Max	0.97	0.016	0.25%	15.28	15.28

Appendix 9: PSD of wind velocity fluctuation for spiral protuberance cable

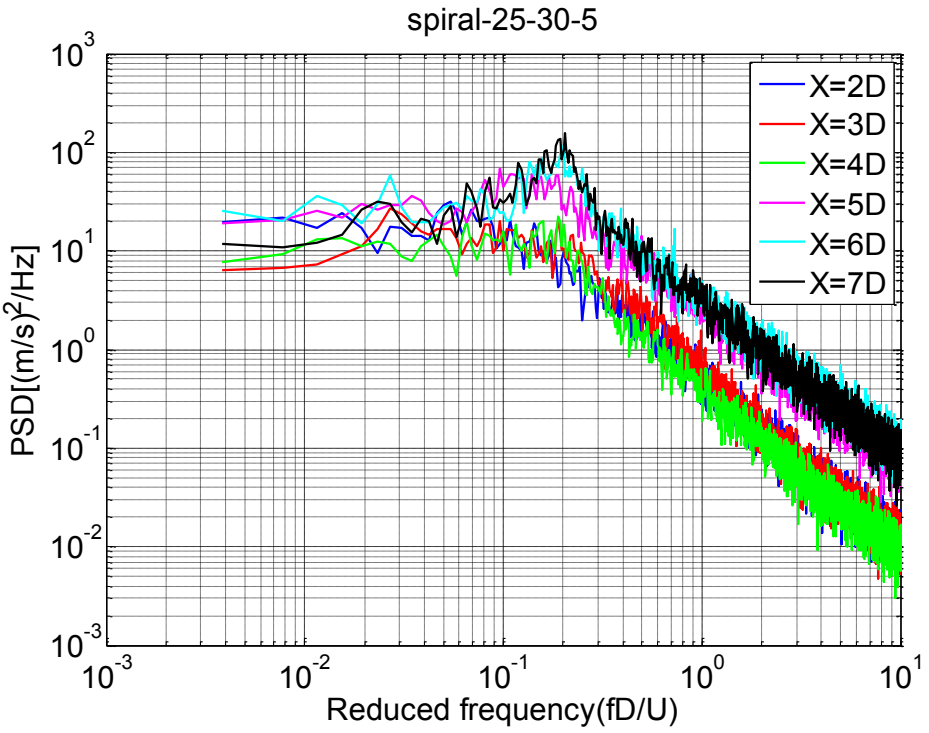

Figure A-9.1 PSD of spiral cable, smooth flow, D=158mm U=5m/s, β=30° and α= 25°

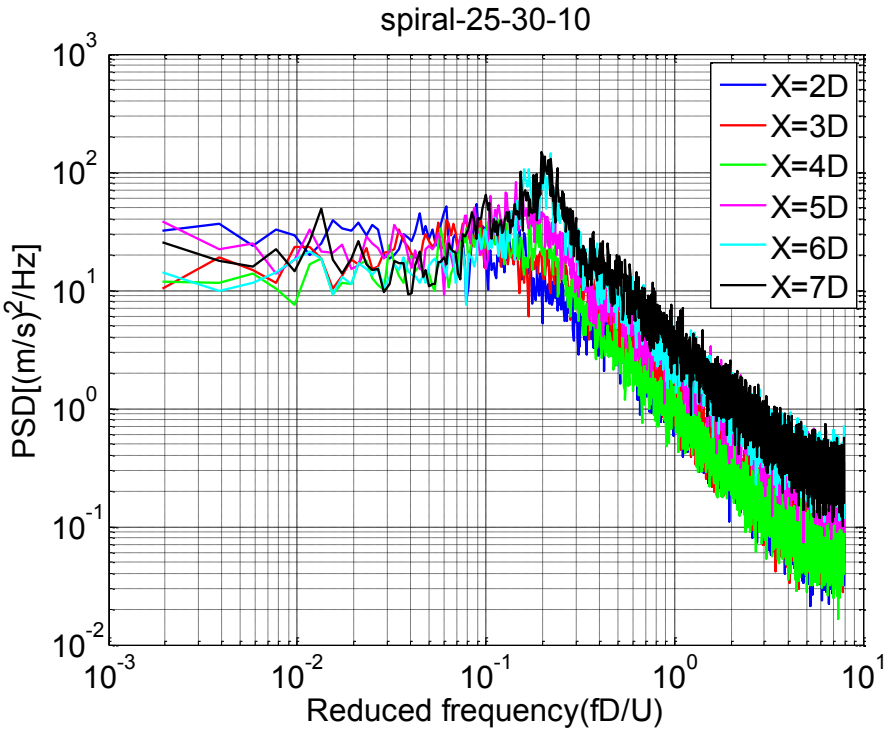

Figure A-9.2 PSD of spiral cable, smooth flow, D=158mm U=10m/s, β=30° and α= 25°

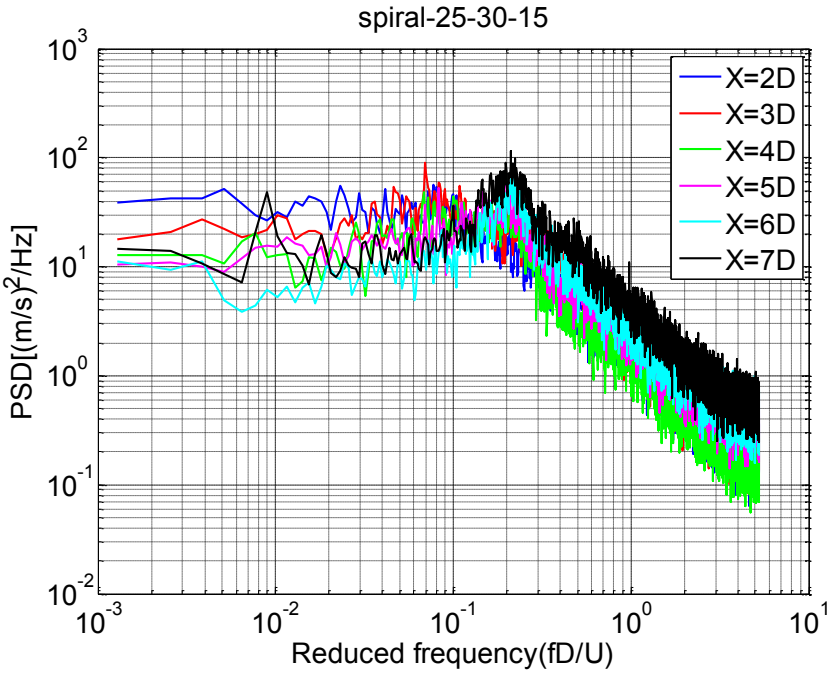

Figure A-9.3 PSD of spiral cable, smooth flow, D=158mm U=15m/s, β=30° and α= 25°

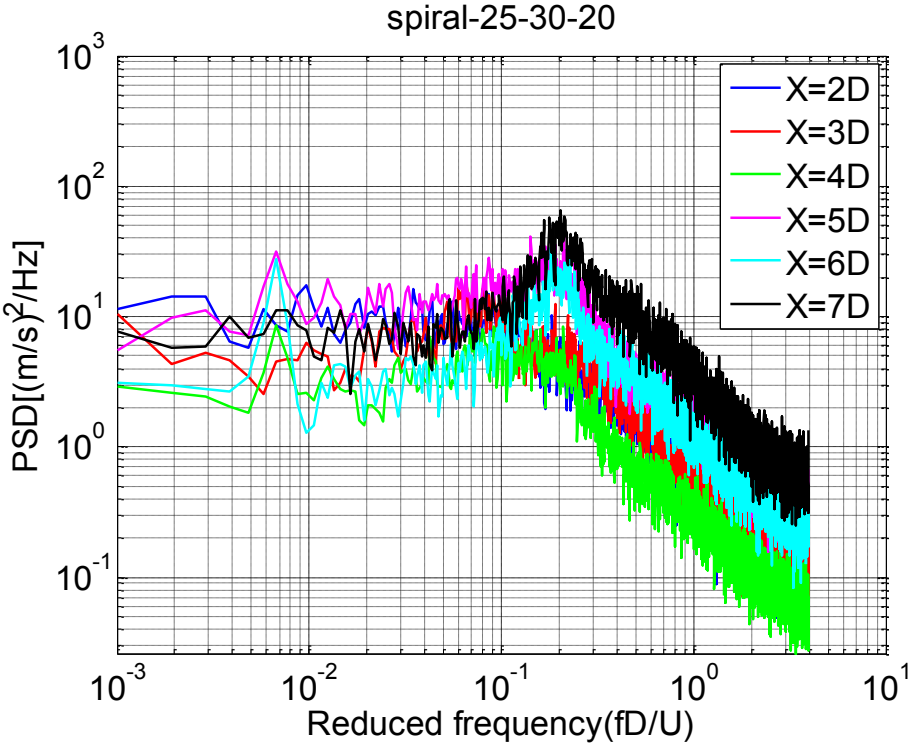

Figure A-9.4 PSD of spiral cable, smooth flow, D=158mm U=20m/s, β=30° and α= 25°

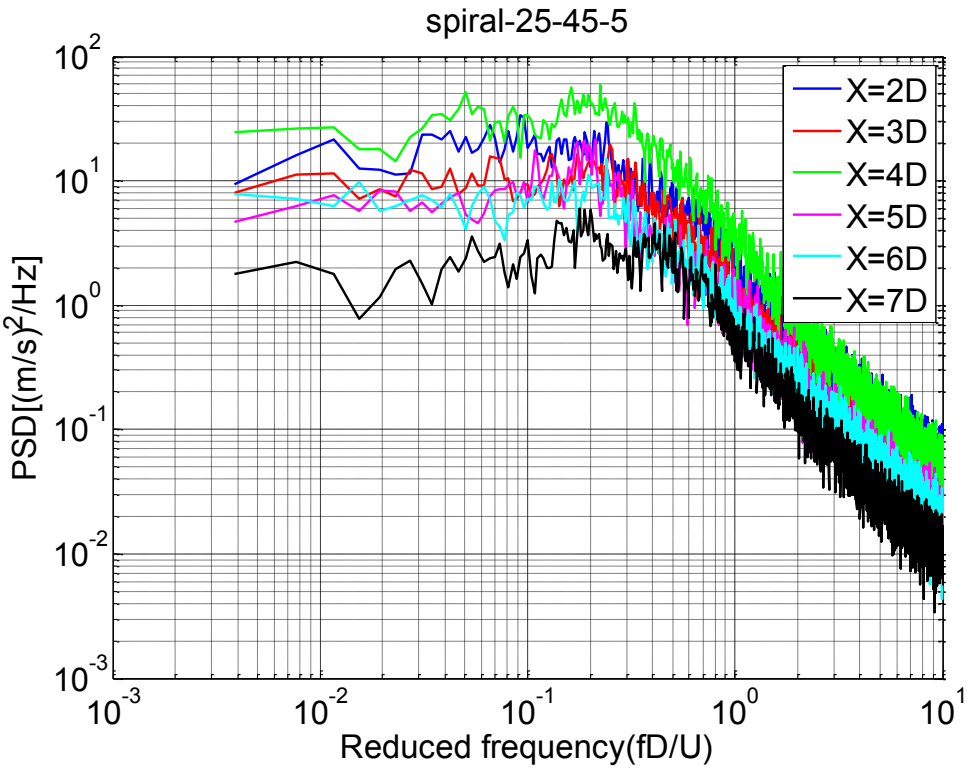

Figure A-9.5 PSD of spiral cable, smooth flow, D=158mm U=5m/s, β=45° and α= 25°

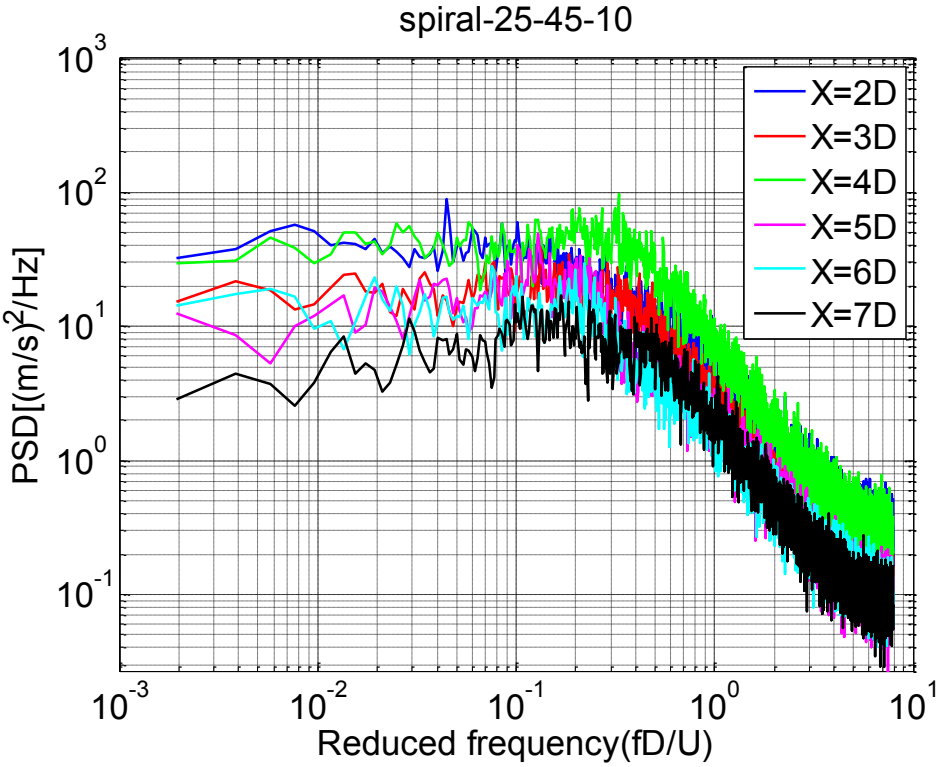

Figure A-9.6 PSD of spiral cable, smooth flow, D=158mm U=10m/s, β=45° and α= 25°

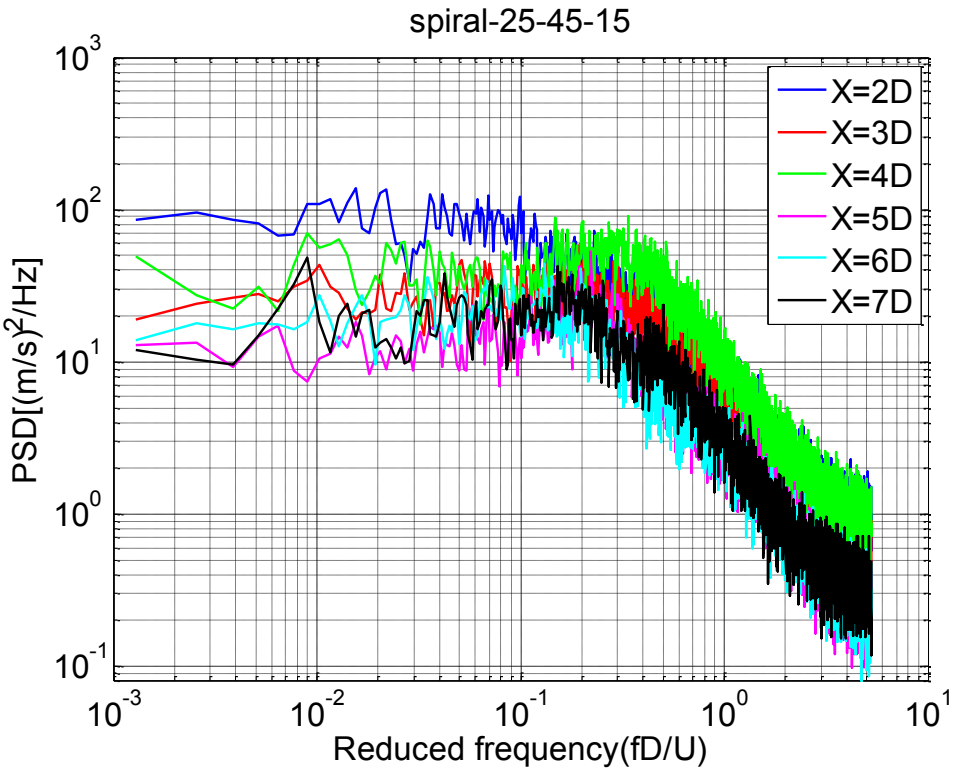

Figure A-9.7 PSD of spiral cable, smooth flow, D=158mm U=15m/s, β=45° and α= 25°

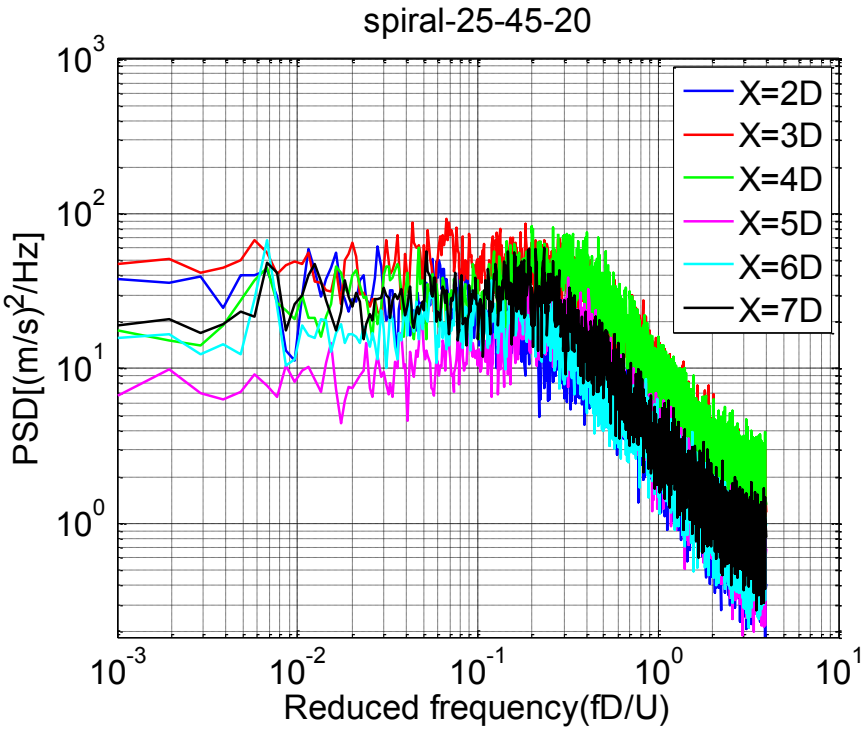

Figure A-9.8 PSD of spiral cable, smooth flow, D=158mm U=20m/s, β=45° and α= 25°

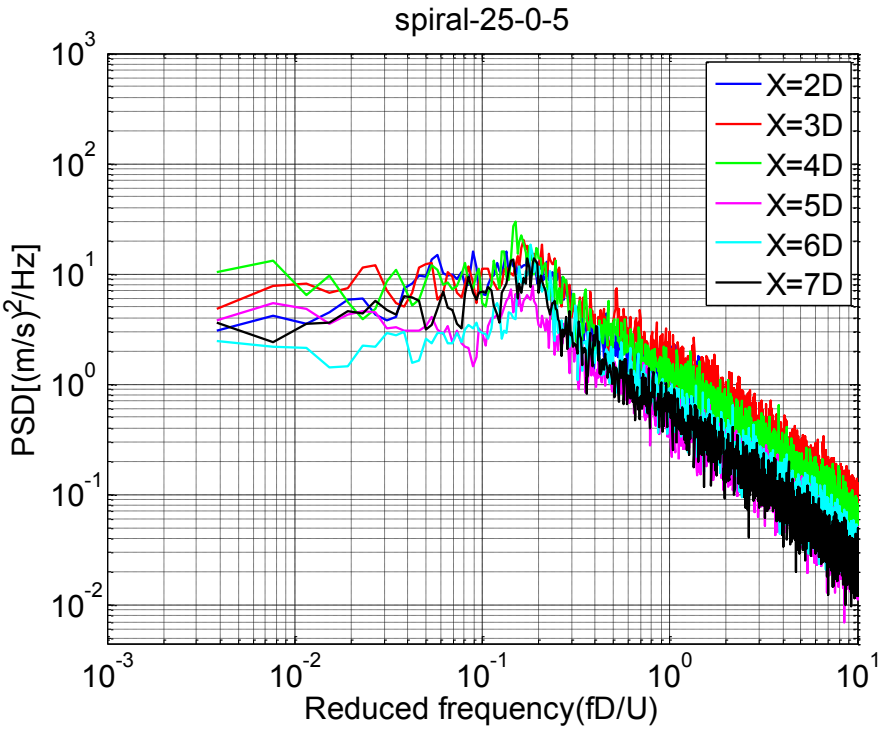

Figure A-9.9 PSD of spiral cable, smooth flow, D=158mm U=5m/s, β=0° and α= 25°

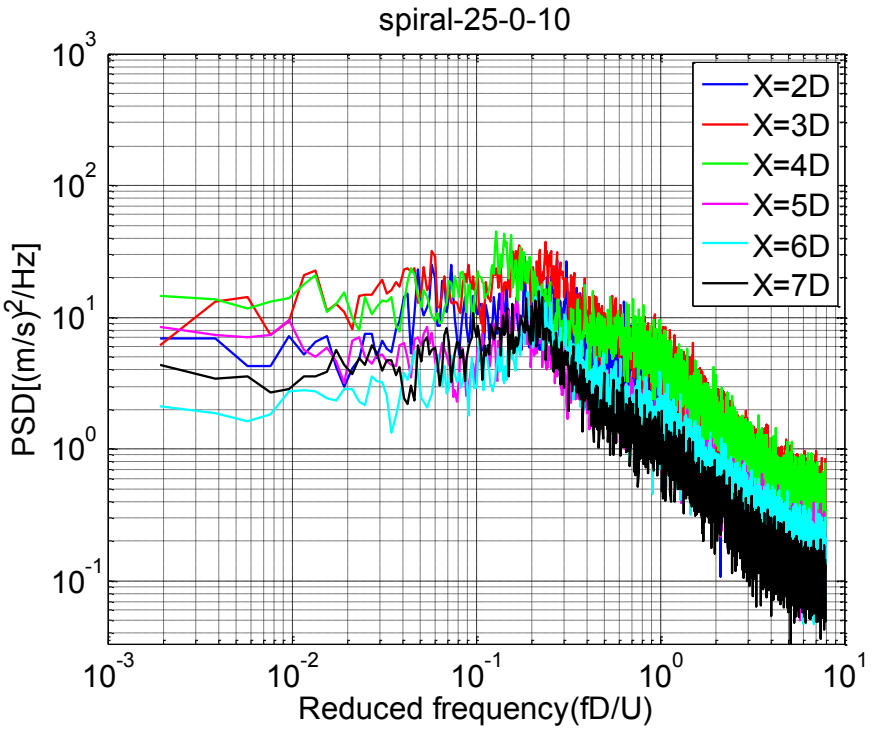

Figure A-9.10 PSD of spiral cable, smooth flow, D=158mm U=10m/s, β=0° and α= 25°

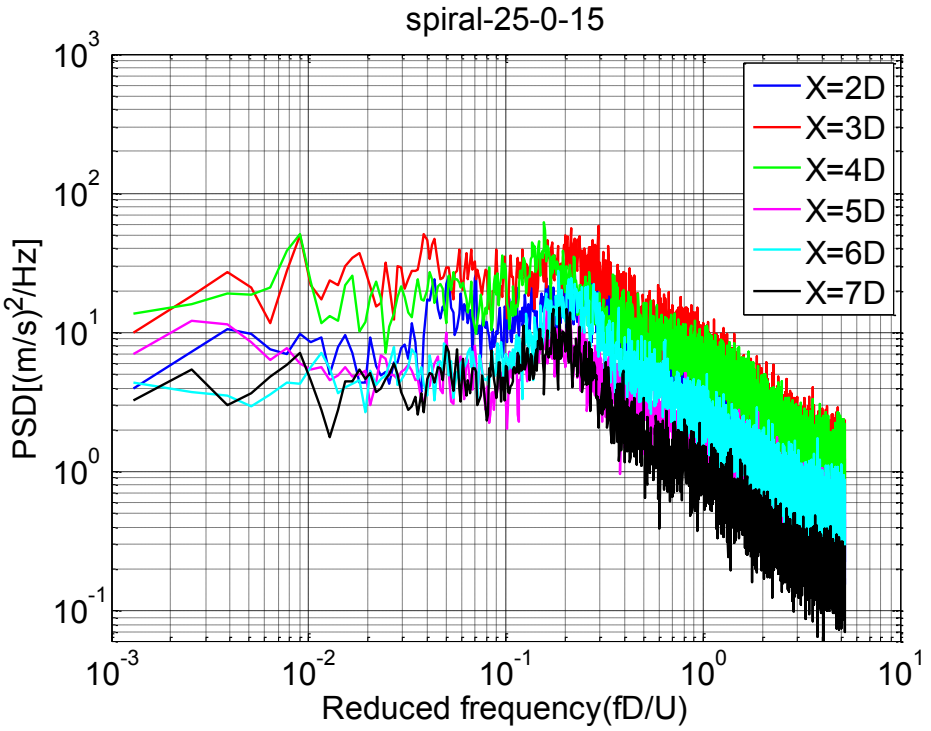

Figure A-9.11 PSD of spiral cable, smooth flow, D=158mm U=15m/s, β=0° and α= 25°

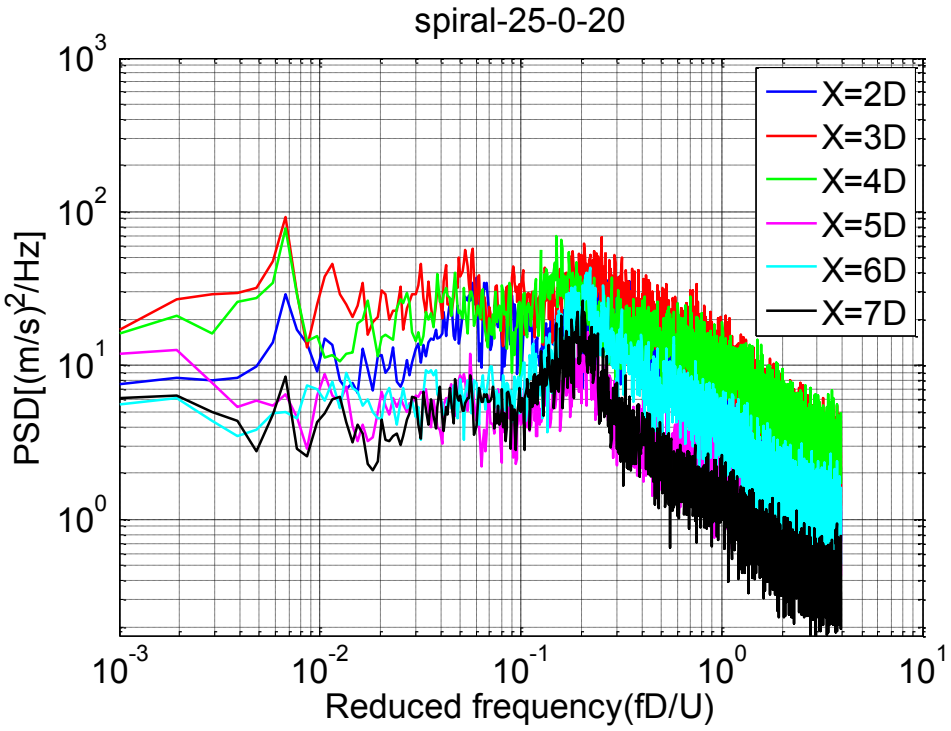

Figure A-9.12 PSD of spiral cable, smooth flow, D=158mm U=20m/s, β=0° and α= 25°

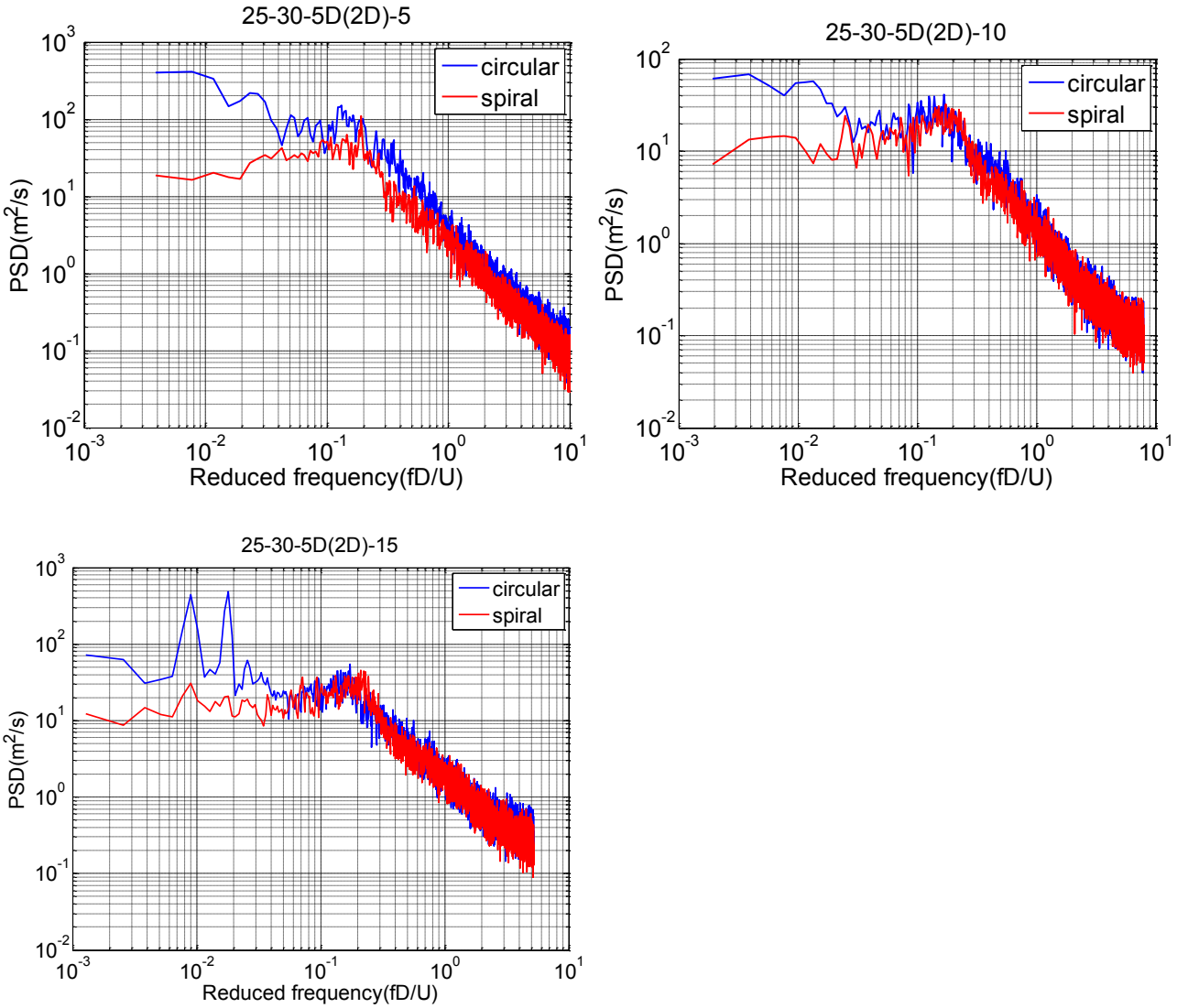

Figure A-9.13 PSD comparison; X/D= 5; D=158mm; U=5; 10 - 15m/s; β=30° and α= 25°

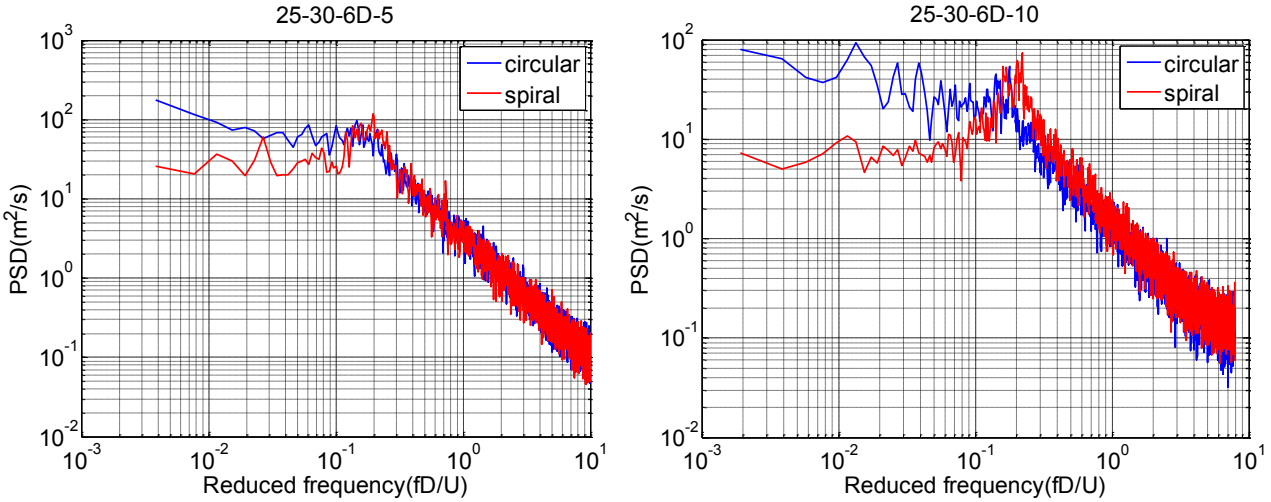

Figure A-9.14 PSD comparison; X/D= 6; D=158mm; U=5-10m/s; β=30° and α= 25°

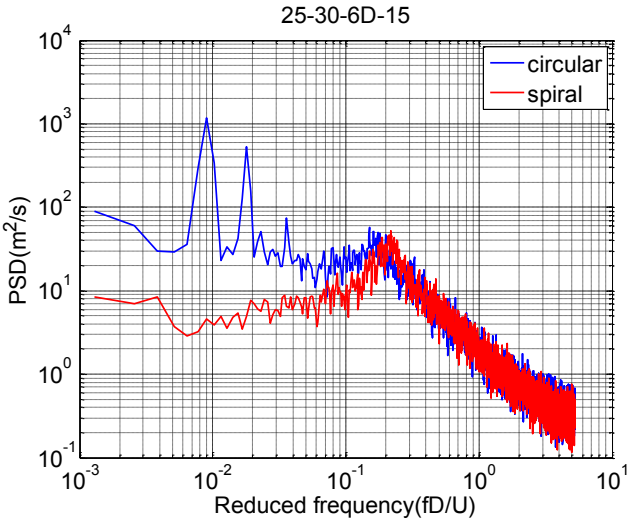

Figure A-9.15 PSD comparison; X/D= 6; D=158mm; U=15m/s; β=30° and α= 25°

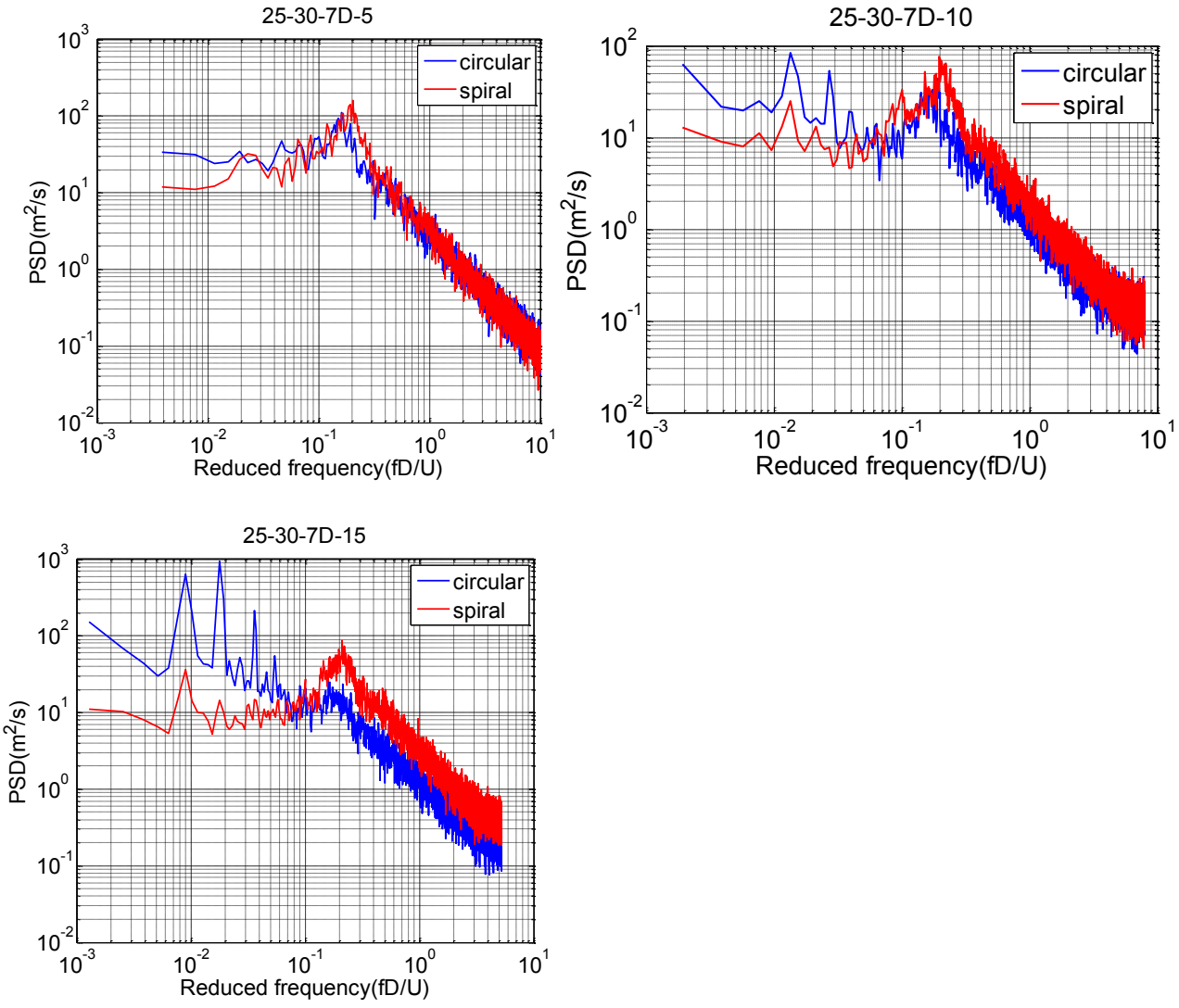

Figure A-9.16 PSD comparison; X/D= 7; D=158mm; U=5-10-15m/s; β=30° and α= 25°

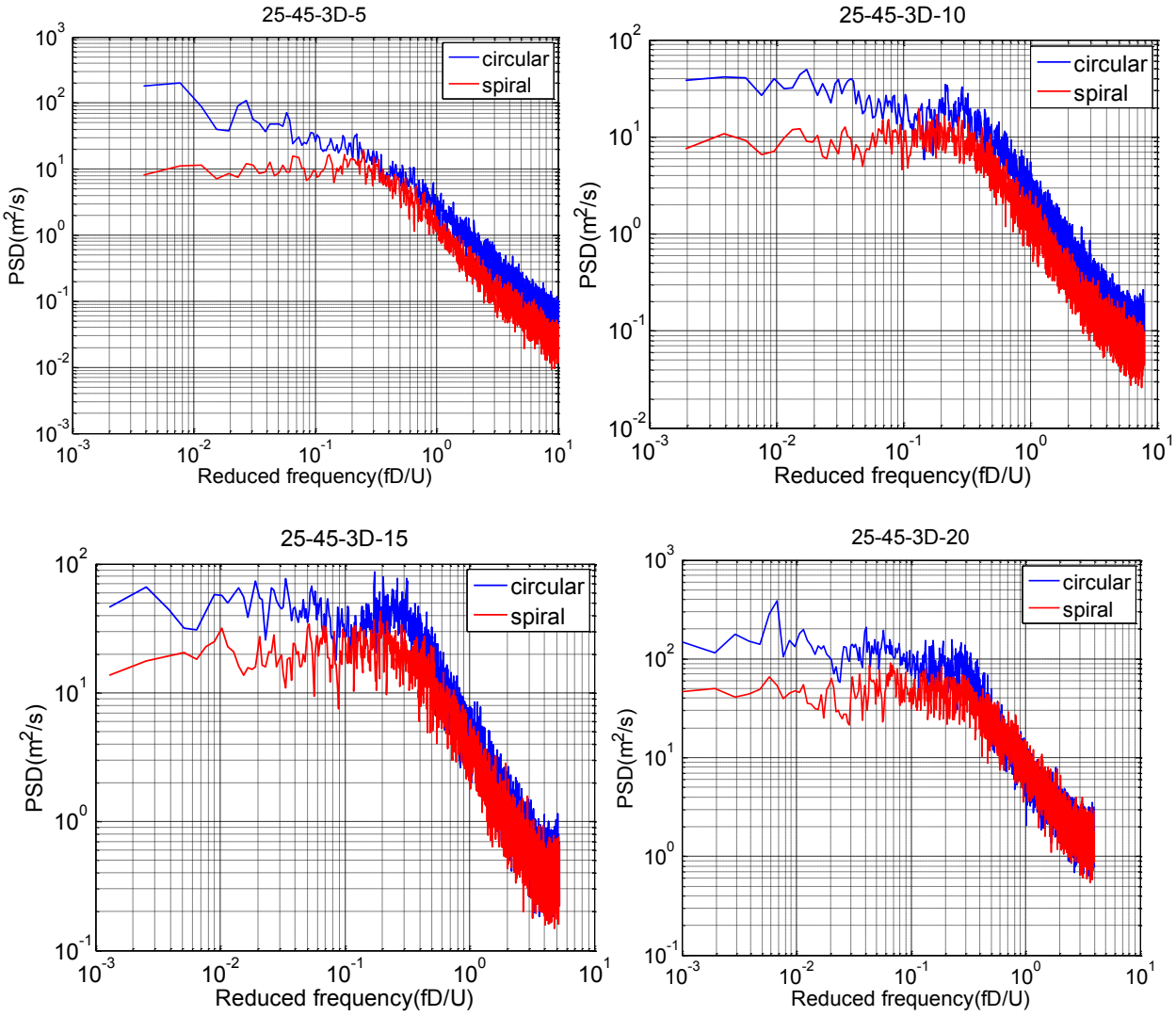

Figure A-9.17 PSD comparison; X/D= 3; D=158mm; U=5; 10; 15; 20m/s; β=45° and α= 25°

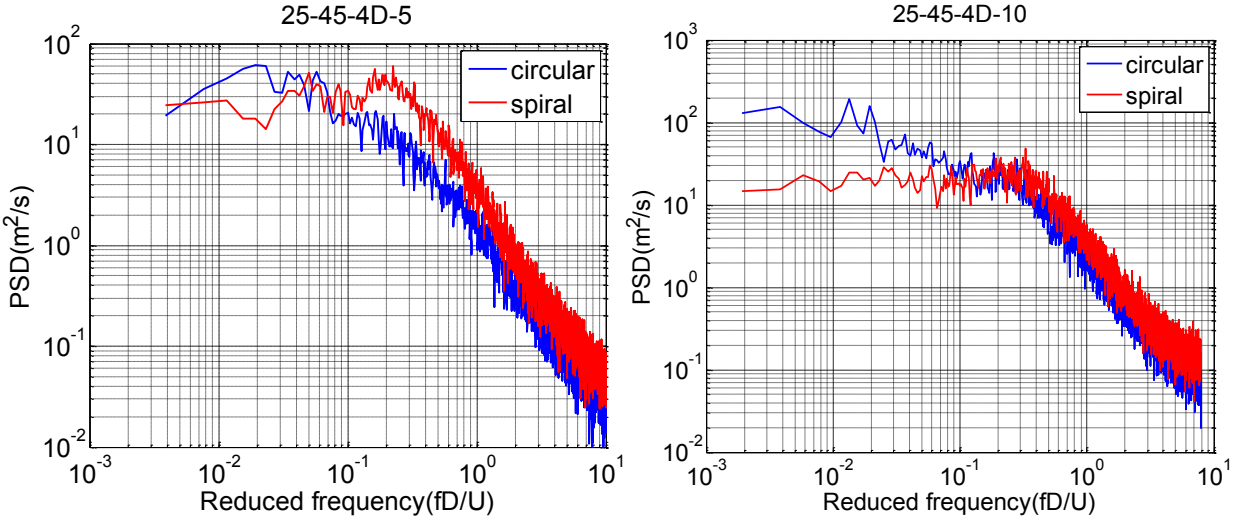

Figure A-9.18 PSD comparison; X/D= 4; D=158mm; U=5; 10 m/s; β=45° and α= 25°

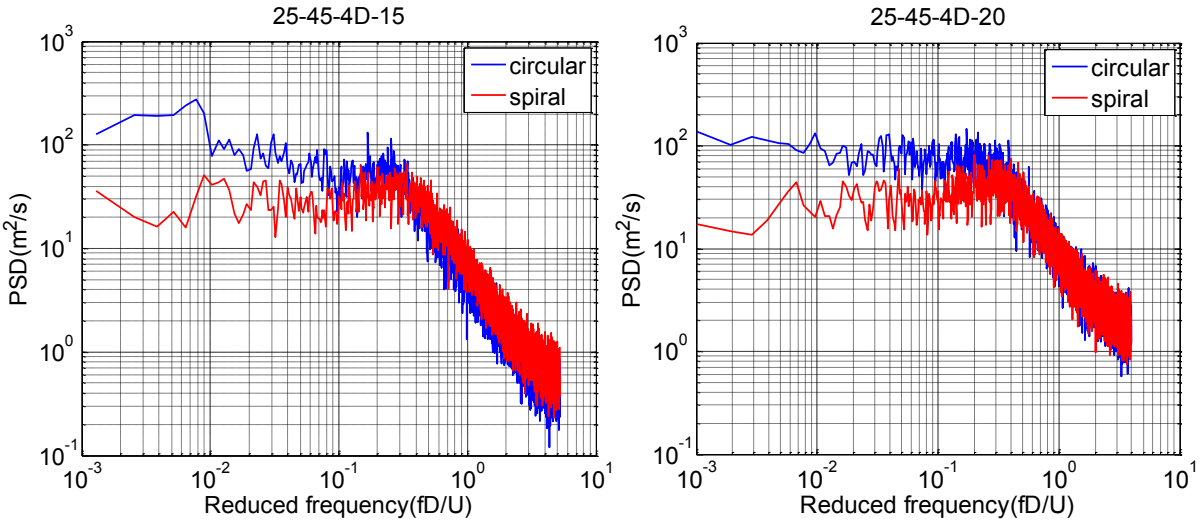

Figure A-9.19 PSD comparison; X/D= 4; D=158mm; U=15; 20 m/s; β=45° and α= 25°

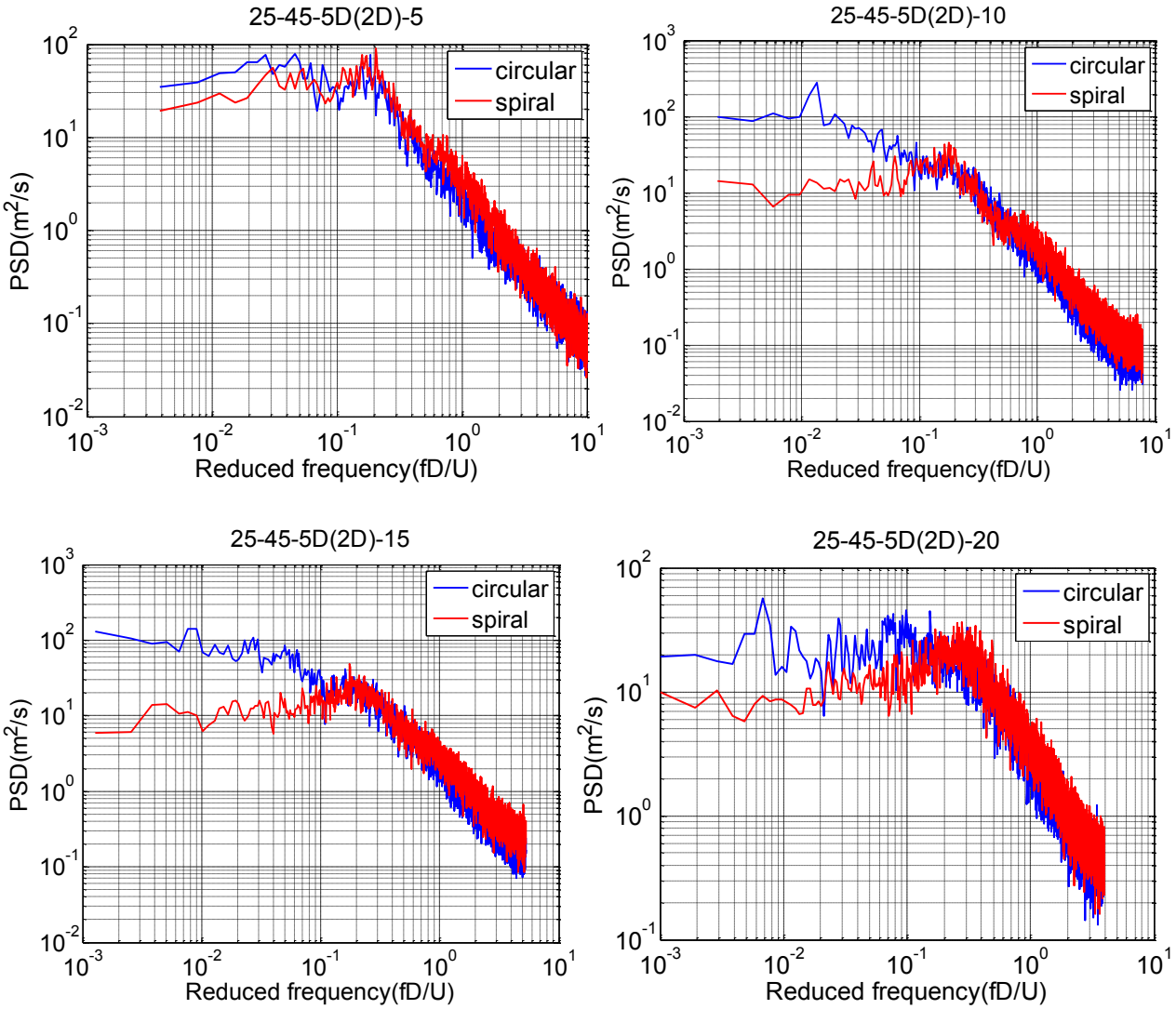

Figure A-9.20 PSD comparison; X/D= 5; D=158mm; U=5; 10; 15; 20 m/s; β=45° and α= 25°

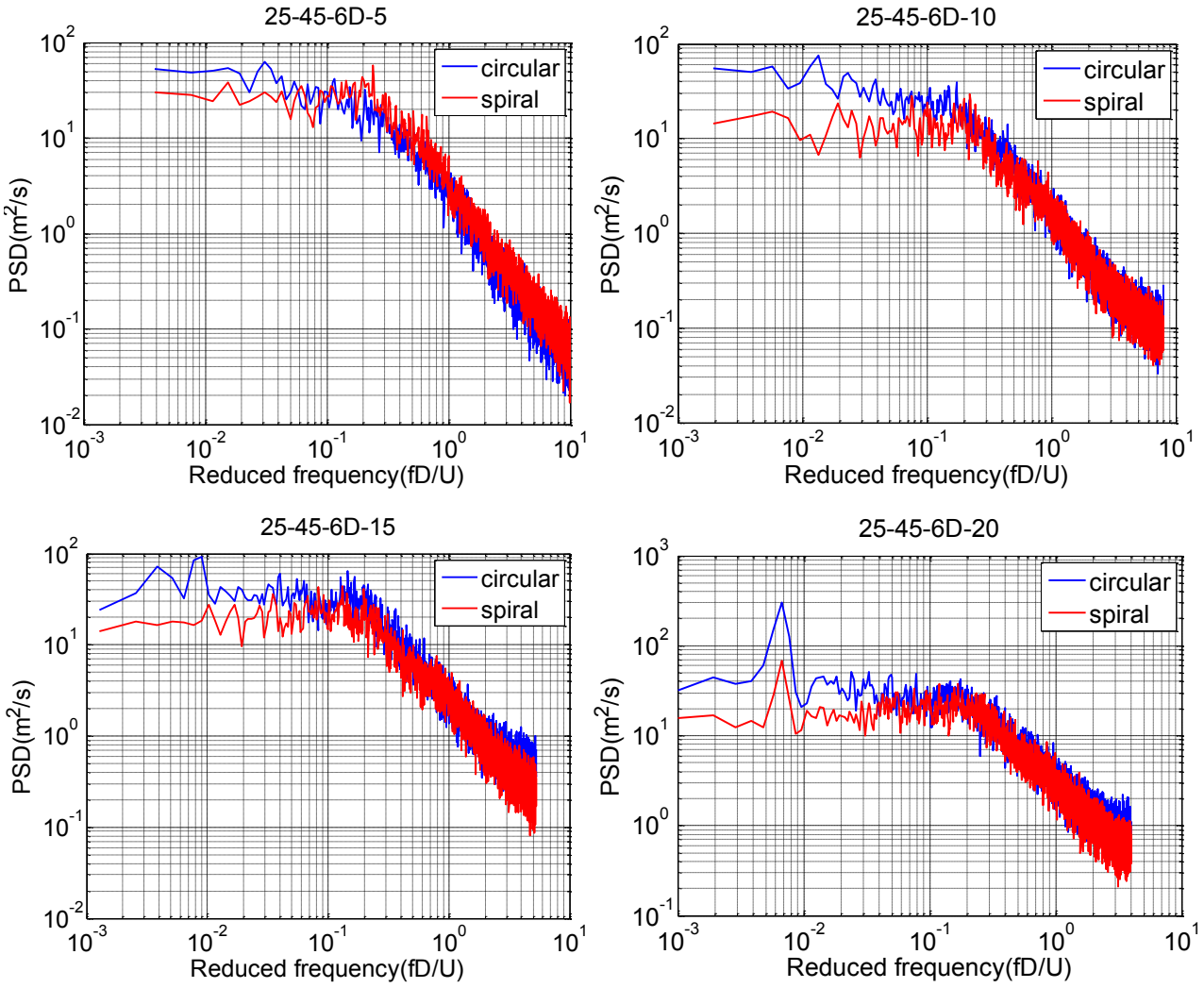

Figure A-9.21 PSD comparison; X/D= 6; D=158mm; U=5; 10; 15; 20 m/s; β=45° and α= 25°

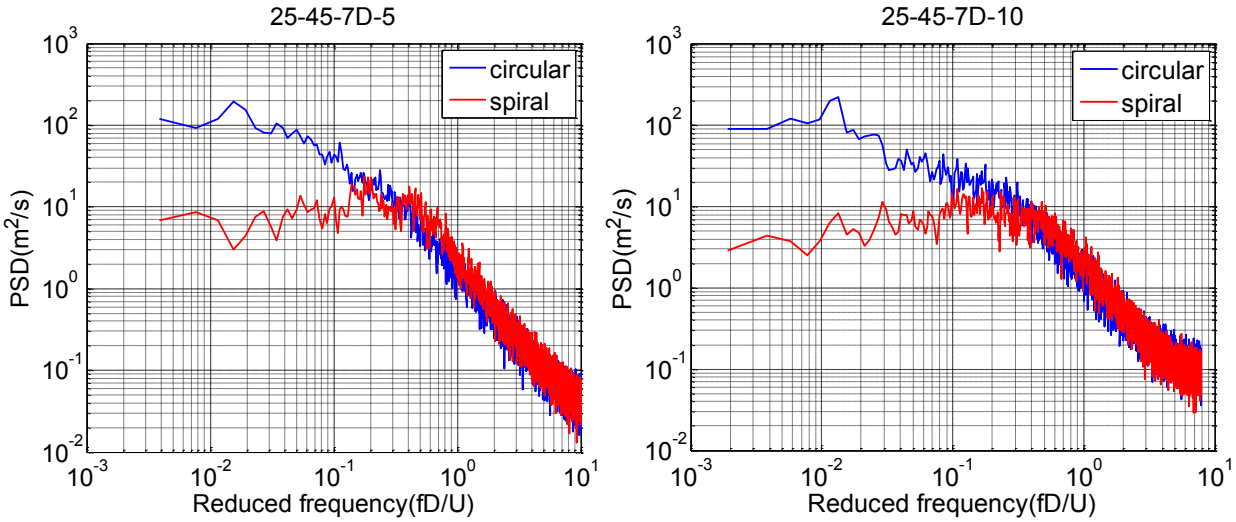

Figure A-9.22 PSD comparison; X/D= 7; D=158mm; U=5; 10; m/s; β=45° and α= 25°

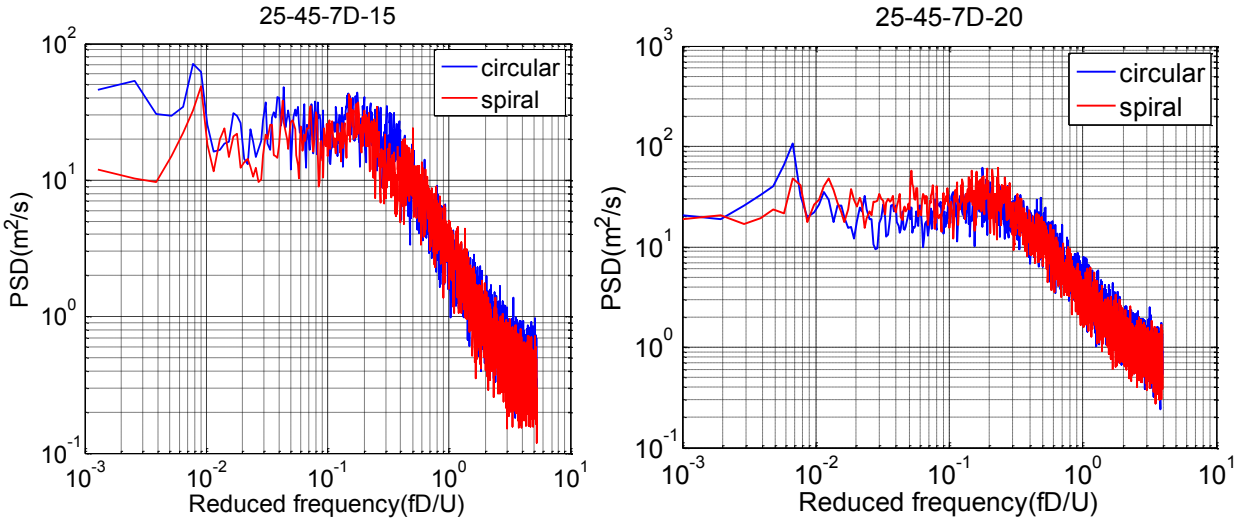

Figure A-9.23 PSD comparison; X/D= 7; D=158mm; U= 15; 20 m/s; β=45° and α= 25°

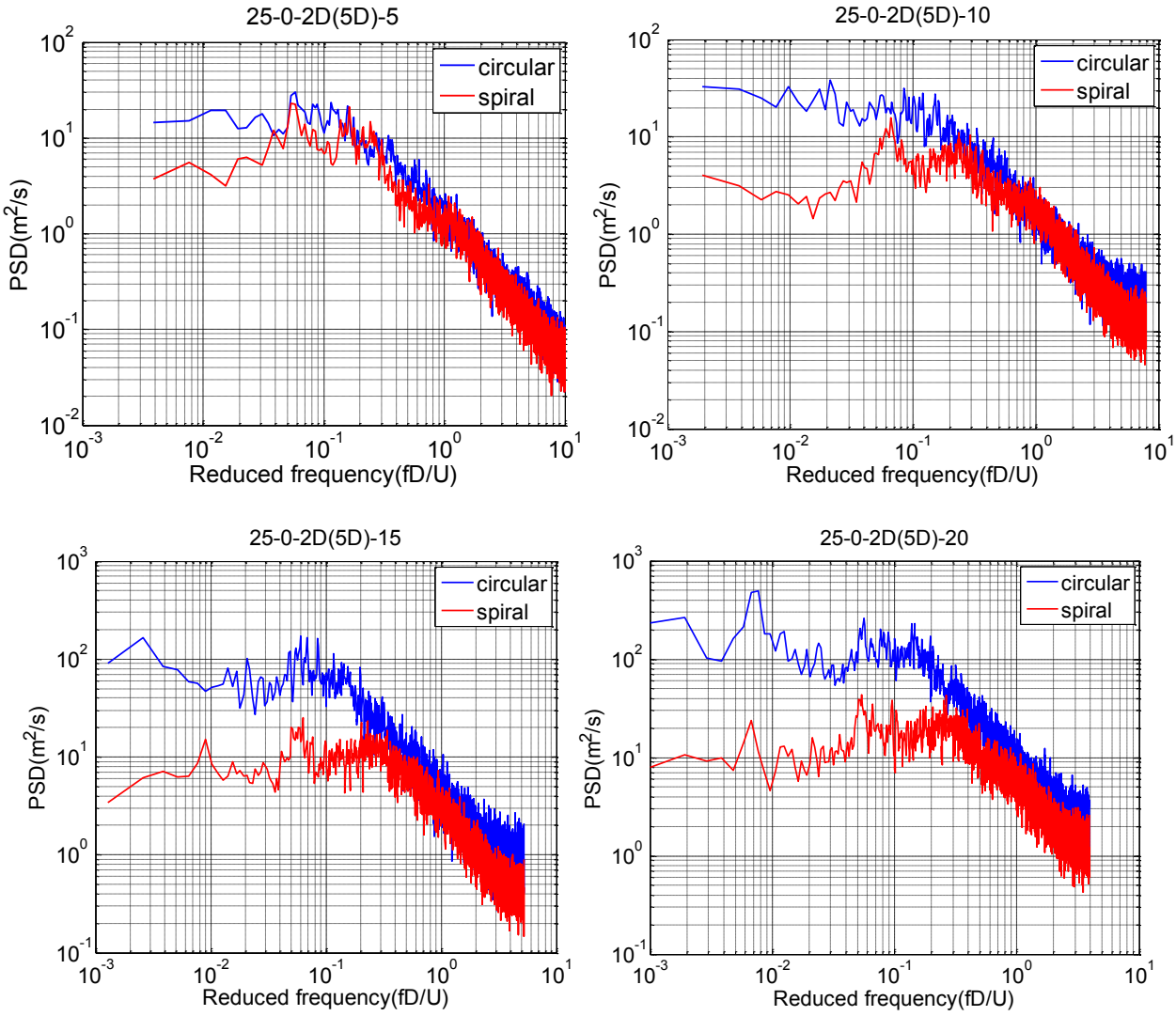

Figure A-9.24 PSD comparison; X/D= 2; D=158mm; U= 15; 20 m/s; β=0° and α= 25°

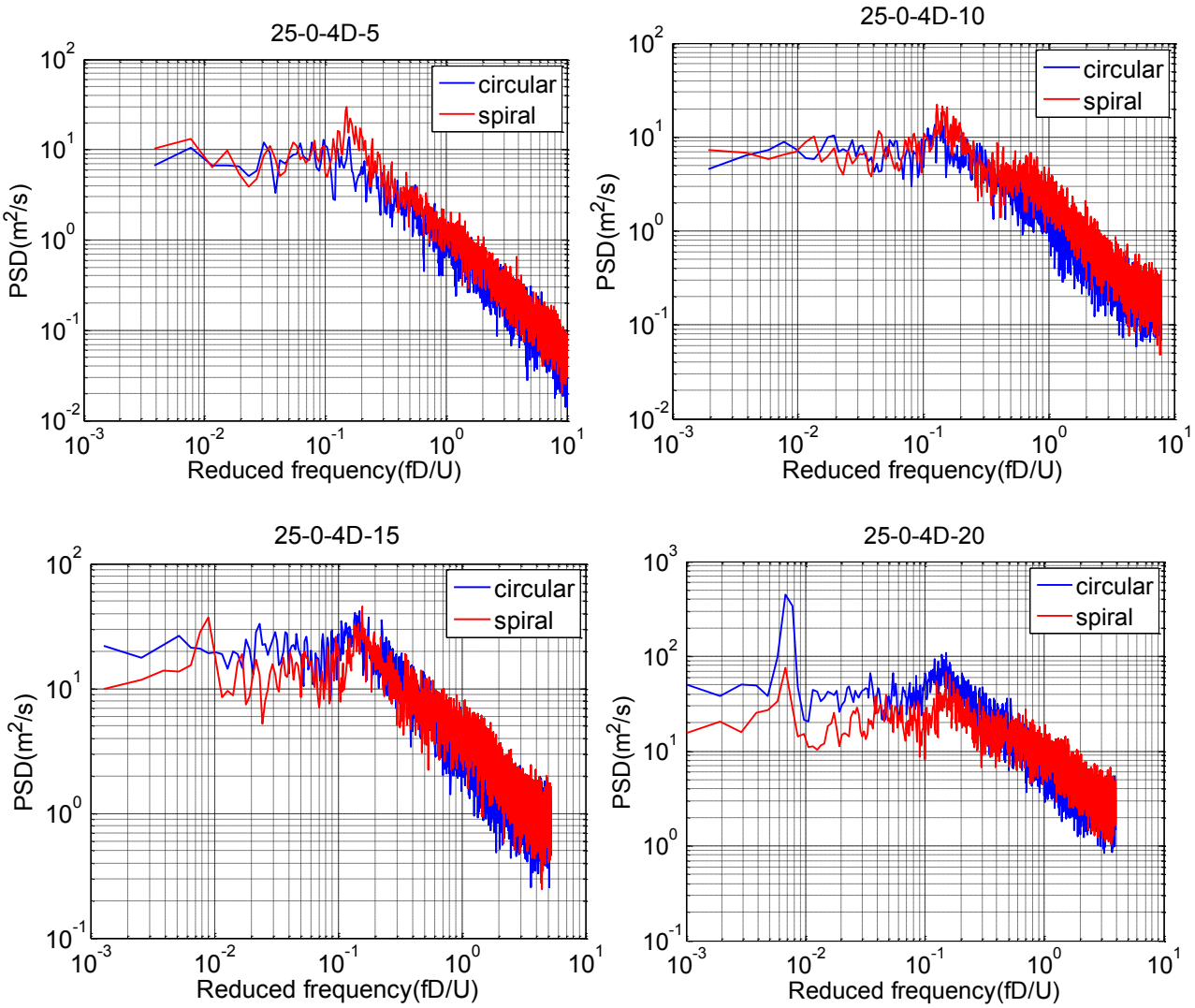

Figure A-9.25 PSD comparison; X/D= 4; D=158mm; U= 5; 10; 15; 20 m/s; β=0° and α= 25°

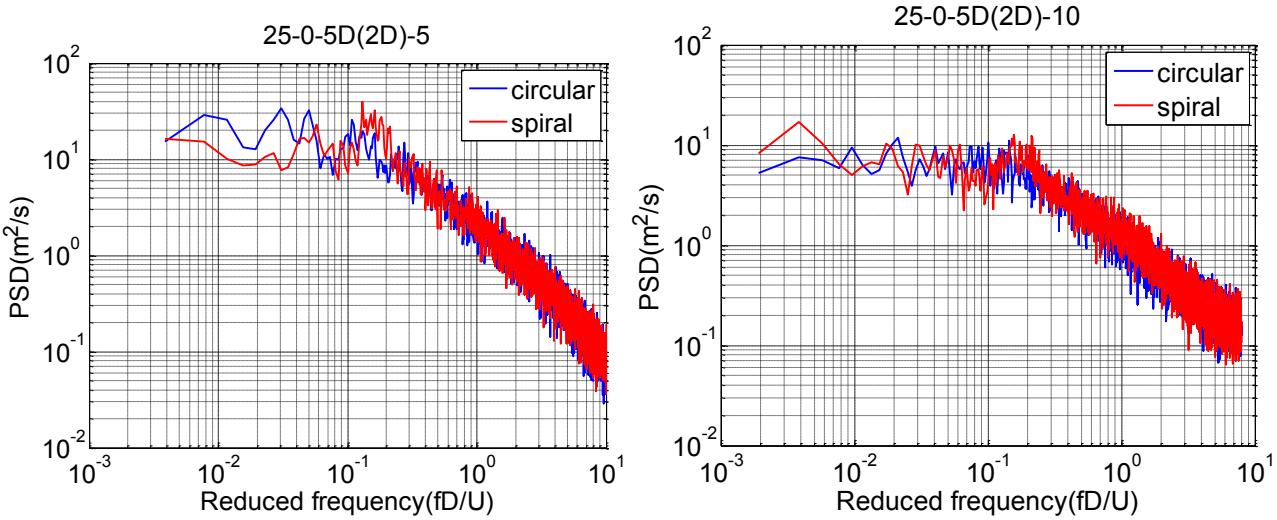

Figure A-9.26 PSD comparison; X/D= 5; D=158mm; U= 5; 10 m/s; β=0° and α= 25°

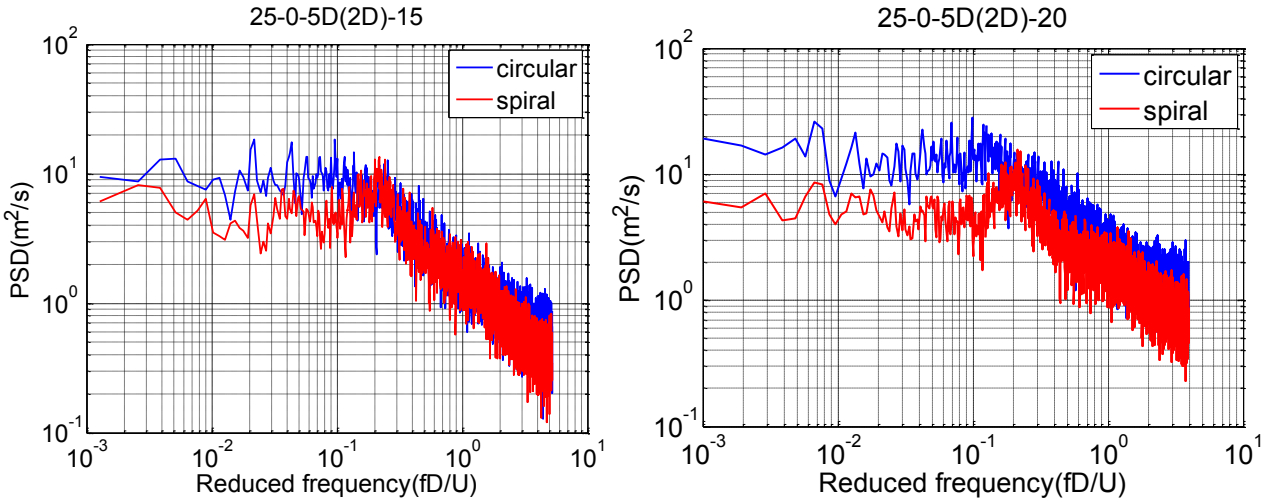

Figure A-9.27 PSD comparison; X/D= 5; D=158mm; U= 15; 20 m/s; β=0° and α= 25°

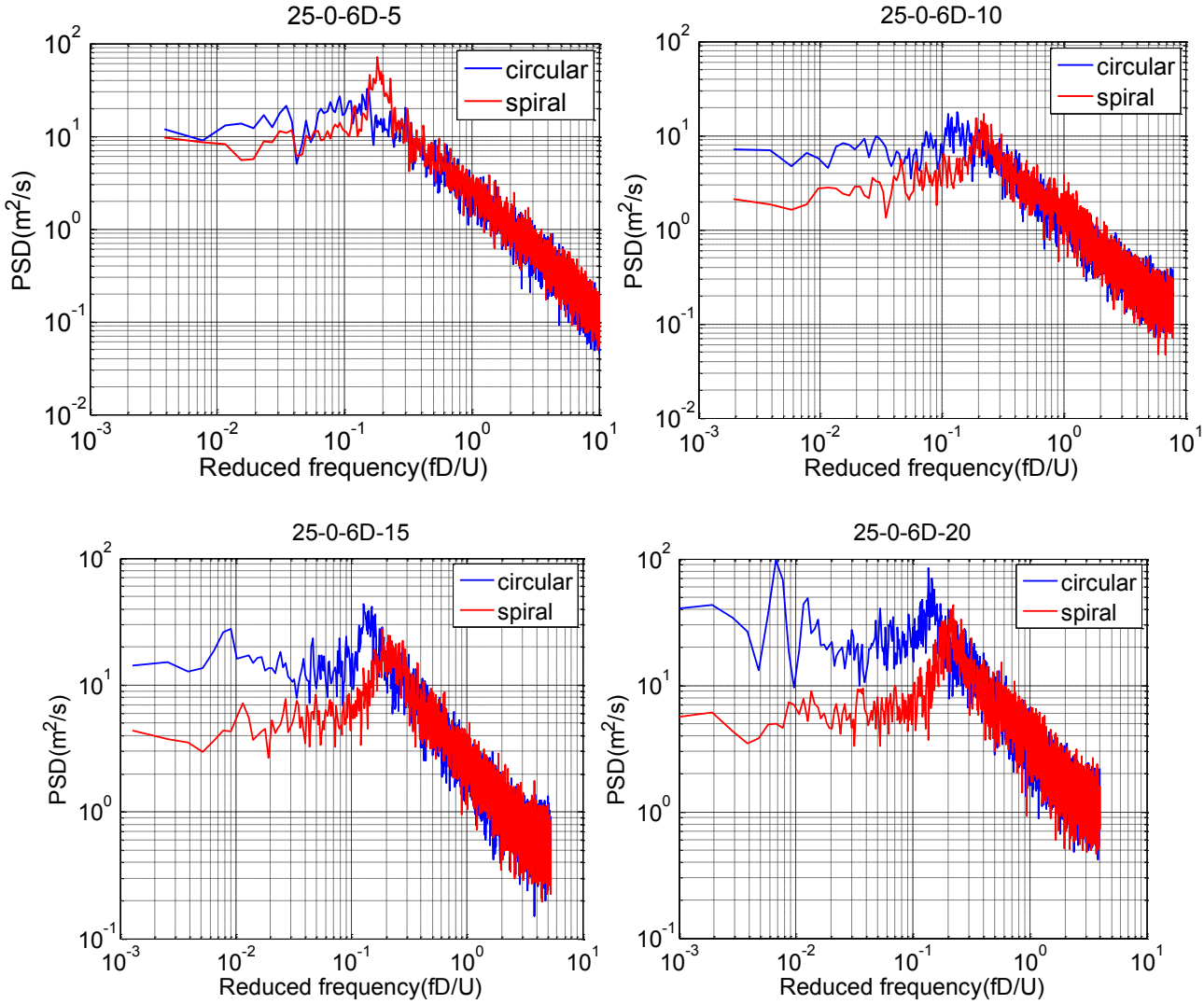

Figure A-8.28 PSD comparison; X/D= 6; D=158mm; U= 5; 10 15; 20 m/s; β=0° and α= 25°

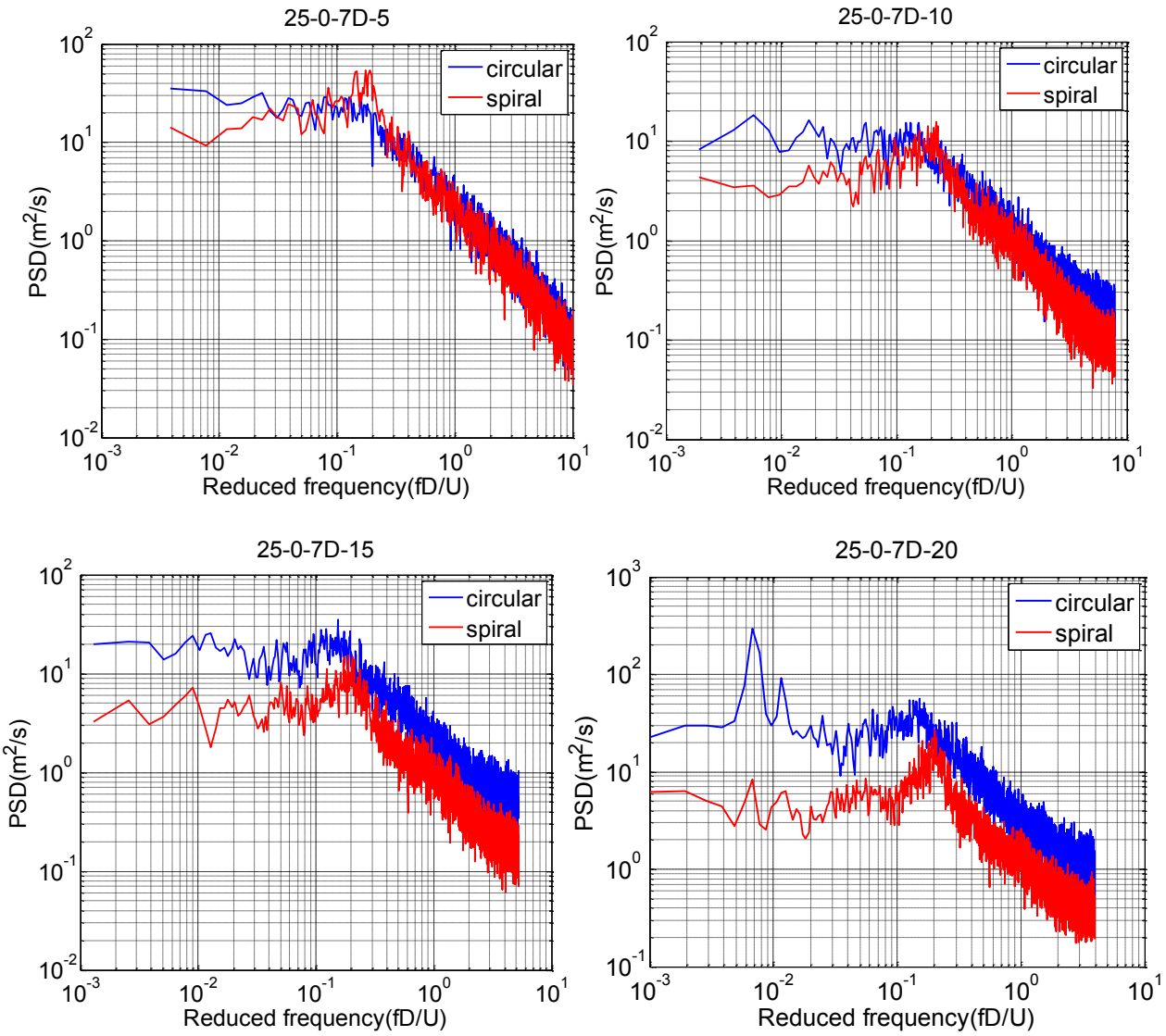

Figure A-9.29 PSD comparison; X/D= 7; D=158mm; U= 5; 10 15; 20 m/s; β=0° and α= 25°

Appendix 10: Wavelet analysis of velocity fluctuating near spiral cable wake

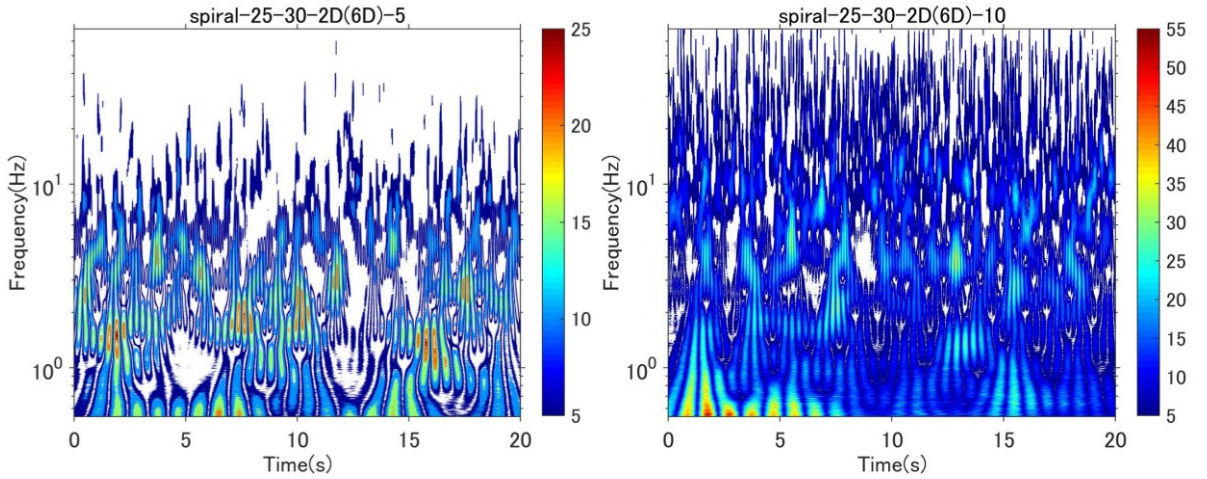

Figure A-10.1 WA of spiral cable, X/D= 2, U=5 and 10m/s, β=30° and α= 25°

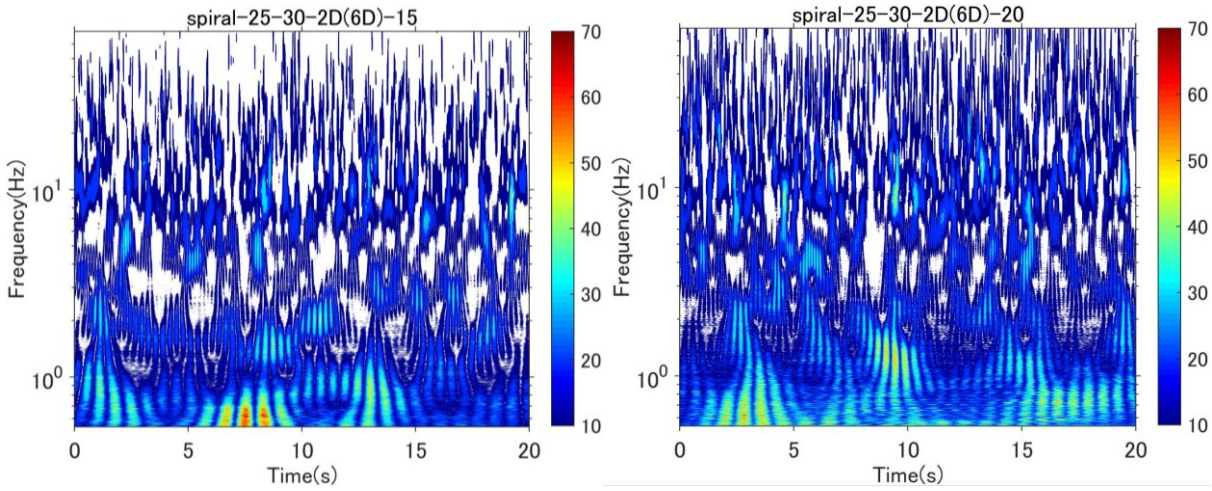

Figure A-10.2 WA of spiral cable, X/D= 2, U=15m/s and 20m/s, β=30° and α= 25°

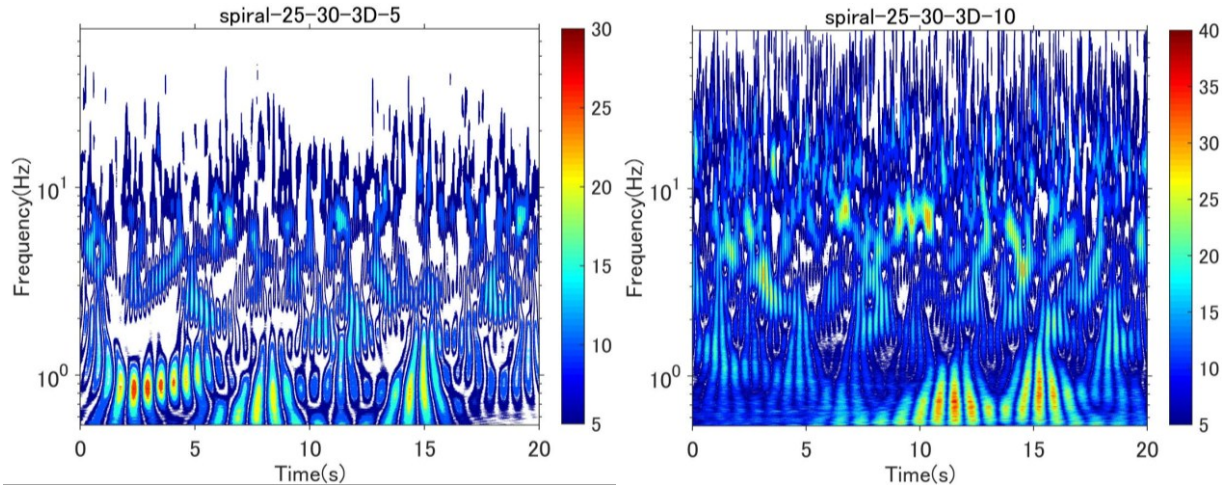

Figure A-10.3 WA of spiral cable, X/D= 3, U=5m/s and 10m/s, β=30° and α= 25°

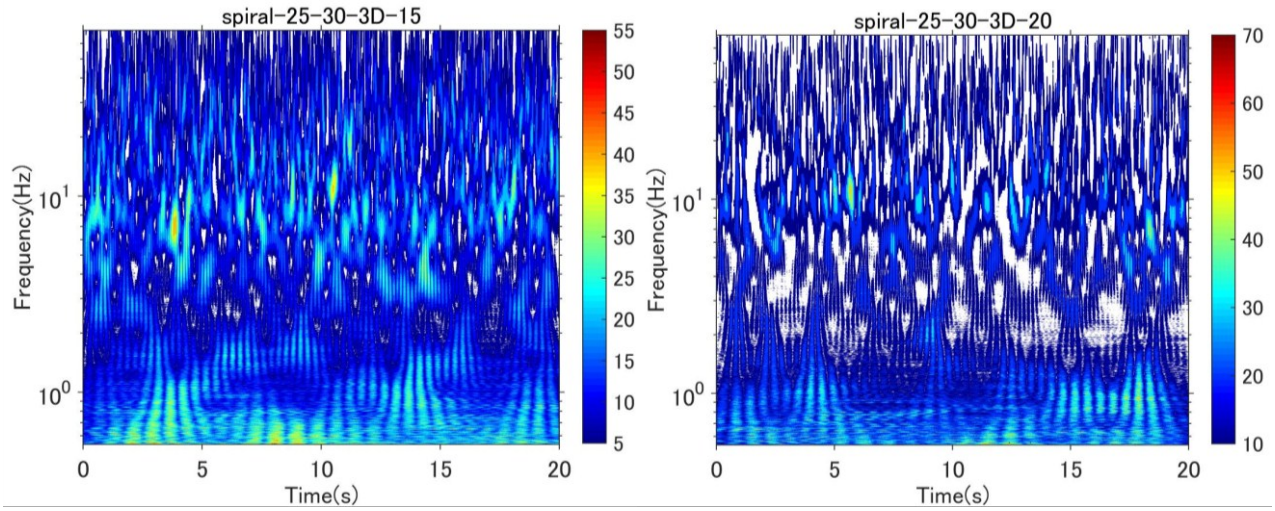

Figure A-10.4 WA of spiral cable, X/D= 3, U=15m/s and 20m/s, β=30° and α= 25°

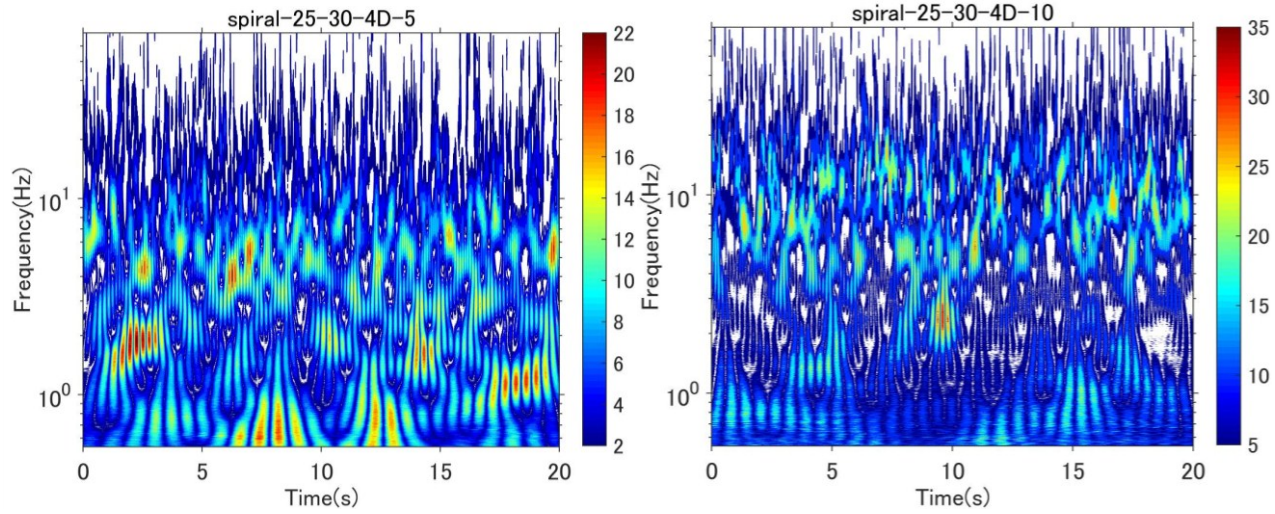

Figure A-10.5 WA of spiral cable, X/D= 4, U=5 and 10m/s, β=30° and α= 25°

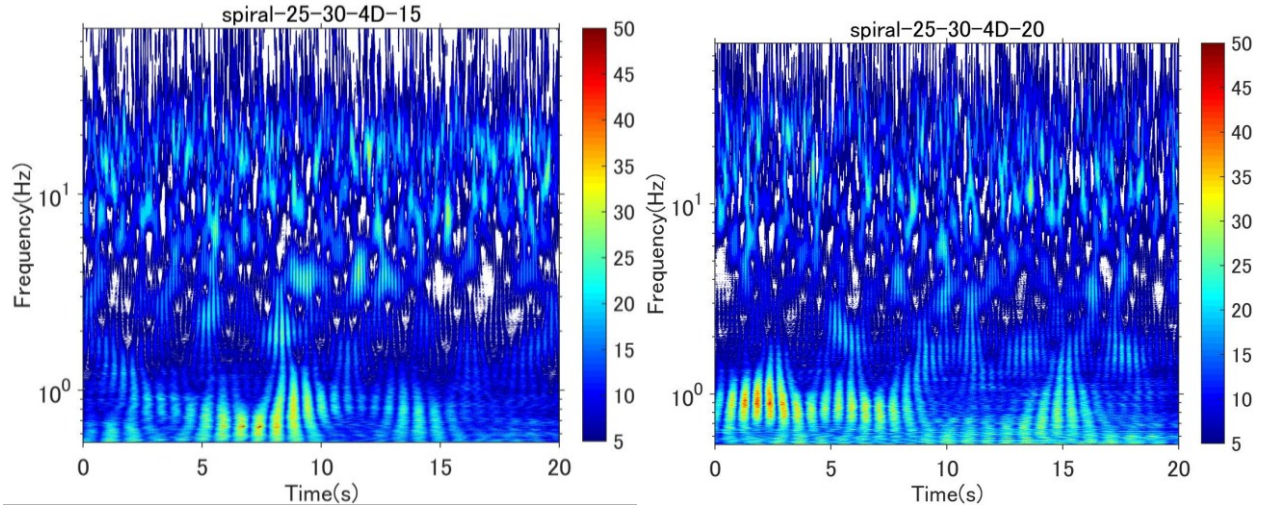

Figure A-10.6 WA of spiral cable, X/D= 4, U=15 and 20m/s, β=30° and α= 25°

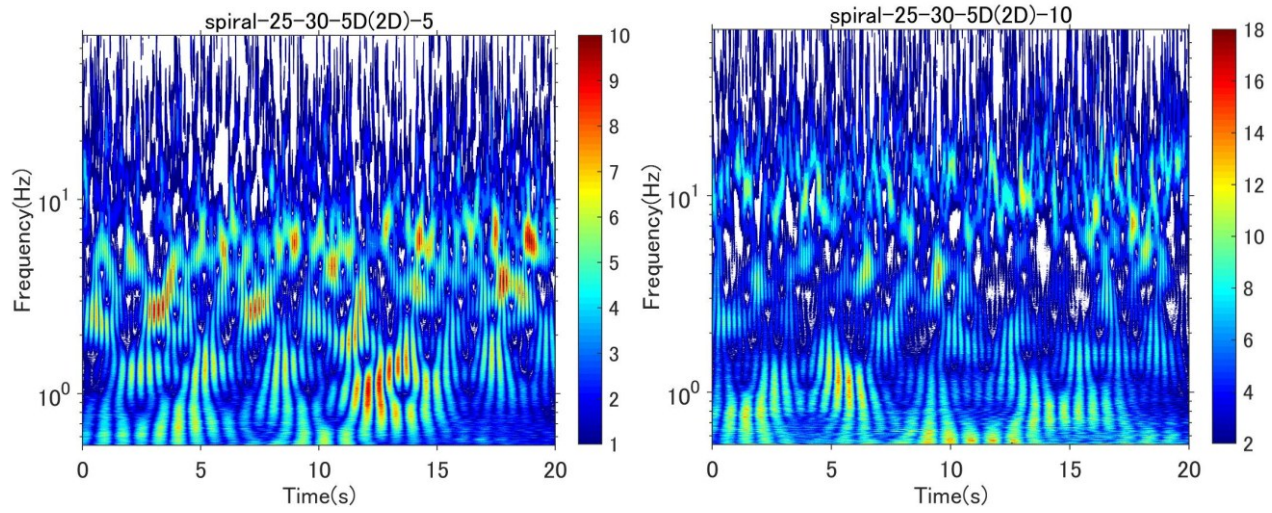

Figure A-10.7 WA of spiral cable, X/D= 5, U=5 and 10m/s, β=30° and α= 25°

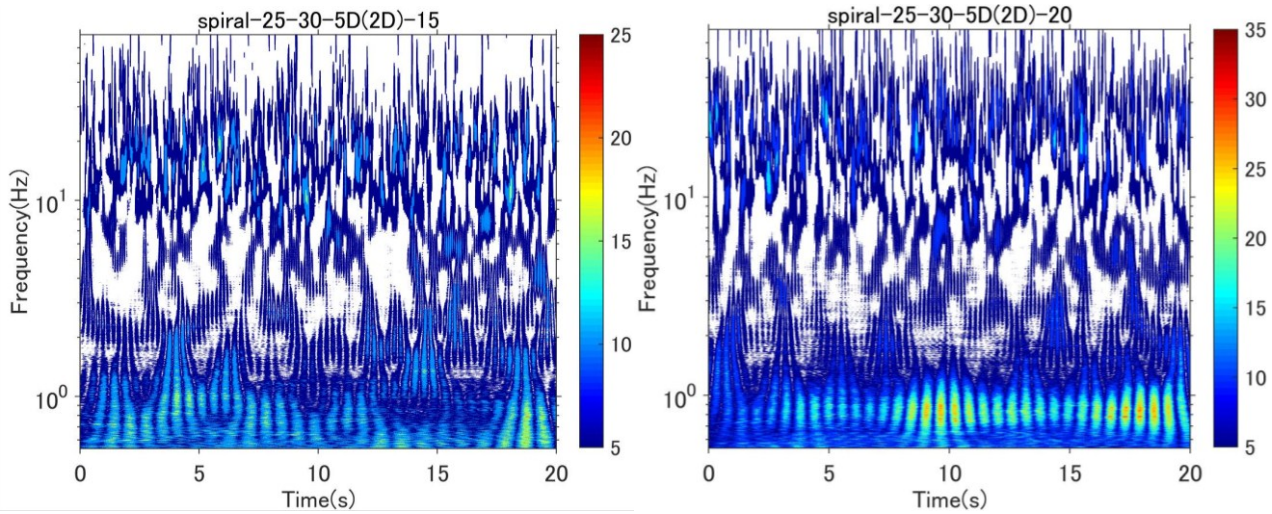

Figure A-10.8 WA of spiral cable, X/D= 5, U=15 and 20m/s, β=30° and α= 25°

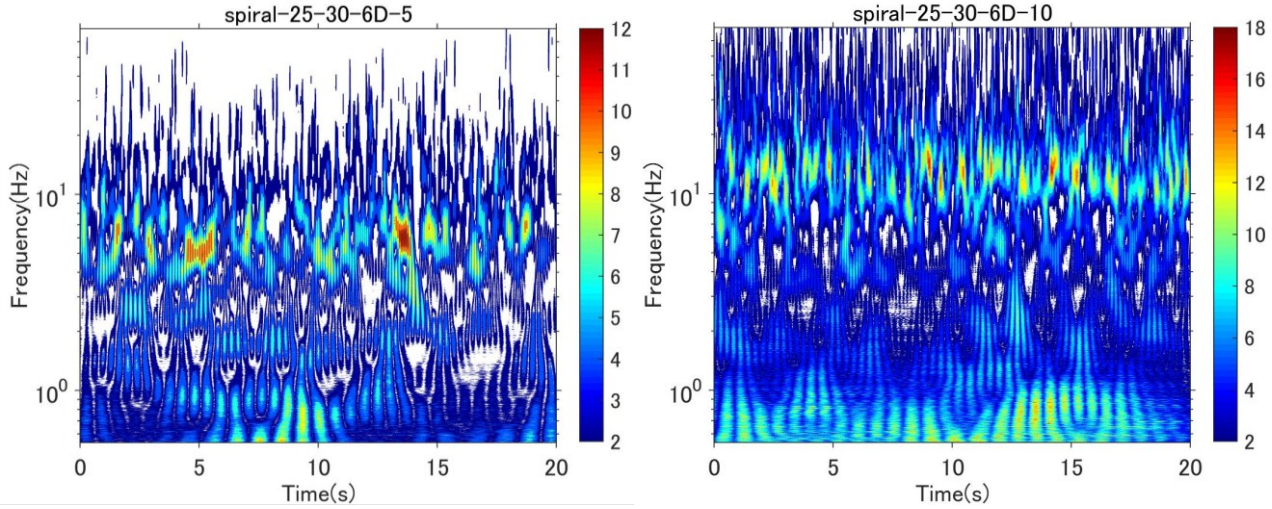

Figure A-10.9 WA of spiral cable, X/D= 6, U=5 and 10m/s, β=30° and α= 25°

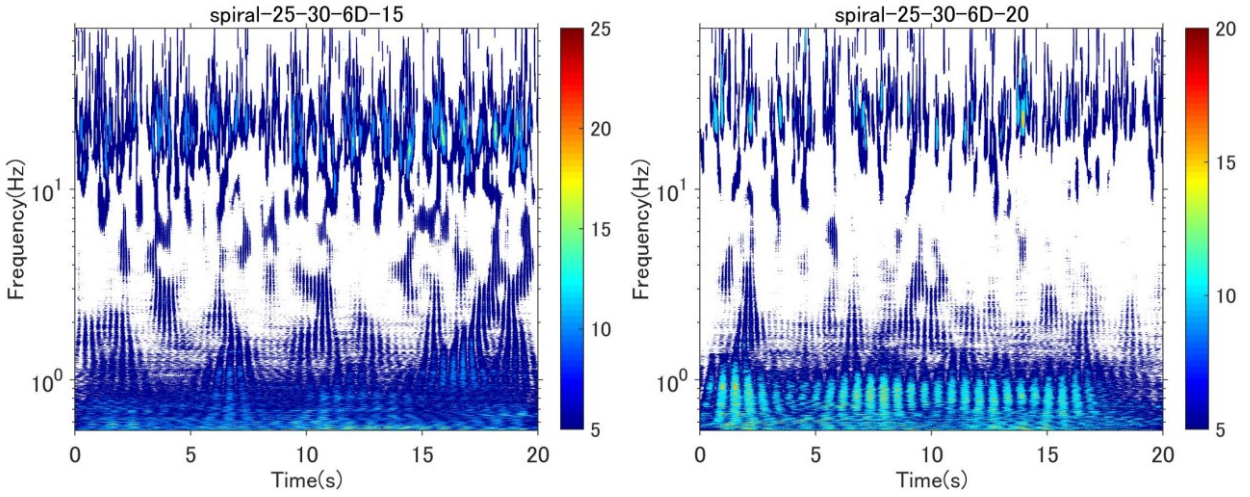

Figure A-10.10 WA of spiral cable, X/D= 6, U=15 and 20m/s, β=30° and α= 25°

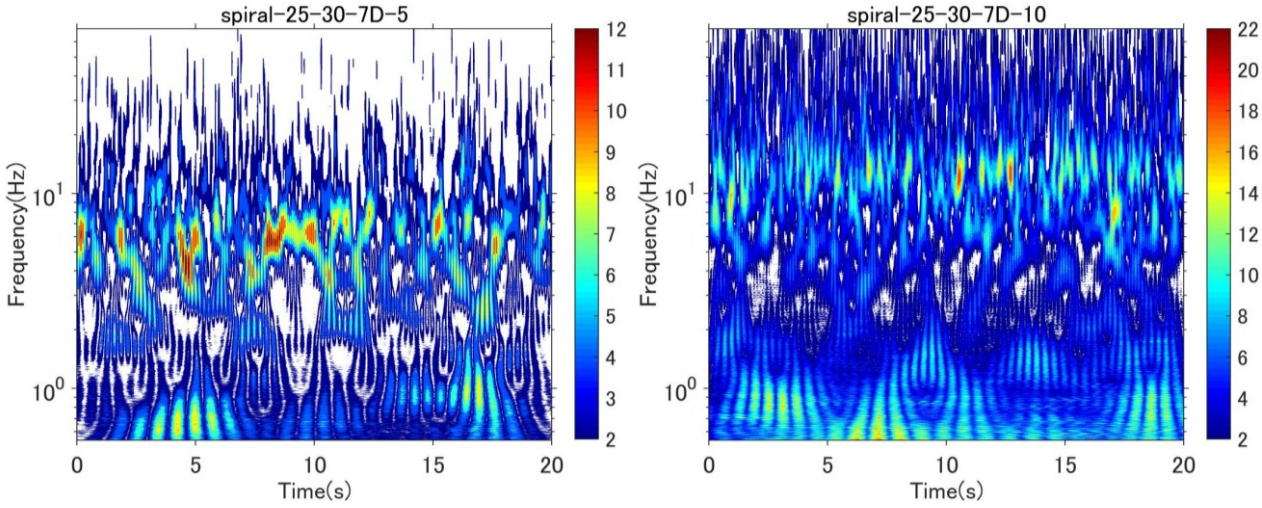

Figure A-10.11 WA of spiral cable, X/D= 7, U=5 and 10m/s, β=30° and α= 25°

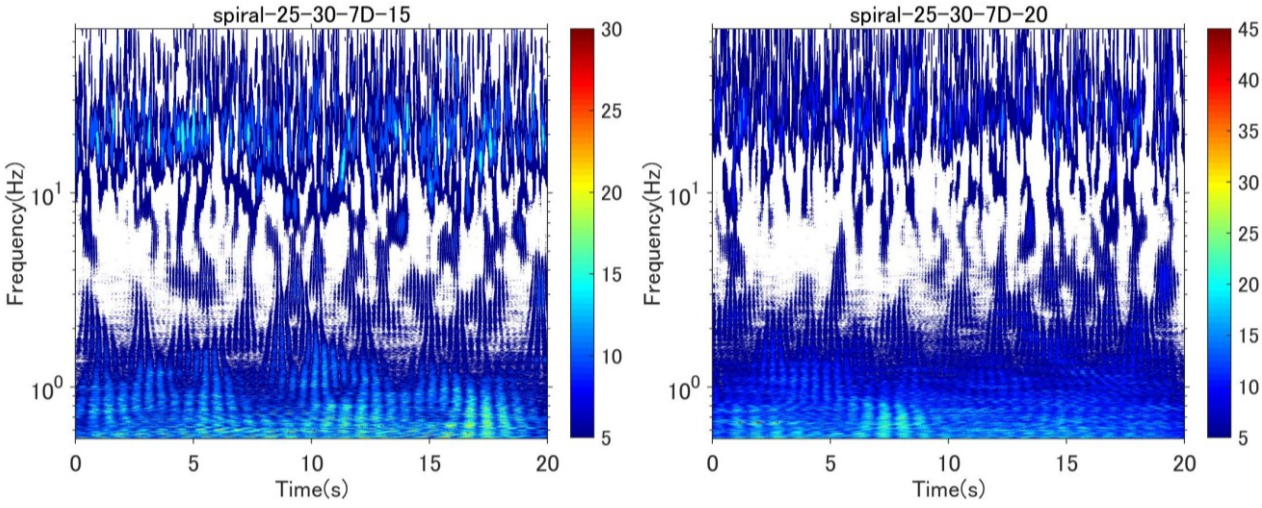

Figure A-10.12 WA of spiral cable, X/D= 7, U=15 and 20m/s, β=30° and α= 25°

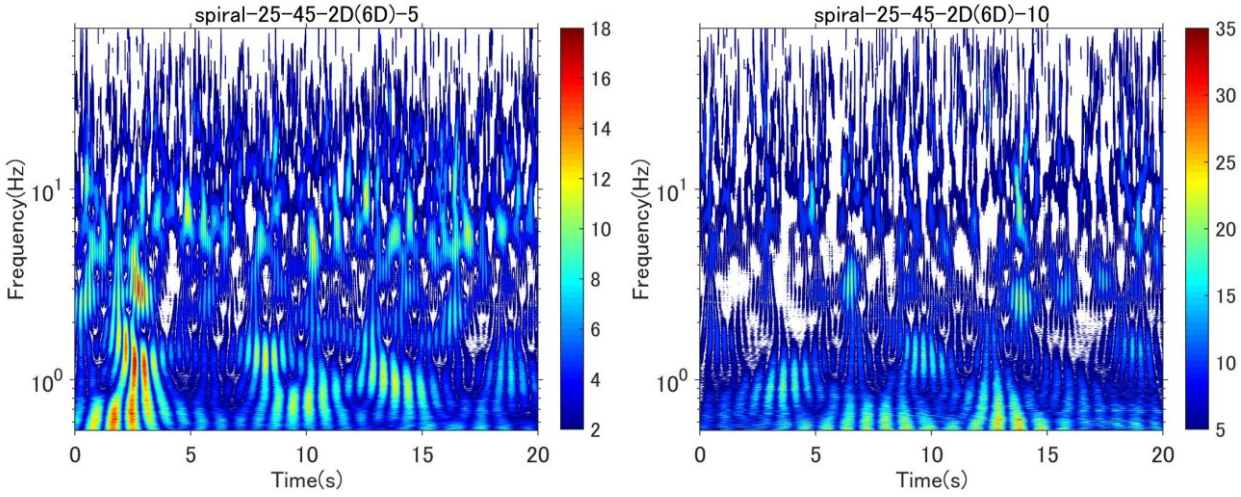

Figure A-10.13 WA of spiral cable, X/D= 2, U=5 and 10m/s, β=45° and α= 25°

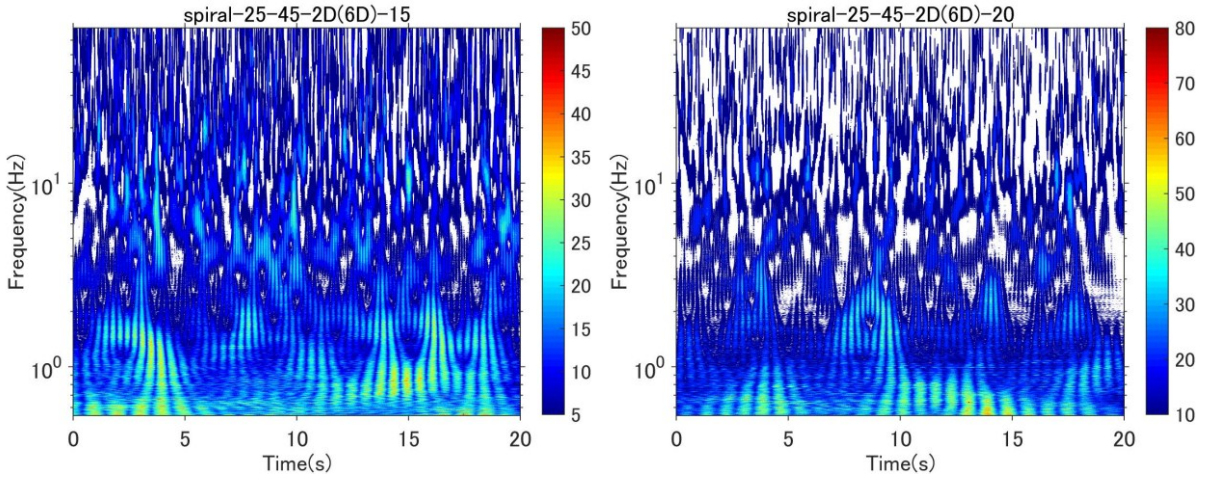

Figure A-10.14 WA of spiral cable, X/D= 2, U=15 and 20m/s, β=45° and α= 25°

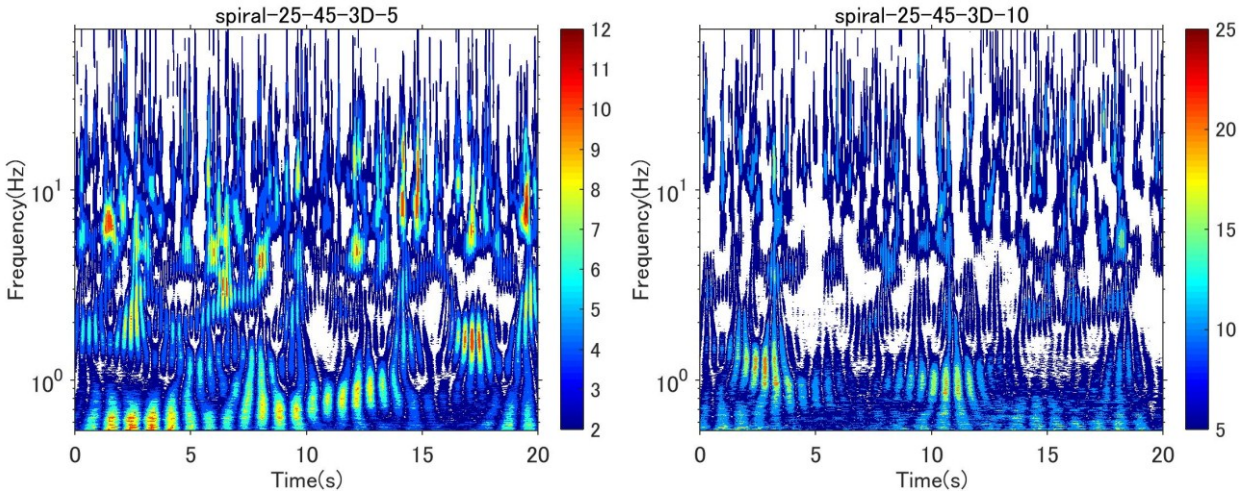

Figure A-10.15 WA of spiral cable, X/D= 3, U=5 and 10m/s, β=45° and α= 25°

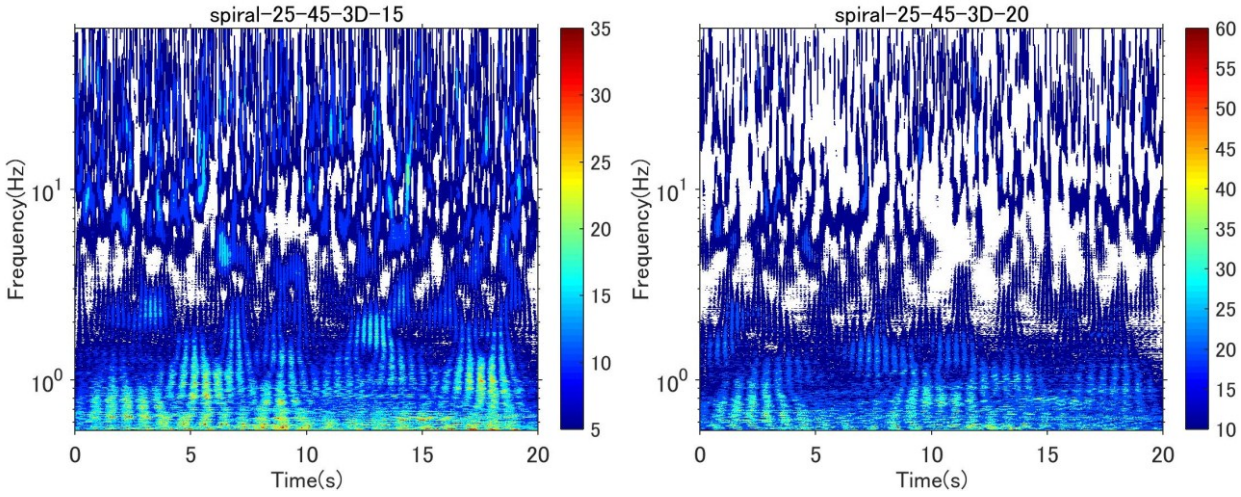

Figure A-10.16 WA of spiral cable, X/D= 3, U=15 and 20m/s, β=45° and α= 25°

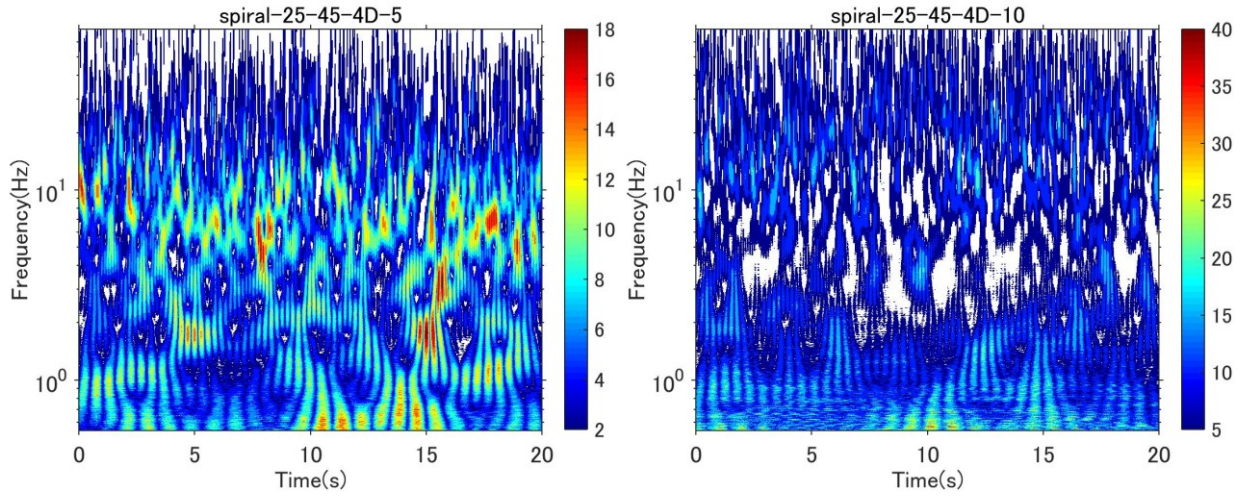

Figure A-10.17 WA of spiral cable, X/D= 4, U=5 and 10m/s, β=45° and α= 25°

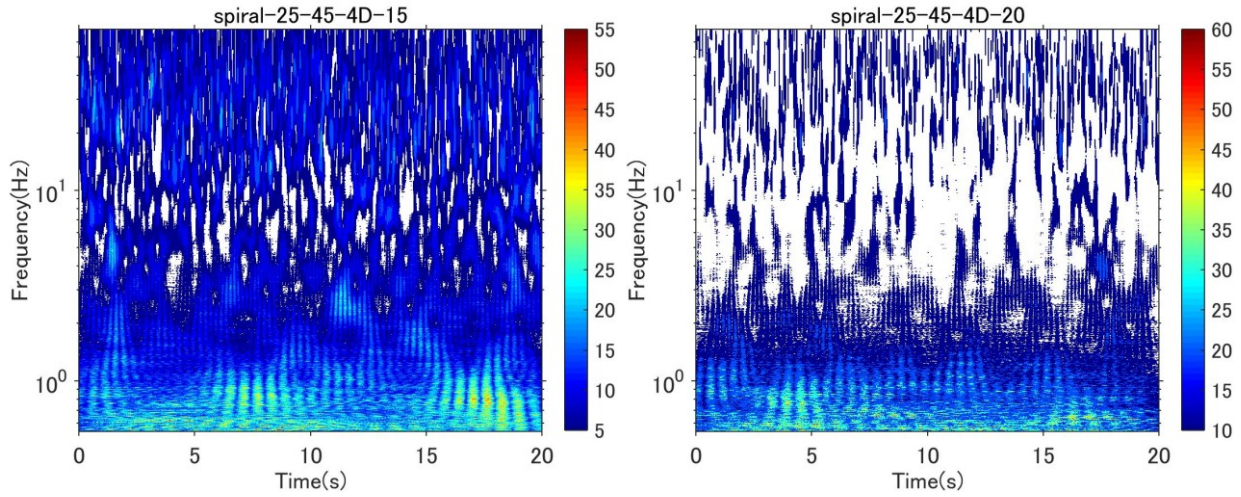

Figure A-10.18 WA of spiral cable, X/D= 4, U=15 and 20m/s, β=45° and α= 25°

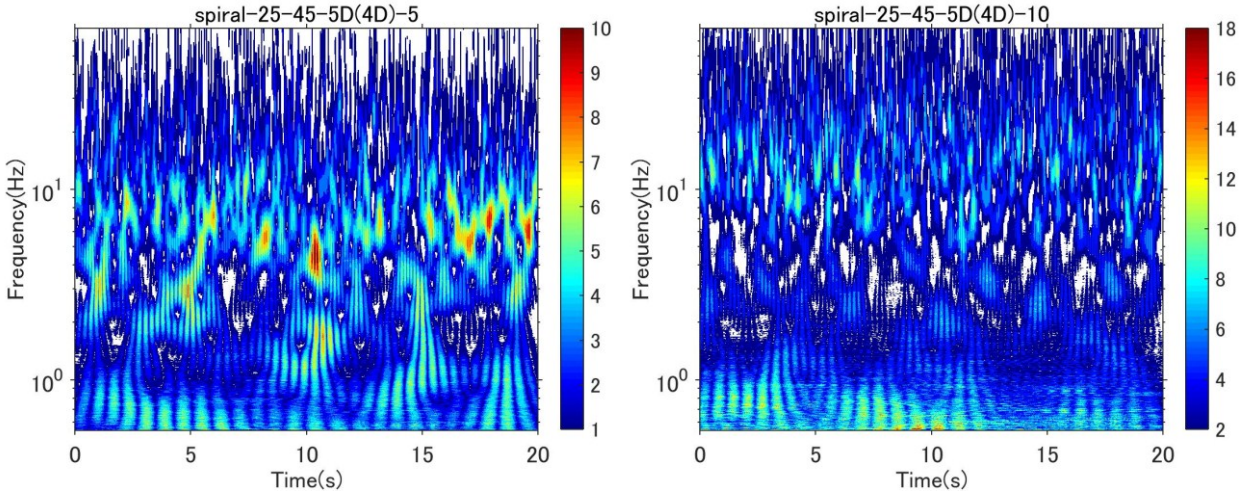

Figure A-10.19 WA of spiral cable, X/D= 5, U=5 and 10m/s, β=45° and α= 25

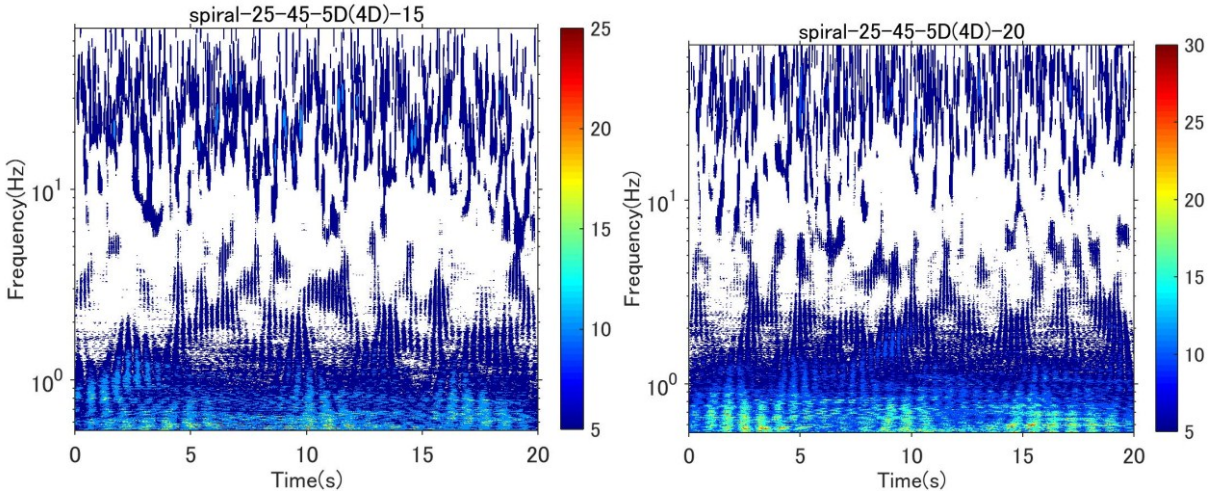

Figure A-10.20 WA of spiral cable, X/D= 5, U=15 and 20m/s, β=45° and α= 25

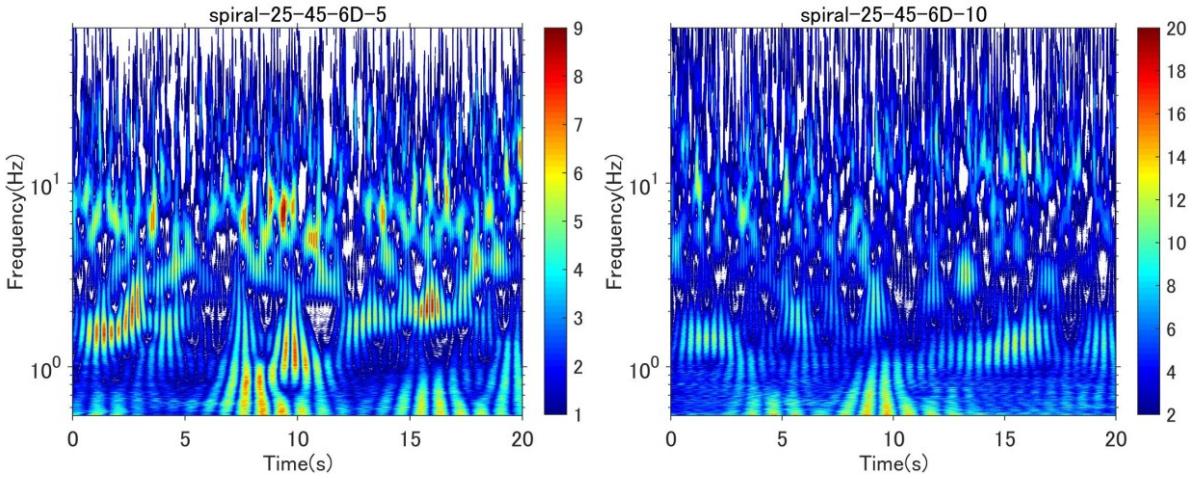

Figure A-10.21 WA of spiral cable, X/D= 6, U=5 and 10m/s, β=45° and α= 25

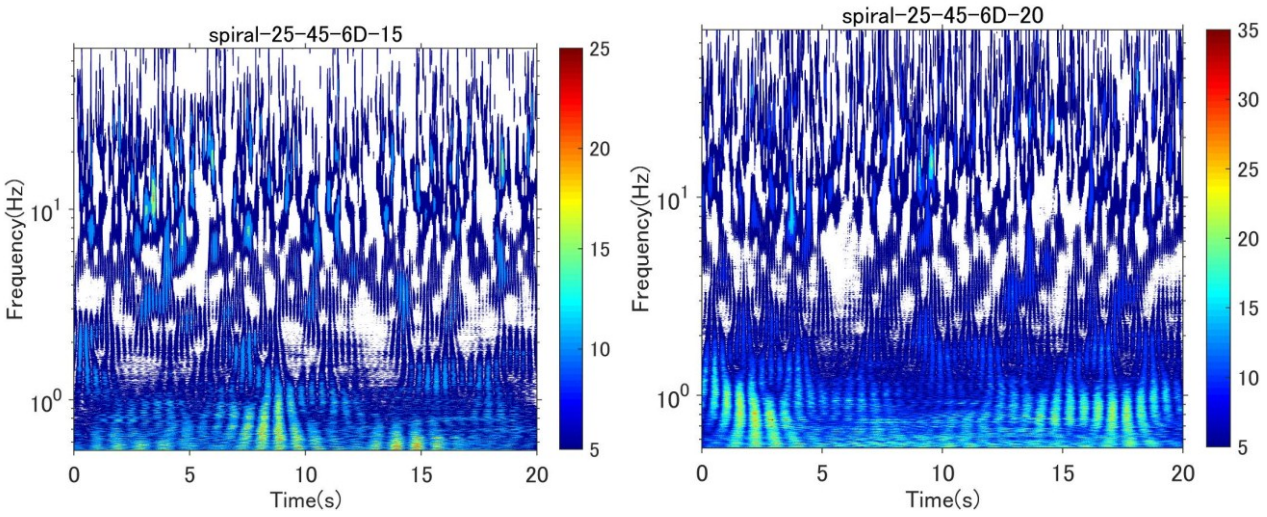

Figure A-10.22 WA of spiral cable, X/D= 6, U=15 and 20m/s, β=45° and α= 25

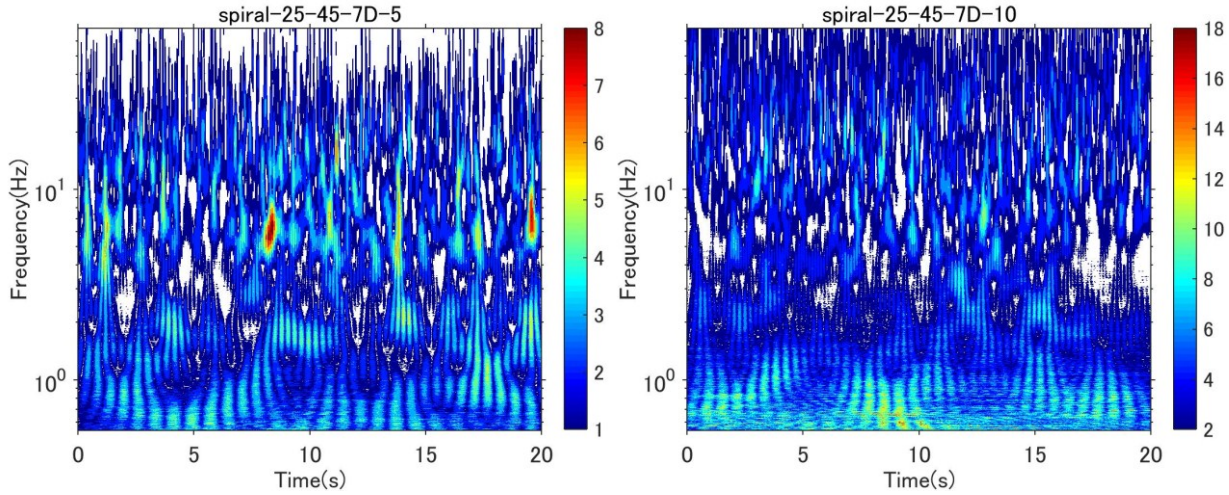

Figure A-10.23 WA of spiral cable, X/D= 7, U=5 and 10m/s, β=45° and α= 25

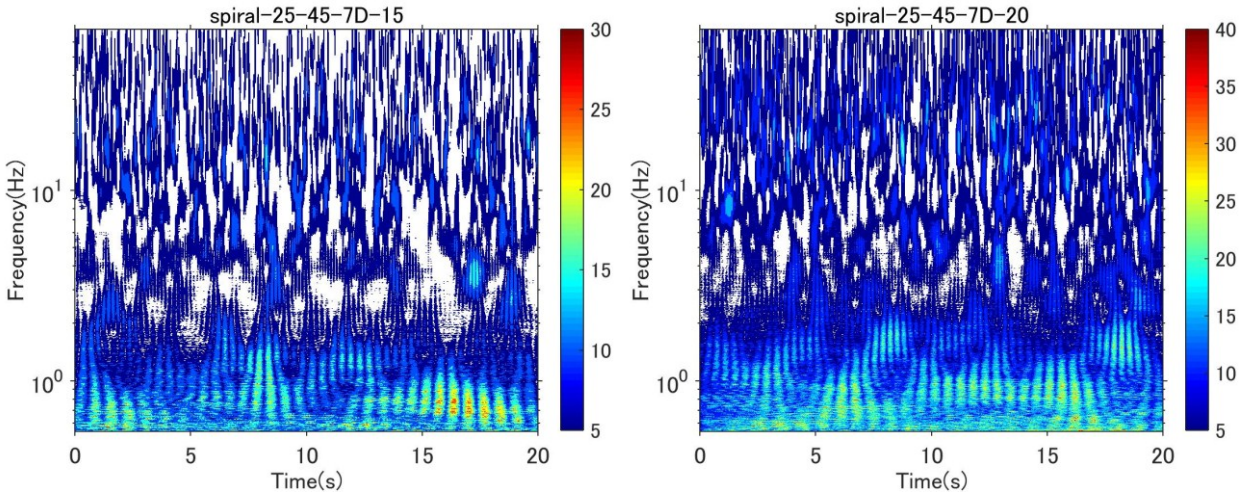

Figure A-10.24 WA of spiral cable, X/D= 7, U=15 and 20m/s, β=45° and α= 25

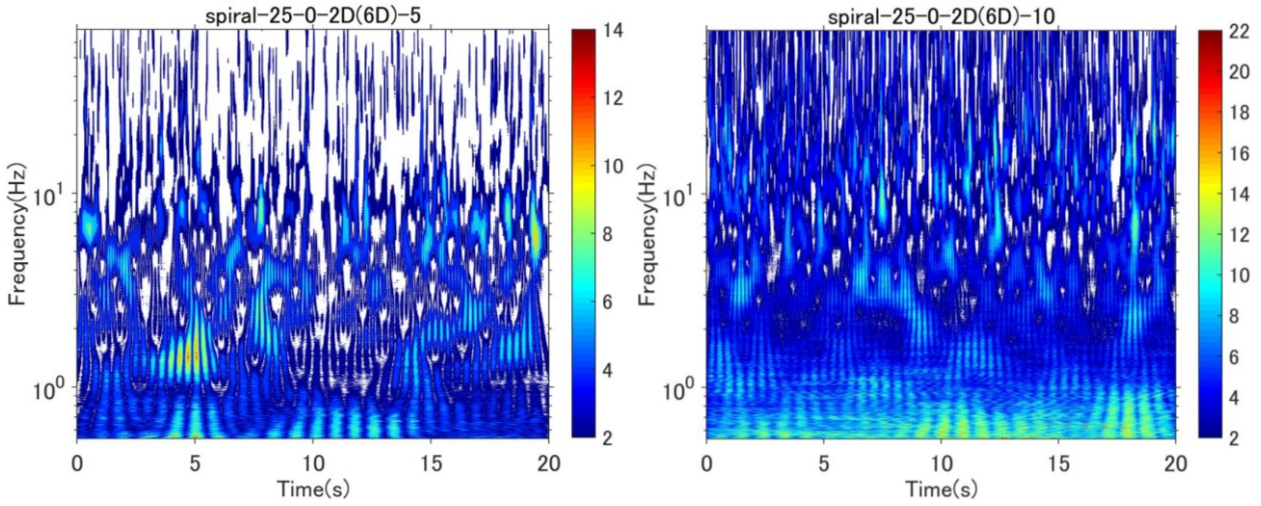

Figure A-10.25 WA of spiral cable, X/D= 2, U=5 and 10m/s, β=0° and α= 25

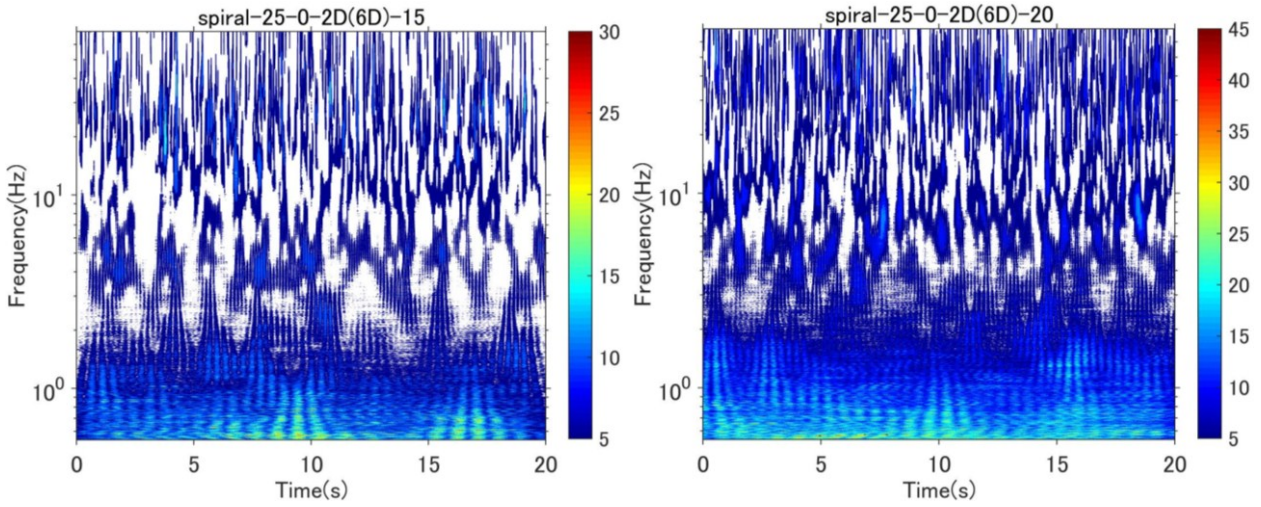

Figure A-10.26 WA of spiral cable, X/D= 2, U=15 and 20m/s, β=0° and α= 25

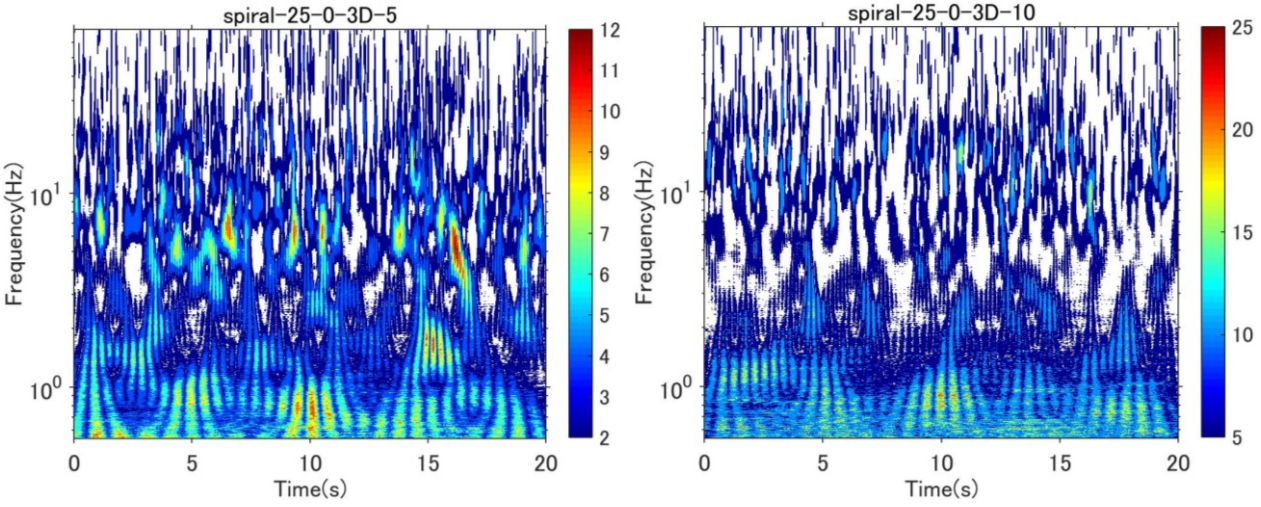

Figure A-10.27 WA of spiral cable, X/D= 3, U=5 and 10m/s, β=0° and α= 25

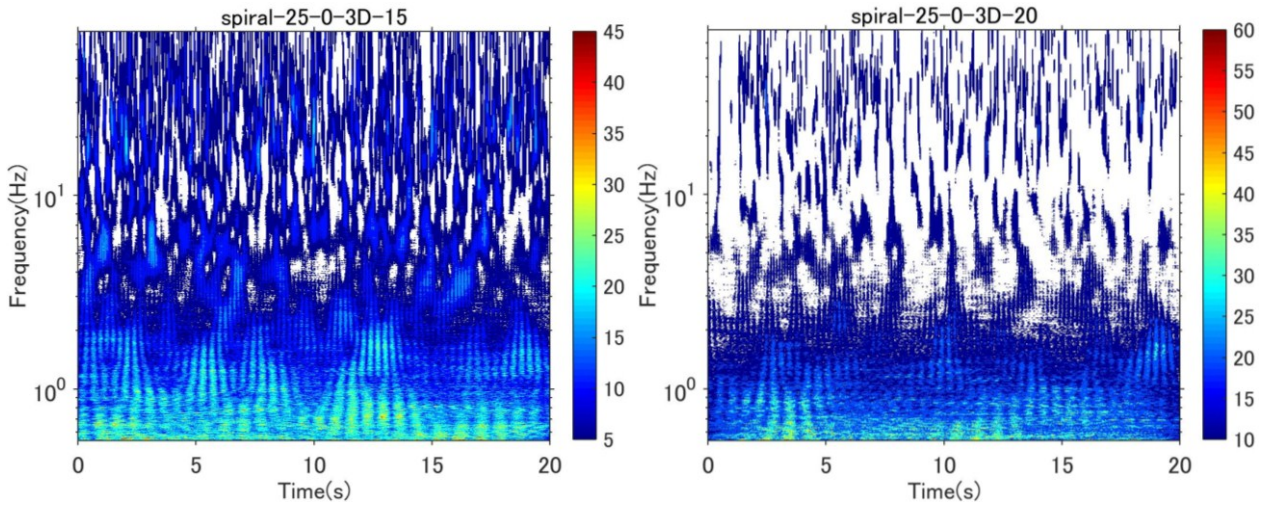

Figure A-10.28 WA of spiral cable, X/D= 3, U=15 and 10m/s, β=0° and α= 25

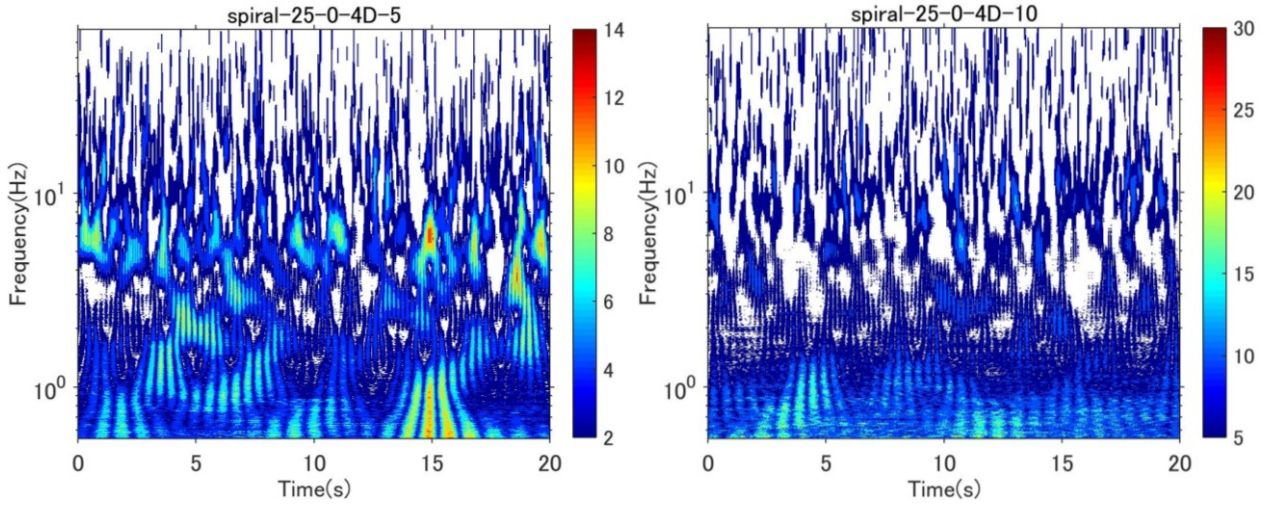

Figure A-10.29 WA of spiral cable, X/D= 4, U=5 and 10m/s, β=0° and α= 25

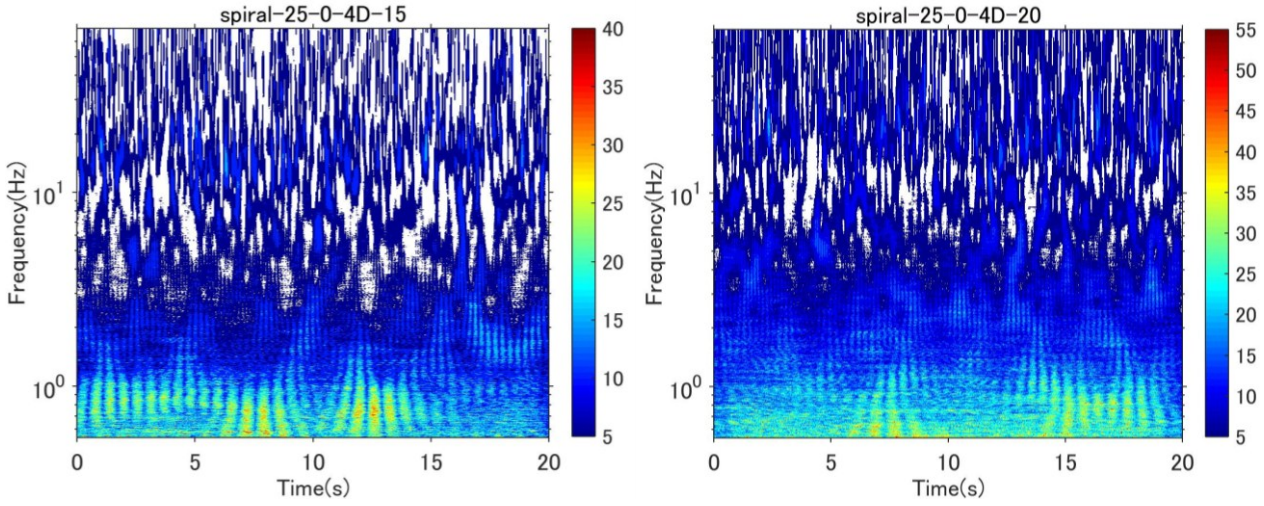

Figure A-10.30 WA of spiral cable, X/D= 4, U=15 and 20m/s, β=0° and α= 25

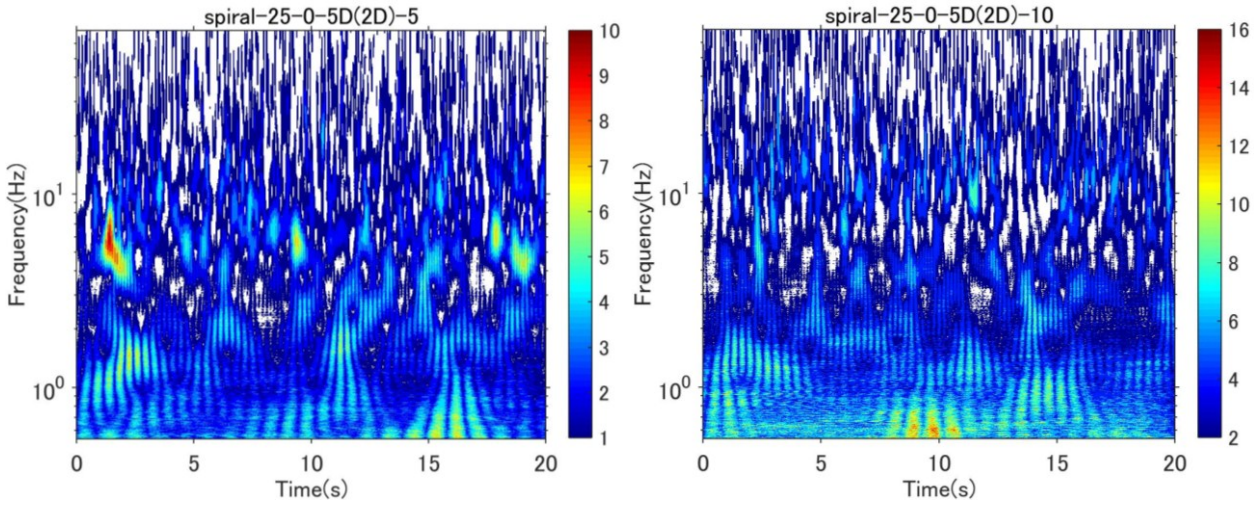

Figure A-10.31 WA of spiral cable, X/D= 5, U=5 and 10m/s, β=0° and α= 25

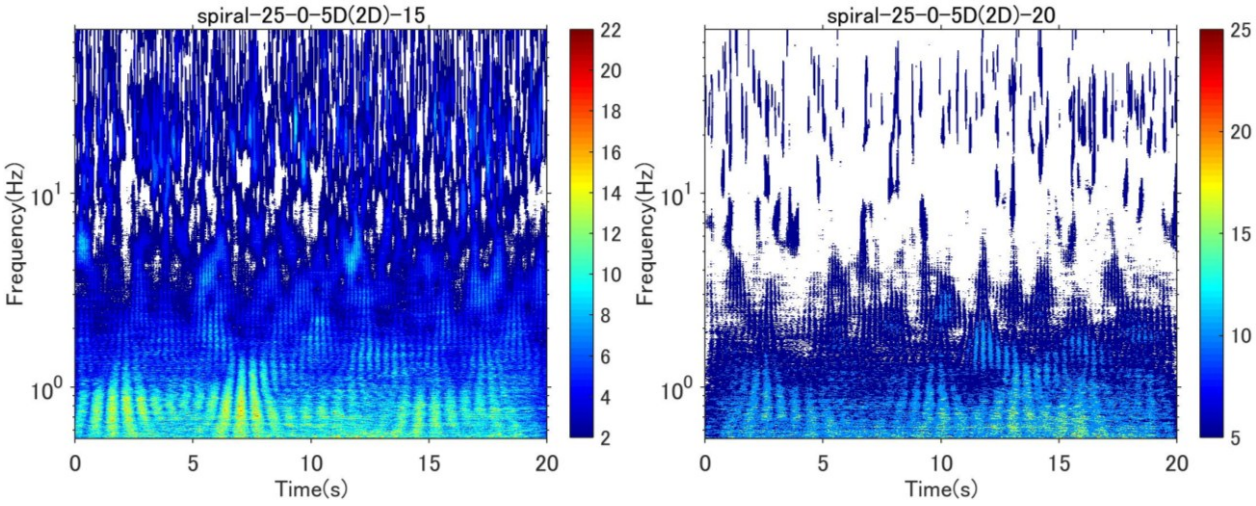

Figure A-10.32 WA of spiral cable, X/D= 5, U=15 and 20m/s, β=0° and α= 25

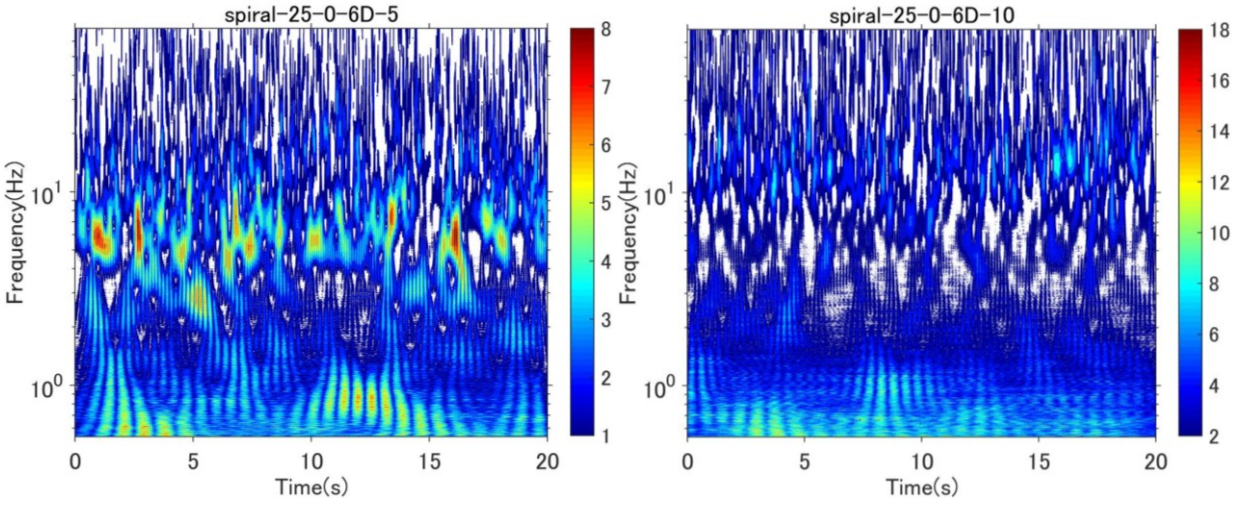

Figure A-10.33 WA of spiral cable, X/D= 6, U=5 and 10m/s, β=0° and α= 25

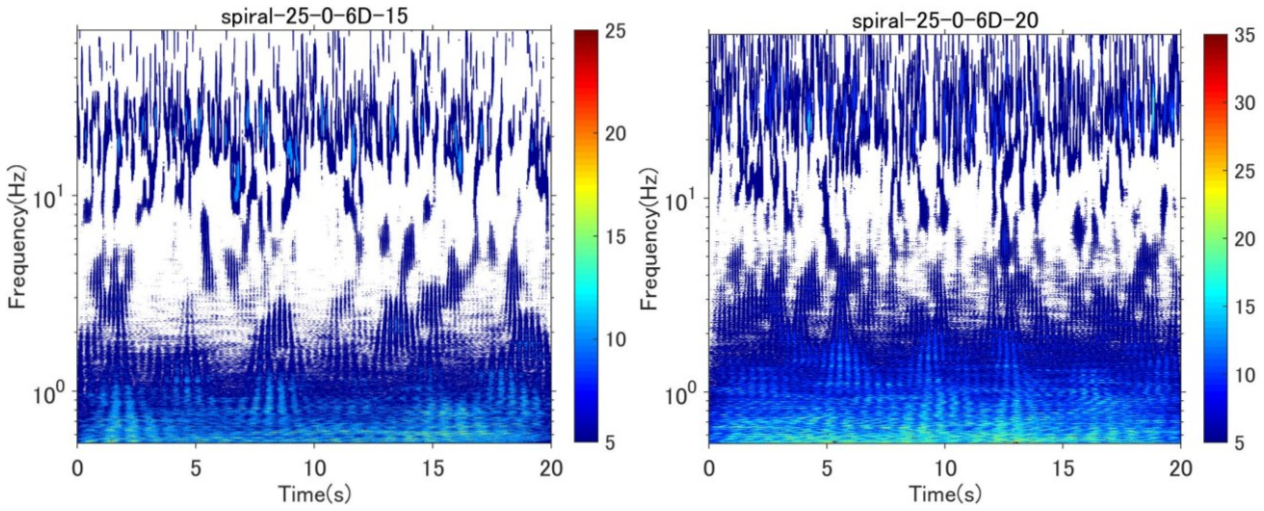

Figure A-10.34 WA of spiral cable, X/D= 6, U=15 and 20m/s, β=0° and α= 25

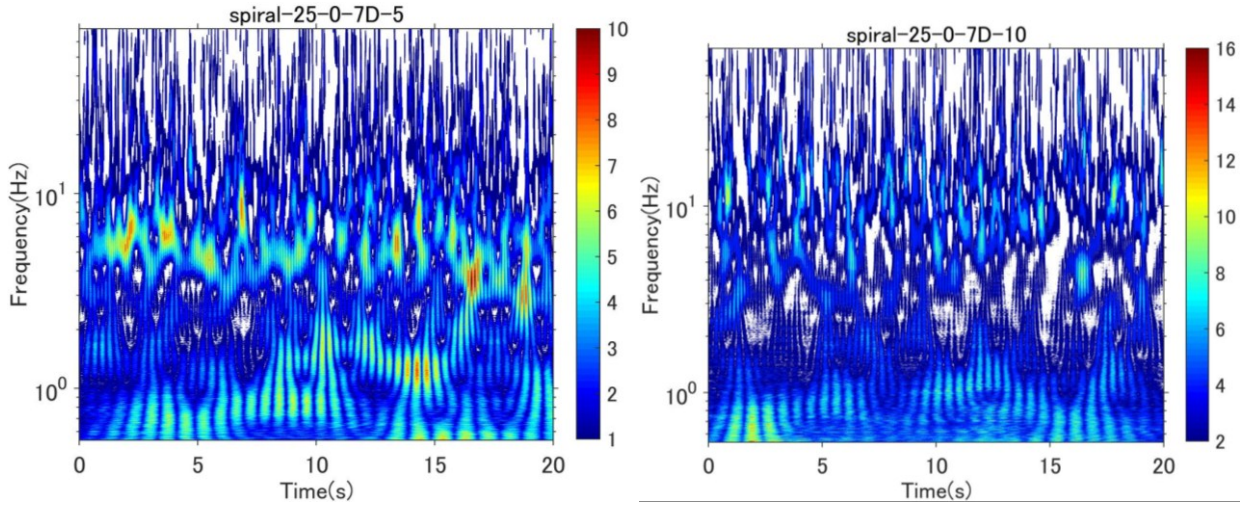

Figure A-10.35 WA of spiral cable, X/D= 7, U=5 and 10m/s, β=0° and α= 25

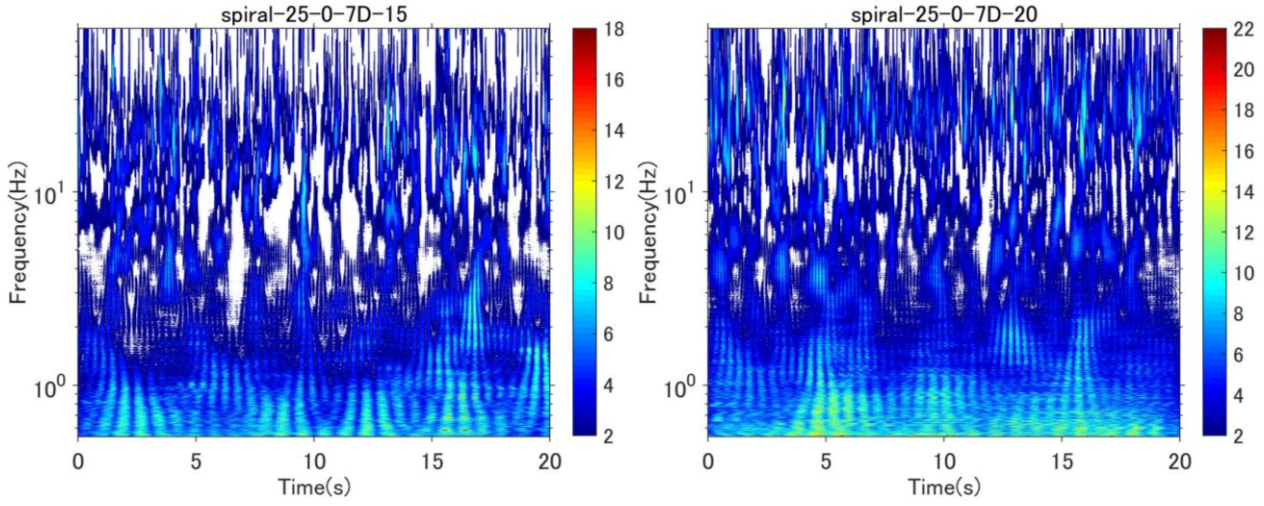

Figure A-10.36 WA of spiral cable, X/D= 7, U=15 and 20m/s, β=0° and α= 25

Appendix 11: Coherence estimation for wake flow near spiral cable wake in span-wise direction

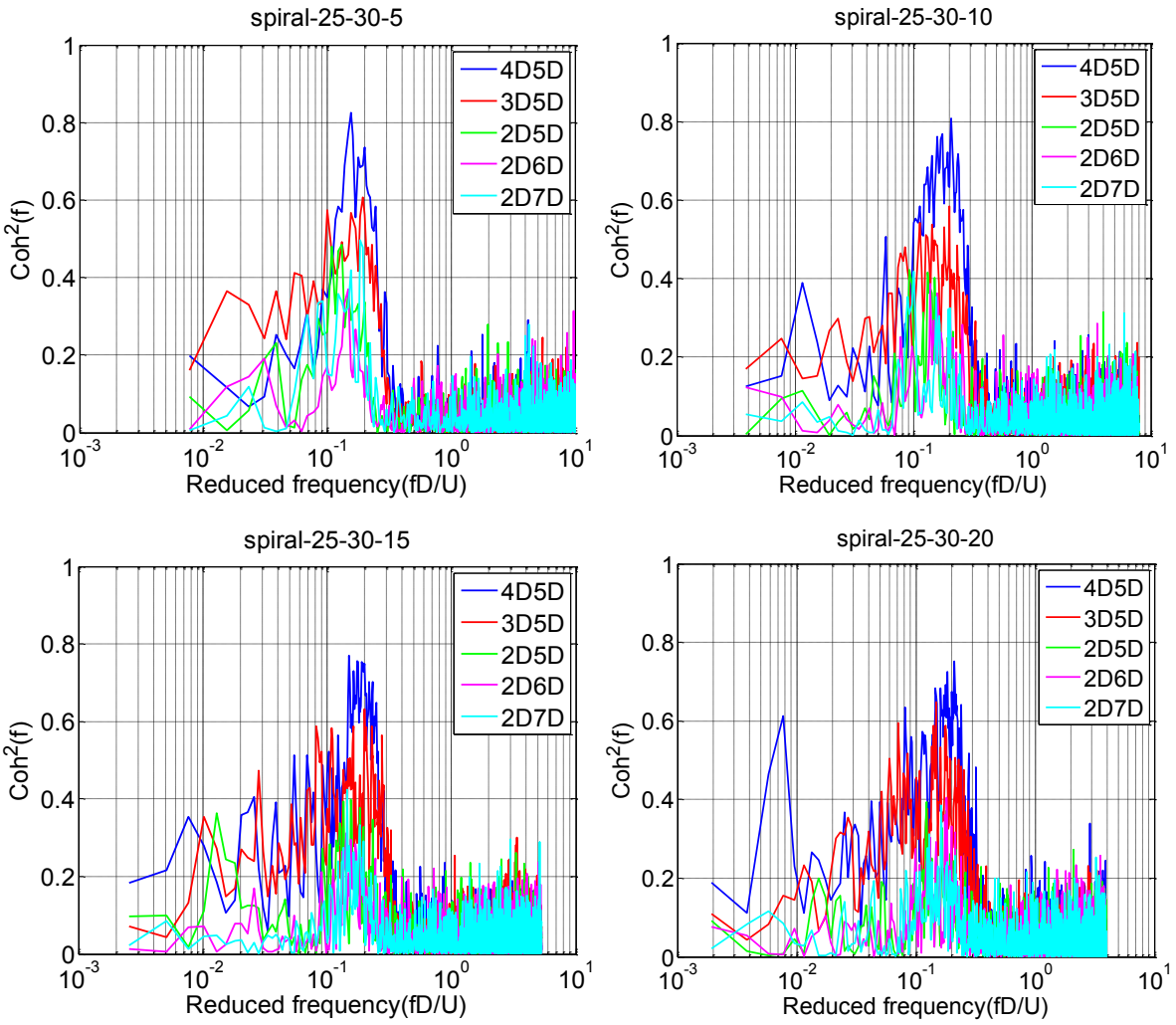

Figure A-11.1 Correlation of wake flow; spiral cable, U=5-10-15- 20m/s, β=30° and α= 25°

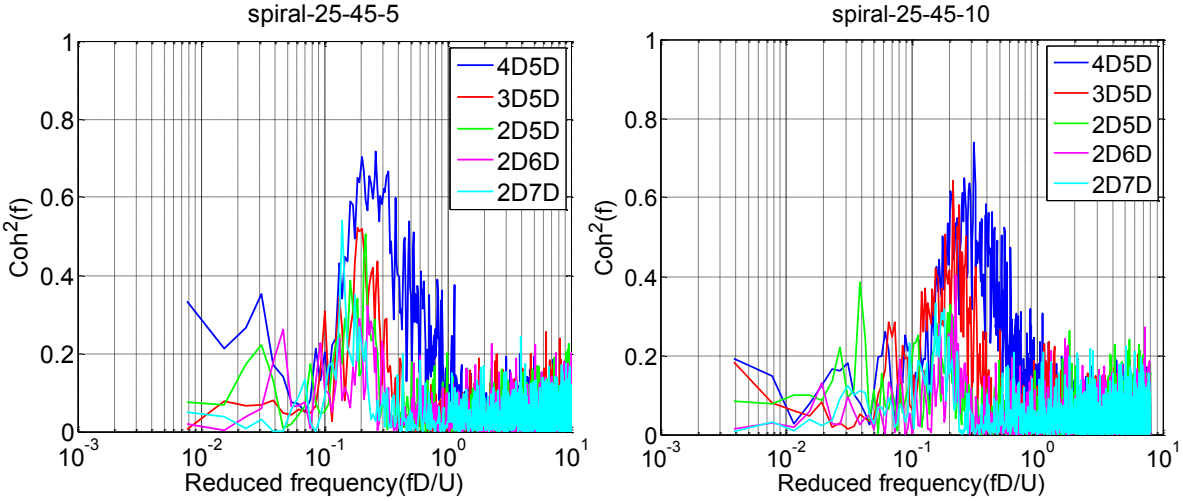

Figure A-11. 2 Correlation of wake flow; spiral cable, U=5m/s and 10m/s, β=45° and α= 25°

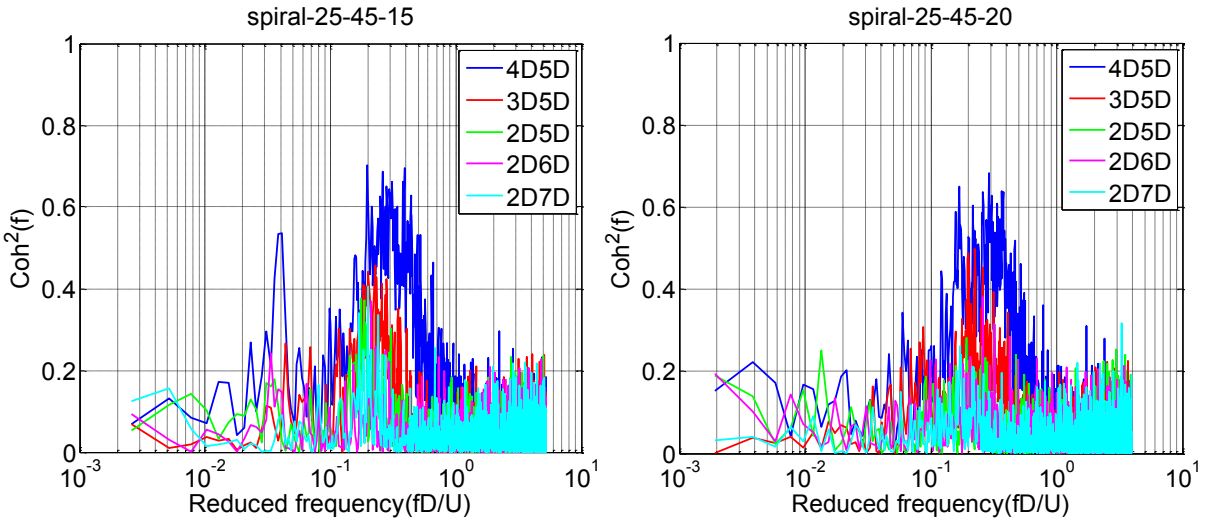

Figure A-11.3 Correlation of wake flow; spiral cable, U=15- 20m/s, β=45° and α= 25°

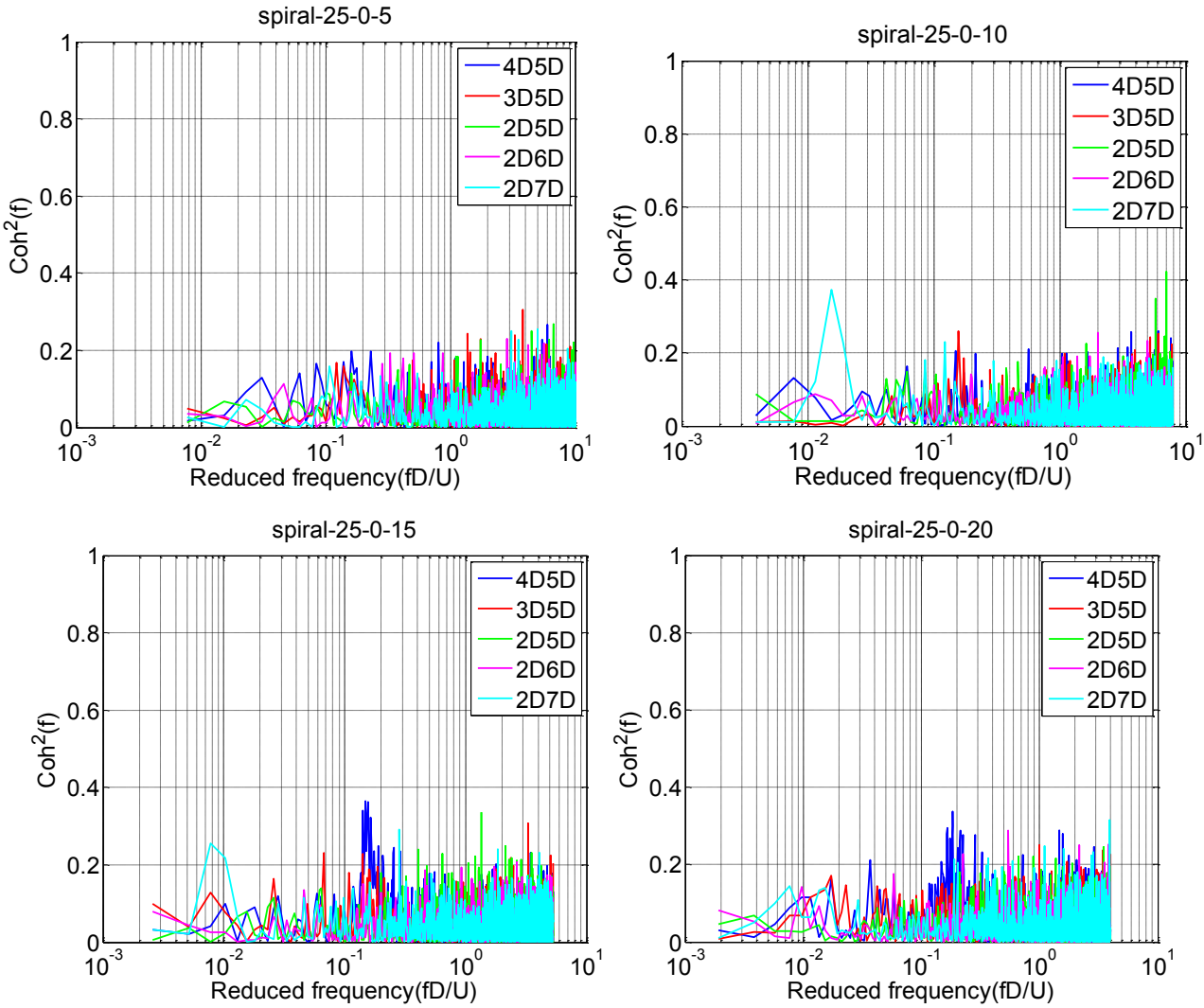

Figure A-11.4 Correlation of wake flow; Spiral cable, U=5-10- 15 and 20 m/s, β=0° and α= 25°

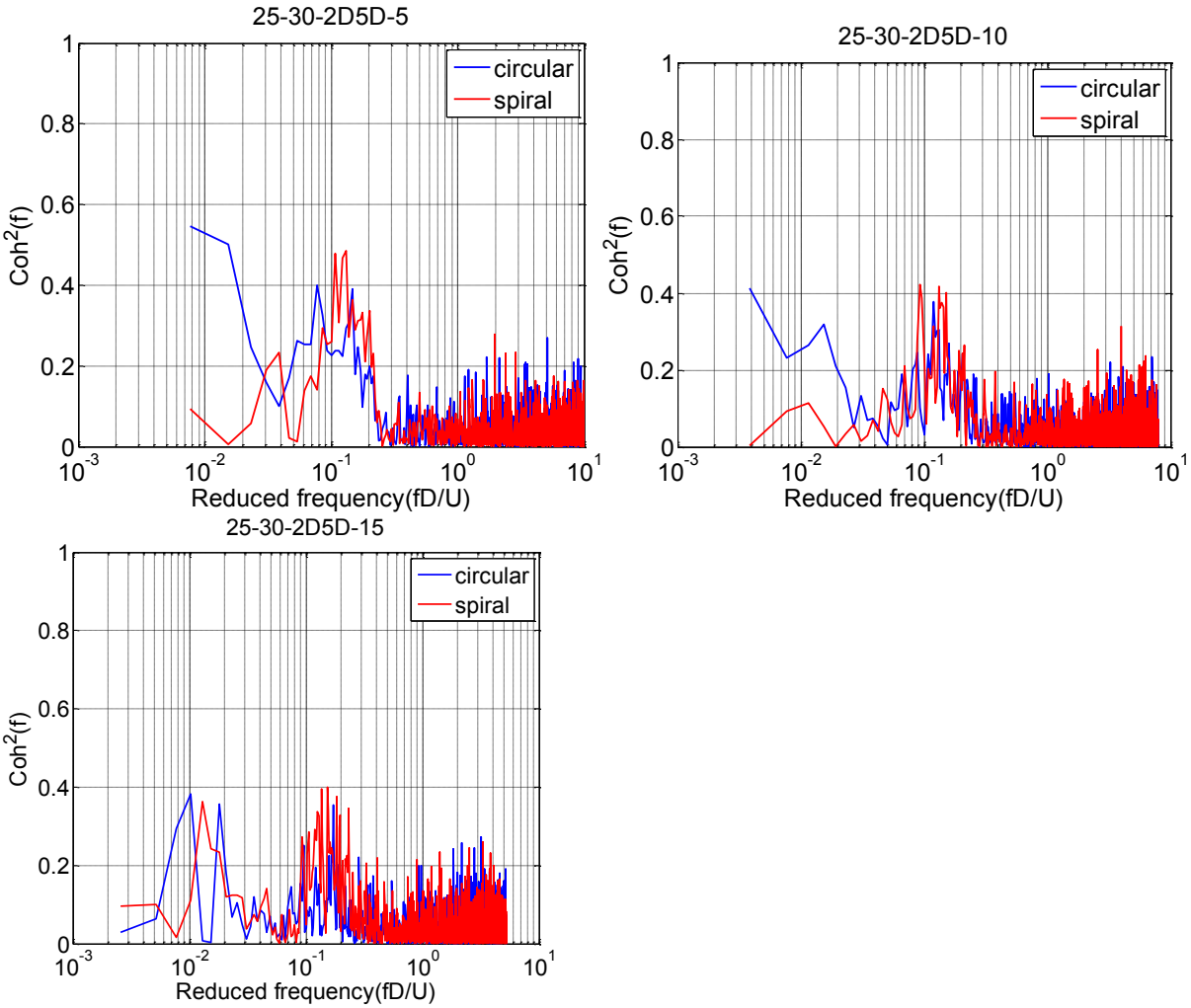

Figure A-11.5 Coherence comparison: circular versus spiral cable, Location 2D- 5D; U=5 and 10m/s and 15m/s β=30° and α= 25°

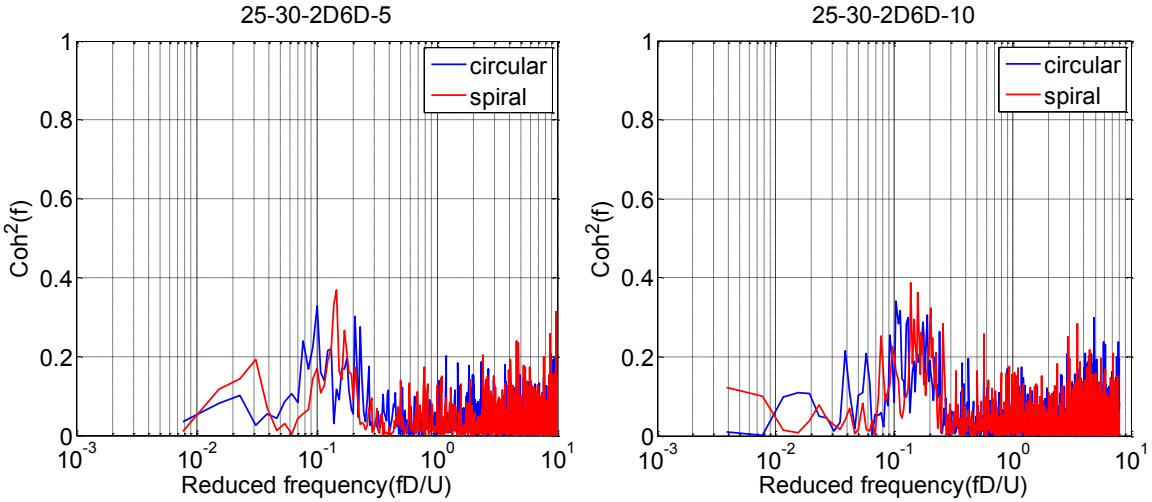

Figure A-11.6 Coherence comparison: circular versus spiral cable, Location 2D-6D; U=5 and 10m/s, β=30° and α= 25°

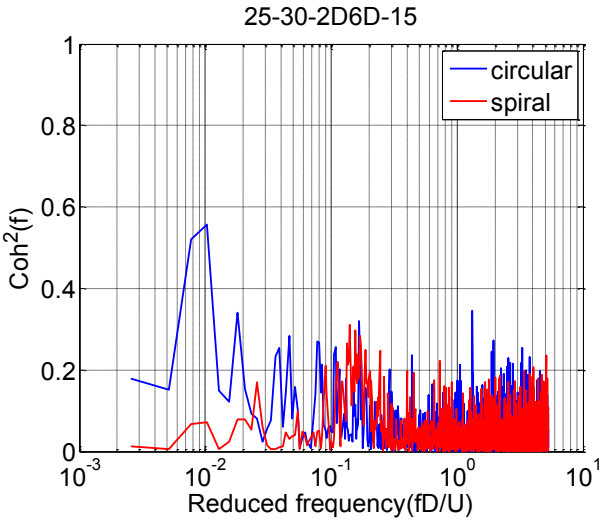

Figure A-11.7 Coherence comparison: circular versus spiral cable, Location 2D-6D; U= 15m/s, β=30° and α= 25°

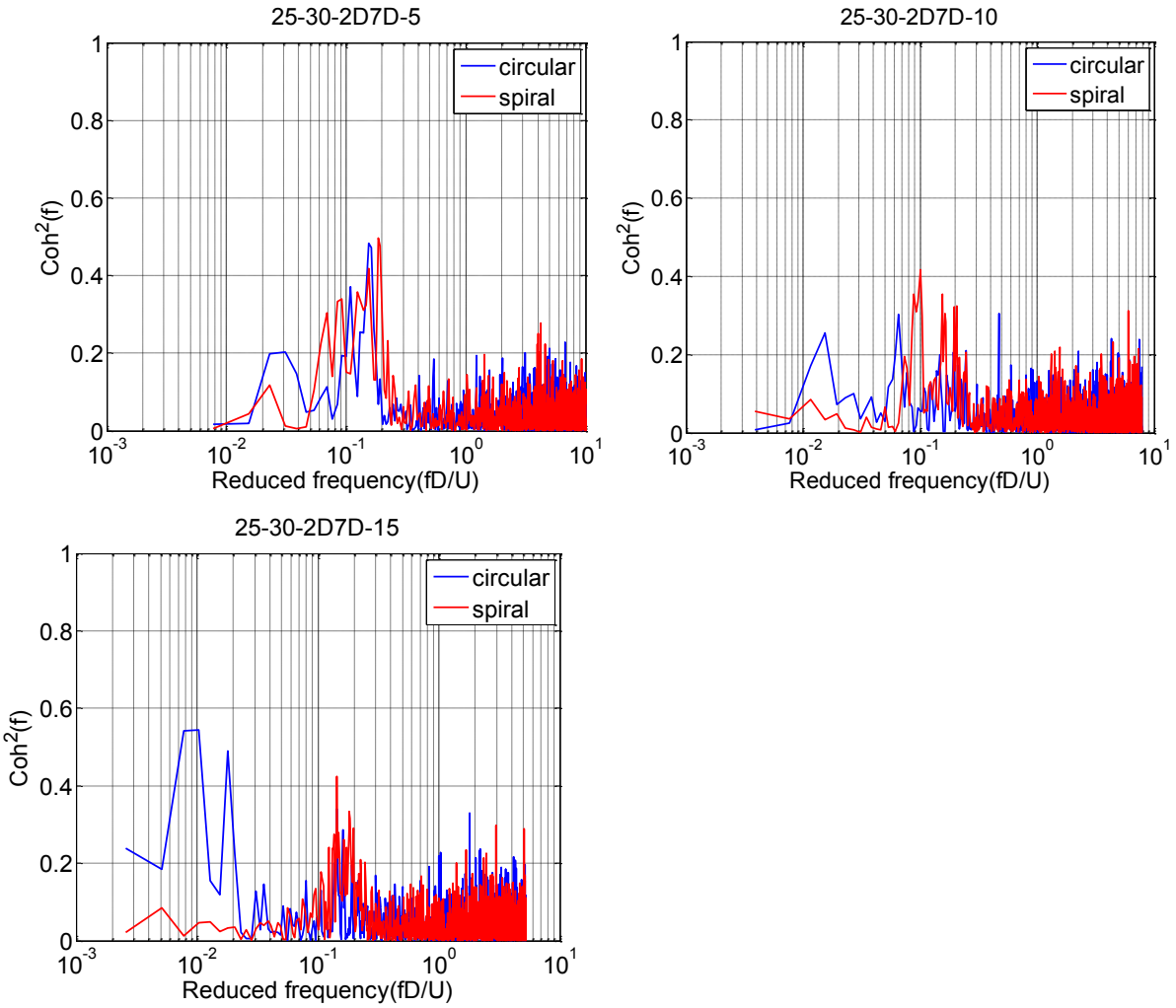

Figure A-11.8 Coherence comparison: circular cable versus spiral cable, 2D-7D; U=5m/s; 10m/s; 15m/s; β=30° and α= 25°

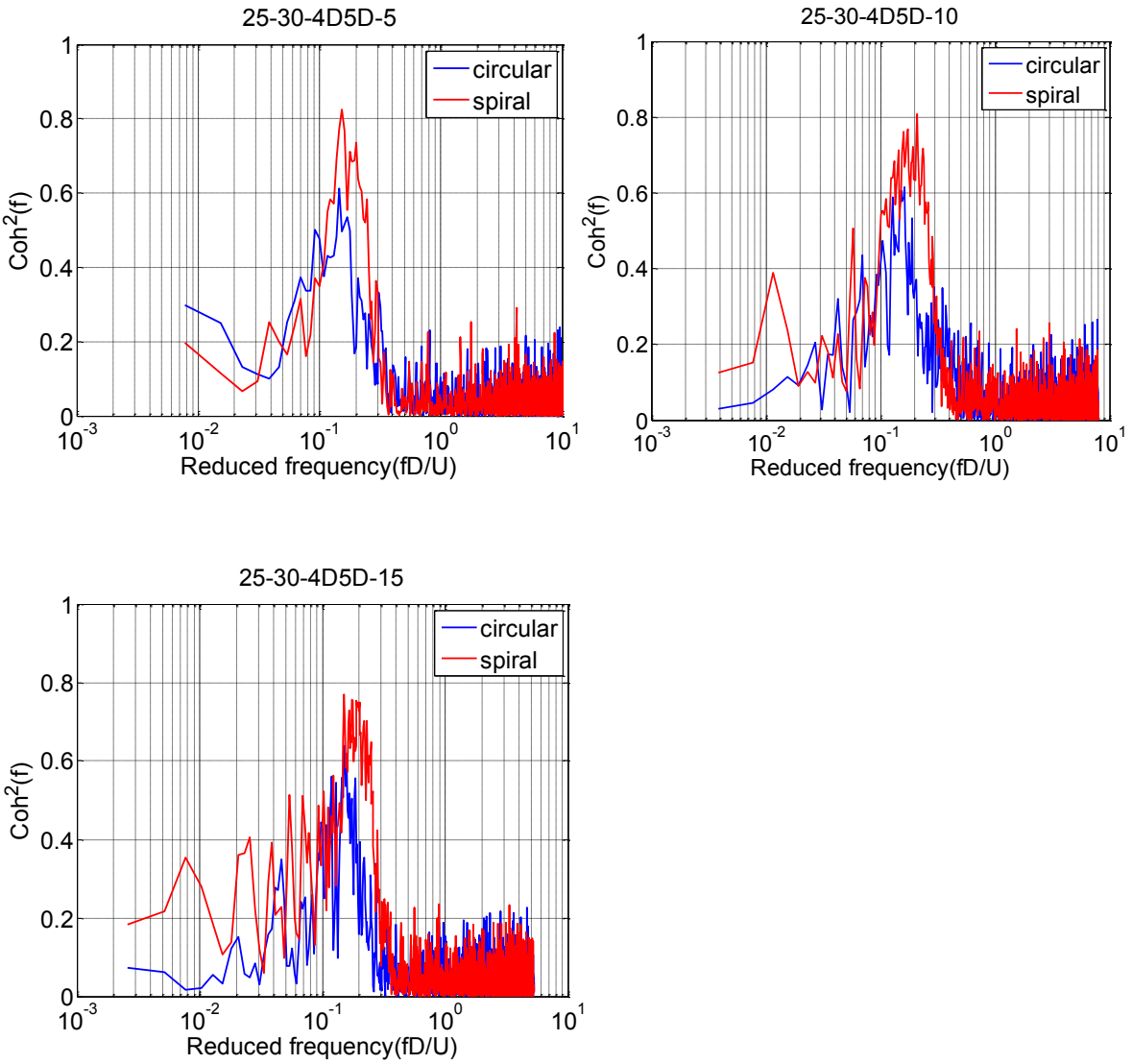

Figure A-11.9 Coherence comparison: circular cable versus spiral cable, 4D-5D; U=5m/s; 10m/s; 15m/s; β=30° and α= 25°

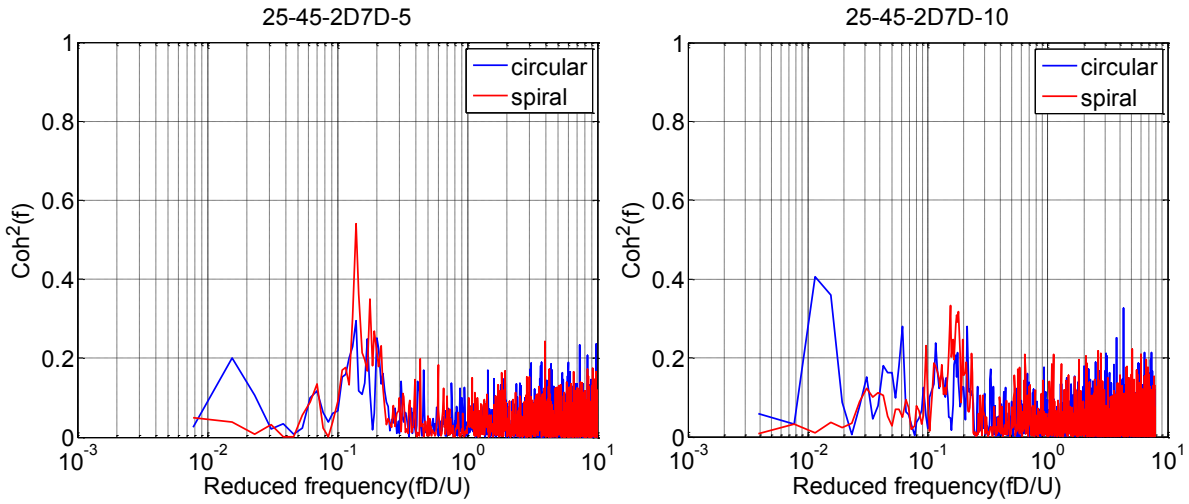

Figure A-11.10 Coherence comparison: circular cable versus spiral cable, 2D-7D; U=5m/s and 10m/s; β=45° and α= 25°

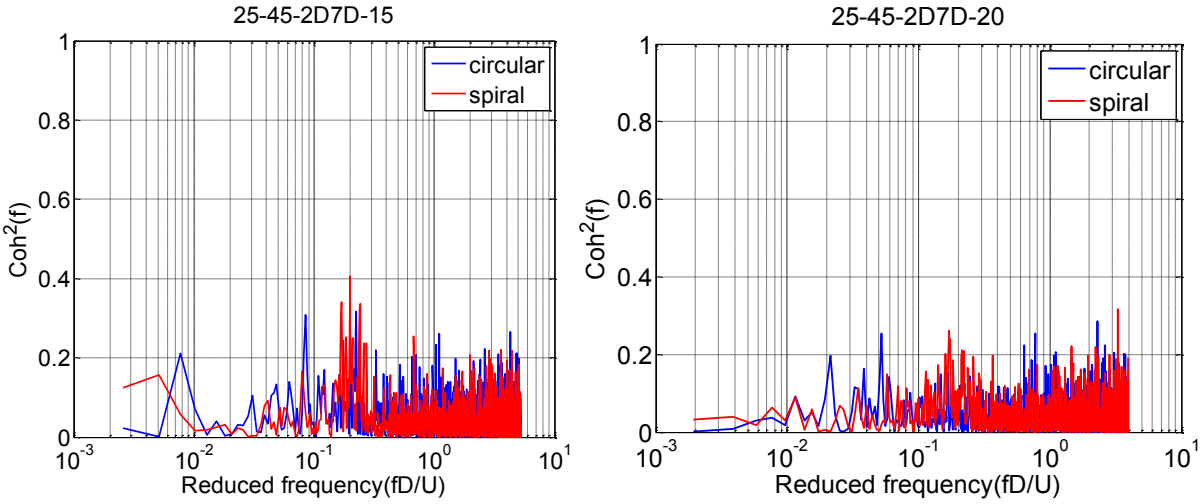

Figure A-11.11 Coherence comparison: circular cable versus spiral cable, 2D-7D; U=15m/s and 20m/s; β=45° and α= 25°

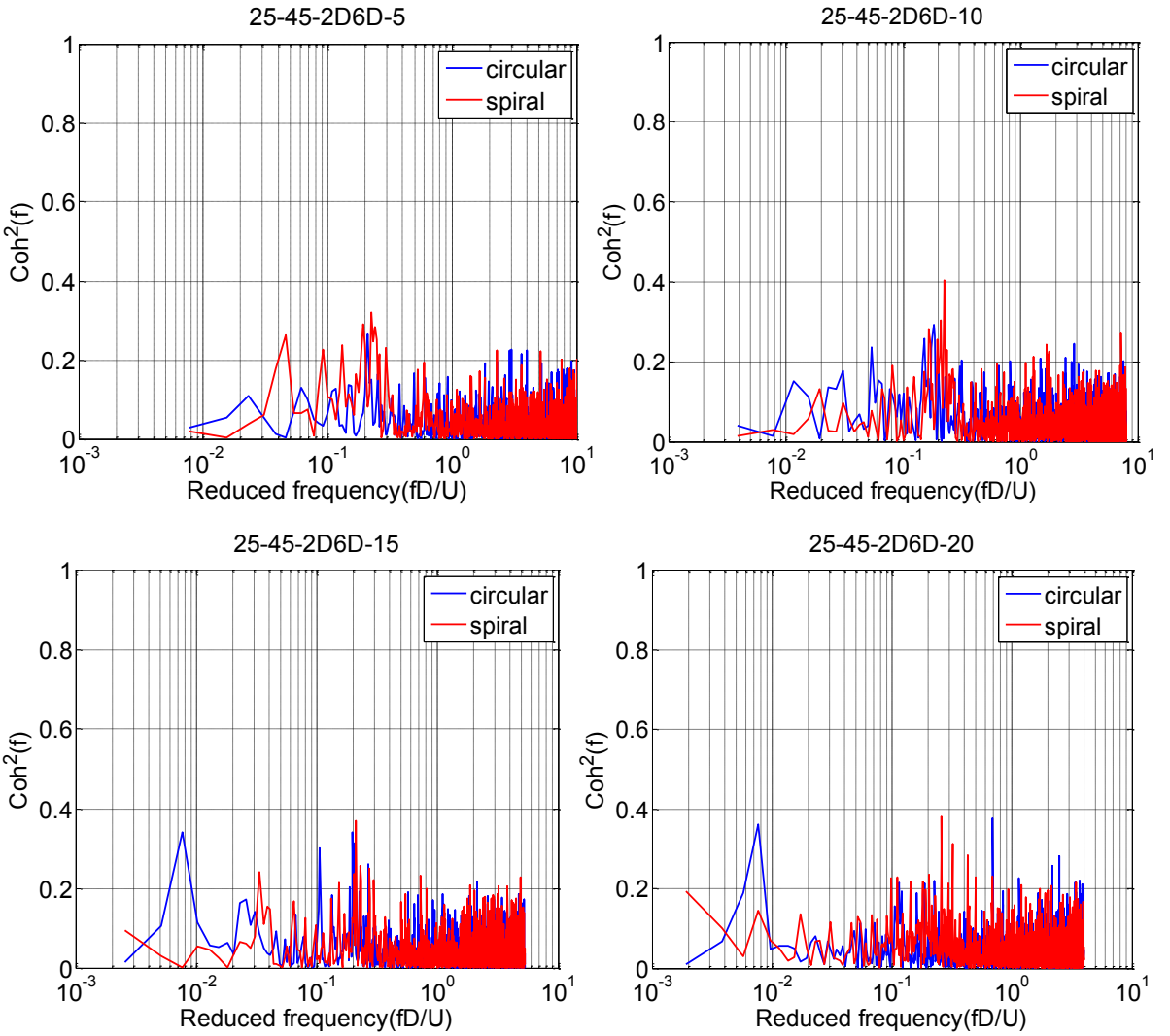

Figure A-11.12 Coherence comparison: circular cable versus spiral cable, 2D-6D; U=5m/s; 10m/s; 15m/s and 20m/s; β=45° and α= 25°

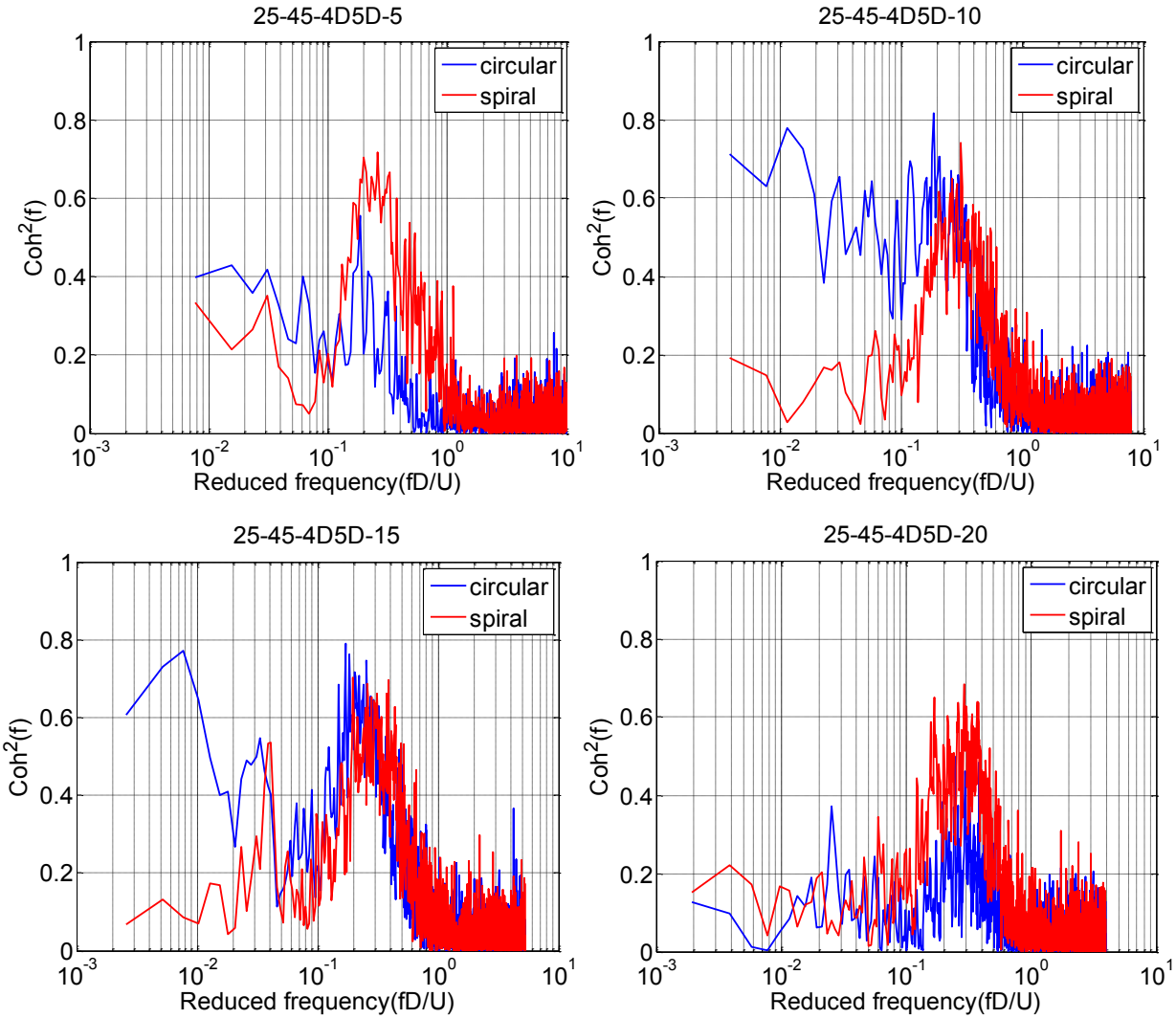

Figure A-11.13 Coherence comparison: circular cable versus spiral cable, 4D-5D; U=5m/s; 10m/s; 15m/s and 20m/s; β=45° and α= 25°

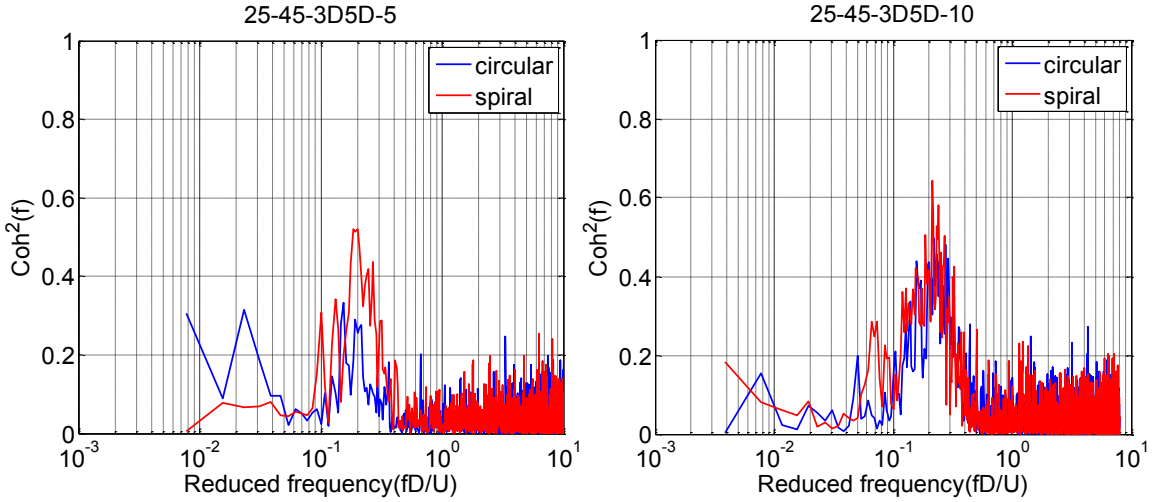

Figure A-11.14 Coherence comparison: circular cable versus spiral cable, 3D-5D; U=5m/s and 10m/s; β=45° and α= 25°

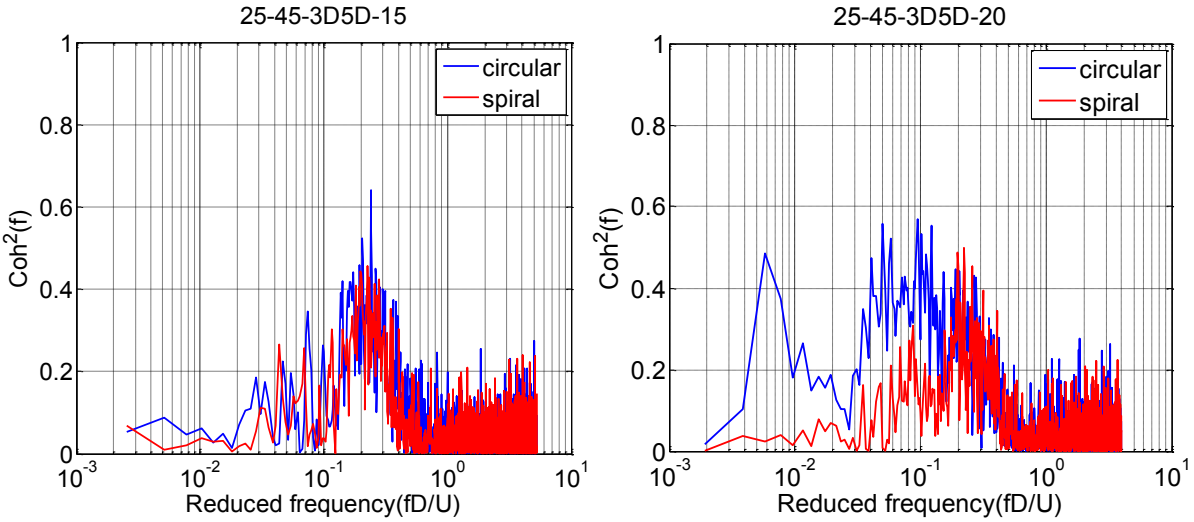

Figure A-11.15 Coherence comparison: circular cable versus spiral cable, 3D-5D; U=15m/s and 20m/s; β=45° and α= 25°

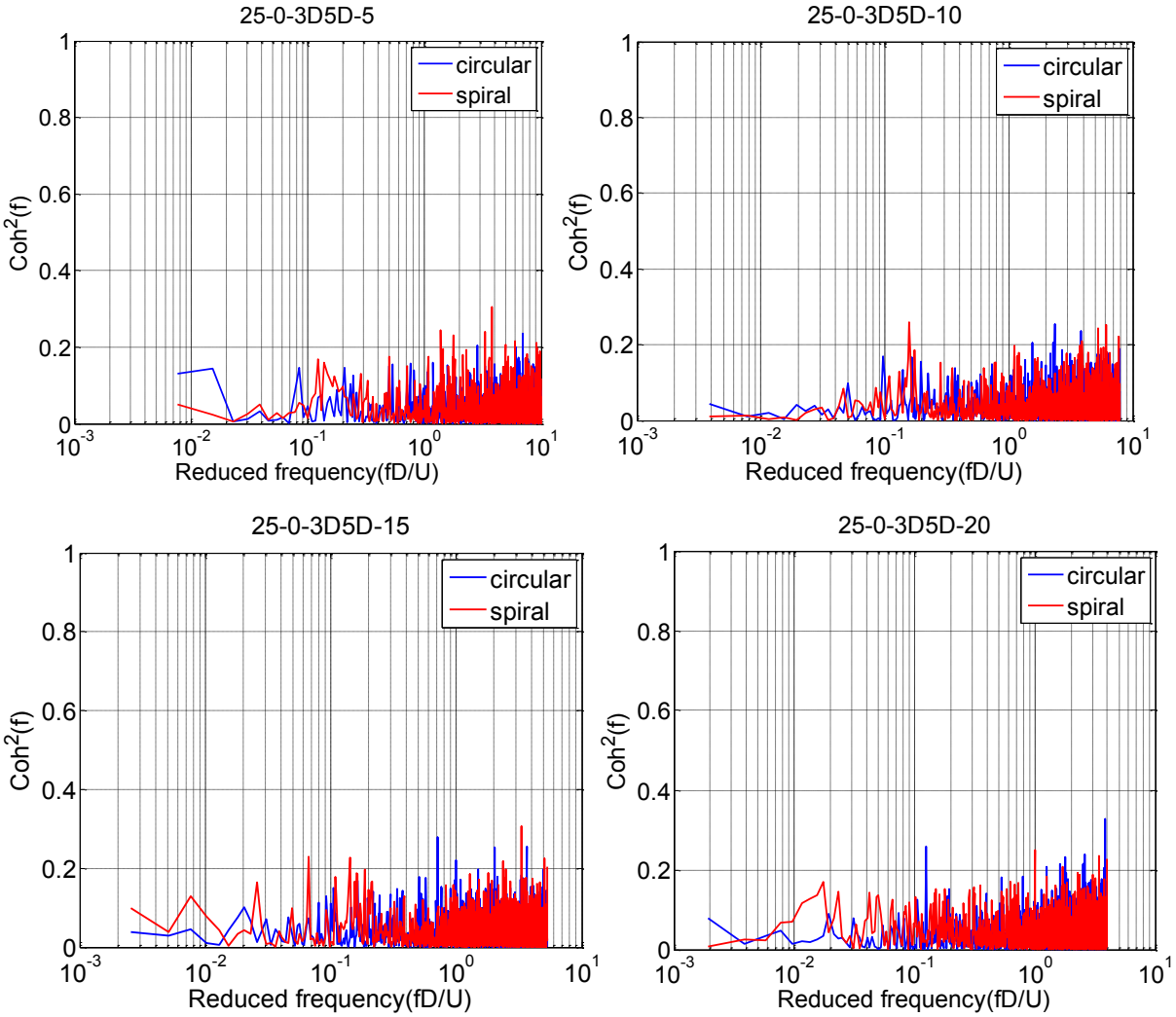

Figure A-11.16 Coherence comparison: circular cable versus spiral cable, 3D-5D; U=15m/s and 20m/s; β=0° and α= 25°

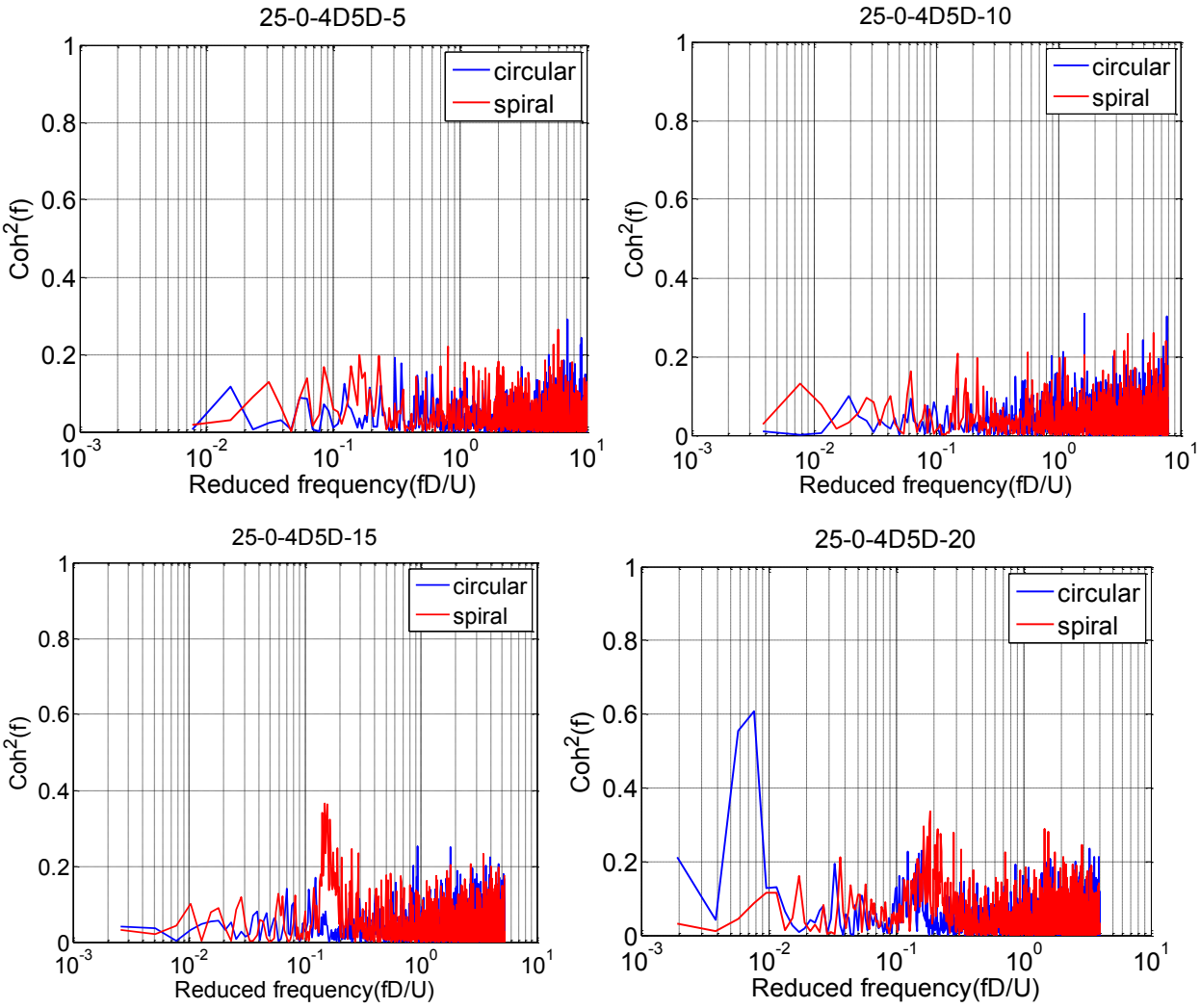

Figure A-11.17 Coherence comparison: circular cable versus spiral cable, 4D-5D; U=5, 10, 15m/s and 20m/s; β=0° and α= 25°

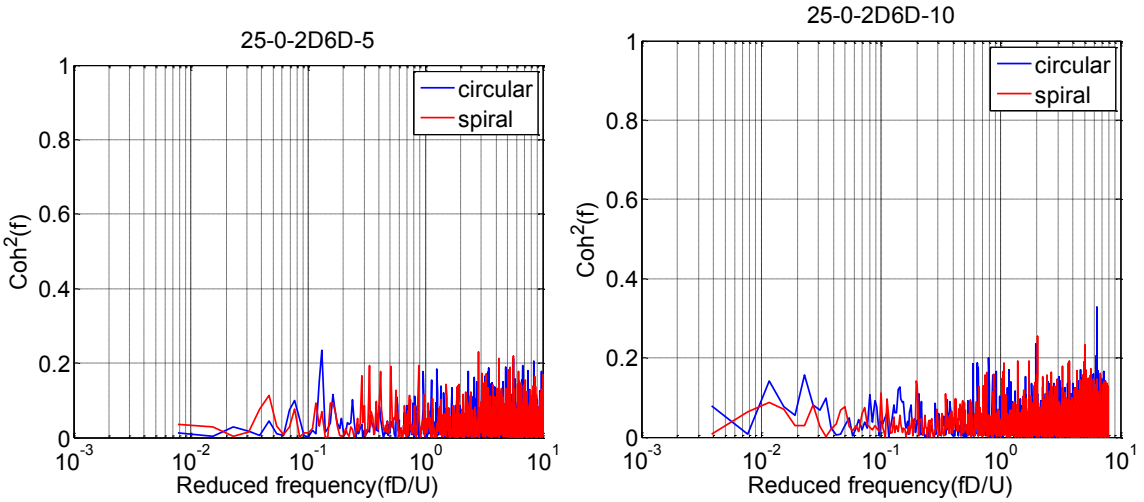

Figure A-11.18 Coherence comparison: circular cable versus spiral cable, 2D-6D; U=5m/s and 10m/s; β=0° and α= 25°

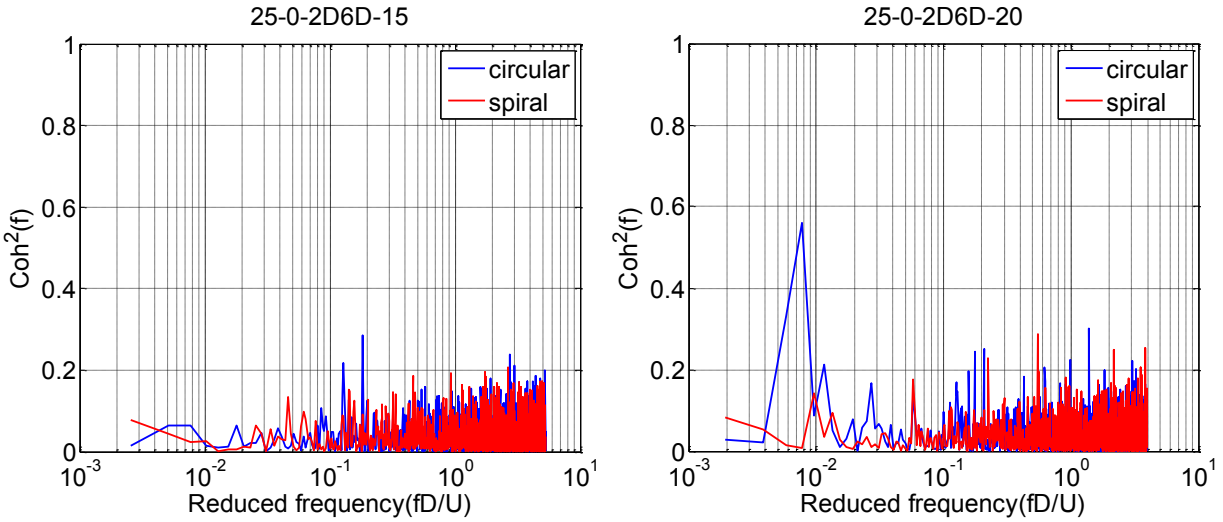

Figure A-11.19 Coherence comparison: circular cable versus spiral cable, 2D-6D; U=15m/s and 20m/s; β=0° and α= 25°

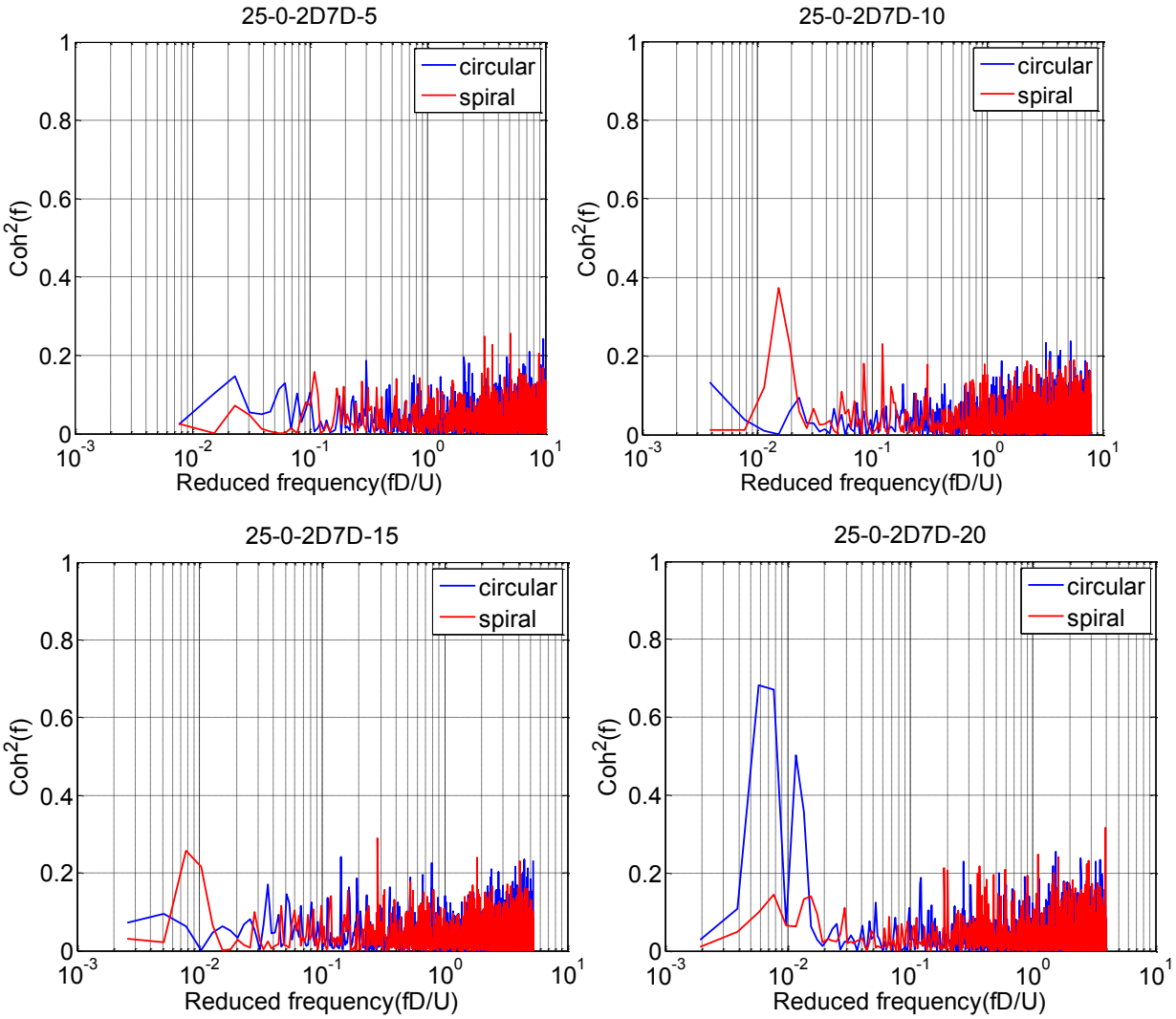

Figure A-11.20 Coherence comparison: circular cable versus spiral cable, 2D-7D; U=5, 10, 15m/s and 20m/s; β=0° and α= 25°